Regulation of neuronal voltage-gated calcium channels via carbon monoxide and amyloid-β

Thesis submitted for the degree of Doctor of Philosophy

School of Chemistry, Food and Pharmacy

Eleni Kaisis

November 2020

Declaration

I confirm that this is my own work and the use of all material from other sources has been properly and fully acknowledged.

Eleni Kaisis

Acknowledgments

I would like to dedicate my PhD thesis to my two grandads. My maternal grandfather Pelopidas who suffered from Alzheimer's disease and was one of the reasons I wanted to pursue this PhD, and my paternal grandfather Yioryos who was always very proud of my academic accomplishments and unfortunately passed away while doing my PhD. I hope you are both very proud of me.

I would also like to say a massive thank you to my husband Luke for standing by me, listening to numerous presentations throughout the years, continuously encouraging me, supporting me throughout this journey and also taking the time to proof-read my whole thesis although barely understanding the science behind it. I could not have done it without your support.

Thank you to both my parents Dora and Vassos Kaisis, and also my brother George and sister Lucia for their encouragements and support and also for all their attempts in trying to understand what I do.

I'd also like to say thank you to all the people I've met through the years I've spent in Hopkins, for being there through both the ups and downs over the years, and all the new friendships I have formed. A few people of note; Nikoleta Vavouraki, Danielle Vaughan, Feroz Ahmad, Andrew Parnell and Tom Vallance. I'd also like to thank my best friend Elina back home for being very proud of me, encouraging me and also being understanding whenever I go radio silent due to work.

Most importantly, I'd like to thank both my supervisors Dr Mark Dallas and Prof Gary Stephens for the continuous guidance and support. I could not have asked for a better supervisory team.

Lastly, I'd like to thank Alzheimer's Association for providing me with the funding for this PhD, and allowing me to carry out research for such an important cause.

Abstract

Alzheimer's disease (AD) is the most frequently occurring form of dementia worldwide. Calcium (Ca^{2+}) is important in maintaining cellular physiology with roles in gene expression, cell proliferation, differentiation and survival. One mechanism by which aggregated amyloid-β (Aβ), a main protagonist in AD, can cause Ca^{2+} dysregulation and subsequent changes in cell activity is through changes in both the expression and activity of VGCCs. Carbon monoxide (CO) acting as a gasotransmitter has shown a range of cytoprotective roles potentially mediated by ion channel-dependant mechanisms. The aim of this study was to identify the effect of protofibrillar $A\beta_{1-42}$ on voltage-gated calcium channels (VGCCs) and to investigate how CO can modulate these channels and therefore interfere with Aβ-mediated cytotoxicity.

Chemical analysis and neuroblastoma activity assays revealed time-dependent (48hr) protofibril formation of $A\beta_{1-42}$ using NH_4OH demonstrating protofibril formation that structurally and functionally resembles aggregated $A\beta_{1-42}$ cytotoxicity seen *in vivo*. Moreover, mimicking the microenvironment of cell membranes, SDS was shown to aid $A\beta_{1-42}$ aggregation. Molecular approaches (qPCR) revealed that within retinoic acid (RTA) differentiated cells protofibril $A\beta_{1-42}$ changes Cav1 expression at gene level, proposed to be representative of Ca^{2+} dysregulation seen at early stages of AD. On the other hand, electrophysiology findings revealed that $A\beta_{1-42}$ is capable of inhibiting Cav2.2 currents of stably transfected HEK293 cells. Reduction in Cav2.2 dependent Ca^{2+} influx represents changes in Ca^{2+} homeostasis seen at late stages of AD where significant neurotransmitter depletion and synaptotoxicity is observed. CO, generated using the donor CORM2 (tricarbonyldichlororuthenium(II) dimer), was shown to inhibit Cav2.2 channels through selective changes in channel kinetics. Further through electrophysiological investigation it was revealed that CO acts similarly to an oxidant, with the reducing agent DTT (dithiothreitol) reversing CO inhibitory effects on the channel.

Findings from the current study aid our understanding of AD by highlighting the different effects of Aβ on Ca^{2+} homeostasis dependent on early or late AD stage. Moreover, this study reveals that CO, might inhibit VGCCs, via an oxidant action, which may be beneficial in targeting Ca^{2+} dyshomeostasis seen at early stage of the disease where neuronal hyperactivity is observed. This study demonstrates the potential of CO, or the activation of CO-dependent pathways as a novel therapeutic against AD.

Abbreviations

Aβ – amyloid-β

AChE – acetylcholinesterase

AD – Alzheimer's disease

ADDLs – Aβ-derived diffusible ligands

ADP – adenosine diphosphate

AICD – APP intracellular domain

ALS – Amyotropic lateral sclerosis

AMP – adenosine monophosphate

AMPK – AMP-activated protein kinase

APOE – apolipoprotein E

APP – amyloid-precursor protein

ATP – adenosine triphosphate

Ba^{2+} – barium

BACE1 – β-secretase gene

$BaCl_2$ – barium chloride

BBB – blood-brain barrier

BDNF – brain derived neurotrophic factor

BPSD – behavioural and psychological symptoms of dementia

Ca^{2+} – calcium

CAMKII – Ca^{2+}/calmodulin dependent protein kinase II

CCB – calcium channel blocker

$CdCl_2$ – cadmium chloride

cDNA – complementary DNA

cGMP – cyclic guanosine monophosphate

ChAT – choline acetyltransferase

CHO cells – Chinese hamster ovary cells

CNS – central nervous system

CO – carbon monoxide

CORM – carbon monoxide releasing molecule

CORM-A1 – Sodium boranocarbonate

CORM1 – manganese decacarbonyl

CORM2 – Tricarbonyldichlororuthenium(II) dimer

CORM3 – Tricarbonylchloro(glycinato)ruthenium (II)

COX – cyclooxygenase

CREB – cAMP response element-binding protein

CsCl – cesium chloride

CSF – cerebrospinal fluid

CVD – cardiovascular disease

DMEM – Dulbecco's Modified Eagle Medium

DMSO – dimethyl sulfoxide

DNA – deoxyribonucleic acid

DTDP – dithiodipyridine

DTT – dithiothreitol

EGTA – egtazic acid

ER – endoplasmic reticulum

FBS – foetal bovine serum

Fe^{3+} – ferrous ion

G418 – geneticin

HEK293 cells – human embryonic kidney 293 cells

HEPES – 4-(2-hydroxyethyl)-1-piperazineethanesulfonic acid

HFIP – hexafluorisopropanol

His – histidine

H_2O_2 – hydrogen peroxide

HO – heme oxygenase

HO-1 – heme-oxygenase-1

HO-2 – heme-oxygenase-2

HO-3 – heme-oxygenase-3

HVA – high-voltage activated

iCORM2 – inactive CORM2

IDE – insulin degrading enzyme

iPSCs – induced pluripotent stem cells

LRP1 – low density lipoprotein receptor-related protein 1

LVA – low-voltage activated

LXR-β – activating liver-X receptor-β

MAPK – mitogen-activated protein kinase

MCI – mild cognitive impairment

MEM – Minimum Essential Medium

$MgCl_2$ – magnesium chloride

MMSE – mini-mental state examination

MRI – magnetic resonance imaging

mRNA – messenger RNA

mTOR – mammalian target of rapamycin

MTT – 3-(4,5-dimethylthiazol-2-yl)-2,5-diphenyltetrazolium bromide

NaOH – sodium hydroxide

NeuN – neuronal nuclear protein

NF-κB – nuclear factor κ-light-chain-enhancer of activated B cells

NH_4OH – ammonium hydroxide

NMDA – N-methyl-D-aspartate

NO – nitric oxide

NOS – nitric oxide synthase

NPCs – Neural Progenitor cells

Nrf2 – nuclear factor erythroid 2–related factor 2

NSAID – non-steroidal anti-inflammatory drugs

NSCs – neural stem cells

PBS – phosphate buffered saline

PCR – polymerase chain reaction

PD – Parkinson's disease

PET – positron emission tomography

PiB – Pittsburgh compound B

PKA – protein kinase A

PMS – phenazine methosulfate

ppm – parts per million

PrP – prion protein

PSEN 1 – presinilin 1

PSEN 2 – presinilin 2

qPCR – quantitative PCR

RBCs – red blood cells

RNA – ribonucleic acid

ROCs – receptor-operated calcium channels

ROS – reactive oxygen species

RTA – retinoic acid

RT-PCR – Real time PCR

Ru – ruthenium

RyRs – ryanodine receptors

SDS – sodium dodecyl sulfate

sGC – soluble guanylyl cyclase

SNAP25 – synaptosomal-associated protein

SOCs – store-operated calcium channels

SOD – superoxide dismutase

TAE – Tris-acetate-EDTA

TEA – triethylamine

TEM – transmission electron microscopy

ThT – Thioflavin

TMO – Trimethadione

Trx – thioredoxin

VAMP-2 – vesicle-associated membrane protein-2

VGCCs – voltage-gated calcium channels

VLDL – very-low density lipoprotein

Table of Contents

Table of Figures

Table of Tables

Chapter 1: Introduction

1.1. Alzheimer's disease

1.1.1. Dementia Prevalence

Dementia is a neurodegenerative disease mainly characterised by cognitive impairment. Alzheimer's disease (AD) is the most common form of dementia and it accounts for around 2/3 of dementia cases, with some individuals exhibiting comorbidities such as the presence of a mixture of dementias (Prince and Jackson, 2009; Qiu, Kivipelto and Strauss, 2009; DeTure and Dickson, 2019). For example, post-mortem studies have revealed that some individuals suffered from a combination of vascular dementia and AD (James *et al.*, 2012; Chui and Ramirez-Gomez, 2015). Other symptoms of dementia include agitation, apathy and changes in the sleep pattern, and also psychological changes such as aggression, depression, stress and hallucinations (Prince and Jackson, 2009; Qiu, Kivipelto and Strauss, 2009; Ryan *et al.*, 2010; Cerejeira, Lagarto and Mukaetova-Ladinska, 2012; Prince, Guerchet and Prina, 2015). These are grouped and collectively termed behavioural and psychological symptoms of dementia (BPSD) (Cerejeira, Lagarto and Mukaetova-Ladinska, 2012). Impairment in thinking, learning and memory process, and also language and orientation may contribute to these symptoms (Prince and Jackson, 2009; Qiu, Kivipelto and Strauss, 2009; Ryan *et al.*, 2010). Although dementia itself is a devastating symptom of the disease, BPSD significantly reduce the quality of life, with individuals exhibiting difficulties in carrying out daily tasks, therefore significantly increasing the burden on carers.

In 2015 approximately 50 million people worldwide were living with dementia, and it is estimated that by 2030 the number of cases will be double (Prince, Guerchet and Prina, 2015). Epidemiological studies revealed that in 2010, around 6.5% of individuals above 65 years of age lived with dementia, with 4.4% of cases due to AD (Lobo *et al.*, 2000; Qiu, Kivipelto and Strauss, 2009). Worldwide, 1 new dementia case arises every ~4 seconds (Prince, Guerchet and Prina, 2015). Although epidemiological studies suggest that dementia cases will rapidly increase over the next decade, a recent study investigating the trend in incidence of dementia in Europe and North America over the last 3 decades has revealed an approximate 13% decrease in dementia incidence per decade (Wolters *et al.*, 2020). The expected increase in dementia cases also has an economic impact, with more carers needed and an increase in demand for

medication requirement for symptomatic relief (Prince, Guerchet and Prina, 2015). In 2015 alone, an approximate £670 billion was spent on dementia worldwide (Prince, Wimo, Guerchet, 2015). In recent years, there has been increased focus in promoting AD awareness, to enhance the public's understanding of the disease, with the aim to help individuals, their families and carers in managing and living with dementia (Prince and Jackson, 2009).

1.1.2. Alzheimer's disease epidemiology

AD was first characterized in a female patient (Auguste D.) who presented signs of cognitive impairment and BPSD by a German physician Alois Alzheimer's in 1901 (Hippius and Neundörfer, 2003; Finder and Glockshuber, 2007; Qiu, Kivipelto and Strauss, 2009). Following the death of the patient in 1906, post-mortem histological and morphological observations revealed the two main AD hallmarks now known as amyloid plaques and neurofibrillary tangles (Hippius and Neundörfer, 2003).

AD is split into two forms dependent on the age that symptoms start developing. Early-onset AD or Familial AD, which accounts for 10% of cases, has been linked to mutations in presenilin 1 and 2 genes (*PSEN 1* & *2*). The majority of these mutations are autosomal missense, found on chromosome 14 and 1 respectively, which encode the PSEN1 and PSEN2 catalytic domains of γ-secretase, an enzyme which leads to amyloid-β (Aβ) peptide production (Levy-Lahad *et al.*, 1995; Rogaev *et al.*, 1995; Qiu, Kivipelto and Strauss, 2009; Sadigh-Eteghad *et al.*, 2015; DeTure and Dickson, 2019). Post-mortem and isolated-Aβ from serum CSF have revealed that Aβ can be present in various lengths in the brain, with $A\beta_{1\text{-}42}$ considered the most toxic form, as it's the most prone to aggregation (Pachahara *et al.*, 2012; Podlisny *et al.*, 1995; Finder and Glockshuber, 2007; Nichols *et al.*, 2015). More than 150 mutations have been identified in *PSEN1* which lead to partial loss of function and a subsequent gain in toxic activity resulting in an increase in both Aβ production and changes in the $A\beta_{1\text{-}40}/A\beta_{1\text{-}42}$ ratio (De Strooper, 2007; Heilig *et al.*, 2010, 2013; Sun *et al.*, 2016). In contrast fewer mutations have been identified in *PSEN2* (Cai, An and Kim, 2015). Although the role of *PSEN1* and *PSEN2* mutations in AD are not fully understood, toxic function might involve changes in $A\beta_{1\text{-}42}$ production or by making the brain more susceptible to AD-mediated cytotoxicity, for example through impairment in Notch signalling responsible for synaptic plasticity (Citron *et al.*, 1997; Marjaux, Hartmann and De Strooper, 2004; Wang *et al.*, 2004; De Strooper, 2007; Heilig *et al.*, 2013). Other mutations which have also been linked to Familial AD, include missense mutations and duplications found on the amyloid-precursor protein (*APP*) gene which encodes the APP peptide that can be cleaved into Aβ (Carter, Desmarais and Bellis, 1992; Rovelet-Lecrux *et al.*, 2006; Qiu, Kivipelto and Strauss, 2009; DeTure and Dickson, 2019). Evidence of the role of APP in

AD originally came from individuals with Trisomy 21 (Down Syndrome) that exhibit amyloid pathology, as the *APP* gene is found within chromosome 21 (DeTure and Dickson, 2019).

Late-onset AD, also known as Sporadic AD, accounts for the majority of AD cases with no direct known genetic causes linked to its development (Prince and Jackson, 2009; Qiu, Kivipelto and Strauss, 2009; DeTure and Dickson, 2019). Ageing (>65 years) constitutes the main risk factor for developing late-onset AD. Epidemiological studies revealed that individuals over 65 years of age have a 10% chance of developing dementia, with risk doubling every ~5 years (Prince and Jackson, 2009; Qiu, Kivipelto and Strauss, 2009; DeTure and Dickson, 2019). The ageing population is expected to increase to 1 billion by 2030, this will inevitably lead to an increase in dementia cases as well (Qiu, Kivipelto and Strauss, 2009). The Framingham Heart study, a cohort study conducted over 30 years, revealed that although ageing is the main AD risk factor, incidence in individuals educated at higher degree level, and with lower vascular disease risk due to early prognosis and diagnosis, report a decline in AD cases over time (Satizabal *et al.*, 2016). Moreover, a recent Lancet report has also linked traumatic brain injury (TBI), smoking, high alcohol consumption, obesity, lack of physical activity, depression and low social contact as additional risk factors accounting for some dementia cases (Livingston *et al.*, 2020). As all these risk factors are considered modifiable, it is believed that the incident of dementia can also be changed if measures are taken against these risk factors.

Several molecules have been found to have a role in Aβ clearance from the brain. Although no genetic causes have been linked to Sporadic AD, the presence of the APOE4 (APOE; apolipoprotein E) allele has shown to increase risk of developing late-onset AD (Qiu, Kivipelto and Strauss, 2009; DeTure and Dickson, 2019). APOE, an apolipoprotein produced by both neurons and glial cells responsible for cholesterol and lipid transport to neurons, has been linked to Aβ processing and specifically, clearance from the brain (Buttini *et al.*, 2010; Liu *et al.*, 2017). In transgenic animal models that overexpress APP (V717F mutation) and that lack the rodent APOE which shares 70% homology with human APOE, show no significant brain Aβ deposition in contrast to animals expressing rodent APOE (Bales *et al.*, 1999). This suggests that APOE can interfere with Aβ

clearance, therefore aiding its accumulation in the brain. APOE has also been shown to have a role in peptide aggregation (Wisniewski *et al.*, 1994; Mouchard *et al.*, 2019). For example Wisniewski and colleagues revealed that *in vitro* APOE, and especially APOE4, accelerates Aβ aggregation into fibrils by direct interaction with the peptide (Wisniewski *et al.*, 1994). In support of this, a study conducted on post-mortem tissue revealed the presence of cleaved-APOE/Aβ small heteroligomer 'complexes' in AD individuals, preventing peptide clearance from the brain (Mouchard *et al.*, 2019). A meta-analysis study revealed that the presence of APOE ε4 allele in Caucasian individuals increases the risk of developing AD by ~3 (one copy) and ~15 (both copies of the alleles are present), compared to the presence of the ε3, and the ε2 isoform which is believed to be protective (Farrer *et al.*, 1997; Liu *et al.*, 2013). The presence of APOE4 allele has also been linked to individuals with Familial AD (Qiu, Kivipelto and Strauss, 2009). In support of this, Bales *et al.* revealed that an increase in Aβ accumulation in the brain was seen at a higher degree when both rodent APOE alleles where present, and this was also shown to be age-dependent (Bales *et al.*, 1999). In contrast to APOE, LRP1 (low density lipoprotein receptor-related protein 1) dependent Aβ clearance through the BBB (blood-brain barrier) via transcytosis occurs in a faster manner (Li *et al.*, 2001; Deane *et al.*, 2008). Deane *et al.* (2008) revealed that APOE4 can interfere with this pathway, by creating a complex with Aβ, and therefore preventing LRP1 from binding. APOE4 dependent Aβ clearance from the brain occurs through a VLDL (very-low density lipoprotein) receptor-dependent mechanism which is slower than the one observed by LRP1, leading to significant Aβ accumulation in the brain (Deane *et al.*, 2008).

Diet has also been identified as a factor that can influence the risk of AD (Scarmeas *et al.*, 2006; Qiu, Kivipelto and Strauss, 2009). For example, some evidence suggests that both food rich in Vitamin E and Vitamin E diet supplementation may reduce progression of AD pathology (Zandi *et al.*, 2004). Additionally, studies have also linked cardiovascular disease (CVD) with dementia, with some studies even referring to AD as a vascular disorder (De La Torre, 2012; Ng, Turek and Hakim, 2013). For example, individuals with hypertension, and hypercholesteremia are at a higher risk of developing AD (Livingston *et al.*, 2020). Impaired blood flow due to CVDs can aid both Aβ and hyperphosphorylated tau protein accumulation in the brain which can lead to the

creation of neurofibrillary tangles (De La Torre, 2012; Ng, Turek and Hakim, 2013). Although CVD increases the risk of developing dementia, pre-clinical studies and clinical trials reveal that use of statins to lower cholesterol levels did not provide conclusive results in reducing cognitive decline linked to dementia (Hajjar *et al.*, 2002; Li *et al.*, 2010; Sano *et al.*, 2011). In contrast, a cohort conducted in 2015 revealed that individuals carrying the APOE4 alleles taking antihypertensive compounds, specifically calcium channel blockers (CCBs), showed reduction in cognitive decline as assessed via a cognitive test (Lovell *et al.*, 2015). Individuals with diabetes, which is also a CVD risk factor, have also shown an increased risk of AD (Qiu, Kivipelto and Strauss, 2009). A population study which followed individuals from around ~50 years of age for an average of 30 years, revealed that individuals with a reduced insulin response have a significantly increased risk of dementia (Rönnemaa *et al.*, 2008). In support, biochemical evidence using insulin degrading enzyme (IDE) knockout mice revealed that IDE not only regulates insulin levels, but can also control Aβ degradation, with a reduction in IDE linked to a reduction in Aβ degradation (Farris *et al.*, 2003). Another study revealed that the density of amyloid plaques, a hallmark of AD, in individuals living with both AD and diabetes was higher than those suffering with AD alone; this links insulin pathology with AD incidence and progression (Janson *et al.*, 2004). In addition to CVD, diabetes and inflammation, lifestyle factors such as low physical activity, increased alcohol consumption, and socioeconomical status, such as low educational level have also been identified as AD risk factors (Qiu, Kivipelto and Strauss, 2009; Etnier *et al.*, 2018; Livingston *et al.*, 2020). Etnier *et al.* proposed that physical activity improved cognitive performance in individuals carrying the APOE4 allele (Etnier *et al.*, 2018).

1.1.3. Alzheimer's pathology

Individuals with mild-cognitive impairment (MCI), which display a noticeable reduction in cognitive function which would not be expected with normal ageing process, are believed to be at higher risk of developing dementia (Petersen *et al.*, 2001). A 2-year longitudinal study, revealed that in a group of 269 individuals diagnosed with mild cognitive impairment that exhibit memory deficits (amnesic MCI), around 20% develop AD per year (Perri *et al.*, 2007). AD is known to affect both grey and white brain matter (Serra *et al.*, 2010). Hippocampal grey matter atrophy is detected in both MCI and AD individuals (Serra *et al.*, 2010). Post-mortem brain tissue and MRI (magnetic resonance imaging) scans from individuals diagnosed with AD has revealed a significant degree of brain atrophy in cortical regions such as within the frontal and temporal lobes, whereas the primary motor and somatosensory regions remain largely unaltered (Bozzali *et al.*, 2002; Serra *et al.*, 2010; DeTure and Dickson, 2019). In contrast, in MCI individuals, brain atrophy is observed at lower degree, with significant white matter atrophy mainly seen in the temporal lobe (Serra *et al.*, 2010). Cognitive impairment observed at early stages of AD is believed to occur due to early stages of synaptic dysfunction, and neuronal loss seen within the temporal regions of the brain (Braak and Braak, 1997; DeTure and Dickson, 2019). For example, evidence obtained from human post-mortem studies, and work carried out on APP transgenic mice, reveals that early-stage synaptic dysfunction could occur due to presence of Aβ oligomers that can change the expression of synaptic proteins such as vesicle-associated membrane protein-2 (VAMP-2), a SNARE protein linked to neurotransmitter vesicle trafficking (Pham *et al.*, 2010). Immunohistochemistry analysis has proposed that the two main hallmarks of AD, also used for post-mortem AD diagnosis, are extracellular amyloid plaques containing Aβ and intracellular neurofibrillary tangles consisting of hyperphosphorylated tau protein. In response to inflammation, microglia can change morphology, becoming activated to phagocytose any 'pathogens' (Newcombe *et al.*, 2018). As inflammation can be noted in AD, activated microglia have also been found around both amyloid plaques and neurofibrillary tangles (Stalder *et al.*, 1999; Hopperton *et al.*, 2018; DeTure and Dickson, 2019). Similarly to this, in response to accumulation of Aβ in the brain and subsequent neuronal damage, 'reactive' astrocytes due to their role in providing

neuronal support, are also found surrounding amyloid plaques (DeTure and Dickson, 2019; Katsouri *et al.*, 2020). The main AD hallmarks, the accompanied oxidative stress, activation of microglia and presence of reactive astrocytes can eventually induce synaptic decline and neuronal loss, which causes the brain atrophy and cognitive impairment seen in AD (Podlisny *et al.*, 1995, 1998; Shao *et al.*, 1999; Urbanc *et al.*, 2002; Barghorn *et al.*, 2005; Finder and Glockshuber, 2007; Ryan *et al.*, 2010; Nimmrich and Eckert, 2013; Nichols *et al.*, 2015; DeTure and Dickson, 2019).

Amyloid plaques are split into two main types known as dense core plaques or diffuse plaques, the latter of which are not usually accompanied by reactive astrocytes and activated microglia (Pike, Cummings and Cotman, 1995; DeTure and Dickson, 2019). Dense core plaques, rich in fibrillar Aβ, have been linked to neuronal cytotoxicity (Urbanc *et al.*, 2002). Staining such as Thioflavin (ThT) can allow both the *in vitro* and *in vivo* visualisation of amyloid plaques within brain tissue, and the monitoring of Aβ aggregation kinetics within the laboratory environment (Walsh *et al.*, 1999; Urbanc *et al.*, 2002; Younan and Viles, 2015; Xue *et al.*, 2017; DeTure and Dickson, 2019). Dense core plaques, also known as neuritic or senile plaques, contain an Aβ core, surrounded by degenerated neurites and microglia activated in response to neuroinflammation, aiding the theory that Aβ drives AD progression through neurodegeneration (Pike, Cummings and Cotman, 1995; Urbanc *et al.*, 2002; DeTure and Dickson, 2019). In some neuritic plaques, the presence of tau has also been noted (Guo, Noble and Hanger, 2017; DeTure and Dickson, 2019). In AD tau undergoes hyperphosphorylation and consequently impaired folding, therefore (as an essential cytoskeleton protein) is unable to support microtubules within axons (Guo, Noble and Hanger, 2017). Evidence suggests that presence of neurofibrillary tangles correlates to AD severity (Nelson *et al.*, 2012). Findings reveals the presence of activated microglia and amyloid plaques in non-cognitive impaired individuals, whereas reactive astrocytes and tau pathology was only detected in individuals with confirmed AD, suggesting that tau pathology correlates better with AD progression, whereas changes in microglia may occur at early stages of the disease (Vehmas *et al.*, 2003).

To evaluate and identify AD status and progression, studies have proposed use of staging schemes. For example, Braak and Braak in the late-1990s suggested a staging

scheme to investigate AD spread in the brain, and therefore identify disease progression. Stage 1 (I) of AD consists of MCI seen due to Aβ deposition and hyperphosphorylated tau seen within the basal frontal and temporal entorhinal regions of the brain, the second stage (II) involves spreading to limbic regions such as the hippocampus, stage 3 (III) involves significant neuronal loss of the cortex, whereas lastly, stage 4 (IV) involves full disease spread, with AD pathology also seen in sensory, visual and motor regions of the brain (Braak and Braak, 1997; Suva *et al.*, 1999; Guo, Noble and Hanger, 2017; Xu *et al.*, 2019). In contrast, some studies suggest that changes in the primary sensory and visual regions of the brain can be seen earlier in AD-related mild cognitive decline and therefore could be considered for early diagnosis of AD (Stephen *et al.*, 2010; Risacher *et al.*, 2020).

1.1.4. Aβ production

A number of physiological roles have been identified for APP including a role in cell proliferation, and more specialised roles such as in neuronal synapse development and a role in early-stages of memory formation (Moya *et al.*, 1994; Luo *et al.*, 1996; Mileusnic *et al.*, 2000; Cárdenas-Aguayo *et al.*, 2014). The transmembrane protein APP can be cleaved differentially via two pathways known as the non-amyloidogenic and amyloidogenic pathway (Finder and Glockshuber, 2007; Cárdenas-Aguayo *et al.*, 2014). Through the non-amyloidogenic pathway APP is cleaved via α-secretase to produce s-APPα that has shown to have a role in neuronal development and to produce neuroprotective effects against excitotoxicity (Mattson *et al.*, 1993; Mattson, 1997; Gakhar-Koppole *et al.*, 2008; Chow *et al.*, 2010). Following this, the cleavage via γ-secretase leads to the production of the amino-terminal APP intracellular domain (AICD) and p3 (Cárdenas-Aguayo *et al.*, 2014). Whereas the amyloidogenic pathway leads to the production of Aβ of mainly 40 or 42 amino acids long. The amyloidogenic pathway cleaves APP via β-secretase giving rise to s-APPβ and CT99 or CT89, followed by γ-secretase, leading to the production of Aβ and AICD (**Fig. 1.1.4.1**) (Podlisny *et al.*, 1995, 1998; Shao *et al.*, 1999; Finder and Glockshuber, 2007; Ryan *et al.*, 2010; Cárdenas-Aguayo *et al.*, 2014; Nichols *et al.*, 2015). The biology of the AICD fragment is not fully understood, however it is believed that further cleavage of AICD via caspases, can lead to the production of fragments which can induce cytotoxicity via DNA fragmentation (Bertrand *et al.*, 2001; Lu *et al.*, 2003). In contrast to s-APPα, s-APPβ role is not fully understood, although a role in axon pruning and neuronal death during development has been proposed (Nikolaev *et al.*, 2009). Analysis of plasma and CSF (cerebrospinal fluid) from individuals with MCI or AD have proven that Aβ is not only produced during pathological conditions, but it is also present in healthy aged individuals, with a significant increase in Aβ, especially $A\beta_{1\text{-}42}$, seen in CSF of both MCI and AD individuals compared to control individuals (Giedraitis *et al.*, 2007). Dependent on the concentration, aggregation status and species, studies have shown that Aβ can exhibit either neurotrophic or neurotoxic effects such as those seen in AD. Similarly to APP, neurotrophic effects of Aβ (pM or low nM concentrations) include a role in cell proliferation, differentiation and memory formation (Luo *et al.*, 1996; Plant *et al.*, 2003;

Chen and Dong, 2009; Garcia-Osta and Alberini, 2009; Fonseca *et al.*, 2013; Bernabeu-Zornoza *et al.*, 2019). For example, non-aggregated $A\beta_{1\text{-}40}$ (1.5 μM; 24-48hr) was shown to induce cell proliferation and induce murine neural progenitor cell (NPG) and neural stem cell (NSC) differentiation into neurons (Chen and Dong, 2009; Fonseca *et al.*, 2013). Whereas, treatment of either human or rodent NSCs with the non-aggregated $A\beta_{1\text{-}42}$ at low μM concentrations increased cell proliferation and caused NSCs to favour differentiation into glial cells (Fonseca *et al.*, 2013; Bernabeu-Zornoza *et al.*, 2019). Due to the neurotrophic role of $A\beta_{1\text{-}40}$, it is believed that changes in the ratio of $A\beta_{1\text{-}40}/A\beta_{1\text{-}42}$, with a noted increase in $A\beta_{1\text{-}42}$ production, may be partly responsible for neuronal loss seen in AD. Evidence indicates that Aβ production can be induced during hypoxic and oxidative stress conditions, with unaggregated Aβ shown to act as an antioxidant (Zou *et al.*, 2002; Pearson and Peers, 2006; Cárdenas-Aguayo *et al.*, 2014). In contrast, abnormal APP processing in AD involving changes in the ratio of $A\beta_{1\text{-}40}/_{1\text{-}42}$ produced, increased production, and impairment in degradation and clearance of the peptide from the brain can aid its accumulation (Hardy and Selkoe, 2002; Dubnovitsky *et al.*, 2013). Abnormally high levels of Aβ in the brain have been linked to numerous neurotoxic mechanisms seen in AD (Ueda *et al.*, 1997; Barghorn *et al.*, 2005; Puzzo *et al.*, 2005; Hermann *et al.*, 2013; Carrillo-Mora, Luna and Colín-Barenque, 2014). For example, downregulation of brain derived neurotrophic factor (BDNF) expression through changes in the phosphorylation of the transcription factor CREB (cAMP response element-binding protein), have been linked to cognitive decline via changes in neurotransmission, synaptic density and neuronal viability (Garzon and Fahnestock, 2007; Fahnestock, 2011).

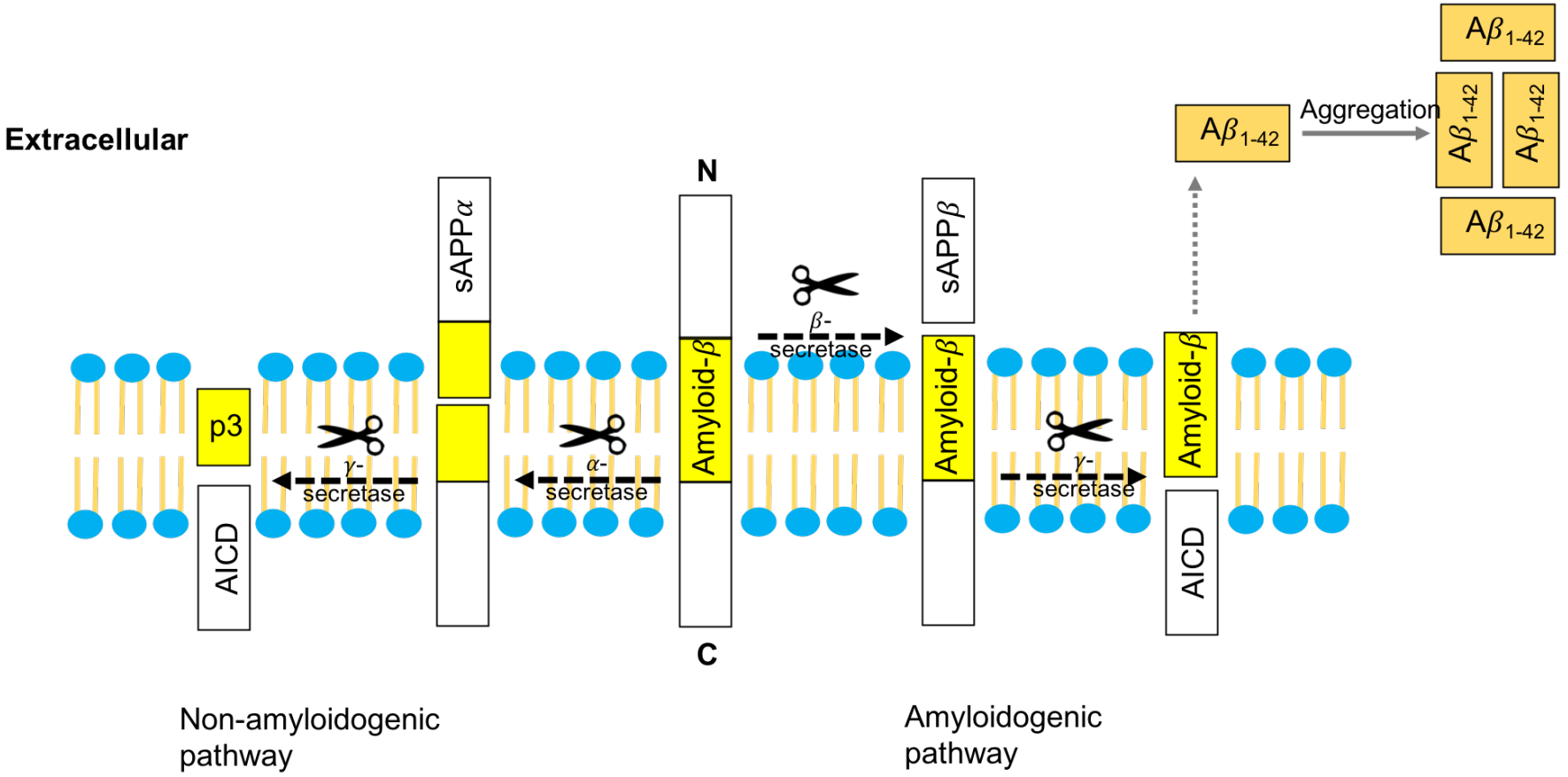

Figure 1.1.4.1: Schematic diagram of APP processing. *APP can be cleaved via two different pathways. The non-amyloidogenic pathway involves α and γ-secretase cleaving APP into sAPPα, AICD and p3. Whereas the amyloidogenic pathway involves APP cleavage via β and γ-secretase leading to the production of sAPPβ, AICD and Aβ. Mutations in the APP, PSEN1 and PSEN2 (catalytic domains of γ-secretase) have been linked to impaired APP processing into Aβ, aiding its accumulation in the brain.*

1.1.5. Amyloid-β cascade hypothesis

The 'amyloid-β cascade hypothesis' proposes that AD pathology largely results due to increased deposition of Aβ in the brain, aiding its aggregation into what is believed to be its cytotoxic form (Hardy and Selkoe, 2002). As a consequence, this initiates a number of neurotoxic mechanisms such as synaptotoxicity, excitotoxicity, mitochondrial dysfunction and oxidative stress that can all ultimately lead to neuronal loss (Hardy and Selkoe, 2002; Barghorn *et al.*, 2005; Nimmrich and Eckert, 2013; Carrillo-Mora, Luna and Colín-Barenque, 2014). Evidence from both *in vitro* and *in vivo* using transgenic animal models, where APP is overexpressed or where the amyloidogenic pathway is promoted, provide support for the amyloid-β hypothesis (Finder and Glockshuber, 2007). Although evidence clearly demonstrates that Aβ has a major role in AD pathology, some studies have shown that tau pathology (and subsequent neuronal loss) is more evident at early Braak I/II stages in the frontal, temporal endorhinal regions of the brain, and the hippocampus compared to presence of Aβ plaques (Arriagada *et al.*, 1992; Gómez-Isla *et al.*, 1996). Even though evidence indicates that tau pathology can precede Aβ plaque formation, and therefore may better correlate to disease progression and severity, some studies have suggested that tau deposition is still dependent on Aβ accumulation and aggregation and that Braak stages I/II may correspond to pre-clinical AD (AD dependent MCI) rather than fully-developed AD; such studies support a critical role for Aβ in AD (Petersen *et al.*, 2006; Bolmont *et al.*, 2007; Fein *et al.*, 2008; Wu *et al.*, 2018). Even though it is widely accepted that Aβ has a significant role in AD pathology, there is also some debate as to whether the toxic effects seen in preclinical animal model studies are a true representation of human pathology. For example, animal models such as the previously mentioned transgenic animal model with the London *APP* mutation induced to overexpress APP, are being genetically manipulated to exhibit AD characteristics (Bales *et al.*, 1999; Daschil *et al.*, 2013). As a number of animal models used for studying AD require genetic manipulation, opposing views exist as to whether different mechanisms underlie disease pathology in animals compared to humans. Another reason which has caused doubt in the Aβ hypothesis, is that some animal models are able to display synaptic loss and cognitive impairment prior to amyloid plaque formation (DaRocha-Souto *et al.*,

2011). In contrast to the belief that amyloid plaques correlate with disease progression, Boncristiano and colleagues in 2005 revealed that in a transgenic animal expressing the *APP* gene with Swedish mutation, which is known to favour amyloidogenic processing of APP, although Aβ plaque formation was evident, no significant degree of synaptic loss was observed (Boncristiano *et al.*, 2005; Shin *et al.*, 2010). Human iPSC (induced pluripotent stem cell) derived neurons are now widely used as a human *in vitro* model to research AD pathology (Arber, Lovejoy and Wray, 2017). Additionally, work conducted in humans on post-mortem tissue revealed that in individuals with MCI, synaptic dysfunction was evident without the presence of amyloid plaques, therefore raising the question whether amyloid plaque formation is indeed a key event correlating to synaptic loss and therefore disease severity (Counts *et al.*, 2014). One possible explanation for the poor correlation of amyloid plaques with cognitive impairment, could be that smaller Aβ aggregates such as oligomeric and protofibrillar Aβ and not mature fibrils (seen in amyloid plaques) are responsible for cytotoxicity (Hardy and Selkoe, 2002; Ryan *et al.*, 2010, 2013; Morris, Clark and Vissel, 2014; Müller-Schiffmann *et al.*, 2016). Due to this, a number of studies are now focusing in investigating the effects of smaller Aβ aggregates, such as Aβ oligomers and protofibrils, due to the lack or reduced degree of toxicity observed with larger aggregates (Barghorn *et al.*, 2005; Nichols *et al.*, 2015).

1.1.6. Aβ assemblies

Studies conducted on post-mortem tissue and isolated-Aβ from serum and CSF have helped in identifying the various lengths of Aβ sequence found within the brain (Podlisny *et al.*, 1995; Finder and Glockshuber, 2007; Nichols *et al.*, 2015). Analysis revealed that Aβ can be present in various lengths ranging from 40 to 43 amino acid long (Pachahara *et al.*, 2012). Although 90% of Aβ found in the human brain consists of the 1-40 sequence, as the 1-42 sequence is more prone to aggregation, a lot of the research on AD pathology has focused on $A\beta_{1-42}$ (Shao *et al.*, 1999; Barghorn *et al.*, 2005; Pachahara *et al.*, 2012; Cárdenas-Aguayo *et al.*, 2014).

It is well documented that Aβ can exist as a number of different assemblies, dependent on its aggregation status (Pachahara *et al.*, 2012; Nicoll *et al.*, 2013). Aβ can exist in its monomeric form, where following changes to its secondary structure, it can then change from α-helices or random coils into β-sheets which are more prone to aggregation (Shao *et al.*, 1999; DeTure and Dickson, 2019). Following changes to its secondary structure, monomeric Aβ (4kDa) can then aggregate into dimers or small soluble and larger oligomers known as the nucleated polymerisation process. Following this, the elongation process starts, which involves Aβ oligomers further rearranging into elongated structures known as protofibrils and eventually mature fibrils displaying crosslinking of β-sheets, which is primarily what is found within amyloid plaques (**Fig. 1.1.6.1**) (Sandberg *et al.*, 2010; DeTure and Dickson, 2019). Various oligomeric species of Aβ exist, ranging from dimers to higher oligomeric assemblies (up to ~3000 kDa) displaying differential degrees of cytotoxicity (Nicoll *et al.*, 2013; Nichols *et al.*, 2015). Dahlgren and colleagues revealed that reduction in neuronal viability was significantly higher when small soluble oligomers (10nM to 1μM) were added compared to treating neuroblastoma cells with larger aggregates (>50kDa) such as Aβ fibrils (Dahlgren *et al.*, 2002). Similarly, research has shown that it is not amyloid fibrils seen in amyloid plaques, but Aβ in its oligomeric state that can induce synaptic dysfunction through changes in neurotransmission and eventually neuronal loss (Nimmrich *et al.*, 2008; Hermann *et al.*, 2013).

A large number of research studies are now using synthetic Aβ which can undergo aggregation in a similar manner to Aβ found *in vivo*, with also similar neurotoxic

effects observed (Ryan *et al.*, 2010). However, even though studies agree that aggregated Aβ can cause neurotoxicity, there is still some dispute as to which aggregated assembly of the peptide is the most toxic and whether a single or multiple assemblies are needed to confer the highest degree of cytotoxicity (Nicoll *et al.*, 2013). In addition, evidence proposes that the neurotoxic effects displayed by aggregated Aβ are not only species dependent, but also concentration-dependent and that this may also influence aggregation status of the peptide (Verma, Vats and Taneja, 2015). For example, Deshpande *et al.* revealed that small oligomers of 15 to 20 monomers in size, can cause mitochondrial dysfunction and therefore initiate cytotoxic pathways at 10nM, although neuronal loss is only seen at higher concentrations (Deshpande *et al.*, 2006). Contradictory to oligomers and Aβ-derived diffusible ligands (ADDLs), a type of small oligomers, Aβ protofibrils require higher concentrations and longer incubation duration to achieve the same degree of cortical neurotoxicity (Deshpande *et al.*, 2006).

Although there is disagreement regarding the degree in which Aβ correlates to disease progression, there is strong evidence that aggregated Aβ indeed has an important role in AD pathology. Therefore more work is needed in order to aid our understanding of Aβ pathology and focusing on Aβ downstream targets may also provide a better understanding of disease progression (Nimmrich *et al.*, 2008; Carrillo-Mora *et al.*, 2014).

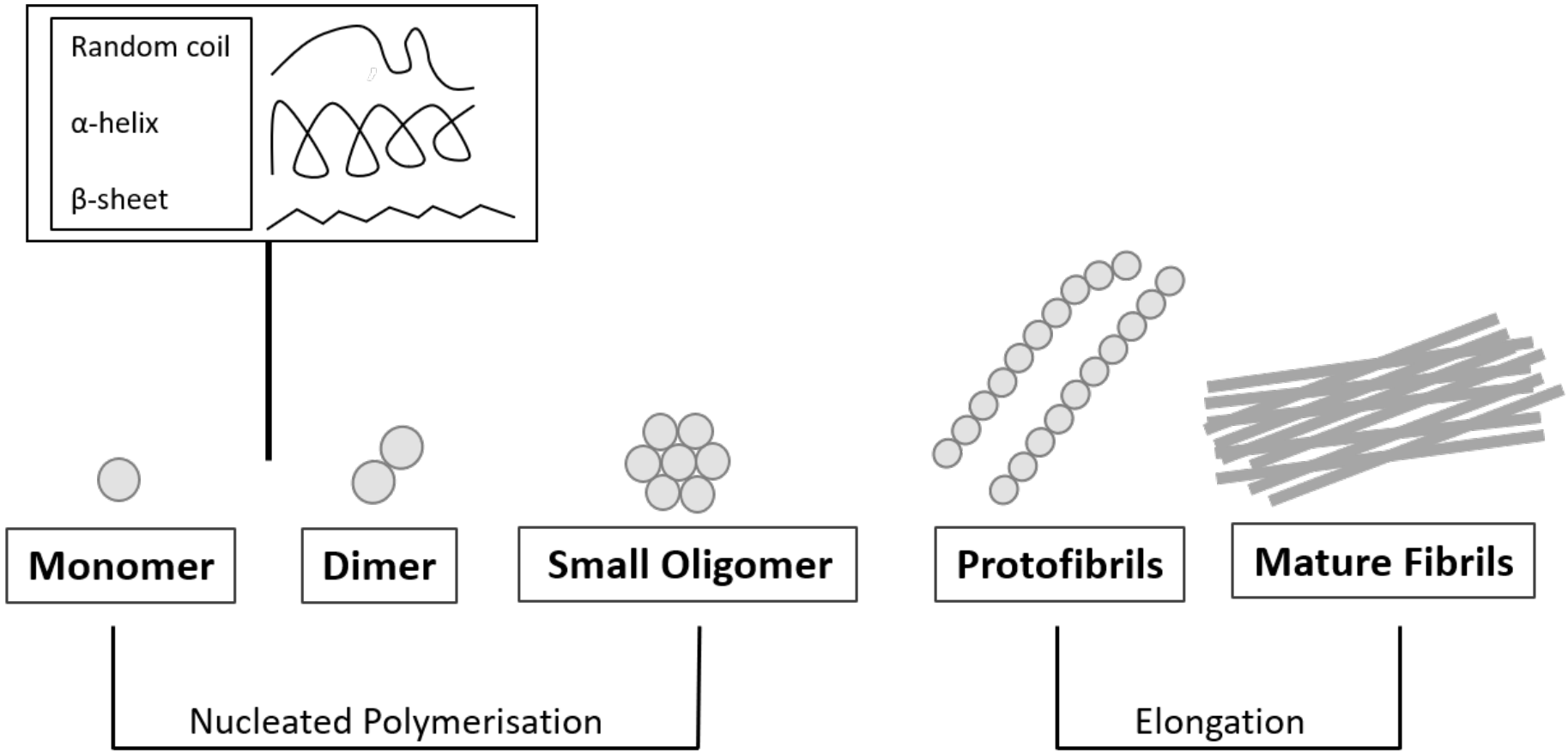

Figure 1.1.6.1: Schematic diagram Aβ aggregation stages. *Monomeric Aβ can undergo changes of its secondary structure into β-sheets which are more prone to aggregation. Aβ can then rearrange into dimers and small oligomers known as the nucleated polymerisation stage of the process. From small oligomers it can then rearrange into elongated structures known as protofibrils or mature fibrils which involves crosslinking of protofibrils into sheets, known as the elongation stage of the aggregation process.*

1.1.7. Alzheimer's diagnosis and therapies

Currently AD diagnosis aims to identify individuals at high risk of developing dementia and to diagnose individuals at early stages. Diagnosis involves neuropsychological tests, such as the mini-mental state examination (MMSE) that aim to assess cognition through testing language fluency, orientation, reasoning and language construction, and patient and carers interviews, and imaging techniques such as MRI and PET (positron emission tomography) scans to quantify brain atrophy (Jack *et al.*, 1999; Ward *et al.*, 2000; Scarmeas *et al.*, 2006; Cerejeira, Lagarto and Mukaetova-Ladinska, 2012; Creavin *et al.*, 2016; Weller and Budson, 2018). Although neuropsychological tests have been routinely used in dementia diagnosis, they can be time-consuming and may not always be able to give a clear indication of an individual's cognitive abilities or distinguish between dementia types. For example, an individual with lower education level but who is healthy, may score lower during a neuropsychological test. An epidemiology study conducted in the early 1990s which followed individuals over 5 to 10 years, revealed that neuropsychological tests were able to accurately predict individuals at risk of developing AD (Tierney *et al.*, 2005). Similarly, a recent systematic review and meta-analysis revealed that neuropsychological tests, especially tests that assess verbal episodic memory and language, are good predictors of individuals at early-stages of dementia (Belleville *et al.*, 2017). The use of radiolabelled amyloid biomarkers (e.g. Pittsburgh compound B;PiB) in combination with imaging techniques such as PET scans are now also used to identify AD severity by checking for amyloid plaque presence in the brain (Ikonomovic *et al.*, 2008; Weller and Budson, 2018; Suppiah, Didier and Vinjamuri, 2019). Although PET scanning has a high degree of accuracy, this process is very costly and therefore not readily available (Clark *et al.*, 2012; Yeo *et al.*, 2015). Moreover, although PET scans using amyloid biomarkers can identify amyloid plaque burden in the brain, this may also lead to mis-diagnosis as other dementia types such as Lewy body dementia may also consist of amyloid plaques in the brain (Kantarci *et al.*, 2012). CSF evaluation measuring the amount of Aβ and both total and hyperphosphorylated tau present within the CSF, and serum tests are now also in development for AD diagnosis, with similar degree of accuracy as PET scans (Palmqvist *et al.*, 2015; Weller and Budson, 2018).

AD pathology has been linked to synaptic loss of cholinergic neurons in regions such as the basal forebrain and hippocampus (Whitehouse *et al.*, 1982; Haam and Yakel, 2017). Neurotransmission in cholinergic neurons occurs via the neurotransmitter acetylcholine which has been implicated in learning and memory (Haam and Yakel, 2017). Studies have shown that both synaptic dysfunction and also reduced acetyltransferase production or changes in the activity of acetylcholinesterase can lead to acetylcholine depletion therefore aiding AD progression (Wilcock *et al.*, 1982; Strada *et al.*, 1992; Wong *et al.*, 1999; Bell *et al.*, 2006). At the present time, therapeutics available for AD treatment, approved for early and mid-moderate stages of AD, are acetylcholinesterase (AChE) inhibitors (e.g. donepezil) which aim to prolong the levels of acetylcholine in the brain (Cacabelos, 2007; Parsons, Stöffler and Danysz, 2007; Birks and Harvey, 2018; Weller and Budson, 2018). Drugs approved for later stages of AD, for targeting mechanisms such as excitotoxicity, are NMDA (N-methyl-D-aspartate) receptor antagonists (e.g. memantine) due to overactive NMDA receptors (Cacabelos, 2007; Parsons, Stöffler and Danysz, 2007; Birks and Harvey, 2018; Weller and Budson, 2018). Although these compounds have been approved for AD treatment for several years and have shown promise in providing symptomatic relief, they have only shown limited effectiveness, and have also been linked to a number of side effects (Ali *et al.*, 2015). Due to this, there is considerable interest in developing other agents that not only delay progression, but may also target specific AD-related cytotoxic mechanisms, with minimal side effects, therefore halting disease progression (Weller and Budson, 2018).

At the moment, drugs which are either in development or tested in clinical trials includes drugs against amyloid, tau, neuroinflammation and also cognitive enhancers (Huang, Chao and Hu, 2020). Drugs that target amyloid aim to either decrease its production or aid amyloid clearance from the brain (Swerdlow, 2007; Doody *et al.*, 2013; Huang, Chao and Hu, 2020). Pre-clinical studies have shown that enzymes that can degrade Aβ such as neprilysin, whose expression and activity is downregulated in AD, have the potential of becoming novel therapeutics for AD (El-Amouri *et al.*, 2008). Compounds that target secretases are also currently under investigation with β-secretase as the main target candidate (May *et al.*, 2011). Although secretases have been considered as a target candidate to treat AD, clinical trials such as that with

verubecestat revealed that β-secretase inhibitors proved ineffective in non-Familial AD (which accounts for the majority of AD cases) (Egan *et al.*, 2018; Volloch and Rits, 2018). This suggests that production of Aβ is induced by differential pathways in early-onset versus late-onset AD, and therefore therapeutics that target the production of Aβ would not be an effective treatment for both AD types. One of the main reasons for failed or interrupted clinical trials such as the ones that target secretases, is the development of unexpected adverse effects (Doody *et al.*, 2013; Salloway *et al.*, 2014; May *et al.*, 2015). For example, targeting γ-secretase brings forward issues such as adverse effects as this secretase also participates in Notch-3 activation, a peptide with critical developmental roles (Swerdlow, 2007). For example, a phase-3 clinical trial using semagacestat (γ-secretase inhibitor) reported gastrointestinal, infection and even skin cancer related adverse effects believed to occur due to changes in Notch-3 signalling (Henley *et al.*, 2014). Therefore, there is considerable interest in developing new therapeutics with increased selectivity and therefore less potential adverse effects. NSAIDs (non-steroidal anti-inflammatory drugs) such as ibuprofen with anti-inflammatory actions are also investigated as potential treatments (Swerdlow, 2007). Although neuroinflammation is a major feature of AD pathology, anti-inflammatories such as NSAIDs in randomized trials have not shown promising results (Pasqualetti *et al.*, 2009; Deardorff and Grossberg, 2017).

In AD, Aβ deposition has also been noted within blood vessels of the CNS (DeTure and Dickson, 2019). Due to this, a number of pre-clinical and clinical studies are investigating the use of antibodies against Aβ. Currently, immunization vaccines against Aβ to induce clearance are been tested, with mixed findings indicating a therapeutic effect (Swerdlow, 2007; Salloway *et al.*, 2014; Huang, Chao and Hu, 2020). Aβ immunization in the PDAPP mouse models (which overexpress human *APP* with a mutation at aa717) led to a significant reduction in cortical amyloid plaque formation and also activation of microglia and reactive astrocytes (Schenk *et al.*, 1999). Contradictory to pre-clinical studies, a double-randomised clinical trial (2001) investigating the effect of Aβ immunization (AN1792) in individuals with AD, although it revealed beneficial effects in reducing hyperphosphorylated tau burden and improving cognitive function, it had to be prematurely stopped due to adverse effects. One of the

serious adverse effects noted in some individuals was the development of encephalitis (Gilman *et al.*, 2005). Post-mortem studies conducted by Masliah and colleagues on an individual who was previously enrolled in the 2001 Aβ immunization clinical trial reported by Gilman *et al.* 2005, but who did not develop encephalitis, revealed a significant reduction in amyloid plaque burden in the frontal and smaller degree of reduction in the temporal regions of the cortex (Masliah *et al.*, 2005). This provides evidence that Aβ immunotherapy may indeed delay AD pathology, although more work is needed in order to develop immunotherapies that do not cause activation of immune response such as those seen in individuals who developed encephalitis. More recently, BIIB037 (drug name: aducanumab), a monoclonal antibody against Aβ has been filed for FDA approval. Although initial results from two late-phase clinical trials revealed mixed findings, re-evaluation of some findings revealed that aducanumab can improve cognitive decline through reduction in amyloid plaque burden (Schneider, 2019). Although these findings suggested it could be an effective therapeutic against AD, it was recently announced it unfortunately was not granted FDA approval. In addition to Aβ immunotherapy, some clinical trials are testing therapies against tau (Congdon and Sigurdsson, 2018; Boxer *et al.*, 2019).

1.2. Voltage-gated calcium channels

1.2.1. Calcium

Calcium (Ca^{2+}) has been linked to a number of physiological processes such as cell viability, differentiation, gene expression, secretion of hormones, muscle contraction, neurotransmitter release and synaptic plasticity within excitable cells (Chin, 1998; Birks and López-Arrieta, 2002; Schneider *et al.*, 2005; Sinnegger-Brauns *et al.*, 2009; Resende *et al.*, 2010; Xu *et al.*, 2011; Daschil *et al.*, 2013; Dolphin, 2013; Brini *et al.*, 2014).

Ca^{2+} influx can be accomplished via at least three types of plasma membrane channels. One type of calcium permeable membrane channels, is the voltage-gated calcium channels (VGCCs) which open in response to changes in the membrane potential (Brini *et al.*, 2014; Zamponi, 2016). Two other types include store-operated calcium channels (SOCs) such as RyRs (ryanodine receptors) present on the ER (endoplasmic reticulum) that allow release of Ca^{2+} from internal stores, and the receptor-operated calcium channels (ROCs) such as ligand-dependent ionotropic receptors (e.g. NMDA receptors) that allow Ca^{2+} influx into the cells from the extracellular space in response to ligand binding (Brini *et al.*, 2014; Zamponi, 2016). For the purpose of this study we will focus on VGCCs.

1.2.2. Voltage-gated calcium channel structure

In the 1980s evidence of the structure of VGCCs had started to emerge. Purification studies and structural analysis of VGCCs revealed three main subunits of ~200 (pore-forming), ~50 and ~30 kDa (accessory subunits) molecular weight, therefore revealing that the VGCCs exist as a complex of various proteins (Curtis and Catterall, 1984; Flockerzi *et al.*, 1986; Takahashi *et al.*, 1987; Witcher *et al.*, 1993; Brini *et al.*, 2014). Further analysis revealed that VGCCs consist of the $\alpha 1$ pore-forming subunit, and the accessory subunits; the intracellular β subunit, the extracellular transmembrane $\alpha 2\delta$ complex connected via disulphide bonds (**Fig. 1.2.2.1**) and sometimes an extracellular γ subunit may also be present (Kamp *et al.*, 2005; Dolphin, 2013; Sousa *et al.*, 2013; Brini *et al.*, 2014; Zamponi, 2016; Qian *et al.*, 2017). The γ subunit has been found to be expressed in skeletal muscle Cav1 channels (Kamp *et al.*, 2005; Striessnig *et al.*, 2014; Zamponi, 2016). The pore-forming subunit, which allows for Ca^{2+} entry, consists of 4 domains (I – IV) each containing 6 transmembrane regions (S1-S6) (Sousa *et al.*, 2013; Zamponi, 2016; Qian *et al.*, 2017). The accessory subunits on the other hand, are responsible for channel trafficking and modulating the gating properties of the channel (Brini *et al.*, 2014; Zamponi, 2016; Lazniewska and Weiss, 2017).

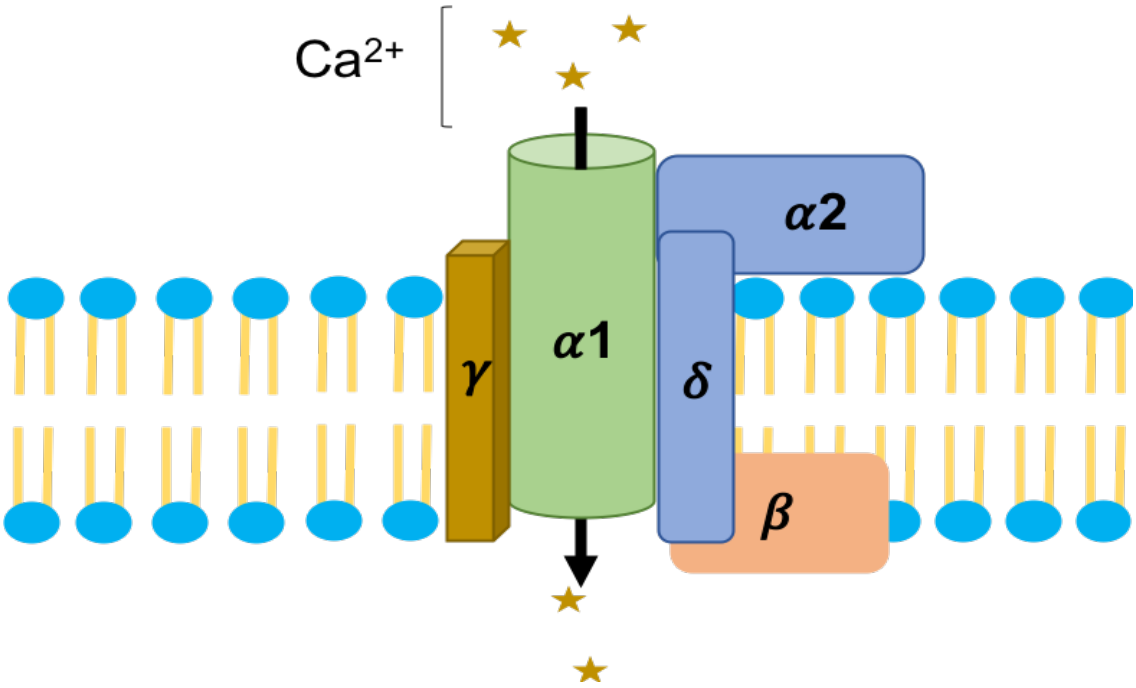

Figure 1.2.2.1: Schematic diagram of voltage-gated calcium channels*. Voltage-gated calcium channels consist of the $\alpha 1$ pore-forming subunit, the intracellular β subunit, the transmembrane $\alpha 2\delta$ complex and also a transmembrane γ subunit may also be present.*

1.2.3. VGCC subtypes and tissue expression

VGCCs can be divided into three main groups based on their α1 pore-forming subunit, and their biophysical and pharmacological properties (Zamponi, 2016). The Cav1 channels, which form L-type currents, consist of Cav1.1, Cav1.2, Cav1.3 and Cav1.4 (Nimmrich and Eckert, 2013; Zamponi, 2016). The Cav2 subfamily consists of the Cav2.1 (P/Q-type current), Cav2.2 (N-type current) and Cav2.3 (R-type current) (Nimmrich and Eckert, 2013; Zamponi, 2016). Lastly, Cav3 channels which form T-type (transient/tiny) currents, consist of Cav3.1, Cav3.2 and Cav3.3 (Barnes and Haynes, 1992; Chin, 1998; Perez-Reyes *et al.*, 1998; Sousa *et al.*, 2013; Zamponi, 2016). VGCCs can also be subdivided into HVA (high-voltage activated) or LVA (low-voltage activated) depending on their activation threshold. Cav1 and Cav2 channels require larger membrane depolarizations to activate, and therefore belong to the HVA group, whereas Cav3 belong to the LVA group with activation seen at lower depolarizations (Nowycky, Fox and Tsien, 1985; Soong *et al.*, 1993; Ertel *et al.*, 2000; Zamponi, 2016). **Figure 1.2.3.1** summarizes the nomenclature of the various members of the VGCCs and the genes that encode the α1 subunit of these channels, based on Ertel *et al.* 2000.

VGCCs have been linked to a number of different roles within the nervous system, often dependent on the subfamily. Cav1.1 channels are primarily expressed within skeletal muscle, whereas Cav1.2 and Cav1.3 are expressed within the cardiac and skeletal muscle, neurons, and also sensory and endocrine cells (Striessnig *et al.*, 2014; Zamponi, 2016). In contrast, Cav1.4 is primarily expressed within immune and retinal cells (Striessnig *et al.*, 2014). Cav1.2 and Cav1.3 expression has also been detected within the central nervous system (CNS), with high variability in biophysical properties of these channels due to subunit splicing and isoform variance as well as association with different β accessory subunits (Striessnig *et al.*, 2014). The majority of Cav1 channels expressed in the brain are Cav1.2, whilst only approximately 10% representing Cav1.3 (Striessnig *et al.*, 2014; Qian *et al.*, 2017). Cav1 channels have been shown to have a role in gene expression and neuronal development, such as during synapse formation and strengthening (Resende *et al.*, 2010; Brini *et al.*, 2014; Striessnig *et al.*, 2014; Zamponi, 2016; Qian *et al.*, 2017). Cav1 channels are known to show sensitivity

to dihydropyridine inhibition, whereas Cav2 and Cav3 are dihydropyridine inhibition insensitive (Nowycky, Fox and Tsien, 1985; Zhang *et al.*, 1993).

All members of the Cav2 subfamily are primarily expressed within neurons and endocrine cells, with several cellular roles (Striessnig *et al.*, 2014). The first evidence of the role of VGCCs in neurotransmission came from studies carried out on squid axons by Katz and Miledi in the 1970s, where it was shown that vesicular fusion and neurotransmitter release was dependent on Ca^{2+} influx through opening of voltage-dependent ion channels (Katz and Miledi, 1970). Cav2.2 was shown to interact directly with the synaptic proteins syntaxin and SNAP25 (synaptosomal-associated protein), proving that Ca^{2+} influx via VGCCs is required for neurotransmitter release (Sheng *et al.*, 1996). A role in neurotransmission has also been observed for Cav2.1, and to a lesser extent Cav2.3, with Cav2.1 also regulating gene expression of proteins such as syntaxin (Kamp *et al.*, 2005; Nimmrich and Eckert, 2013; Brini *et al.*, 2014; Zamponi, 2016). In contrast to Cav1 channels, which can be found predominately in postsynaptic sites, Cav2 channels are predominately found at presynaptic sites (Witcher *et al.*, 1993; Nimmrich and Eckert, 2013; Striessnig *et al.*, 2014; Zamponi, 2016). In addition to neurotransmission, Cav2.3 channels have also been shown to have a role in cell apoptosis (Kamp *et al.*, 2005). Inhibition of Cav2 channels has been achieved using a range of toxins, including conotoxins and agatoxins derived from cone snail and spider venom, respectively, and other divalent cations such as Ni^{2+} and Cd^{2+} a global-VGCC modulator (Witcher *et al.*, 1993; Zhang *et al.*, 1993; Randall and Tsien, 1995; Ertel *et al.*, 2000).

Both Cav3.1 and Cav3.3 are primarily found within CNS neurons (Soong *et al.*, 1993; Perez-Reyes *et al.*, 1998; Striessnig *et al.*, 2014). Cav3.1 is also expressed within cardiac cells. Cav3.2 on the other hand, is predominantly found within kidney and liver cells (Striessnig *et al.*, 2014). Evidence has shown that the expression of Cav3 channels is higher during early stages of neuronal development (Aguado *et al.*, 2016). A role for Cav3 channels within neuronal excitability has also been proposed (Aguado *et al.*, 2016; Zamponi, 2016). Inhibition of Cav3 channels has been observed with Ni^{2+} and pharmacological agents such as mibefradil dihydrochloride (Soong *et al.*, 1993; Perez-Reyes, Lee and Cribbs, 1999).

A number of pathways have been reported to change the expression and activity of VGCCs. For example, post-translational modifications of VGCCs such as phosphorylation, N-glycosylation of asparagine and redox modulation have been reported to change the activity of VGCCs (Takahashi *et al.*, 1987; Scragg *et al.*, 2008; Lazniewska and Weiss, 2017; Qian *et al.*, 2017). Studies starting as early as the 1980s revealed several phosphorylation sites within the $\alpha 1$ subunit (Takahashi *et al.*, 1987). Recent studies, further revealed Ser^{1928} as one of the site by which PKA (protein kinase A) can phosphorylate Cav1.2 channels, an event which can lead to an increase in Ca^{2+} influx (Qian *et al.*, 2017). Numerous sites in both the pore-forming subunit and accessory subunits have been noted as sites of N-glycosylation (Lazniewska and Weiss, 2017). For example N-glycosylation of the $\alpha 2\delta$ accessory subunit is believed to occur as a process for stabilizing the interaction of this complex with the $\alpha 1$ pore-forming subunit of the channel (Lazniewska and Weiss, 2017).

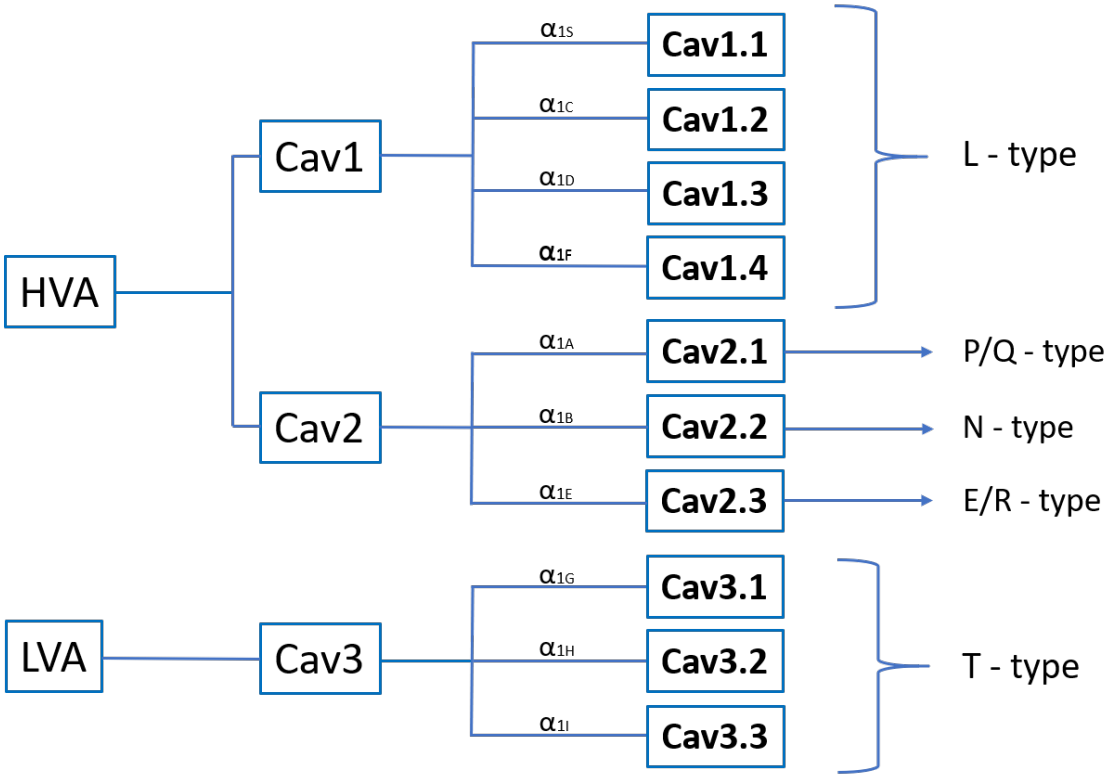

Figure 1.2.3.1: Nomenclature of VGCCs. *VGCCs are split into three subgroups; Cav1 (Cav1.1 - Cav1.4) also known as the L-type currents, the Cav2 (Cav2.1 - Cav2.3) also known as P/Q, N and E/R-type respectively, and lastly the Cav3 (Cav3.1 – Cav3.3) channels also known as T-type currents. Members of the Cav1 and Cav2 subfamilies belong to the high voltage activated (HVA) group, whereas members of the Cav3 sufamily belong to the low voltage activated (LVA) group. The various genes that encode the $\alpha 1$ subunit of each member of the VGCC subfamily are also shown in the figure.*

1.2.4. VGCC impairment in Alzheimer's disease

Calcium dyshomeostasis has been linked to several vascular and cardiovascular conditions such as stroke, myocardial infarction, and also neurodegenerative conditions such as AD, Parkinson's disease, psychiatric disorders, epilepsy and pain (Kim and Rhim, 2011; Zamponi, 2016).

An abundance of *in vivo* and *in vitro* studies revealed that aggregated Aβ can cause neuronal dysfunction, synaptic loss and eventually neuroapoptosis (Ueda *et al.*, 1997; Dahlgren *et al.*, 2002b; Shin *et al.*, 2010; Mezler *et al.*, 2012; Valerie *et al.*, 2013). There is accumulating evidence that suggests that part of Aβ's pathological effects seen in AD involves modulation of ion channels. In AD, the 'calcium hypothesis' proposes that one of the toxic effects of Aβ includes Ca^{2+} dyshomeostasis; this can potentially lead to cell apoptosis, due to Ca^{2+} being fundamental in maintaining correct cell function. One prominent way by which Aβ can cause changes in Ca^{2+} influx, is through modulation of VGCCs (Anekonda *et al.*, 2011; Kim and Rhim, 2011; Nimmrich and Eckert, 2013).

A mechanism by which Aβ has been proposed to cause calcium dysregulation is through change in VGCC expression. For example, a study conducted by Anekonda *et al. (*2011) revealed that oligomeric Aβ can cause overexpression of Cav1.2 at both mRNA (messenger RNA) and protein level, which can result in neurotoxicity. Neurotoxicity was reduced with the Cav1 blocker isridipine (Anekonda *et al.*, 2011). In support, Chiou (2006), revealed that 20μM $A\beta_{25-35}$ treatment caused a time-dependent upregulation in Cav1.2, Cav2.1 and Cav2.2 at both mRNA and protein level in SH-SY5Y neuroblastoma cells. This upregulation, was suggested to involve activation of NF-κB and subsequent upregulation of VGCC α1 subunit expression (Chiou, 2006). In contrast, Daschil *et al.*, (2013) proposed that VGCC-dependent Ca^{2+} dysregulation does not form part of the mechanism by which Aβ causes cytotoxicity, but occurs as a result of the Aβ-mediated cytotoxicity. Daschil and colleagues revealed that in transgenic mice which exhibit both APP and Aβ upregulation (due to London V717I) and Swedish (K670M/ N671L) *APP* mutations, respectively, an upregulation in Cav1.2 α1 was only seen at late disease stages, where plaque formation in reactive astrocytes was reported (Daschil *et al.*, 2013). These findings may suggest a differential pattern in Aβ-mediated neuronal and glial Ca^{2+} dysregulation. Ueda and colleagues revealed that incubation of both cortical

and hippocampal neurons with protofibrillar 10μM $A\beta_{25-35}$ induced a significant Ca^{2+} influx, which in turn induced ROS production, initiating cell apoptosis (Ueda *et al.*, 1997). Ueda proposed that the increase in Ca^{2+} influx by $A\beta_{25-35}$ through L-type channels observed via electrophysiological studies could be through increasing Cav1 expression at protein level, or via Aβ changing channel kinetics, and therefore allowing more Ca^{2+} influx (Ueda *et al.*, 1997).

Another potential mechanism by which Aβ can modulate VGCCs is through subunit/protein-protein interaction. Kim and Rhim demonstrated that treatment with nM concentrations of $A\beta_{25-35}$ caused an upregulation of Cav1.2 at the mRNA level, accompanied by an increase in the number of functional channels present at the cell membrane of hippocampal neurons. Further experiments in Cav1.3-transfected HEK293 cells (containing $\alpha 1_D$ and β_3 subunits) with $A\beta_{25-35}$ acute treatment caused a marked increase in both Cav1.3 amplitude and conductance, but did not significantly change the activation and deactivation voltages (Kim and Rhim, 2011). Immunoprecipitation experiments supported that this effect could be due to direct interaction with the β_3 subunit of the VGCCs (Kim and Rhim, 2011).

Alzheimer's and Prion (PrP) diseases are both linked to impaired peptide processing (Aβ and PrP respectively) which can lead to neuronal dysfunction and eventually apoptosis (Westergard, Christensen and Harris, 2007; Senatore *et al.*, 2012). Due to this, it has been suggested that similar pathogenic mechanisms may underlie these diseases. Under physiological conditions PrP can interact and block β-secretase; whilst under pathological conditions, such as AD, Aβ accumulation can hinder this process, causing a further upregulation in its production (Kellett and Hooper, 2009). Senatore *et al.* (2012) proposed a direct interaction of misfolded-PrP with the accessory $\alpha 2\delta$ subunit, preventing VGCC translocation to the cell membrane, and consequently reducing neurotransmitter release (Senatore *et al.*, 2012). This direct interaction of PrP with VGCCs, raises the question whether Aβ may also modulate VGCCs in a similar manner.

Another potential mechanism by which Aβ may impair VGCC function is via modulating VGCC channel kinetics. In 2008, Nimmrich *et al.*, noted that incubation with globulomer $A\beta_{1-42}$ did not cause a decrease in neurotransmitter release through pore

formation, as proposed by the amyloid-pore formation hypothesis, but rather through a decrease in VGCC-dependent Ca^{2+} influx (Nimmrich *et al.*, 2008). Electrophysiological experiments indicated that Aβ-mediated reduction in Ca^{2+} influx occurred through changes in P/Q-type channel kinetics, with slope and V_{half} (half activation voltage) remaining unaltered (Nimmrich *et al.*, 2008). By contrast, Mezler *et al.* (2012), showed that treatment of X*enopus laevis* oocytes with oligomeric Aβ increased both the amplitude, and also caused a hyperpolarized shift in the activation of recombinant Cav2.1 channels, through interacting with the pore-forming α1 subunit (Mezler *et al.*, 2012). In support of Mezler's work, Hermann and colleagues, through whole-cell patch clamp, revealed that Aβ globulomers not only modulated Cav2.1 kinetics, but also increased the activity of Cav2.2 channels, through an increase in amplitude and also shift of V_{half} towards more hyperpolarized values (Hermann *et al.*, 2013). This effect of Aβ on Cav2.2 channels could be prevented through the use of VGCC blockers (Hermann *et al.*, 2013), suggesting that CCBs may be beneficial in preventing Aβ-mediated synaptic dysfunction via impairment in neurotransmission. Contradictory findings concerning the mechanism by which Aβ affects Cav2 kinetics could be due to differences in the concentration of the peptide used, the aggregation state of the peptide, and also whether the channel was within its conducting or non-conducting state.

It is widely accepted that Ca^{2+} dyshomeostasis constitutes part of the AD pathology (Lopez *et al.*, 2008; Daschil *et al.*, 2013; Gholamipour-Badie *et al.*, 2013). Several studies have demonstrated that CCBs can suppress Aβ toxicity in the brain, as seen in various *in vivo* animal models and cell lines (Ueda *et al.*, 1997; Yagami *et al.*, 2004; Anekonda *et al.*, 2011; Mezler *et al.*, 2012; Gholamipour-Badie *et al.*, 2013; Hermann *et al.*, 2013; Nimmrich and Eckert, 2013). Currently, several pharmaceutical agents which target VGCCs and interfere with their pathophysiological action, have already been tested or are currently in clinical trials to combat AD (Zamponi, 2016). Although it has been shown that CCBs can suppress Aβ neurotoxicity mediated through VGCCs, as yet clinical trials with VGCC blockers have failed to exhibit significant effects in interrupting or delaying AD pathology (Birks and López-Arrieta, 2002; Anekonda *et al.*, 2011; Gholamipour-Badie *et al.*, 2013). A systematic review conducted by Birks and Lopez-Arrieta in 2002 (updated in 2010), revealed that the Cav1 blocker nimodipine was

only beneficial in short term improvement of cognitive function. One reason that clinical trials have failed to exhibit significant findings could be due to drug low brain bioavailability of the CCB currently tested (Anekonda *et al.*, 2011). Selectivity issues may also be a reason for a failed clinical trial (Nimmrich and Eckert, 2013). Formulation changes may increase drug bioavailability, and therefore may make compounds more effective against AD.

Overall there is contradictory evidence as to the mechanism(s) by which Aβ may modulate VGCCs, possibly due to methodological differences or differential effects dependent on the VGCC subtype. Identifying endogenous signalling molecules, or developing new compounds which may be able to interfere with VGCC-dependent Aβ-mediated neurotoxicity without disturbing the physiological activity of other ion channels, may be of therapeutic interest in improving, delaying or even halting AD progression.

1.3. Carbon Monoxide

1.3.1. Carbon Monoxide as an exogenous gas

Carbon monoxide (CO) is an odourless and colourless gas, most widely known for its deleterious effects, but as described more fully below can also act as a endogenous gasotransmitter. Exogenous CO gas can be produced from carbon-based fuels, from various home appliances and vehicles (Wilkinson and Kemp, 2011). In the UK alone, around 50 individuals die annually due to exogenous CO-poisoning, with around 200 individuals requiring hospitalization (Wilkinson and Kemp, 2011). A large number of worldwide deaths reported due to CO poisoning were due to CO-release from running vehicles in enclosed spaces. Cigarette smoking can also be a source of CO, with smoking for 5mins leading to up to 4% oxygen displacement from haemoglobin (Omaye, 2002). Toxic levels of CO consist levels higher than 200ppm for acute, and 30ppm for chronic exposure (Wilkinson and Kemp, 2011). Exposure to 1000ppm or 0.1% CO for as low as an 1h can lead to respiratory failure, hypoxia and even death (Peterson and Stewart, 1975; Omaye, 2002).

CO poisoning has determinantal effects to the human body. CO-dependent cytotoxicity involves CO binding onto haemoglobin to form the carboxyl-haemoglobin complex, which can cause a reduction in the amount of oxygen transported and can be released to tissue by RBCs (red blood cells) causing hypoxia (Omaye, 2002). Haemoglobin shows an approximate 200-fold higher affinity to CO compared to oxygen (Omaye, 2002; Gorman *et al.*, 2003; Motterlini, 2007). Moreover, CO can act cytotoxically via block of cytochrome oxidase of complex IV of the electron transport chain, causing the body to switch to anaerobic respiration, causing tissue damage and even death (Omaye, 2002).

1.3.2. Carbon monoxide as a gasotransmitter

Although CO as a toxic gas, can cause cytotoxicity through a hypoxia-related manner, endogenously as a product of heme catabolism, it can have vital roles in metabolism (Wu and Wang, 2005; Peers, Dallas and Scragg, 2009). CO as an important participant in cell signalling, within physiological levels, can be critical for correct cell function (Wu and Wang, 2005; Zeynalov and Doré, 2009).

Endogenously, the majority of CO is released through heme processing. RBC heme catabolism can be catalyzed by the enzyme heme oxygenase (HO-1 or HO-2 isoforms), an enzyme of 30kDa in size, which can be found in a number of cells, including glial cells and neurons (Schipper, Cissé and Stopa, 1995; Maines, 1997). A third HO isoform exists, known as HO-3 with limited heme catabolism activity (McCoubrey and Maines, 1994; Hayashi *et al.*, 2004). Heme oxygenase uses oxygen to catabolize heme into biliverdin, ferrous ion (Fe^{3+}) and CO due to the cleavage of the porphyrin ring A and B (Tenhunen, Marvel and Schmid, 1969; Maines, 1997). Biliverdin is then further metabolised into bilirubin, both known antioxidants (Maines, 1997; Omaye, 2002; Jayanti *et al.*, 2020). All of the products generated during heme catabolism are known to have a role in both iron and bile metabolism. Although heme catabolism comprises a physiological process, stressful conditions can also cause an upregulation in heme oxygenase, prompting heme processing. Heme oxygenase expression has been shown to upregulate in response to events that induce oxidative stress, due to an increase in metals ions such as heme and also due to presence of sulfhydryl compounds (Applegate, Luscher and Tyrrell, 1991; Schipper, Cissé and Stopa, 1995; Schipper, 2000).

CO as a gasotransmitter, can act as a signalling molecule to maintain cell function, similarly to the gasotransmitter nitric oxide (NO). Within the cardiovascular system, it has been shown that CO can act as a vasodilator by inducing muscle relaxation (e.g. via cGMP (cyclic guanosine monophosphate) pathways) and also induce changes in platelet aggregation (Motterlini, 2007; Kaczara *et al.*, 2020). CO has also shown to have anti-inflammatory properties. For example, studies using animal models of ischemic stroke, showed that 125 or 250ppm CO inhalation (less than 24hr) led to a reduction in both inflammation and cell damage, during restoration of oxygen flow (Vieira, Queiroga and Alves, 2008; Zeynalov and Doré, 2009; Wang *et al.*, 2011; Mahan

et al., 2012). One potential mechanism by which CO may exhibit these cytoprotective effects, is through activation of antioxidant pathways, such as activation of Nrf2 pathways that induces transcription of antioxidant genes including HO and SOD (superoxide dismutase) (Wang *et al.*, 2011). CO has been shown to have anti-inflammatory and anti-apoptotic effects in preventing rejection of lung transplants (Song *et al.*, 2003). In addition to anti-inflammatory properties, CO has also shown to have a role within cell proliferation. Duckles and colleagues noted that CO reduced proliferation of smooth muscle cells via inhibition of Cav3 channels (Duckles *et al.*, 2015). Moreover, CO has also shown to prevent apoptosis. For example, pre-treating astrocytes with CO prior to induction of oxidative stress prevented cell death through changes in the expression of anti-apoptotic proteins (e.g. bcl-2) (Almeida *et al.*, 2012). In another study, it was shown that CO, generated using the CO-releasing molecule CORM2, had anti-apoptotic effects by preventing neuroblastoma cell death induced by $A\beta_{1-42}$ (Hettiarachchi *et al.*, 2014). Kim *et al.* (2018) revealed that CO is not only able to prevent some of the toxic effects of Aβ, but it can also reduce Aβ production through reducing the expression of β-secretase via a pathway that involves block of NF-κB binding onto *BACE1* (gene that encodes β-secretase) (Kim *et al.*, 2018).

1.3.3. Carbon monoxide as a novel therapeutic

As a number of papers have proposed that CO can have vast cytoprotective roles, there is considerable interest in investigating CO as a novel therapeutic in treating various diseases, such as AD. Due to the concerns associated with the use of CO gas as a treatment, there is some stigma in using CO as a therapeutic. In order to study CO cytoprotective effects in a safe and controllable environment with the laboratory, Moterllini's research group started developing compounds in the early 2000s that allow the release of CO in a trackable manner, so-called carbon monoxide releasing molecules (CORMs) (Motterlini *et al.*, 2002; Motterlini, 2007; Wilkinson and Kemp, 2011). The first compounds to be developed, CORM1 (manganese decacarbonyl) and CORM2 (tricarbonyldichlororuthenium(II) dimer) were manganese and ruthenium based respectively. Both of these compounds are capable of rapid CO release, in response to light or ligand substitution respectively (Motterlini *et al.*, 2002; Motterlini, 2007). In contrast to CORM1 and CORM2 which require DMSO as a solvent, compounds CORM-A1 (sodium boranocarbonate) and CORM3 (tricarbonylchloro(glycinato)ruthenium (II)) were developed as water soluble compounds (Motterlini *et al.*, 2002; Motterlini, 2007). Similarly to CORM2, CORM3 is also a ruthenium based compound capable of rapid CO release (Clark *et al.*, 2003). Contrary to the transition-metal containing CORM compounds, CORM-A1 contains a carboxylic group capable of slow CO release in response to changes in the pH or temperature (Motterlini, Mann, *et al.*, 2005; Motterlini, Sawle, *et al.*, 2005).

1.3.4. Heme oxygenase and Alzheimer's disease

Numerous neurodegenerative diseases have shown that part of their pathogenesis involves induction of oxidative stress and presence of free radicals (Schipper, Cissé and Stopa, 1995). A downregulation in antioxidants, an upregulation in lipid peroxidation products and also redox active iron that can induce ROS release has been noted in AD (Schipper, Cissé and Stopa, 1995; Wojsiat *et al.*, 2018). It is believed that oxidative stress comprises one of the pathways that lead to cell dysfunction and eventually neuronal death, although it is still not fully understood at which stage in disease progression this occurs (Schipper, Cissé and Stopa, 1995; Pappolla *et al.*, 1998; Schipper, 2004). The increase in heme, and oxidative stress observed in AD brains induces HO-1 expression which is proposed to act as a defence mechanism against free radicals (Schipper, Cissé and Stopa, 1995; Wojsiat *et al.*, 2018). Ca^{2+} dysregulation mediated oxidative stress (through changes in Ca^{2+} influx) may also account for the increase in HO-1 expression seen in AD (Ueda *et al.*, 1997; Pappolla *et al.*, 1998; Schipper, 2004).

Findings obtained from experimental work done on mice has revealed that during ageing, an upregulation in HO-1 expression in the liver is seen in response to oxidative stress, although no change in brain HO-1 expression is noted (Barnes *et al.*, 1998). Immmunohistochemistry and fluorescence imaging studies on slices from human AD brains reveal HO-1 upregulation in the cerebral cortex, hippocampus and subcortical white matter compared to brains of healthy age matched controls; these studies suggest that elevated expression of HO-1 in the brain is not a physiological event observed during normal ageing (Schipper, Cissé and Stopa, 1995; Schipper, 2000). Co-localisation of HO-1 in human brain regions where amyloid plaques and neurofibrillary tangles were evident, indicated a link for HO-1 with the presence of these two main hallmarks of AD (Schipper, Cissé and Stopa, 1995; Schipper, 2000). An upregulation in HO-1 expression has also been noted in astrocytes and microglia in response to neuroinflammation (Schipper, Cissé and Stopa, 1995; Fernández-Mendívil *et al.*, 2020). Oxidative stress is known to increase HO expression, therefore co-localisation of HO-1 within regions where amyloid plaques and neurofibrillary tangles are present, may occur as a neuroprotective measure (Schipper, Cissé and Stopa, 1995; Hettiarachchi *et*

al., 2014). In support, another study, revealed co-localisation of both HO-1 and also CuZn-superoxide dismutase 1 (CuZn-SOD1), another marker of oxidative stress, in regions where amyloid plaques are present in animals overexpressing mutant APP (Pappolla *et al.*, 1998; Peers, 2011). As upregulation of HO-1 was also observed in areas with low amyloid plaque density it was proposed that HO-1 upregulation occurs as a response to amyloid accumulation and aggregation and therefore precedes plaque formation (Pappolla *et al.*, 1998).

Upregulation of HO-1 in AD is believed to occur as a protective measure. Infante *et al.* (2010) revealed that HO-1 can halt cholesterol-dependent increase in Aβ generation by inducing glial cholesterol conversion into oxysterols, and consequently activating liver-X receptor-β (LXR-β) which in turn cause changes in gene expression and eventually reduction in Aβ (Infante *et al.*, 2010). Interestingly, individuals with a specific polymorphism at the promoter region of HO-1 (-413), and LXR-β polymorphisms in introns 2 (rs2695121), 5 (rs1052533), and 7 (rs1405655), exhibit an increased risk of developing AD (Infante *et al.*, 2010).

It is widely accepted that HO-1 can exhibit antioxidant properties. In transgenic animals that suffered an ischemic stroke, HO-1 overexpression minimized cell damage and maintained cell viability by reducing release of ROS and also upregulating expression of pro-apoptotic proteins such as bcl-2 (Panahian, Yoshiura and Maines, 1999; Schipper, 2004). Moreover, heme catabolism by HO-1 leads to the production of products such as biliverdin with known antioxidant properties (Maines, 1997; Takahashi *et al.*, 2000; Schipper, 2004; Jayanti *et al.*, 2020).

Although evidence suggest that HO-1 upregulation in AD occurs as a protective measure, some studies reveal that function of HO-1 in AD is impaired and therefore cannot exhibit its protective effects. Co-immunoprecipitation experiments revealed that HO-1 can interact with APP (Takahashi *et al.*, 2000). This demonstrates that especially in Familial AD where *APP* mutations can be present, upregulation of HO-1 as a defence mechanism against oxidative stress will be unable to confer cytoprotection due to APP interacting with HO-1 consequently aiding neuronal toxicity (Schipper, 2000; Takahashi *et al.*, 2000). Animal models that lack HO and express mutant APP can display similar features to late onset AD.

1.3.5. Carbon monoxide modulation of ion channels

There is considerable evidence that suggests that some of the cytoprotective effects elicited by HO-1 are partly due to CO (Wu and Wang, 2005; Hettiarachchi *et al.*, 2014). It has been proposed that one mechanism by which CO acts cytoprotectively is through modulation of ion-channels (Wu and Wang, 2005; Peers, 2011).

Zeynalov and Doré (2009) revealed that following an ischemic stroke, degree of cerebral tissue damage and oedema decreases with inhalation of physiological levels of CO. It was suggested that the mechanism by which CO confers these protective effects is through activation of Ca^{2+}-dependent K^+ channels that causes vasodilation of blood vessels. Kv2.1 channels are known to have a role in cell apoptosis (Al-Owais *et al.*, 2012). Elevated K^+ efflux initiates pro-apoptotic pathways, such as caspase activation, and upregulates endonuclease function (Szabò, Zoratti and Gulbins, 2010). Al-Owais *et al.* (2012) demonstrated that both HO-1 and its heme catabolism product CO have important roles in maintaining cell survival. Oxidative stress-mediated cell death was inhibited by CO through an ion channel-dependent manner that involved inhibition of neuronal Kv2.1 channels (Al-Owais *et al.*, 2012). In contrast to K^+ channels, in a study investigating the effect of CO on cardiac arrythmias revealed that it can activate Nav1.5 channels through a NO, nitrosylation pathway (Dallas *et al.*, 2012). In support to this, Al-Owais and colleagues demonstrated that CO modulation of ion channels, in this case, Kv1.5, not only involves NO, it also involves the activation of guanyl cyclase and therefore CO-mediated inhibition of these channels also involves the cGMP pathway (Al-Owais *et al.*, 2017). Similarly, Viera's study revealed that activation of mitochondrial K_{ATP} through a sGC (soluble guanylyl cyclase) and NO-dependent pathway is part of the mechanism by which CO is able to reduce tissue damage and cell death following an ischemic stroke (Vieira, Queiroga and Alves, 2008).

It has been widely accepted that part of the amyloid pathology seen in AD involves calcium dysregulation through modulation of VGCCs (Zamponi, 2016). As several studies have revealed that CO can modulate VGCCs, there is considerable interest in investigating the mechanism(s) by which CO may interfere with Aβ-mediated calcium impairment through VGCCs seen in AD.

Although it has been proposed that CO-mediated prevention of apoptosis is through K^+ channels, VGCCs have also been implicated. For example, Hettiarachchi *et al.* (2014), revealed that both HO-1 and CO prevented protofibrillar $A\beta_{1-42}$-mediated neuronal cell apoptosis through caspase activation. Part of the $A\beta_{1-42}$ neurotoxicity involved increasing the activity of Cav1 channels, which in turn caused activation of CAMKKII and subsequent phosphorylation and activation of AMPK (Hettiarachchi *et al.*, 2014). CO released through CORM2 treatment inhibited both the phosphorylation and subsequent activation of AMPK (Hettiarachchi *et al.*, 2014).

Within the cardiovascular system, CO has been shown to decrease myocardial infarction-mediated tissue damage (Scragg *et al.*, 2008; Peers, 2011). As inhibition of Cav1 channels expressed in HEK293 cells induced neuroprotection, it was proposed that CO protective effects are through a Cav1-dependent manner (Peers, 2011). Work carried out by Scragg and colleagues revealed that specific cysteine residues (1787 - 1818 aa) residing within the pore-forming subunit of Cav1 channels are essential for CO modulation of cardiac Cav1 channels (Scragg *et al.*, 2008; Peers, 2011). Supporting this, it was shown that both CO released from CORM2 and also dissolved CO changed L-type channel kinetics via inhibition of L-type currents seen in both recombinant and native Cav1 channels (Scragg *et al.*, 2008). However, in disagreement to Scragg *et al.,* another study demonstrated that administering low levels of exogenous CO to both intestinal smooth muscle cells that natively express these channels, and Cav1 stably transfected HEK293 cells caused an increase in L-type current amplitude (Lim *et al.*, 2005). It was proposed that this increase in Ca^{2+} influx occurred through an increase in NO release (via NO synthase) and a subsequent increase in cGMP production through sGC and activation of PKA (Lim *et al.*, 2005). In contrast, Scragg *et al.* (2008) revealed that CO-mediated inhibition of Cav1 channels was through release of ROS from complex III of the electron transport chain, as the use of MnTMPγP, an antioxidant halted its inhibitory effect, revealing that CO works through a redox-dependent pathway. Differences in the effect of CO on Cav1 channels seen within studies, could be due to differences in the source and dose of CO used, the subunit composition of the Cav1 channels investigated and also CO exhibiting tissue specific effects. It has long been known that T-type channels have a role in cell proliferation (Duckles *et al.*, 2015). Duckles *et al.* (2014) revealed that CO (through HO-1) can have anti-proliferative effects in smooth muscle

cells by a mechanism involving a reduction in Cav3 current conductance. A reduction in Cav1 conductance was also seen, although was not correlated to proliferation (Duckles *et al.*, 2015). Unlike other studies, Boycott and colleagues, revealed that CO modulation of Cav3 channels involves hindering Trx (thioredoxin)-mediated redox modulation of Cav3.2 channels, by interacting with it, therefore inhibiting T-type currents (Boycott *et al.*, 2013).

To summarise, it is well established that CO can influence cell function and also confer cytoprotection. CO modulation of ion channels depends on tissue specificity and the ion channel targeted. It is widely accepted that calcium dysregulation through impairment of VGCC function consists one of the pathways by which Aβ confers neurotoxicity. As the manner by which CO modulates ion channels is not fully understood, it is therefore important to further investigate the effects of CO on VGCCs, which may identify CO as a novel therapeutic for diseases such as AD.

1.4. Aims and Objectives

This project was divided into two sections. It is widely accepted that one mechanism by which Aβ in AD confers cytotoxicity may be through calcium dysregulation (Zamponi, 2015). Although studies have shown that one way by which Aβ can cause calcium dysregulation is through changes in the expression and activity of VGCCs, studies report differences in the mechanism by which Aβ modulates these channels. Therefore, as a first step in the study, the effect of Aβ on our neuronal cell line model (SH-SY5Y cells) was investigated. Thus the aims were to:

- Define VGCC expression profile within undifferentiated and RTA-differentiated SH-SY5Y cells
- Identify which VGCC subtypes have a role in cell viability and activity
- Establish a consistent protocol for Aβ aggregation into protofibrils
- Identify changes in VGCC expression and activity with $A\beta_{1-42}$ protofibril treatment

CO as an endogenous signalling molecule has been shown to have a number of important roles in metabolism. For example, studies have demonstrated CO can act cytoprotectively by preventing cell death, displaying anti-inflammatory effects and prevent oxidative stress-dependent cell dysfunction (Vieira, Queiroga and Alves, 2008; Zeynalov and Doré, 2009; Hettiarachchi *et al.*, 2014). CO cytoprotection has been shown to occur through several mechanisms, including ion channel modulation, such as through redox modulation and nitrosylation (Lim *et al.*, 2005; Scragg *et al.*, 2008). Due to this, there is considerable interest in testing CO as a potential therapeutic for neurodegenerative diseases such as AD. Therefore, the second step of this study was to investigate the effect of CO on our neuronal cell line model and also on Cav2.2 stably transfected HEK293 cells in order to identify the mechanism by which CO modulates presynaptic Cav2.2 channels. Aims here were to:

- Identify non-neurotoxic CO concentrations via the use of CORM2
- Investigate the effect of CO in preventing protofibrillar $A\beta_{1-42}$-mediated neurotoxicity in SH-SY5Y cells

- Identify CO-mediated changes in N-type channel kinetics in Cav2.2-stably transfected HEK293 cells
- Identify the mechanism by which CO changes VGCC channel kinetics

This work aims to further our understanding of protofibril $A\beta_{1-42}$-mediated changes in VGCC expression and activity, as well as investigate the mechanism by which CO may interfere with the noted Ca^{2+} dysregulation. This will aid our understanding of AD by identifying changes in Ca^{2+} homeostasis mediated by $A\beta$. Moreover identifying how CO may modulate VGCCs may help in the development of better therapeutics that not only aim to provide symptomatic relief, but also target $A\beta$-mediated cytotoxic mechanisms, with the ultimate goal of halting AD progression, and even possibly prevent it from developing.

Chapter 2: Materials and Methods

2.1. Cell Culture

2.1.1. Cell Lines

SH-SY5Y human neuroblastoma cells

SH-SY5Y neuroblastoma cells (ECACC, UK) were cultured in Dulbecco's Modified Eagle Medium (DMEM)-GlutaMAX (Life Technologies, UK) with low glucose concentration (1g/L), containing 2mM L-glutamine (Life Technologies, UK) and supplemented with 10% fetal bovine serum (FBS; Life Technologies, UK) and 1% penicillin/streptomycin (Life Technologies, UK).

Differentiation medium was DMEM-GlutaMAX supplemented with 10μM RTA (retinoic acid), to allow SH-SY5Y differentiation. Following cell passaging, cells were allowed to settle in T75 flasks overnight, and then the medium was replaced with RTA-containing medium. Cells were left in differentiation medium for 3 days prior to experimental use.

Cav2.2 ((α_{1B} ($Ca_v2.2$), β_{1b}, and $a_2\delta$ subunits))-stably transfected HEK293 cells

Stably-transfected HEK293 expressing Cav2.2 calcium channels (α_{1B} ($Ca_v2.2$), β_{1b}, and $a_2\delta$ subunits) (McDavid and Currie, 2006), were cultured in Minimum Essential Medium (MEM; Life Technologies, UK) supplemented with 2mM L-glutamine (Life Technologies, UK) , 0.5mg/ml geneticin (G418; Sigma Aldrich, UK), 10% FBS (Life Technologies, UK) and 1% penicillin/streptomycin (Life Technologies, UK).

BV2 mouse-microglia cells

Microglia BV2 cells (gift by Dr Eder, St. George's University) were cultured in DMEM-GlutaMAX (Life Technologies, UK) with low glucose concentration (1g/L), containing 2mM L-glutamine (Life Technologies, UK), supplemented with 10% FBS (Life Technologies, UK) and 1% penicillin/streptomycin (Life Technologies, UK).

2.1.2. Cell Passaging and Plating

All cell lines were incubated at 37°C with 5% CO_2 (95% O_2), and were passaged when reaching approximately 80% confluency. Once desired confluency had been reached, cells were then washed in phosphate-buffered saline (PBS; Life Technologies, UK) twice prior to passaging and plating. TrypLE-express (Life Technologies, UK) was used for detachment of cells. Following detachment, cells were resuspended in appropriate medium, and then centrifuged at 1500rpm for 5min at room temperature for cell collection. The medium was then discarded, and cells (pellet) were resuspended in fresh media for experimental use or cell passaging. For cell passaging, cells were resuspended in 5ml medium and placed in T75 flasks to allow growth at 1:5-1:25 dilution for SH-SY5Y and HEK293 cells, and 1:50-1:100 dilution for BV2 cells. For experimental use, cells were resuspended in 1ml medium for cell counting and then plating.

All cell work was performed under sterile conditions.

2.1.3. Cell Counting

Cell count was quantified using Moxi Flow (Orflo, USA) or a standard haemocytometer. Desired number of cells were plated for each experiment. Cells were plated onto 96-well plates for cell viability experiments (25,000-50,000 cells/well) and 6-well plates for quantitative polymerase chain reaction (qPCR) experiments (200-400,000 cells/well). For electrophysiology experiments, cells were resuspended in 5ml medium and then plated onto coverslips at 1:40-1:100 dilution.

2.1.4. Cryopreservation

For cryopreservation the cell passaging protocol was followed up to the cell collection step (centrifugation). Media was then removed, and cells (pellet) were resuspended in FBS-containing 10% dimethyl sulfoxide (DMSO; Thermo Fisher Scientific, UK) for cryopreservation (4.5ml per confluent T75 flask). Cells in freezing medium were then transferred into cryovials (1.5ml/cryovial) and placed in a -80°C freezer overnight, in a polyethylene foam container, to allow gradual freezing. Following this, the cryovials were transferred into liquid nitrogen tanks to allow long-term cryopreservation.

For cell thawing, cryovials were placed in a water bath at 37°C to allow gradual thawing. Cells were then placed in T25 flasks, containing appropriate medium to allow

expansion. Over a few days, the medium was gradually replaced with fresh medium, to achieve complete removal of DMSO. Once desired confluency had been reached, cells were then transferred into T75 flasks and passaged.

2.2. Calcium Channel Blocker Preparation

For studying VGCC activity, various calcium channel blockers (CCBs) were used. Nifedipine (Cav1 blocker), ω-agatoxin IVA (Cav2.1 blocker), ω-conotoxin GVIA (Cav2.2 and to a less extent Cav2.1 blocker) and mibefradil dihydrochloride (Cav3 blocker but also with actions at Cav1) were prepared as stocks, aliquoted out, and placed in -20°C for long-term storage. Whenever a blocker was needed, one aliquot would be thawed for experimental use. Cadmium chloride ($CdCl_2$) was prepared fresh prior to each experiment. Final working concentrations were prepared in DMEM medium. A list of the various blockers, their supplier, stock concentration, working concentration and solvent used can be found in **Table 2.2.1**.

***Table 2.2.1: CCB preparation**. List of the VGCC modulators used, their supplier, stock concentration and VGCC target(s). Cadmium chloride was prepared fresh prior to each experiment. All other CCBs were prepared, aliquoted out and stored at -20°C for long-term storage.*

Pharmacological Tools	Supplier	Stock/Solvent	Working Concentration	Target
Cadmium Chloride	Sigma Aldrich, UK	50mM in dH_2O	100nM - 50μM	Pan-VGCC blocker (Chow, 1991)
Nifedipine	Abcam, UK	100mM in DMSO ↓ 5mM in medium	5μM	Cav1 (Ortner and Striessnig, 2016)
ω-Agatoxin IVA	Abcam, UK	50μM in dH_2O	50nM and 200nM	Cav2.1 (Bourinet *et al.*, 1999)
ω-Conotoxin GVIA	Abcam, UK	10μM in dH_2O	10nM and 1μM	Cav2.2 (Lewis *et al.*, 2000)
Mibefradil Dihydrochloride	Sigma Aldrich, UK	5mM in dH_2O	5μM	Cav3 & Cav1 (Cribbs *et al.*, 1998; Perez-Reyes *et al.*, 1998)

2.3. CORM2/iCORM2 preparation

To minimise loss of CO, CORM2 (Sigma Aldrich, UK) was prepared as 100μM-100mM stocks (in DMSO) immediately prior to experimental use. To achieve working concentration, an initial 1:1000 dilution of the stock was carried out in medium, followed by a serial dilution to achieve lower concentrations. For electrophysiology experiments, dilution of stock into working concentration was carried out in extracellular solution. For the inactive form (iCORM2), CORM2 was left at room temperature at least overnight, with the lid loosely attached to allow CO release.

2.4. Redox agents

Stocks of the oxidising agent dithiodipyridine (DTDP; Sigma Aldrich, UK) and reducing agent dithiothreitol (DTT; Sigma Aldrich, UK) were prepared fresh in DMSO, prior to each experiment. For electrophysiology experiments, in order to achieve working concentrations, a 1:1000 dilution of the stock was carried out in extracellular solution.

2.5. Amyloid-β preparation

2.5.1. NH_4OH protocol

Human synthetic Aβ (Abcam: $A\beta_{1\text{-}42}$ #ab120301, $A\beta_{42\text{-}1}$ #ab120481) was dissolved in 1% ammonium hydroxide (NH_4OH; Sigma Aldrich, UK) (in PBS), to obtain 1mg peptide film. The percentage of purity of the peptide was taken into consideration when calculating the volume of NH_4OH needed to be used. Following this, the Aβ was left at room temperature for 30min and then placed in a speed-vac until the peptide film is obtained (~20min). Peptide film was then dissolved into the 5mM stock using 10mM sodium hydroxide (in dH_2O) (NaOH; Sigma Aldrich, UK). Aβ was then sonicated for 10min in order to prime the peptide for aggregation. Control Aβ kept as 'monomeric' did not undergo any sonication. Both the peptide film and the 5mM stock were stored at -20°C until use.

Prior to experimental use, the 5mM stock was sonicated for a further 10min and then further diluted into the 100μM usable stock over a 48hr incubation period. Firstly, the 5mM stock was diluted in PBS and 2% sodium dodecyl sulfate (SDS; Invitrogen, UK), and then incubated over 24hr. The volume of SDS was 10% of the 400μM Aβ minus the 5mM stock volume. Following this, the 400μM Aβ was then diluted into the 100μM usable stock using PBS and incubated for another 24hr.

In order to minimise chances of potential aggregation, monomeric (control) Aβ was diluted from the 5mM stock directly to the 100μM usable stock prior to experimental use.

For experimental purposes, in order to achieve various working concentrations (1nM - 10μM), the 100μM $A\beta_{1-42}$/$A\beta_{42-1}$ stock was further diluted in medium.

2.6. Transmission Electron Microscopy

Aggregation process of both $A\beta_{1-42}$ and $A\beta_{42-1}$ preparations was investigated using a transmission electron microscope (TEM; Jeol 2100 Plus, 200kV). Firstly, the Aβ preparations (30μl) were loaded onto 300-mesh sized carbon grids (HC300Cu films, EM Resolutions, UK). Following this, the grids were then stained with 1-2% w/w uranyl acetate (Agar, UK) in dH_2O for visualisation purposes (~1min). The grids were then washed with dH_2O to remove excess stain (for ~1min) and then left to dry prior to use (~5min). Image analysis, via measuring protofibril length, was achieved using Image J.

2.7. Cell viability assays

For investigating metabolic activity, and specifically cell respiration, XTT or MTT cell viability assays were carried out. Here on onwards, for simplification purposes, metabolic activity investigated by XTT/MTT assay is referred to as cell activity.

2.7.1. XTT assay

SH-SY5Y/BV2 cells were plated in sterile standard flat-bottom 96-well plates and left to adhere overnight. Cells were then treated with 1-100nM, or 1-10μM concentrations of $A\beta_{1-42}$/$A\beta_{42-1}$, CCBs ($CdCl_2$, nifedipine, ω-agatoxin IVA, ω-conotoxin GVIA, and mibefradil dihydrochloride) or CORM2/iCORM2, their corresponding vehicle controls and 10mM hydrogen peroxide (H_2O_2; Thermo Fisher Scientific, UK). Working concentrations of the treatments were prepared using the cells corresponding medium.

Following 24hr treatment of the cells, 1:10 XTT solution in DMEM serum-free medium was added to the cells, with a total well volume of 100μl. Cells were incubated with the XTT solution for 3-4hr. For the preparation of the final XTT solution 1:200 PMS (phenazine metholsulfate) was added to the XTT. The XTT solution consisted of 1mg/ml XTT (Molecular Probes, UK) dissolved in DMEM serum-free medium, and 5mM PMS (Sigma Aldrich, UK) dissolved in PBS. Plates were read at 450nm (650nm reference readings) using a standard colorimetric reader (Molecular Devices, SPECTRAmax 340 PC). For analysis purposes, results were normalised and plotted as a percentage of their corresponding vehicle control.

2.7.2. MTT assay

SH-SY5Y cells were plated in sterile standard flat-bottom 96-well plates and left to adhere overnight. Cells were then treated with combinations of various concentrations of $A\beta_{1-42}$ and CCBs ($CdCl_2$, nifedipine, ω-agatoxin IVA, ω-conotoxin GVIA, and mibefradil dihydrochloride) or CORM2/iCORM2, and their corresponding vehicle controls for 24hr. Additionally, 10mM H_2O_2 as a positive control was used. Working concentrations of the treatments were prepared using the cells corresponding medium.

Following the treatment of cells, MTT (3-(4,5-dimethylthiazol-2-yl)-2,5-diphenyltetrazolium bromide; Sigma Aldrich, UK) was prepared as a 5mg/ml stock in PBS. The MTT solution was loaded onto the cells at 1:10 dilution in their corresponding medium. Cells were incubated with the MTT solution for 3-4hr. Following incubation, once the formazan crystals are formed, the MTT solution was removed from the cells, and the formazan crystals are dissolved in 50μl DMSO, carefully to avoid the formation of bubbles. Plate were then pulse-span using a standard plate centrifuge. The plate was

then incubated for 5-10min and read at 575nm (650nm reference readings) using a standard colorimetric reader (Molecular Devices, SPECTRAmax 340 PC). For analysis purposes, results were normalised and plotted as a percentage of their corresponding vehicle control.

2.8. Polymerase Chain Reaction

2.8.1. RNA extraction

SH-SY5Y cells were plated in standard flat-bottom 6-well plate and left to adhere overnight. Cells were then treated with 100nM and 1μM $A\beta_{1-42}$ and their corresponding vehicle control (PBS) for 24hr. Following this, the treatments were removed and 1ml Trizol (Thermo Fisher Scientific Scientific, UK) was added directly onto the cells for 5min for cell lysis and lysates were then transferred into Eppendorf tubes. RNA separation from protein and DNA was achieved via adding 200μl chloroform (Thermo Fisher Scientific, UK) into each tube. Samples were then mixed vigorously for 20s and centrifuged at 12,000G for 10min at 4^{o}C. Following centrifugation, the RNA 'layer' was carefully removed from each tube and was then placed into new Eppendorf tubes. Isopropanol (Thermo Fisher Scientific, UK) 500μl was added in each tube, and tubes were then mixed and centrifuged at 17,000G for 14min at 4^{o}C. The supernatant was then discarded, and 75% ice-cold ethanol was added into each tube. The tubes were mixed and then centrifuged at 17,000G for 5min at 4^{o}C, supernatant was removed and the isolated RNA extracts (pellets) were then left to air dry for ~20min. RNA was then resuspended in 15μl nuclease-free water and heated at 60^{o}C for 10min using a heat block. The Eppendorf tubes were then pulse-spun and kept on ice for total-RNA measurement.

Total-RNA (ng/μl) was measured via loading 1.5μl per sample onto a Nanodrop 2000 (Applied Biosystems/Thermo Fisher Scientific, UK). Nuclease-free water was used for Nanodrop blanking. Samples were read at 260nm (for DNA) and 280nm (for protein) with an ideal wavelength ratio of 1.8 to 2.1 for RNA.

Results where then used to calculate the volume of total-RNA which is required to achieve a concentration of 1000ng/sample. The required amount was then transferred

into new Eppendorf tubes and was topped-up to total volume of 3.85µl (using nuclease-free water) ready for complementary DNA (cDNA) synthesis.

For long-term storage (up to a year), RNA extracts were kept at -20°C.

2.8.2. cDNA synthesis

Total RNA (1000ng/sample) was reverse-transcribed into cDNA using TaqMan® reverse transcription reagents (Applied Biosystems/Thermo Fisher Scientific, UK) in a T100 Thermal cycler (Biorad). In each 200µl PCR-tube a total of 6.15µl Master mix and 1000ng total RNA in 3.85µl was added (**Table 2.8.2.1**). cDNA synthesis protocol steps are shown below:

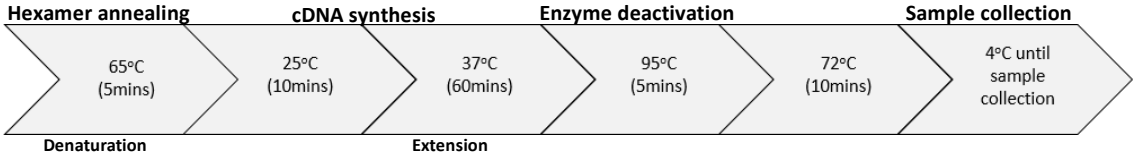

Following reverse transcription, samples were diluted 1:5 in nuclease-free water for qPCR. For long-term storage (up to a year) both RNA and cDNA was kept at -20°C. cDNA synthesis steps involve; hexamer primer annealing for ensuring that the whole RNA template is ready for reverse transcription, reverse transcription (Reverse transcriptase, dNTPs, RT buffer) of RNA template into cDNA, and also enzyme deactivation step.

Table 2.8.2.1: Master Mix for cDNA synthesis.

	Volume µl (per sample)	Final concentration
10x Reverse transcription buffer	1	1x
2.5mM dNTPs	2	0.5mM
25mM $MgCl_2$	2.2	5.5mM
50 µM Random Hexamers	0.5	2.5µM
20U/µl RNase Inhibitor	0.2	0.4U/µl
50U/µl Reverse Transcriptase	0.25	1.25U/µl
	TOTAL: 6.15µl	
RNA (1000ng)	3.85	
	TOTAL: 10µl	

2.8.3. qPCR

Standard qPCR with Sybr Green (Sigma Aldrich, UK), using PCR compatible 96-well plates (MicroAmp Fast Optical 96-well reaction plates, Applied Biosystems, UK) was carried out. PCR plates were run using StepOne Plus Real-Time PCR System (Applied Biosciences). List of primers and master mix used for running the PCR plates can be found in **Table 2.8.3.1** and **2.8.3.2** respectively. A total of 2µl cDNA (or nuclease-free water as a negative control) and 8µl Master mix was added into each well for qPCR. PCR protocol steps are shown below:

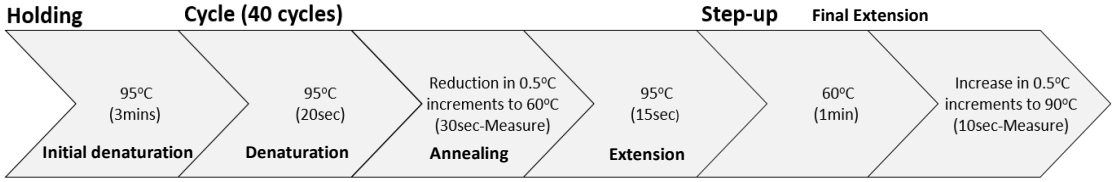

qPCR steps involve; a denaturation step where the double stranded DNA template strands separate, the annealing step where primers bind to the target DNA sequence, and the extension step where new DNA strands are made. This cycle is repeated 40 times for amplification.

Relative gene expression was calculated using Ct values (cut-off point Ct 37) and data were normalised to the housekeeping gene β-actin. Changes in gene expression were presented as an mRNA fold-change in VGCC expression of vehicle control treated (PBS) compared to $A\beta_{1\text{-}42}$ treated cells. Nuclease-free water was used as the negative control (no template control). Reaction specificity (e.g. exclusion of presence of primer-dimers) was done by looking at melting curves.

Table 2.8.3.1: Primer design for VGCC mRNA expression analysis via qPCR. *Previously described primers were used* (Sousa *et al.*, 2013)*. Amplicon size (nt = nucleotides) and primer melting temperature (Tm) are also shown in the table. Primer pairs for β-actin, Cav1.3, Cav1.4, Cav2.1, Cav2.2, Cav3.2, Cav3.3 are exon-exon spanning primers.*

	Forward Primer	**Reverse Primer**
B-actin	5'-CCAACCGCGAGAAGATGA-3'	5'-CCAGAGGCGTACAGGGATAG-3'
(97nt)	Tm: 65.2 º	Tm: 63.5 º
Cav1.1	5'-TCATCCTCAGTGAGATCGACA-3'	5'-TCCACCCAGGCAATACAGTC-3'
(62nt)	Tm: 63.6 º	Tm: 64.9 º
Cav1.2	5'-CGTGGCTGCTCCTCCTATTA-3'	5'-GGCTCCCATAGTTGGAACCT-3'
(103nt)	Tm: 64.1 º	Tm: 64.1 º

Cav1.3	5'-GGCTGGACAGATGTGCTCTAC-3'	5'-CCCAAAGATGACGAGACTGAC-3'
(87nt)	Tm: 63.8 º	Tm: 63.7 º
Cav1.4	5'-AACACACCCCTCAAGAATGC-3'	5'-GCCGTGACACGTCTCCAT-3'
(63nt)	Tm: 63.9 º	Tm: 65.2 º
Cav2.1	5'-TGGAACATCTTCGACTTTGTGA-3'	5'-GCTCAGGTTGATGAAGTTATTCG-3'
(93nt)	Tm: 64.5 º	Tm: 63.6 º
Cav2.2	5'-AACAGAGATTGCGGAAACGA-3'	5'-GATGCGGATGGTGTAGCC-3'
(106nt)	Tm: 64.6 º	Tm: 64.3 º
Cav3.1	5'-GGTGTGGTGGTGGAGAACTT-3'	5'-CATCGTCCAGCATTAGATTCC-3'
(124nt)	Tm: 63.9 º	Tm: 63.3 º
Cav3.2	5'-CGCTGCTCATGCTCTTCAT-3'	5'-AACTTGCAGCCGAAAAGGT-3'
(64nt)	Tm: 64.4 º	Tm: 63.7 º
Cav3.3	5'-CAATGGACTGGATGCTGTTG-3'	5'-ATCCAGGGGTTGTGGTTG-3'
(60nt)	Tm: 64.2 º	Tm: 63.4 º

Table 2.8.3.2: Master Mix for qPCR.

	Volume µl (per well)	**Final Concentration**
FastStart Universal Sybr Green Master (ROX) 2x	5	1x
10µM Forward Primer	0.5	0.5µM
10µM Reverse Primer	0.5	0.5µM
Nuclease-free water	2	-
	TOTAL: 8µL	
cDNA	2	
	TOTAL: 10µL	

2.8.4. PCR gel

qPCR products were subjected to gel electrophoresis in order to identify whether the various VGCCs are expressed within undifferentiated and differentiated SH-SY5Y cells.

Firstly a 1.5% agarose gel was prepared, consisting of 0.9g agarose (Invitrogen/ Thermo Fisher Scientific, UK) and 60ml 1x Tris-acetate-EDTA (TAE; Promega). The agarose mix was subjected to heat (1-3min) to allow complete dissolution and allowed to cool down to 50^{o}C. Sybr 'Safe' 6µl (Invitrogen/ Thermo Fisher Scientific, UK) was then added to the agarose mix, and the agarose was then poured into an agarose gel casting

tray and left to solidify. Samples were run on agarose gels of 7x7cm in size (Mini-Sub Cell GT, BIO-RAD, UK) with space for 15 samples.

For sample preparation, qPCR products (10μl) were mixed with 2μl DNA loading buffer dye (6x; Thermo Fisher Scientific, UK). Additionally, a ladder (ACTGene 100bp PCR DNA ladder; Thermo Fisher Scientific, UK) sample was also prepared, consisting of 2μl DNA ladder, 2μl DNA loading buffer and 8μl nuclease-free water. Once the gel was submerged in 1x TAE, the samples were loaded into the wells. The gels were ran at 70V for approximately 40min, to allow samples to run down ¾ of the gel. Following gel electrophoresis, images of the PCR bands were taken using a gel doc (Syngene U:Genius-3 gel doc).

2.9. Electrophysiology

2.9.1. Cell preparation

For electrophysiology, both SH-SY5Y cells and stably-transfected HEK293 cells were plated on uncoated sterile coverslips (22x22mm) at 1:40, 1:80 or 1:100 dilutions using their corresponding medium. Cells were left to adhere overnight at 37^{o}C and 5% CO_2 in a sterile 6-well plate.

2.9.2. Preparation of glass electrodes

Glass electrodes (O.D. 1.5mm, I.D. 0.86mm, 10cm length borosilicate glass capillaries; Intracel) were fabricated using an Intracel P-1000 micropipette puller. Electrodes used for whole cell patch clamp experiments had a resistance range between 4 and 10 MΩ. Resistance was monitored throughout the duration of the experiment. Glass electrodes were filled with intracellular solution composed of: 120mM CsCl; 20mM TEA; 10mM EGTA; 2mM $MgCl_2$; 10mM HEPES; 2mM ATP (pH 7.2 using CsOH) using a MF34G micro-loader tip (World Precision Instruments), attached to a 0.2μm filter and a non-metallic syringe needle. Glass electrodes were tapped for removal of any bubbles prior to use.

Fresh intracellular solution was prepared approximately each month, and osmolarity (~270 mOsm) was monitored using a standard osmometer (OSMOMAT 030,

Gonotec). The intracellular solution was aliquoted (5ml/vial) and kept at -20^{o}C until use. Whenever needed, an aliquot was thawed and used for a max of 5 days (short-term storage 4^{o}C).

2.9.3. Earth electrode

The earth electrode consisted of a silver chloride wire which was routinely chlorinated to avoid drifting during recording.

2.9.4. Whole-cell patch clamp

Prior to the start of whole-cell patch clamp experiments, coverslips were transferred to a bath containing extracellular solution composed of: 95mM NaCl (ThermoFischer Scientific, UK); 10mM $BaCl_2$; 2mM $MgCl_2$; 10mM HEPES; 10mM glucose; 5mM TEA (pH 7.4 using NaOH). All chemicals for electrophysiology solutions were purchased from Sigma Aldrich (UK), unless otherwise stated. Barium (Ba^{2+}) was used as the 'drive force' to study VGCCs as it is known to keep cells stable and prevent channel inactivation, therefore, allowing the study of the currents for a longer period of time.

Fresh extracellular solution was prepared approximately every month, and osmolarity (~270 mOsm) was measured using an osmometer. The extracellular solution was kept at 4^{o}C for short-term storage. Both intracellular and extracellular solutions were left to reach room temperature (21^{o}C) prior to experimental use.

Once the coverslip was placed in the extracellular solution, the glass electrode was slowly lowered into the extracellular bath (**Fig. 2.9.4.1A**). Prior to this, positive pressure was applied to the glass electrode using a 5ml syringe. The pressure was held via closing the syringe valve. Using the microscope, the glass electrode was then lowered and focused above the cell. Continuous monitoring of pipette offset was carried out, in order to make sure all recordings start at baseline 0pA. Following this, the glass electrode was then slowly lowered onto the cell (**Fig. 2.9.4.1B**). To help achieve a giga-seal (>1GΩ), negative pressure was applied using the syringe, which was released to aid seal formation. Once a giga-seal was formed, resting potential was changed to -70mV (**Fig. 2.9.4.1C**). In order to achieve whole-cell configuration, small negative pressure was then applied via the syringe, to 'break the membrane' (**Fig. 2.9.4.1D**). Cell stability was monitored throughout the experiment.

2.9.5. Whole-cell patch clamp protocols

To study VGCC currents, a multi-step protocol was applied, from a holding potential of -70mV, in 10mV increments from -70 to +50mV (200ms). Data from multi-step recordings were used to plot the current/voltage (I/V) relationship. Additionally, a single-step protocol, to +10mV from a holding potential of -70mV, was also applied. Recordings of cells demonstrating a poor quality seal or high current leakage were not included in data analysis. Extracellular solution was applied via a continuous tube-perfusion system. Working concentration of the various compounds, was achieved using extracellular solution and perfused.

All electrophysiology experiments were carried out at room temperature (~21^{o}C). Whole cell patch clamp recordings were acquired using Axopatch 200B (Axon Instruments), using the software Clampex10.3 via a Digidata 1440A (Axon Instruments). Electrophysiology recordings were analysed using Clampfit10.3.

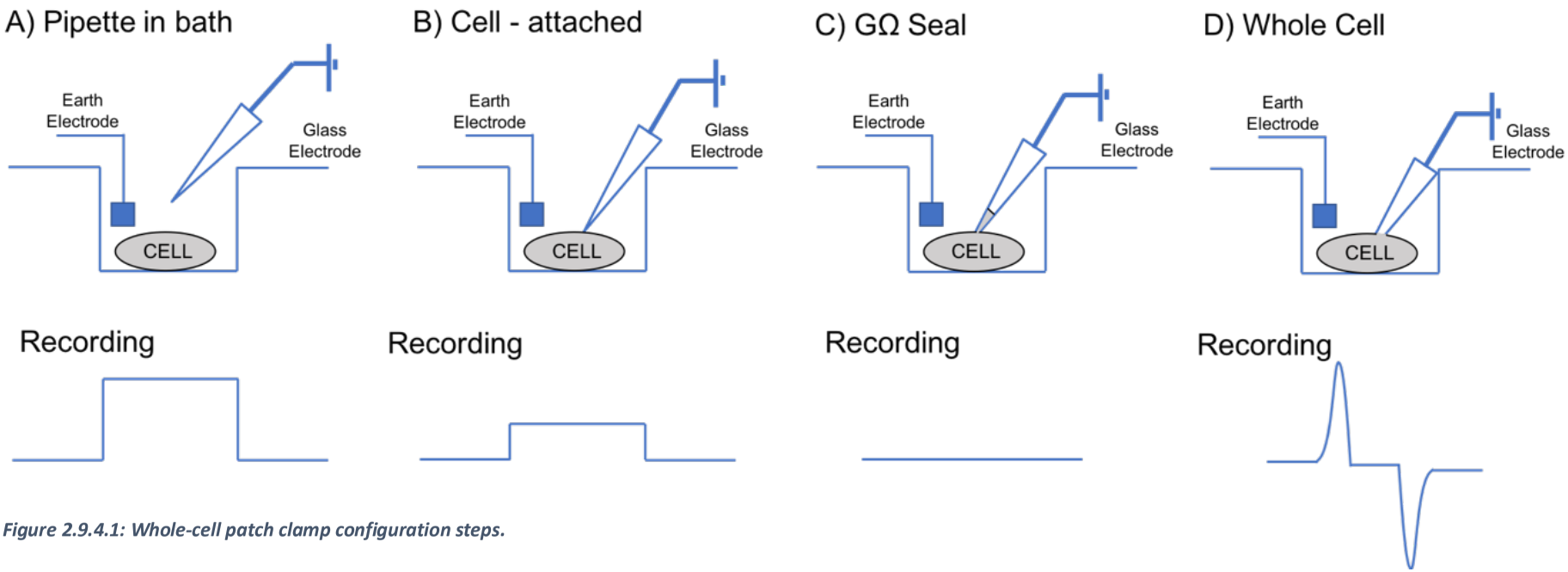

Figure 2.9.4.1: Whole-cell patch clamp configuration steps.

2.10. Statistical Analysis

Statistical analysis and plotting of graphs was performed using GraphPad Prism 7.0. For statistical analysis all data were firstly tested for normality (Shapiro-Wilk) and examined for outliers (Grubb's). Data are plotted as average ± SEM with number of biological replicates (n) stated in Figure legends. At least 3 technical replicates per treatment were performed. Values of $P \leq 0.05$ were considered significant.

For both Aβ protofibril length analysis and cell viability experiments, One-way ANOVA followed by Tukey post-hoc test was used for multiple comparison of data demonstrating normal distribution. For data not following normal distribution unpaired T-test followed by Kolmogorov-Smirnov was used.

For qPCR data comparison of only two treatment groups unpaired Welch T-test was performed.

For electrophysiology experiments, I/V relationships were first fitted with a modified Boltzmann fit equation ($Y=(G_{max}*(X-Vrev))/(1+exp((X-V50)/k))$ (Vogl *et al.*, 2015). Data obtained from the Boltzmann fit analysis were then subjected to one-tailed unpaired Welch T-test for the population studies (Aβ experiments) and one-tailed paired T-test for all other experiments.

Chapter 3: Voltage-gated calcium channel regulation of cell activity

3.1. Introduction

SH-SY5Y human neuroblastoma cells, subcloned from SK-N-SH first isolated from a bone-marrow biopsy in 1970, demonstrate characteristics of an immature neuronal phenotype and can easily be differentiated into terminally differentiated cells (Biedler and Schachner, 1978; Morton *et al.*, 1992; Kovalevich and Langford, 2013; Sousa *et al.*, 2013; de Medeiros *et al.*, 2019). This allows the study of a more representative mature neuronal phenotype, therefore providing an excellent *in vitro* model for use within the neuroscience field and studying neurodegenerative diseases such as AD (Morton *et al.*, 1992; Kovalevich and Langford, 2013; de Medeiros *et al.*, 2019). SH-SY5Y cells can easily be manipulated, expanded, and can be differentiated into specific neurons (Kovalevich and Langford, 2013). Treating cells with 10μM retinoic acid (RTA) for ~3 days is widely used for inducing SH-SY5Y differentiation towards a phenotype more closely representing primary cholinergic neurons. Differentiation consists of changes in cell activity including reduced proliferation and neurochemical phenotype changes such as neurite creation, expression of both neuronal and cholinergic-specific markers (e.g. tyrosine hydroxylase, NeuN, AChE and ChAT) (Lopes *et al.*, 2010; Kovalevich and Langford, 2013; de Medeiros *et al.*, 2019). Additionally, as SH-SY5Y cells are not primary cells, no ethical considerations are linked with their use (de Medeiros *et al.*, 2019).

Both electrophysiological and molecular approaches have shown that SH-SY5Y neuroblastoma cells express VGCCs and therefore are considered a good model for investigating Ca^{2+} homeostasis (Spoerri, Dozier and Roisen, 1990; Morton *et al.*, 1992; Chiou, 2006; Sousa *et al.*, 2013). VGCCs are known to have a role in cell viability, cell proliferation and differentiation, gene expression, and neurotransmission (Chin, 1998; Sinnegger-Brauns *et al.*, 2009; Resende *et al.*, 2010). Due to the involvement of both Ca^{2+} and VGCCs in AD amyloid pathology, as a first step in this study, the expression and the role of the individual VGCCs in neuronal differentiation and survival was investigated. Better understanding of VGCCs involvement in neuronal survival and differentiation can aid our understanding of their role in neurodegenerative diseases such as Alzheimer's.

3.1.1. Aim

The aim of the study was to firstly verify and identify VGCC subtype expression in the neuronal model SH-SY5Y cells, and also identify their role in overall neuronal cell function. Moreover, the effect of physiological CO levels on maintaining neuronal activity in the presence of CCBs was also investigated.

3.1.2. Objectives

- To identify which VGCC subtypes are expressed at mRNA level in SH-SY5Y cells in contrasting differentiation states.
- To investigate which VGCC subtypes have a role in neuronal activity using SH-SY5Y cells in contrasting differentiation states.
- To investigate VGCC expression at the functional level in undifferentiated SH-SY5Y cells.
- To examine the effect of physiological CO levels in neuronal activity using SH-SY5Y cells in contrasting differentiation states.
- To investigate the effect of CO in modulating CCB-mediated changes in neuronal activity using SH-SY5Y cells in contrasting differentiations states.

3.1.3. Hypotheses

- Inhibiting VGCCs using either the global-VGCC blocker $CdCl_2$ or more selective blockers (CCBs) should impair neuronal cell (metabolic) activity.
- CO, through CORM2 treatment, at physiological levels should not impair cell (metabolic) activity.

3.2. Results

3.2.1. VGCC expression profile and activity in neuroblastoma cells

For the purpose of this study, SH-SY5Y neuroblastoma cells of both undifferentiated and RTA-differentiated state were used. Verification of SH-SY5Y differentiation was done via monitoring morphological changes. Morphological observations in this study reveal that undifferentiated cells grow in clusters and show neuroblast-like phenotype, whereas RTA-differentiated cells form processes and therefore appear more elongated, with an accompanied reduction in cell proliferation (**Fig. 3.2.1.1**).

In order to verify that SH-SY5Y indeed express VGCCs, gene expression analysis via PCR was carried out in order to identify which VGCCs were present at mRNA level in both undifferentiated and differentiated SH-SY5Y cells. Representative PCR gels (using end-point qPCR products) revealed mRNA expression of Cav1.2, Cav1.3, Cav2.2 and Cav3.1 within undifferentiated cells (**Fig. 3.2.1.2A**). On the other hand, in differentiated cells a loss in Cav3.1 expression was seen. Moreover, low mRNA expression for Cav1.4 was also detected (**Fig. 3.2.1.2B**). Quantification analysis of the qPCR data revealed no significant fold-change in mRNA expression of Cav1.2, Cav1.3 and Cav2.2 upon SH-SY5Y differentiation (n=7) (**Fig. 3.2.1.3A-C**). Whereas, a significant reduction in Cav3.1 mRNA expression of 0.7 ± 0.1 fold-change was seen upon SH-SY5Y differentiation (n=7; $P<0.0001$) (**Fig. 3.2.1.3D**).

Undifferentiated SH-SY5Y cells (n=6) were also confirmed to express inward currents at the functional level using whole-cell patch clamp recordings (**Fig. 3.2.1.4**).

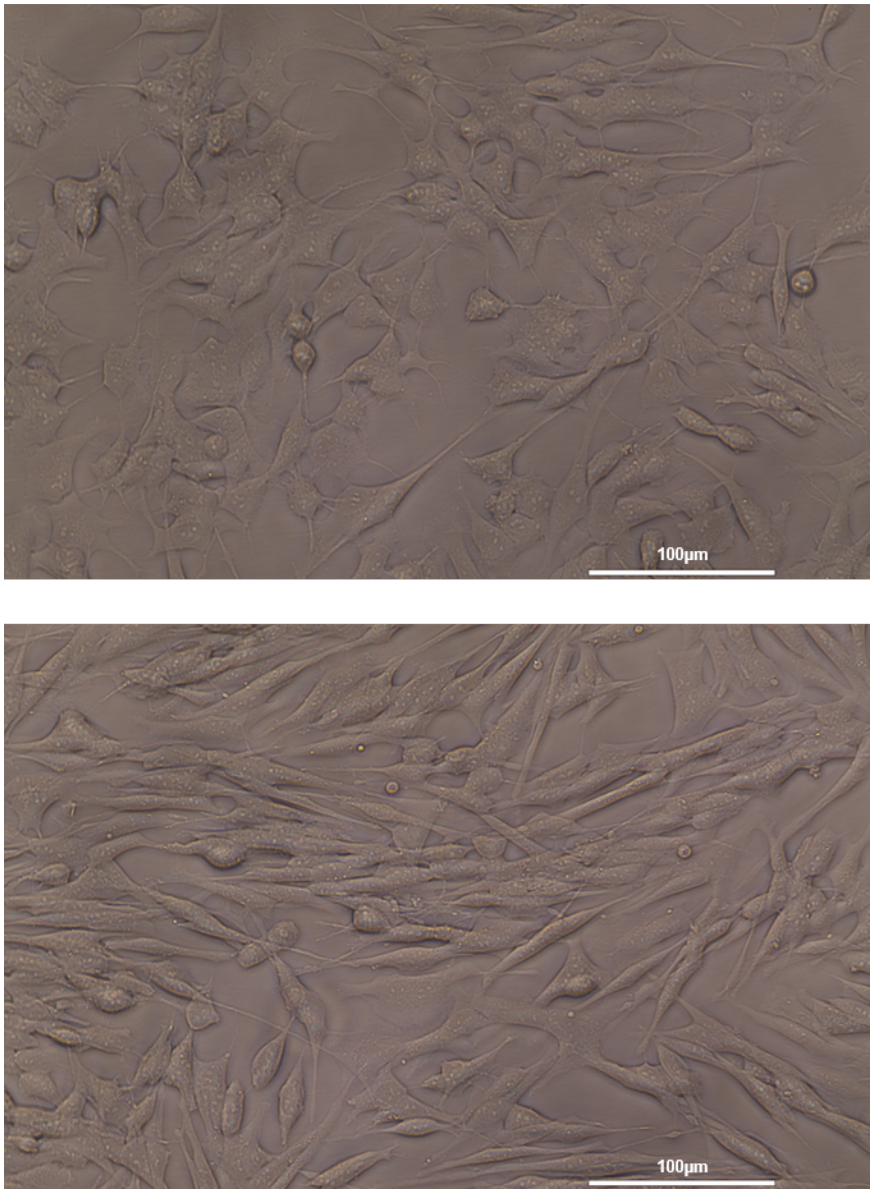

Figure 3.2.1.1: Undifferentiated and RTA-differentiated SH-SY5Y cells. *Representative images of SH-SY5Y cells prior (top panel – undifferentiated) and after 3-day differentiation in the presence of 10µM RTA (bottom panel-differentiated).*

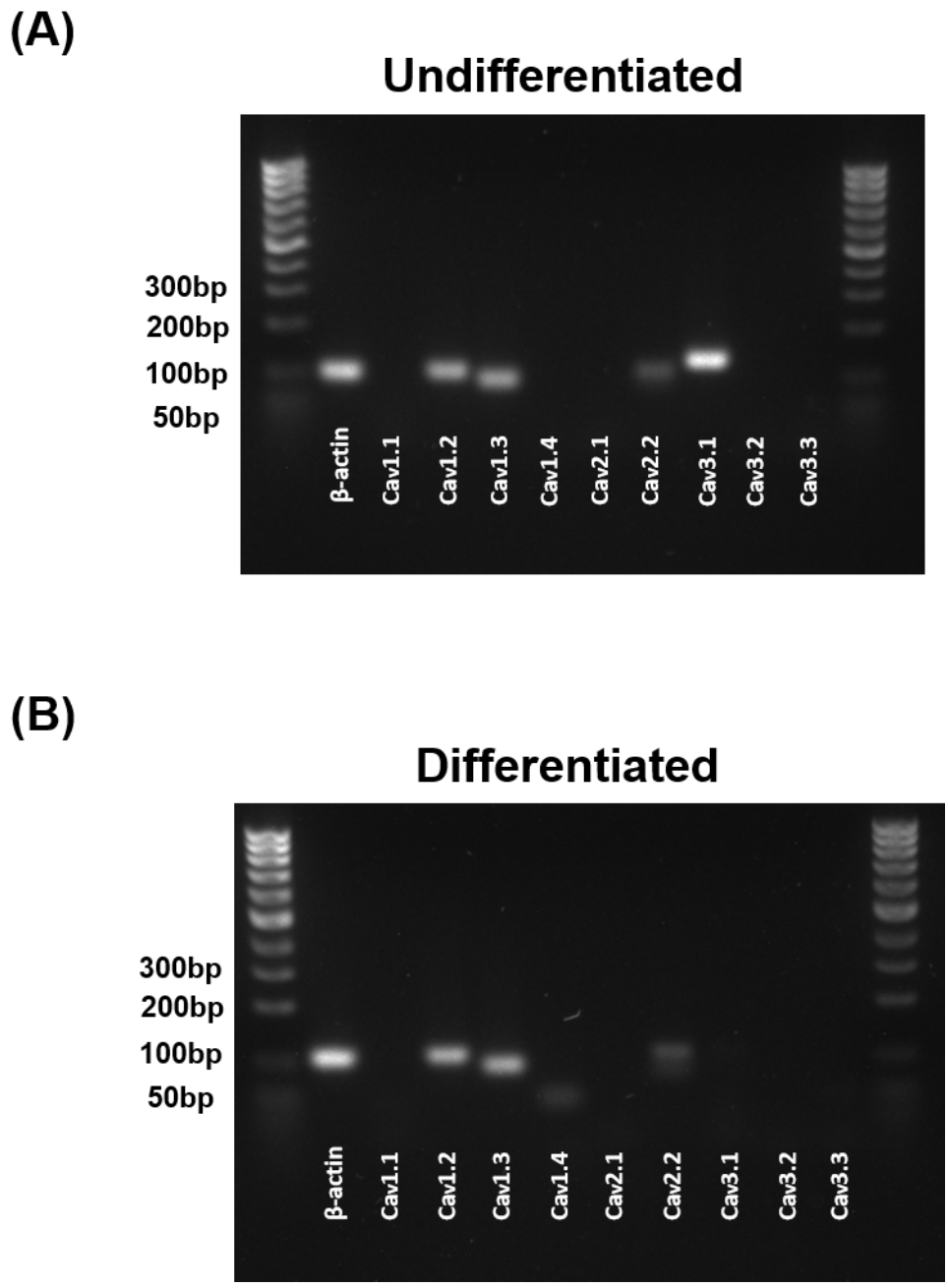

Figure 3.2.1.2: Neuroblastoma VGCC gene expression. *Representative images of gels from end-point qPCR products indicating VGCC mRNA expression in neuroblastoma cells of both differentiation states.* ***(A)*** *Within undifferentiated SH-SY5Y cells Cav1.2, Cav1.3, Cav2.2 and Cav3.1 expression was detected at mRNA level.* ***(B)*** *Within differentiated cells Cav1.2, Cav1.3, Cav1.4, Cav2.2 and a loss of Cav3.1 mRNA expression was observed. For gene expression experiments, B-actin was used as the housekeeping control.*

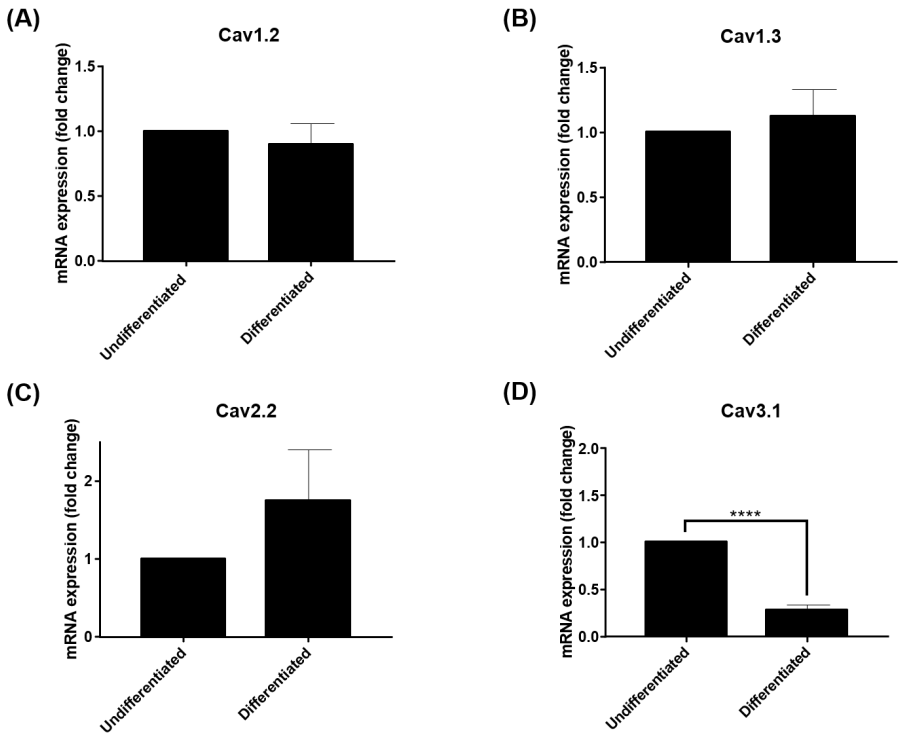

Figure 3.2.1.3: Changes in VGCC expression dependent on neuroblastoma differentiation state. *Changed in VGCC mRNA expression with SH-SY5Y differentiation were investigated via qPCR. No change in the mRNA expression of* ***(A)*** *Cav1.2 (n=7),* ***(B)*** *Cav1.3 (n=7) and* ***(C)*** *Cav2.2 (n=7) was seen with SH-SY5Y differentiation.* ***(D)*** *In contrast, a significant reduction in Cav3.1 (n=7) mRNA expression was seen with SH-SY5Y differentiation. Data (mean ±SEM) were normalized to β-actin and subjected to one-tailed unpaired Welch T-test. (****=P<0.0001)*

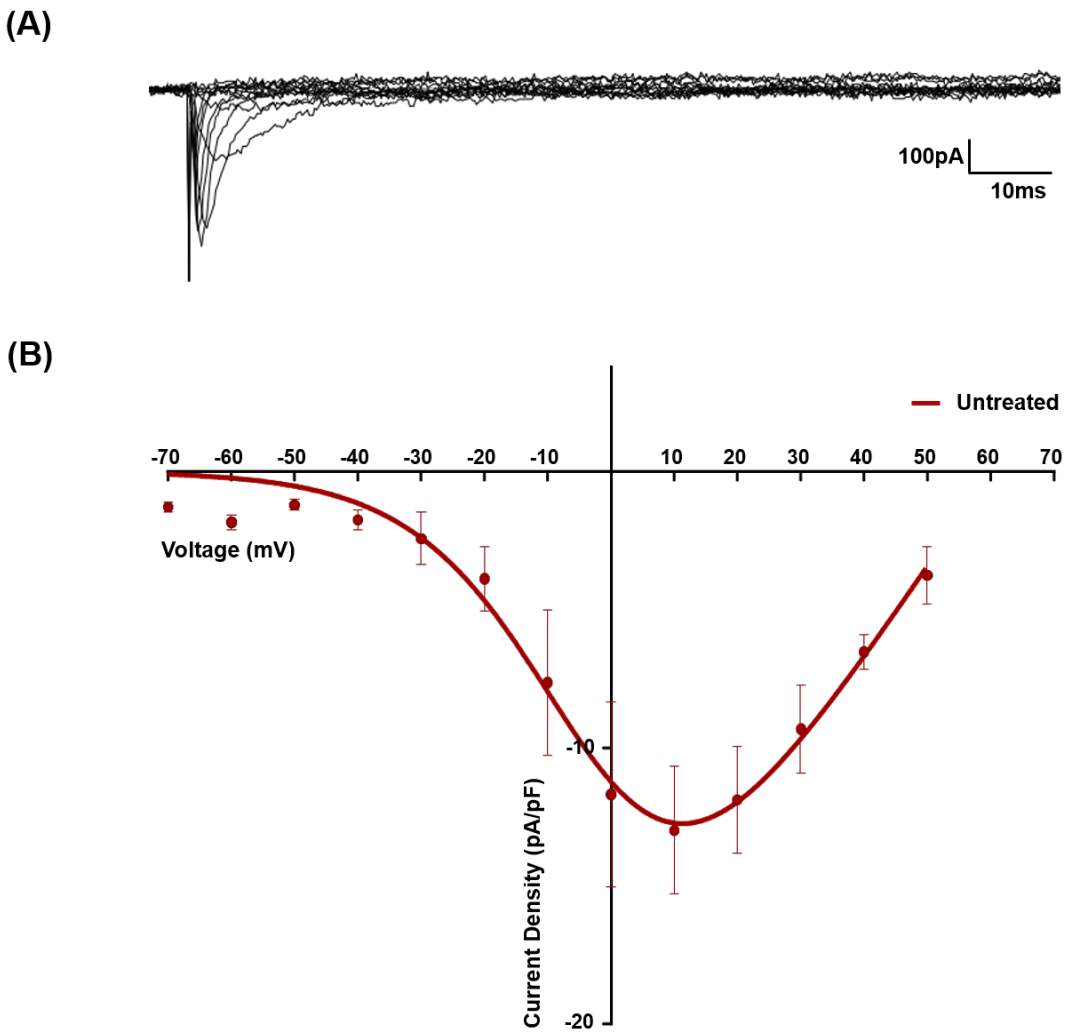

Figure 3.2.1.4: Inward currents in neuroblastoma cells. *Inward currents recorded within undifferentiated SH-SY5Y cells via whole-cell patch clamp.* ***(A)*** *Example trace of a mixture of inward currents recorded within an untreated SH-SY5Y cell (-70 to +50mV at 10mV intervals)* ***(B)*** *Current-voltage relationship of inward currents recorded within undifferentiated SH-SY5Y cells fitted with the Boltzmann fit equation (n=6). Clampfit 10.3 was used for trace analysis, and GraphPad for plotting current-voltage relationship and Boltzmann fit analysis.*

3.2.2. VGCC role in overall cell activity

Ca^{2+} is important in maintaining cell homeostasis, with a number of cellular roles. As a first step in studying calcium homeostasis, the role of VGCCs in cell (metabolic) activity of SH-SY5Y cells of both differentiation states was investigated via XTT and MTT viability assays.

A significant reduction in cell activity by 51.6 ± 8.7% (n=7; P<0.05), 65.0 ± 8.6% (n=5; P<0.01) and 66.2 ± 9.0% (n=5; P<0.01) was seen in undifferentiated SH-SY5Y treated with the global VGCC blocker $CdCl_2$ at 50, 100 and 200μM with the (IC_{50}= 27.7μM) compared to vehicle control treated cells. Within differentiated SH-SY5Y cells, a reduction in activity was seen by 26.4 ± 11.8% (n=5; P<0.05), 70.0 ± 13.5% (n=5; P<0.001) and 70.9 ± 13.5% (n=5; P<0.001) was seen with $CdCl_2$ at 50, 100 and 200μM (IC_{50}= 45.6μM) respectively compared to vehicle control treated cells. Interestingly, lower concentrations of $CdCl_2$ caused a significant increase in RTA-differentiated SH-SY5Y cell activity. A significant increase by 48.3 ± 13.5 (n=5; P<0.05), 58.6 ± 14.3% (n=4; P<0.01) and 46.5 ± 13.5 % (n=5; P<0.05) was seen with $CdCl_2$ at 100nM, 1 and 10μM respectively. Further comparison of changes in cell activity seen by $CdCl_2$ reveal no significant differences between undifferentiated (HillSlope: 2.0 ± 0.9) compared to differentiated (HillSlope: 5.9 ± 18.4) cells (**Fig. 3.2.2.1**).

In order to identify which VGCC subtypes have a role in cell activity, more specific VGCC blockers (CCBs) were used. Within undifferentiated cells a significant reduction in activity was seen with 1μM ω-conotoxin-GVIA (26.5 ± 8.0%; n=3; P<0.05) and 5μM mibefradil dihydrochloride (74.5 ± 6.8%; n=5; P<0.0001), blockers of Cav2 and Cav3 channels respectively. No change in activity of undifferentiated SH-SY5Y cells was seen with 5μM nifedipine (15.5 ± 6.8%; n=5), 10nM ω-conotoxin-GVIA (15.2 ± 6.8%; n=5), 50 or 200nM ω-agatoxin-IVA (21.0 ± 6.8%; n=5 and 15.1 ± 8.0%; n=3) (**Fig. 3.2.2.2A**). Within differentiated cells, a significant reduction in activity was only observed with 1μM ω-conotoxin-GVIA, of 27.5 ± 5.6% (n=5; P<0.001). In contrast to undifferentiated cells, treatment with 5μM mibefradil dihydrochloride did not cause any change in activity of differentiated cells (13.0 ± 5.6%; n=5). No change in activity was seen in differentiated cells with 5μM nifedipine (1.3 ± 5.6%; n=5), 10nM ω-conotoxin-GVIA (4.1 ± 5.6%; n=5),

and 50 or 200nM ω-agatoxin-IVA (3.6 ± 5.6%; n=5 and 5.8 ± 5.6; n=5) treatment compared to vehicle control (**Fig. 3.2.2.2B)**.

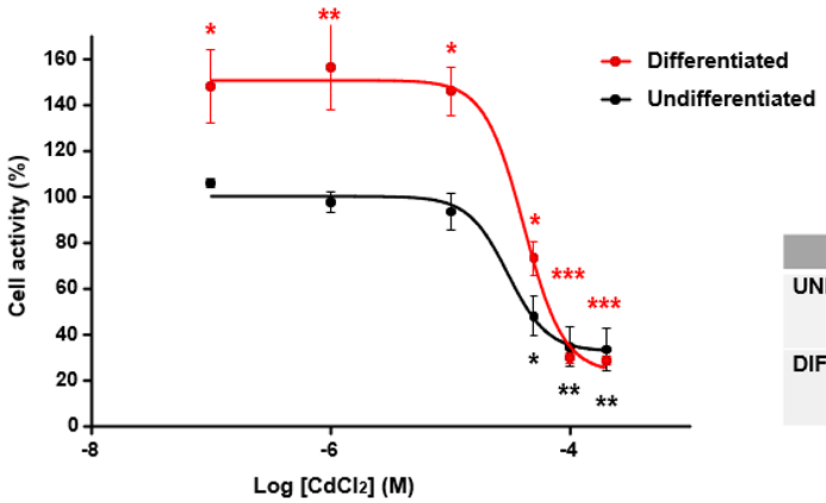

	Hillslope
UNDIFFERENTIATED	2.0 ± 0.9
DIFFERENTIATED	5.9 ± 18.4

Figure 3.2.2.1: $CdCl_2$ mediated cytotoxicity in neuroblastoma cells. *The effect of $CdCl_2$ was investigated in both undifferentiated and RTA-differentiated SH-SY5Y cells via XTT assay. A significant reduction in undifferentiated SH-SY5Y activity was seen with 50, 100 and 200µM (24hr; n=5-7). Within differentiated cells, a similar effect was seen with the same concentrations, whereas 100nM, 1 and 10 µM significantly increased cell activity (24hr; n=5). HillSlope analysis of dose-response curves for undifferentiated and differentiated SH-SY5Y cells treated with $CdCl_2$ revealed no significant difference. Data (mean ±SEM) were normalised to the corresponding vehicle control (dH2O). Statistical analysis for undifferentiated cells was carried out via Kruskal-Wallis and post-hoc Dunn's test. Statistical analysis for differentiated cells was carried out via One-way ANOVA and post-hoc Tukey test. (*=P<0.05, **=P<0.01, ***=P<0.001)*

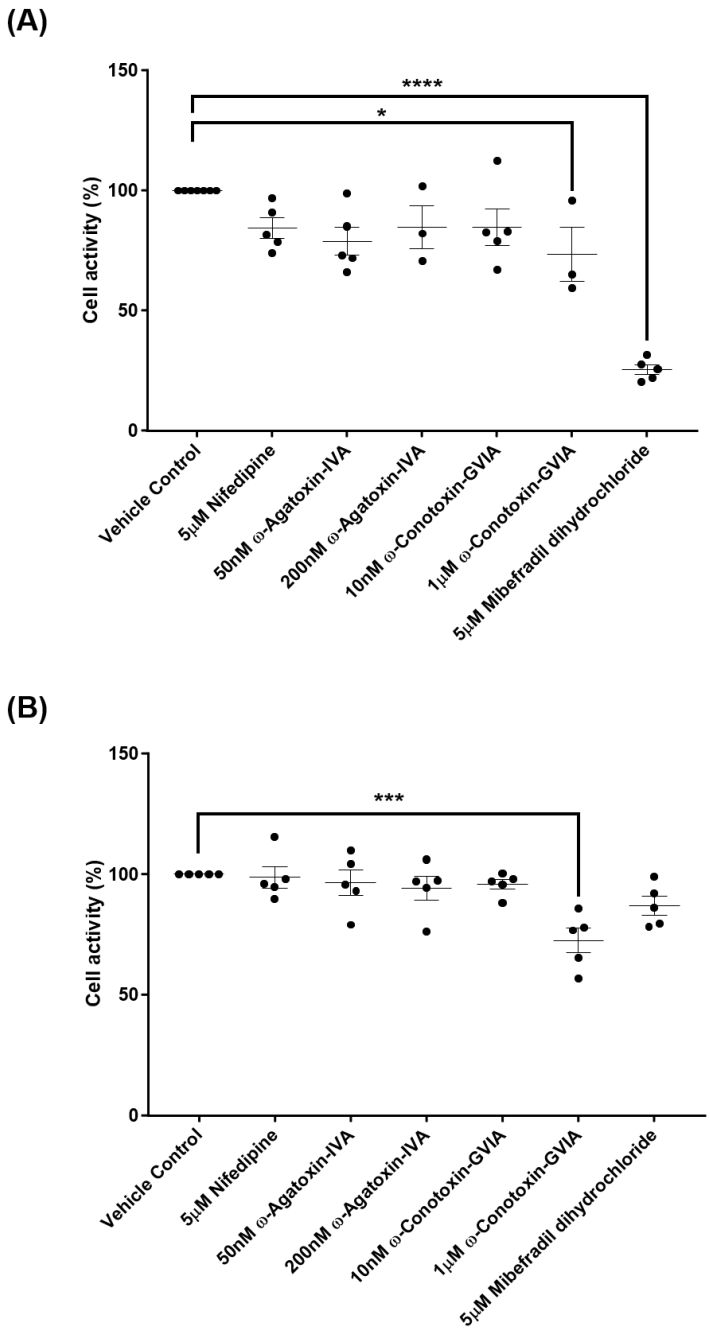

Figure 3.2.2.2: Calcium channel blocker (CCB) mediated cytotoxicity in neuroblastoma cells. *The effect of selective-VGCC blockers was investigated in both undifferentiated and differentiated SH-SY5Y cells via XTT and MTT assay respectively (24hr).* ***(A)*** *A significant reduction in undifferentiated SH-SY5Y viability was observed with 1μM ω–conotoxin-GVIA (n=3) and 5μM mibefradil dihydrochloride (n=5).* ***(B)*** *Within differentiated cells, only 1μM ω–conotoxin-GVIA (n=5) significantly reduced viability. Data (mean ±SEM) were normalised to the corresponding vehicle control (DMSO/dH2O). Statistical analysis was carried out via One-way ANOVA and post-hoc Tukey test. (*=P<0.05, ***=P<0.001, ****=P<0.0001)*

3.2.3. Effect of CO on neuronal cell activity

CORM2, a carbon-monoxide releasing molecule was used to study the effects of CO in SH-SY5Y neuroblastoma cell (metabolic) activity (via MTT) of cells of both differentiation states.

In both undifferentiated and differentiated SH-SY5Y cells, 1-100μM CORM2 (n=5) did not significantly alter cell activity (**Fig. 3.2.3.1A and B**). The positive control 10mM H_2O_2 caused a 97.5 ± 5.6% (n=5; P<0.0001) reduction in undifferentiated SH-SY5Y activity. A similar degree in reduction in activity (97.5 ± 3.9%; n=5; P<0.0001) was also seen when differentiated cells were treated with 10mM H_2O_2.

Similar to CORM2, no change in activity was also observed when the inactive control (1-100μM iCORM2; n=5) was added to SH-SY5Y of both differentiation states (**Fig. 3.2.3.1C and D**). Whereas the 10mM H_2O_2 caused a 97.5 ± 4.2% and 97.4 ± 5.8% (both n=5; P<0.0001) reduction in activity in undifferentiated and differentiated SH-SY5Y cells respectively.

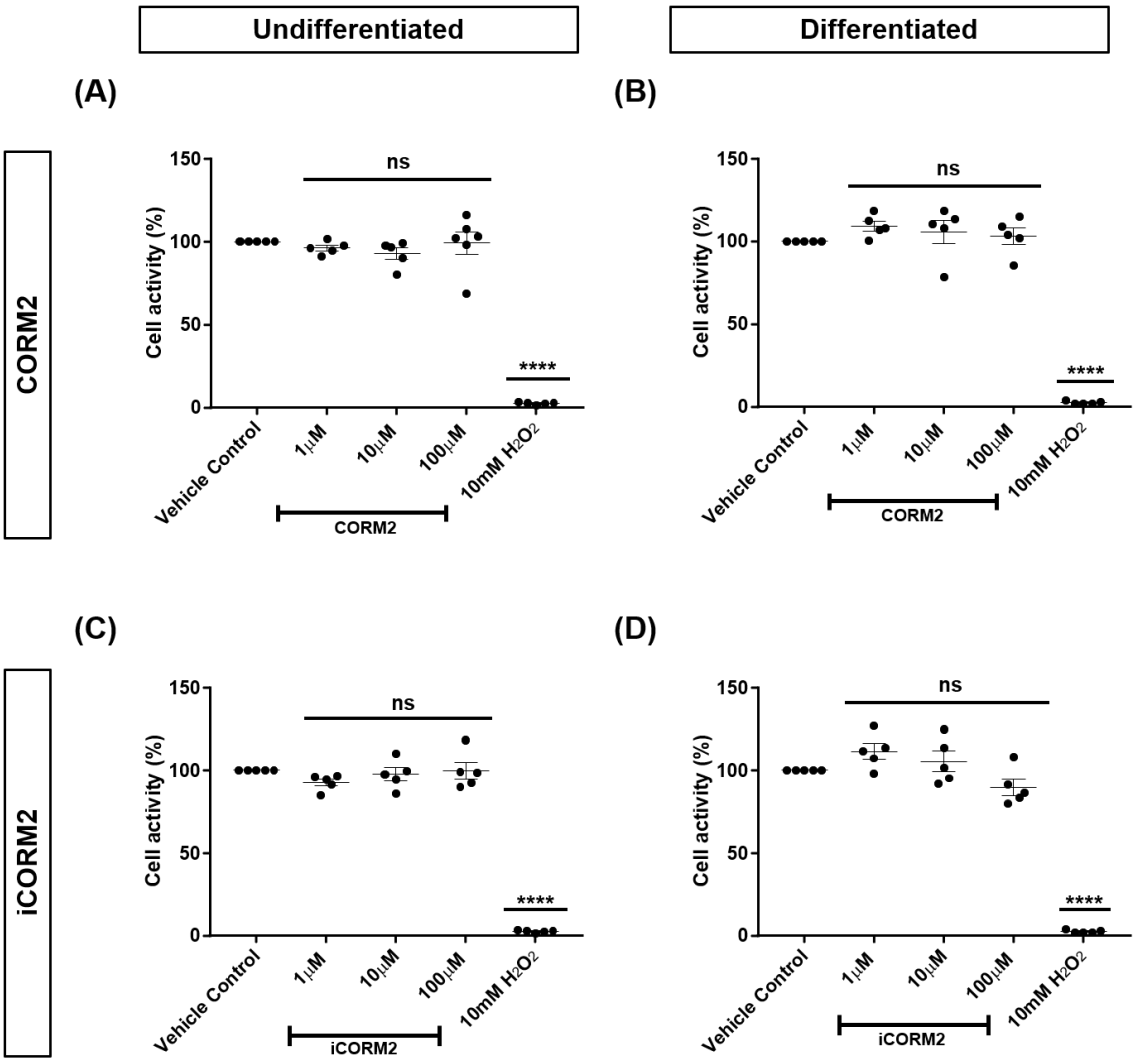

Figure 3.2.3.1: Carbon monoxide (CO) effect on neuroblastoma cells. *The effect of CO, through CORM2, was investigated in neuroblastoma cells of both differentiation states, via MTT assay.* ***(A+B)*** *No significant change in SH-SY5Y activity of both differentiation states was observed with 1- 100μM CORM2 (24hr; n=5).* ***(C+D)*** *No significant change in SH-SY5Y viability of both differentiation states was observed with 1- 100μM inactive control (iCORM2) (24hr; n=5). Hydrogen peroxide (10mM) was used as a positive control in cell activity experiments. Data (mean ±SEM) were normalised to the corresponding vehicle control (DMSO). Statistical analysis was carried out via One-way ANOVA and post-hoc Tukey test. (****=P<0.0001)*

3.2.4. Effect of CO on CCB-mediated changes in cell activity

Following the identification of a distinct VGCC mRNA profile in SH-SY5Y cells dependent on differentiation state, and verifying that CORM2 at the concentrations tested does not alter SH-SY5Y activity, the effect of CO on CCB-mediated changes in cell (metabolic) activity was investigated via MTT assay.

Within undifferentiated and differentiated cells CORM2 (1-100μM; n=5) was unable to prevent changes in cell activity induced by the pan-VGCC blocker $CdCl_2$. $CdCl_2$ alone caused a 81.7 ± 3.3% (n=10; P<0.0001) reduction in undifferentiated SH-SY5Y activity, whereas $CdCl_2$ in combination with 1μM, 10μM and 100μM caused a 79.0 ± 4.2% (n=4), 81.7 ± 4.2% (n=4) and 90.0 ± 3.9% (n=5) reduction, which was not significantly different than $CdCl_2$ treated cells alone. No significant changes in $CdCl_2$-mediated changes in activity were also seen when undifferentiated cells were treated with $CdCl_2$ in combination with 10μM and 100μM iCORM2 (78.3 ± 4.2%; n=4 and 89.5 ± 3.9%; n=5), compared to $CdCl_2$ alone (**Fig. 3.2.4.1A**). Within differentiated cells, $CdCl_2$ alone caused a 52.9 ± 7.7% (n=5; P<0.0001) reduction, whereas $CdCl_2$ in combination with 1μM, 10μM and 100μM iCORM2 caused a 59.3 ± 7.7% (n=5), 55.0 ± 7.7% (n=5) and 71.2 ± 7.7% (n=5) in cell activity in differentiated SH-SY5Y cell activity respectively. No significant change in $CdCl_2$-mediated changes in activity were seen when differentiated cells were treated with $CdCl_2$ in combination with 1μM (49.3 ± 7.7%; n=5), 10μM (52.6 ± 7.7%; n=5) and 100μM iCORM2 (53.3 ± 7.7%; n=5) compared to $CdCl_2$ alone (**Fig. 3.2.4.1B**). Additionally, a significant reduction by 97.7 ± 3.3% (n=10; P<0.0001) in undifferentiated and by 97.4 ± 7.7% (n=5; P<0.0001) in differentiated cell viability were seen with the positive control 10mM H_2O_2.

Similar to $CdCl_2$, 1 and 10μM CORM2 were also unable to prevent changes in cell activity induced by CCBs (n=4) in both undifferentiated (**Fig. 3.2.4.2A-D**) and differentiated SH-SY5Y cells (**Fig. 3.2.4.3A-C**). Additionally, 10mM H_2O_2 caused a significant reduction in cell activity by 95.7 ± 11.5% (n=4; P<0.0001) in undifferentiated and by 95.8 ± 7.7% (n=4; P<0.0001) in differentiated cells.

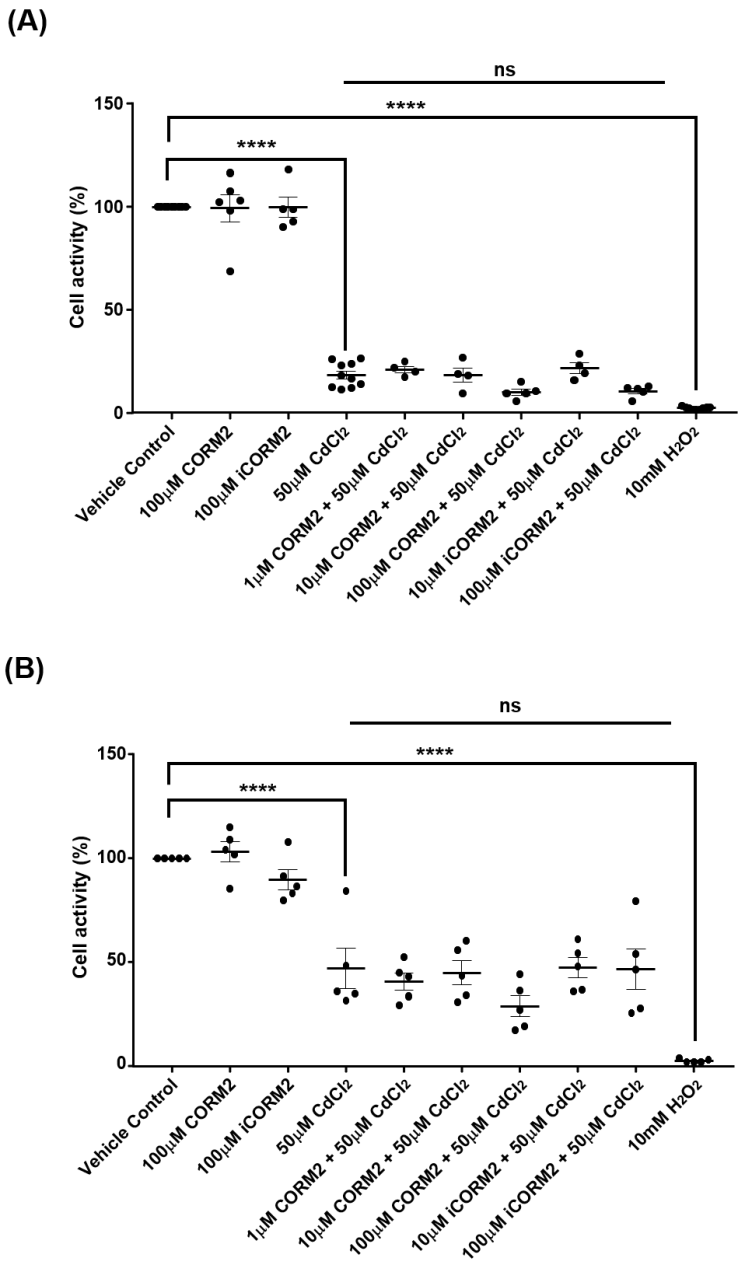

Figure 3.2.4.1: CO effect in modulating $CdCl_2$ mediated neurotoxicity. *The effect of CO, via CORM2, was investigated on $CdCl_2$ mediated changes in cell activity, via MTT assay. Both (1-100μM) CORM2, and its inactive form (10 and 100μM) were unable to prevent reduction in activity, mediated by 50μM $CdCl_2$ in both* ***(A)*** *undifferentiated (n=5-10) and* ***(B)*** *differentiated SH-SY5Y cells (24hr; n=5). A significant reduction in activity was observed with the positive control 10mM H_2O_2. Data (mean ±SEM) were normalised to the corresponding vehicle control (DMSO + dH2O). Statistical analysis was carried out via One-way ANOVA and post-hoc Tukey test. (****=P<0.0001)*

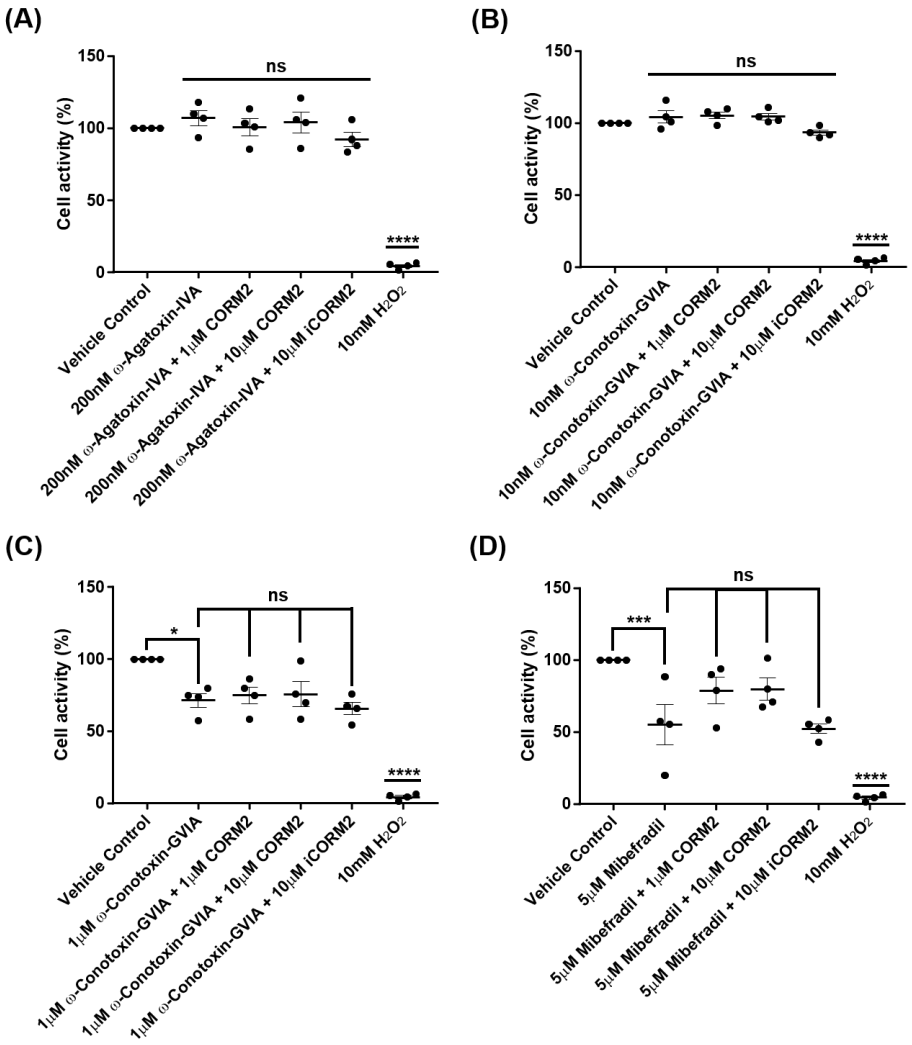

Figure 3.2.4.2: CO effect in modulating CCB mediated neurotoxicity in undifferentiated SH-SY5Y cells. *The effect of CO, via CORM2 was investigated on CCB mediated changes in cell activity, via MTT assay. Both (1 and 10μM) CORM2, and its inactive form (10 μM) were unable to prevent changes in cell activity mediated by* ***(A)*** *200nM ω-agatoxin-IVA* ***(B)*** *10nM ω-conotoxin-GVIA* ***(C)*** *1μM ω-conotoxin-GVIA, and* ***(D)*** *5μM mibefradil dihydrochloride (24hr; n=4). A significant reduction in activity was observed with the positive control 10mM H_2O_2. Data (mean ±SEM) were normalised to the corresponding vehicle control (DMSO + dH2O). Statistical analysis was carried out via One-way ANOVA and post-hoc Tukey test. (***=P<0.001, ****=P<0.0001)*

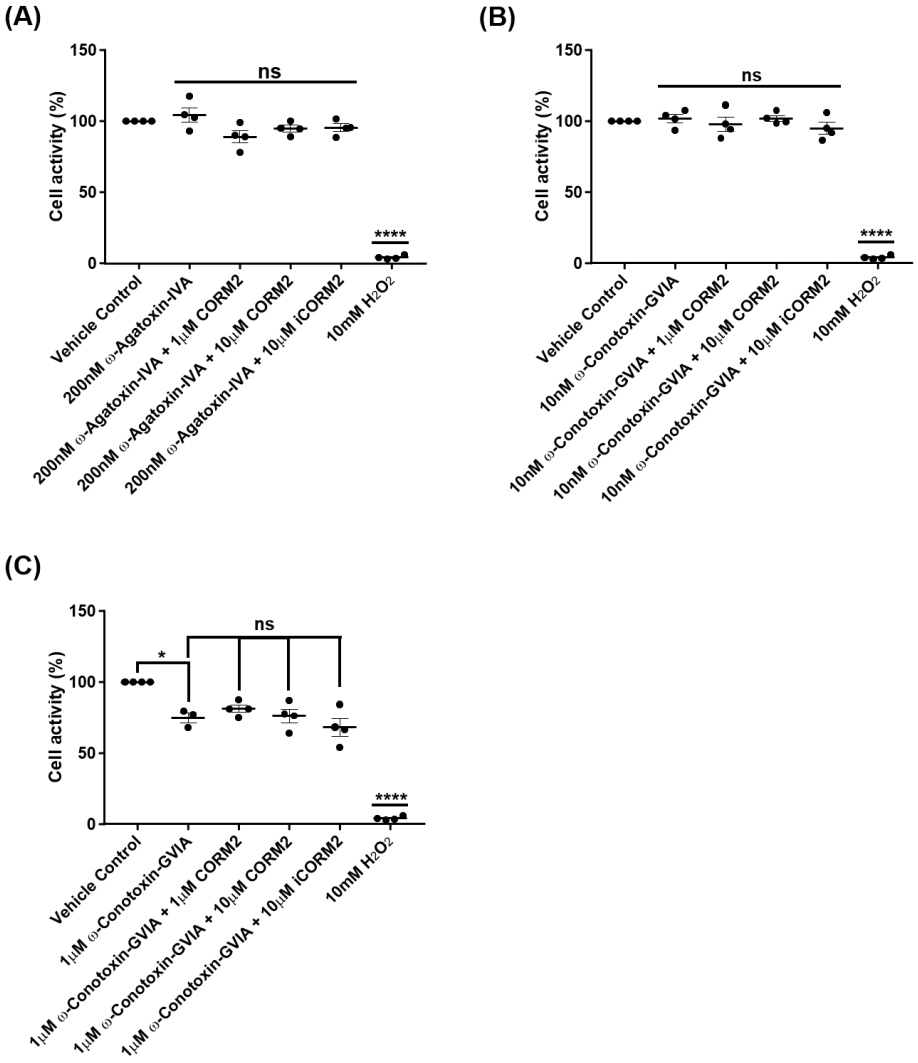

Figure 3.2.4.3: CO effect in modulating CCB mediated neurotoxicity in differentiated SH-SY5Y cells. *The effect of CO, via CORM2 was investigated on CCB mediated changes in cell activity, via MTT assay. Both (1 and 10μM) CORM2, and its inactive form (10 μM) were unable to prevent changes in cell activity mediated by* ***(A)*** *200nM ω-agatoxin-IVA* ***(B)*** *10nM ω-conotoxin-GVIA* ***(C)*** *1μM ω-conotoxin-GVIA (24hr; n=4). A significant reduction in activity was observed with the positive control 10mM H_2O_2. Data (mean ±SEM) were normalised to the corresponding vehicle control (DMSO + dH2O). Statistical analysis was carried out via One-way ANOVA and post-hoc Tukey test. (*=P<0.05, ****=P<0.0001)*

3.3. Discussion

VGCC expression in neuroblastoma cells

- *Morphological observations verify retinoic acid-dependent SH-SY5Y differentiation.*
- *VGCC gene expression profile in SH-SY5Y cells of both differentiation states reveals loss of Cav3.1 expression with cell differentiation, resembling VGCC expression in neurons with roles in neuronal development and differentiation.*

For the purposes of this study, SH-SY5Y neuroblastoma cells in both undifferentiated and RTA-differentiated state were used as *in vitro* neuronal models for studying neurodegeneration. As a first step, SH-SY5Y RTA-differentiation was verified via monitoring morphological changes. Morphological observations in this study reveal that undifferentiated SH-SY5Y cells grow in clusters and show neuroblast-like phenotype. By contrast, RTA-differentiated cells form processes and therefore appear more elongated, with an accompanied reduction in cell proliferation. In support of this, previous research where RTA was added to SH-SY5Y cells as a methodology to induce cell differentiation, revealed similar morphological changes (Lopes *et al.*, 2010; de Medeiros *et al.*, 2019). These findings support the use of SH-SY5Y as an immature neuronal cell line model that can be differentiated into neuronal-like cells more closely resembling primary neurons for studying AD.

Similar to primary neurons, SH-SY5Y cells are known to express an array of VGCC subtypes, with evidence indicating that VGCC-dependent Ca^{2+} influx is important in regulating neuronal survival, development and differentiation (Spoerri, Dozier and Roisen, 1990; Morton *et al.*, 1992; Reeve, Vaughan and Peers, 1994; Pravettoni *et al.*, 2000; Chiou, 2006; Resende *et al.*, 2010; Sousa *et al.*, 2013; Aguado *et al.*, 2016). In the current study, expression of Cav1.2, Cav1.3, Cav1.4 (very low), Cav2.2 and Cav3.1 at gene level was noted in undifferentiated cells. Whereas RTA differentiation led to a significant reduction or even in some instances, complete loss of Cav3.1 expression. Lack of expression of Cav1.1, Cav2.1, Cav3.2 and Cav3.3 within SH-SY5Y of both differentiation states could indicate either complete lack of expression or primer failure. In support of a role for VGCCs in neuronal development and differentiation, Spoerri and colleagues revealed that VGCC-dependent Ca^{2+} influx is needed for mouse neuroblastoma Neuro-2A cell neuritogenesis, assessed via cell imaging and use of pharmacological tools (Spoerri, Dozier and Roisen, 1990). Agreeing with findings in this study, differential VGCC expression profile is observed dependent on the stage of cell

development and differentiation (Spoerri, Dozier and Roisen, 1990; Morton *et al.*, 1992; Reuveny and Narahashi, 1993; Reeve, Vaughan and Peers, 1994; Pravettoni *et al.*, 2000; Bertolesi *et al.*, 2003; Sousa *et al.*, 2013).

In this study, gene expression analysis revealed Cav1 VGCC α1 subunit mRNA expression for only Cav1.2 and Cav1.3 in both undifferentiated and differentiated SH-SY5Y cells, indicative of either very low or no expression for Cav1.1 and Cav1.4. Whole-cell patch clamp recordings reveal a mixture of inward currents, which once plotted with the Boltzmann fit analysis, I/V relationship resembles HVA currents, with similar biophysical properties (activation voltage (V) and Vmax) to Cav1 channels recorded as those noted by Reeve and colleagues in undifferentiated SH-SY5Y cells (Reeve, Vaughan and Peers, 1994). It is known that in contrast to their Cav2 and Cav3 counterparts, Cav1 channels are not as widely expressed within the CNS (Chin, 1998; Resende *et al.*, 2010; Aguado *et al.*, 2016). Despite this, Cav1 channels play a key role in neuronal proliferation, development and subsequent differentiation (Chin, 1998; Resende *et al.*, 2010; Aguado *et al.*, 2016). In support to findings in the current study, as Cav1.1 is predominantly expressed in skeletal muscle (Striessnig *et al.*, 2014), it is expected that very low or no expression at all for Cav1.1 will be seen in neuronal cell lines such as SH-SY5Y cells. Evidence has shown that Cav1 channels not only have a role at early stages of neuronal development such as neurite outgrowth and synapse formation, but also in gene transcription (eg CREB-dependent transcription) and subsequent regulation of synaptic plasticity and strengthening of differentiated neurons (Spoerri, Dozier and Roisen, 1990; Pravettoni *et al.*, 2000; Bertolesi *et al.*, 2003; Zhang *et al.*, 2006; Striessnig *et al.*, 2014). In support of this, when murine CSC (embryonal carcinoma) and MSC (mesenchymal) stem cells were induced to undergo neuronal differentiation, BayK8644 Cav1 agonist increased cell proliferation and neuronal differentiation as assessed via monitoring nestin levels, a marker of neuronal development and differentiation (Resende *et al.*, 2010). In contrast, Cav1 blockers such as nifedipine reduced cell proliferation and neuronal differentiation (Resende *et al.*, 2010). Therefore, in this study expression of Cav1 channels within undifferentiated cells may suggest a role for Cav1 in cell proliferation and development. In further support of findings in this study where expression of Cav1.2 and Cav1.3 is detected within undifferentiated neuroblastoma cells, in 1992, Barnes and Haynes confirmed the expression of Cav1 channels at the

functional level within undifferentiated Y79 retinoblastoma cells, which are capable of undergoing neuronal differentiation (Barnes and Haynes, 1992). This suggests a role for Cav1 channels at early stage of neuronal development. More recently, a rodent whole brain genome analysis study revealed very low mRNA expression for Cav1.1 and Cav1.4 in comparison to Cav1.2 and Cav1.3 in the CNS (Sinnegger-Brauns *et al.*, 2009). Cav1.2 and Cav1.3 are expressed throughout the hippocampus, and are also detected in the cerebral cortex and cerebellum, with Cav1.2 being the most expressed L-type channel in the CNS (Hell *et al.*, 1993). A 2014 review conducted by Striessnig *et al.*, revealed that the majority of L-type channels expressed in the brain are Cav1.2, with approximately 10% due to Cav1.3 and that site of expression is predominantly postsynaptic (Striessnig *et al.*, 2014). Moreover, recently, alternative splicing of the VGCC α1 subunit has been identified as a factor that can add heterogeneity in VGCC subtype expression in the CNS (Bock *et al.*, 2011). These observations support this study where expression of only Cav1.2 and Cav1.3 was detected in SH-SY5Y cells of both differentiation states, confirming SH-SY5Y cells as an appropriate 'neuronal' cell model closely resembling VGCC expression seen in primary neurons, and therefore an excellent *in vitro* model for studying neurodegeneration. Sousa *et al.* (2013) revealed that from the Cav1 subfamily, only Cav1.3 mRNA expression was detected in undifferentiated SH-SY5Y cells, with expression also confirmed at the functional level via binding assays and the use of pharmacological tools (Sousa *et al.*, 2013). Although in our study Cav1.2 expression was also detected, possible explanations for discrepancies within this study and the study conducted by Sousa *et al.*, could be due to differences in the cell line supplier, heterogeneity within the cell population, and also Sousa *et al.* failed to specify whether the cDNA synthesized underwent any dilutions prior to PCR, therefore Cav1.2 although expressed might have been too low for detection. Gene expression detection via qPCR here, rather than conventional PCR could be more sensitive in picking up expression of genes at very low levels. In further support of our findings, a previous study on undifferentiated SH-SY5Y cells, confirmed mRNA expression of Cav1.3, with lower Cav1.2 expression which remained undetected in some technical experimental repeats (Chiou, 2006), suggesting heterogeneity within the cell population. In agreement to this study, where Cav1.2 and Cav1.3 mRNA expression was also confirmed not only in undifferentiated, but also differentiated cells, findings by Morton *et al.* (1992), revealed

functional Cav1 channels within RTA-differentiated SH-SY5Y cells, although which Cav1 subtypes are present was not addressed.

It is known that Cav2 channels are highly expressed in the CNS, with the predominant Cav2 channels being Cav2.2 which is found throughout the brain (Sheng *et al.*, 1996; Chin, 1998; Pravettoni *et al.*, 2000). In this study, from the Cav2 channel subfamily only mRNA expression of Cav2.2 α1 subunit was detected in both undifferentiated and differentiated SH-SY5Y cells. Given the lack of evidence for Cav2.3 expression in neuroblastoma cells, and due to its limited expression in various parts of the nervous system (Schneider *et al.*, 2005; Sousa *et al.*, 2013), Cav2.3 expression was not investigated in this study. Numerous studies have linked Cav2 channels to neuronal development (Pravettoni *et al.*, 2000). In contrast to neurite outgrowth during early stages of neuronal development which requires Cav1 channel opening, Cav2.2 channels are needed at later stages, such as during synaptic vesicle recycling (Pravettoni *et al.*, 2000). In support of findings from this study, Sousa *et al.* (2013) confirmed Cav2.2 expression at both mRNA and protein level, evident from electrophysiology and CCB radioligand binding assays, whereas no mRNA expression was detected for Cav2.1 and Cav2.3 in undifferentiated SH-SY5Y cells (Sousa *et al.*, 2013). Cav2 channels have also shown a prominent role in terminally differentiated cells (Pravettoni *et al.*, 2000). Neurotransmitter release, seen in differentiated neurons, is highly regulated by Cav2 channels (Sheng *et al.*, 1996; Pravettoni *et al.*, 2000; Kamp *et al.*, 2005). For example, Sheng *et al.*, in isolated rat brain synaptosomes, revealed that Cav2.2 channels are able to interact with syntaxin and SNAP25, and consequently participate in neurotransmitter release (Sheng *et al.*, 1996). Therefore, in support of a role for Cav2 channels in terminally differentiated cells, in this study, Cav2.2 expression was also confirmed within RTA-differentiated SH-SY5Y cells which are known to express synaptic markers once they undergo terminal differentiation (Kovalevich and Langford, 2013; Teppola *et al.*, 2016; Jahn *et al.*, 2017).

In contrast to the expression of both Cav1 and Cav2 channels and their role in neuronal development and differentiation, studies agree that expression of Cav3 channels is primarily observed within undifferentiated cells, with a proposed role for Cav3 channels in cell proliferation and development prior to cells undergoing terminal differentiation (Barnes and Haynes, 1992; Bertolesi *et al.*, 2003; Aguado *et al.*, 2016; Kim

et al., 2018). Findings in this study indicate a significant reduction, or in some instances a complete loss of Cav3.1 mRNA expression upon cell differentiation. Cav3.2 and Cav3.3 were not detected in SH-SY5Y of either differentiation states. Evidence from studies conducted on neural progenitor cells (NPCs) isolated from Sprague-Dawley rat embryos, reveal only Cav3.1 and Cav3.2 mRNA expression at early embryonic stages of development compared to later stages of neuronal development in the cortex (Kim *et al.*, 2018). This agrees with findings from this study, and the notion that Cav3 channels are needed at early stages for cell proliferation and for induction of differentiation, where differentiation may lead to either a loss or reduction in Cav3 expression. In further agreement, previous studies have revealed Cav3.1 and Cav3.2 gene expression in Y79 retinoblastoma cells is significantly reduced when cells are induced to terminally differentiate into neurons (Barnes and Haynes, 1992; Bertolesi *et al.*, 2002). Bertolesi *et al.* detected significantly higher expression of Cav3.1 compared to Cav3.2 in undifferentiated Y79 cells (Bertolesi *et al.*, 2002). Differences in findings within these studies and our study could be due to differences in the primers used, and also although Cav3.2 mRNA expression was not detected, Cav3.2 might still be expressed in SH-SY5Y cells, but at very low levels. Cav3 channels are also known to have a role in cell viability and proliferation (Valerie *et al.*, 2013). In support of this, a study conducted by Valerie and colleagues showed that siRNA-induced knock-down of all Cav3 subtypes can result in a reduction in glioblastoma cell number (Valerie *et al.*, 2013). Immunohistochemistry analysis revealed high expression of Cav3.1 in the cerebellum and Cav3.3 in the hippocampus of mice (Aguado *et al.*, 2016; Dumenieu *et al.*, 2018). It is known that Cav3.2 is primarily expressed in cardiac, kidney and liver cells, and not predominantly found in neurons like the other Cav3 counterparts (Striessnig *et al.*, 2014). Consistent with findings from this study, and further supporting the expression and role of Cav3 channels in cell proliferation in undifferentiated cells, Sousa *et al.* only detected Cav3.1 mRNA expression out of all the members of the Cav3 subfamily within undifferentiated SH-SY5Y cells (Sousa *et al.*, 2013).

To conclude, in support of only Cav1.2 and Cav1.3 expression of the Cav1 family detected in the CNS, this study has detected Cav1.2 and Cav1.3 at transcript level in SH-SY5Y cells of both differentiation states. Moreover, in agreement with the role of Cav2 channels during neuronal development, and more specialised neuronal functions such

as neurotransmission following neuronal differentiation, Cav2.2 was detected in SH-SY5Y of both differentiation states. Lastly, Cav3 channels have been shown to have an important role during early stages of neuronal development and differentiation, suggesting that terminal differentiation would cause loss or reduction in expression. Indeed, in this study, SH-SY5Y differentiation led to a significant reduction in Cav3.1 expression. These findings provide evidence that SH-SY5Y VGCC expression profile is similar of that seen in undifferentiated cells capable of undergoing neuronal differentiation, and terminally differentiated neurons, therefore supporting the use of SH-SY5Y cells to study neurodegeneration.

VGCC role in cell survival and activity

- *Global VGCC blocker $CdCl_2$ significantly alters SH-SY5Y activity of both differentiation states.*
- *Selective CCBs reveal a role for Cav2.2 and Cav3.1 in SH-SY5Y cell activity and survival.*

A plethora of studies have investigated the role of Cd^{2+}, a metal divalent ion, in calcium-related induced neurotoxicity in primary neurons and neuronal cell lines via a VGCC-dependent manner, with different signalling cascades being proposed (Swandulla and Armstrong, 1989; Chow, 1991; Thévenod and Jones, 1992; Taylor, Batten and Peers, 1999; Xu *et al.*, 2011; Saddala *et al.*, 2017). In this study, treatment with the pan-VGCC modulator $CdCl_2$ led to a concentration-dependent reduction in cell (metabolic) activity in SH-SY5Y cells of both differentiation states, with a significant reduction seen from 50μM $CdCl_2$. Studies in the late 1990s, conducted in chicken sensory neurons and frog sympathetic neurons, reveal that the effect of Cd^{2+} (20 and 1μM respectively) is voltage-dependent, with Cd^{2+} modulating VGCCs during their activation state, changing this into 'an opened blocked state' (Swandulla and Armstrong, 1989; Thévenod and Jones, 1992). Inhibition could be reversed at very high hyperpolarised or positive voltage values (Swandulla and Armstrong, 1989; Thévenod and Jones, 1992). Further studies proposed that Cd^{2+}, at high μM concentrations, can reversibly block squid calcium currents by permeating the VGCC pore and binding onto a specific site in the pore, hence preventing the entry of Ca^{2+} (Chow, 1991). Similarly to findings in this study where reduction in cell activity was seen from 50μM $CdCl_2$ and higher, Taylor and colleagues demonstrated that Cav2.2-dependent Ca^{2+} influx in PC12 (pheochromocytoma) cells was inhibited by 200μM Cd^{2+} (Taylor, Batten and Peers, 1999). In a study where CHO cells were stably transfected with the Cav1 channel, acute treatment with 50-100μM Cd^{2+} caused cell death due to accumulation of Cd^{2+} intracellularly, an effect that could be blocked with the Cav1 blocker nimodipine, suggesting that Cd^{2+} can cause cell apoptosis through a VGCC-dependent manner at μM concentrations (Marchetti, 2013). Building on this, more recently, Saddala and colleagues demonstrated that use of the Cav1 blocker amlodipine was able to prevent Cd^{2+} entry through VGCCs, and therefore neurotoxicity, by acting as a $CdCl_2$ antagonist preventing its binding onto the VGCC pore (Saddala *et al.*, 2017). Due to the important role of VGCCs in cell activity and survival, taken together, these findings suggest that the concentration-dependent reduction in cell activity seen in this study is due to $CdCl_2$ modulation of VGCCs. In contrast to other

studies, Xu *et al.* (2011) demonstrated that $CdCl_2$,in a concentration-dependent manner (>2.5μM), induced cell death of SH-SY5Y, PC12 and primary mouse neurons partly through an increase in intracellular Ca^{2+}, and subsequent activation of MAPK (mitogen-activated protein kinase) and mTOR (mammalian target of rapamycin) pathways, mediated by ROS release and oxidative stress (Xu *et al.*, 2011). Although unlike other studies Xu and colleagues proposed Cd^{2+} neurotoxic mechanism partly involves an increase in Ca^{2+} influx from the extracellular, rather than a reduction, the manner by which $CdCl_2$ directly modulates VGCCs at the functional level was not investigated. Differences in findings between Xu *et al.* 2011 compared to other studies could be due to differences in the metholodology such as treatment duration. For example, Xu and colleagues studied the effect of Cd^{2+} over 24hr whereas studies involving electrophysiology experiments investigated the effect of Cd^{2+} over a short period of time (<1hr) suggesting that Cd^{2+} may have differential effect on VGCCs dependent on treatment duration.

In order to further investigate and identify the role of specific VGCC subtypes in regulating cell (metabolic) activity, a number of studies have used pharmacological tools with a higher degree of selectivity. In the current study, Cav2.2 and Cav3.1 channels, as revealed by pharmacological blockage by ω-conotoxin-GVIA and mibefradil respectively, have been identified as VGCCs with an important role in SH-SY5Y viability and activity. Calcium dyshomeostasis has been linked to cancer progression (Zawadzki *et al.*, 2008). In 2015, a meta-analysis, using a microarray database, showed that in a number of cancers, a change in the expression of various VGCC isoforms is detected; this indicates a pivotal role for VGCCs in promoting cell survival and growth (Valerie *et al.*, 2013; Wang *et al.*, 2015). For example, in glioblastomas a 5.8 fold upregulation of Cav2.1 gene expression was detected (Wang *et al.*, 2015). Similarly, an upregulation in Cav3 expression is also detected in glioblastoma tumours (Valerie *et al.*, 2013). A study conducted on both primary colon cancer cells and a widely-used colon cancer cell line (HT-29), revealed that use of the Cav1 agonist Bay K8644 induced cell death in a manner involving increase in Ca^{2+} entry (Zawadzki *et al.*, 2008). Whereas, the use of the CCB verapamil prevented cell death, proving that Cav1 channels have an important role in cell survival (Zawadzki *et al.*, 2008). In contrast to Zawadzki *et al.*, this study revealed that the use of the Cav1 blocker nifedipine did not cause any change in cell activity.

Differences in findings could be due to differences in the cell types tested, and additionally in pathological conditions such as seen in cancer, different pathways may control cell survival and death. Evidence from preclinical cancer models suggest that inhibition of Cav3 channels not only can reduce cell proliferation, it can also induce cell apoptosis (Sheehan *et al.*, 2013; Valerie *et al.*, 2013). Sheehan and colleagues showed that block of Cav3 channels by mibefradil (μM concentrations), was able to reduced cell proliferation of C6 glioblastoma cells both *in vitro* and also *in vivo* when cells were injected in Sprague-Dawley rats (Sheehan *et al.*, 2013). Another study demonstrated that 5μM mibefradil caused an approximate 40% reduction in glioblastoma viability by initiating pro-apoptotic pathways, such as an increase in caspase3/7 activity, and reduction in the expression of the anti-apoptotic protein bcl-2 (Valerie *et al.*, 2013). Valerie and colleagues also revealed that pharmacological inhibition of Cav3 channels causes a subsequent block of mTORC2/Akt pathway, through preventing phosphorylation of Akt (position: Ser473 and Thr308) and consequently initiating cell death (Valerie *et al.*, 2013). Although through the use of mibefradil it was concluded that block of Cav3 channels can induce cell death, inhibition of Cav1 channels cannot be excluded as mibefradil is known to block both L-type and T-type channels in a concentration-dependent manner (Perez-Reyes, Lee and Cribbs, 1999; Valerie *et al.*, 2013). Studies have shown that mibefradil can block Cav3 channels at IC_{50} 1μM, whereas for inhibition of Cav1 channels 14 times higher concentration is needed (Perez-Reyes, Lee and Cribbs, 1999; Bertolesi *et al.*, 2002). Valerie and colleagues, in order to exclude that the effects of mibefradil could be due to block of Cav1 channels, repeated experiments in the presence of nifedipine and verapamil; these Cav1 blockers failed to prevent a similar degree of cytotoxicity (Valerie *et al.*, 2013). Findings by Valerie *et al.* support findings from this study where 5μM mibefradil caused a significant change in cell activity of undifferentiated SH-SY5Y cells, whereas 5μM nifedipine treatment failed to cause any change in activity, suggesting that mibefradil-mediated changes in activity are due to inhibition of Cav3 and not Cav1 channels. Further supporting the current study, Kim *et al.* (2018) demonstrated that NPCs isolated from Sprague-Dawley rat embryos showed a significant degree of reduction in viability when treated with 0.15-10μM mibefradil (5μM mibefradil - 50% reduction). Similar to Valerie's study, Kim and

colleagues proposed that reduction in cell viability via inhibition of Cav3 channels causes a subsequent prevention of Akt phosphorylation at Ser473 and GSK3b (Kim *et al.*, 2018). Incubation of NPCs with micromolar concentrations of nifedipine failed to cause a change in cell viability (Kim *et al.*, 2018). On the other hand, mibefradil treatment of cortical neurons caused a lower degree of reduction in viability, suggesting that terminally differentiated cells are more resistant to Cav3 inhibition. Agreeing with the notion that Cav3 channels have an important role in cell proliferation and therefore their expression reduces with cell differentiation (Barnes and Haynes, 1992; Bertolesi *et al.*, 2002, 2003; Aguado *et al.*, 2016; Kim *et al.*, 2018), findings from previous studies agree with results from the current study where no expression for Cav3.1 is detected in RTA-differentiated cells, and subsequently no changes in differentiated SH-SY5Y activity was observed with mibefradil treatment. In contrast to other studies, Bertolesi *et al*. (2002), demonstrated that treating both human retinoblastoma cells and also C6 rodent glioblastoma cells with mibefradil (IC_{50} 1 and 5μM respectively) a significant reduction in cell growth and proliferation through a cell cycle independent pathway is observed. As no changes in anti-apoptoptic bcl-2 expression and pro-apoptotic bax expression was seen with mibefradil treatment, Bertolesi *et al.* (2002), suggested that its mode of action may involve necrosis rather than apoptosis.

Previous studies have shown that inhibition of VGCCs with or without exposure to an apoptotic stimulus, can confer neuroprotection (Pringle *et al.*, 1996; Zawadzki *et al.*, 2008; Wildburger *et al.*, 2009; Lecht *et al.*, 2012). Cultures (8-days) of hippocampal neurons from E18 mice when treated with the Cav3 blocker trimethadione (TMO), although a very high concentration (600μM; 48hr) was needed, less reduction in neuronal viability compared to untreated neuronal cultures was seen via lactate dehydrogenase assays (Wildburger *et al.*, 2009). A similar degree of neuronal protection was also observed with 1μM nimodipine treatment (Wildburger *et al.*, 2009). Cortical neurons on the other hand, demonstrated a lower degree of reduction in viability with similar TMO concentrations, suggesting differential expression profile of Cav3 channels dependent on neuronal type and CNS region (Wildburger *et al.*, 2009; Aguado *et al.*, 2016). Interestingly, 0.5 and 1μM mibefradil, demonstrated protection, whereas treatment with 10μM induced neurotoxicity (Wildburger *et al.*, 2009). Treating 'aged-

neuronal cultures' (15-day cultures) with nimodipine, also exhibited neuroprotective effects, whereas TMO was unable to prevent significant neuronal loss (Wildburger *et al.*, 2009). This suggests that ageing may be linked to changes in the expression of specific VGCC subtypes. In neuron differentiated PC12 cells, oxygen/glucose deprivation (up to 5hr) to mimic ischaemic hypoxia conditions, caused an increase Ca^{2+} influx, where exposure to micromolar concentrations of the Cav1 CCBs nifedipine and nimodipine reduced caspase activation and lactate dehydrogenase release (Lecht *et al.*, 2012). Additionally, nifedipine at concentrations as low as 1μM conferred neuroprotection to hippocampal neurons exposed to similar ischaemic conditions (Lecht *et al.*, 2012). Similarly, Pringle and colleagues showed that hippocampal organotypic slice cultures exposed to 3hr of hypoxia or 1hr of ischemic conditions treatment with 300nM ω-conotoxin-MVIIA (EC_{50}= 50nM) an N-type CCB, lower degree of neuronal loss was observed (Pringle *et al.*, 1996). Whereas co-incubation of hippocampal neurons with nifedipine, failed to prevent neuronal loss, suggesting neuronal loss due to stressful stimuli such as hypoxia involve an increase in Ca^{2+} influx through Cav2 and not Cav1 channels (Pringle *et al.*, 1996).

In parallel with previous findings, this study indicated lack of neurotoxicity with nifedipine, and in line with the absence in Cav2.1 expression in SH-SY5Y cells, lack of toxicity with the Cav2.1 blocker ω-agatoxin-MVIA. In contrast, a significant reduction in cell activity was observed with 1μM ω-conotoxin-GVIA, a Cav2.2 blocker in line with Cav2 channel expression in both undifferentiated and differentiated SH-SY5Y cells and its role in neuronal development and specialised neuronal functions such as neurotransmission seen post-differentiation. A reduction in SH-SY5Y activity was also noted with the Cav3.1 blocker mibefradil dihydrochloride in undifferentiated cells. In support of no Cav3.1 expression in differentiated cells, mibefradil was unable to cause changes in SH-SY5Y activity.

CO effect on CCB-mediated neurotoxicity

- *Physiological levels of CO do not change SH-SY5Y cell activity of either differentiation states.*
- *CO is unable to prevent changes in SH-SY5Y activity mediated by CCBs in cells of either differentiation states.*

Although CO is commonly known as a toxic odourless gas, endogenously it has a number of important cellular roles, with preclinical studies investigating the use of CO as a potential therapeutic. It has been proposed that one mechanism by which CO can act cytoprotectively is through modulation of VGCCs (Lim *et al.*, 2005; Scragg *et al.*, 2008; Boycott *et al.*, 2013; Hettiarachchi *et al.*, 2014; Duckles *et al.*, 2015). In the current study, as a first step in investigating the cytoprotective role(s) of CO in neuroblastoma cells, SH-SY5Y of both differentiation states, were treated with either CORM2 or its inactive control (iCORM2) for 24hr at concentrations 1-100μM. The CORM2 concentrations tested, which correspond to physiological CO levels, did not confer any neurotoxicity in SH-SY5Y of either differentiation states. Further experiments revealed that CORM2 was unable to modulate CCB-mediated changes in SH-SY5Y cell (metabolic) activity.

A study conducted in 2005 showed that administration of low levels of exogenous CO solution to Cav1.2 (α1 and β2 subunits) stably transfected HEK293 cells, and intestinal smooth muscle cells that natively express VGCCs, caused an increase in intestinal Cav1 currents (Lim *et al.*, 2005). CO-mediated increase in intestinal Cav1 currents involves increasing NO production via NOS (nitric oxide synthase) and subsequent increase in cGMP via sGC and ultimately activation of PKA (Lim *et al.*, 2005). In contrast to Lim's research, Scragg *et al.* (2008) revealed that CORM2 , and dissolved carbon monoxide, can both inhibit the activity of recombinant and native cardiac Cav1 channels via a redox manner, rather than a NO, cGMP and PKG pathway (Scragg *et al.*, 2008). This involved an increase in release of ROS from complex III of the electron-transport chain, which caused changes in channels kinetics via modulation of specific cysteine residues (a.a. 1787-1818 region), with the α1 pore-forming subunit essential for CO sensitivity of the L-type channels (Scragg *et al.*, 2008). Opposing finding in Scragg's vs Lim's study, where activation of Cav1 channels via CO was observed, could be due to differences in the source and dose of CO used. Additionally expression of accessory subunits of these channels could also have an effect in how CO modulates

Cav1 channels. Lim's study also focused on the effect of CO on Cav1.2 channels expressed within intestinal smooth muscle cells, whereas Scragg's study focused on the effect of CO within cardiomyocytes. Although both studies agree CO can act as a VGCC modulator, differences in the manner in which it modulates these channels could be due to tissue specific differences in the mechanism underlying its activity. Interestingly, a study conducted on low-voltage activated VGCCs revealed that CO can indirectly inhibit Cav3.2 (T-type channels) through CO interacting with thrioredoxin (Trx), and therefore hindering Trx regulatory activity on these channels (Boycott *et al.*, 2013). Similarly to Boycott *et al.* (2013), research done by Duckles proposed that CO can modulate VGCCs by reducing Cav3.1 and Cav3.2 channel conductance, and therefore exhibiting anti-proliferative properties (Duckles *et al.*, 2015). A similar reduction in channel conductance was also seen in Cav1 channels (Duckles *et al.*, 2015). Although these studies prove that CO can act as a VGCC modulator, they fail to address whether CO confers cytoprotection in a VGCC manner. In contrast to the previously mentioned studies, Hettierachchi *et al.* (2014), showed that CO has the potential to act cytoprotectively against Aβ toxicity in a VGCC-dependent manner. It was revealed that part of $A\beta_{1\text{-}42\text{-}}$ mediated apoptosis involved an increase in Cav1 channel activity, which in turn caused activation of CAMKKII and subsequent phosphorylation and activation of AMPK. CORM2 was able to prevent Aβ-mediated apoptosis via prevention of phosphorylation and the consequent activation of AMPK (Hettiarachchi *et al.*, 2014). Although previous research has shown that CO can act as a VGCC modulator through modulating VGCC activity, the current study was unable to prove CO cytoprotection through preventing CCB-mediated changes in SH-SY5Y cell activity. Contradictory findings could be due to differences in methodology between studies, but it may also suggest that even though CO may modulate VGCC activity, in this case, CO cytoprotection may occur through a VGCC-independent manner. For example, Zeynalov and Doré (2009), through the use of rodent animal models, demonstrated that administration of high physiological concentrations of CO (125 and 250ppm), immediately following an ischemic stroke and during times of oxygen flow restoration, protected cerebral tissue from further damage. This cytoprotection occurred through arteriole dilation through activation of Ca^{2+}-dependent K^{+} channels which prevented further cerebral tissue damage by preventing inflammation and maintaining cell viability

(Zeynalov and Doré, 2009). Similarly, another study was able to show that in an animal model of lung transplants, CO exhibited anti-inflammatory effects through reduction in mRNA expression of pro-inflammatory genes such as IL-6, therefore reducing inflammation and cell death, ultimately preventing transplant rejection (Song *et al.*, 2003). In support of this, another study revealed that inhalation of physiological levels of CO prior to ischemic injury reduces neuronal loss observed in the hippocampus and the cortex (Mahan *et al.*, 2012). Although a number of studies suggest that CO may confer cytoprotection through a VGCC independent pathway, some studies have suggested that CO may not directly target VGCCs, but may target Ca^{2+} influx dependent pathways such as through changes in mitochondria activity. One manner by which CO may confer these anti-apoptotic effects, may be through antioxidant pathways, including through an increase in NOS (nitric oxide synthase) activity and NO production, and activating mitochondrial K_{ATP} channels, rather than VGCCs (Vieira, Queiroga and Alves, 2008; Wang *et al.*, 2011). Moreover, studies conducted on primary astrocytes treated with CO, CO prevented oxidative stress or inflammation induced apoptosis through mitochondrial targeting involving an increase in bcl-2 anti-apoptotic protein, accompanied by an increase in ATP production, changes to COX (cyclooxygenase) activity and lastly mitochondria biogenesis (Zuckerbraun *et al.*, 2007; Almeida *et al.*, 2012). In further support of a role of CO on mitochondria, Lo Iacono *et al.* showed that administration of CORM3 (μM range) upregulates mitochondrial respiration, accompanied by a reduction in membrane potential and reduction in H_2O_2 production from complex II (Iacono *et al.*, 2011). CO pre-treatment of isolated mitochondria from primary astrocytes prevented oxidative stress-dependent cell death due to mitochondrial permeabilization through glutathionylation of adenine nucleotide translocase, the antiporter found on the inner membrane of mitochondria responsible for ADP intake and ATP export (Queiroga *et al.*, 2010). Another study revealed that in primary hippocampal neurons, pre-treatment with CO was able to prevent hypoxia induced cell death through caspase 3, through upregulation of anti-apoptotic bcl-2 expression and subsequent inhibition of ROS production and cytochrome c release (Queiroga *et al.*, 2012). In further support of CO's role in inhibition of cell apoptosis, Song *et al.* revealed that 250ppm CO not only prevents T-lymphocyte activation and

proliferation, it also inhibits cell apoptosis through block of caspase 3 and 8, in a cGMP and MAPK independent pathway (Song *et al.*, 2004).

Although a number of studies suggest that CO can act cytoprotectively through ion channels, in the current study CORM2 was unable to prevent CCB-mediated changes in SH-SY5Y activity. This suggests that although CO may modulate VGCC activity, CO cytoprotection may occur through a VGCC independent manner.

3.4. Summary

VGCC-dependent calcium dyshomeostasis is a pathway that has been linked to AD pathology. Treating SH-SY5Y cells with RTA suggests that cells can differentiate into cells more closely representing primary neurons, with differential VGCC expression profile dependent on differentiation state. In support of a role for both Cav1 and Cav2 channels during neuronal development, and also in more specialised roles following neuronal differentiation, Cav1.2, Cav1.3 and Cav2.2 expression was confirmed in SH-SY5Y of both differentiation states. In contrast, agreeing with the idea that Cav3 channels are required during early stages of development (Barnes and Haynes, 1992; Bertolesi *et al.*, 2003; Aguado *et al.*, 2016; Kim *et al.*, 2018), a reduction in Cav3.1 expression was seen with RTA differentiation of SH-SY5Y cells. This suggests that the SH-SY5Y neuroblastoma VGCC profile closely resembles that of primary neurons, therefore SH-SY5Y neuroblastoma cells are an appropriate system for studying VGCC-dependent calcium dyshomeostasis in neurodegenerative diseases.

It is widely accepted that VGCCs have a key role in neuronal activity and survival (Pringle *et al.*, 1996; Wildburger *et al.*, 2009; Kim *et al.*, 2018). This study, through the use of the global VGCC blocker $CdCl_2$ and selective CCBs ω-conotoxin-GVIA and mibefradil identified Cav2.2 and Cav3.1 to have a role in SH-SY5Y cell activity. These results support the hypothesis that blocking selective VGCCs, due to their important roles within cell development, differentiation and survival, will have an impact on overall neuronal metabolic activity.

Agreeing with the hypothesis that CO (via CORM2 treatment) at physiological concentrations should not alter overall neuronal activity, this study has proven that CORM2 treatment alone has no effect on neuronal metabolic activity. Although a number of studies have proposed that CO can act neuroprotectively through an ion channel-dependent manner (Scragg *et al.*, 2008; Vieira, Queiroga and Alves, 2008; Zeynalov and Doré, 2009; Boycott *et al.*, 2013; Hettiarachchi *et al.*, 2014; Duckles *et al.*, 2015), CORM2 was unable to change CCB-mediated changes in SH-SY5Y metabolic activity of cells of either differentiation states. This suggests that although CO may modulate VGCC activity, in this case, CO cytoprotection may occur through a VGCC-independent manner.

To conclude, these findings aid our understanding of the role of individual VGCC members in neuronal viability and differentiation. Further experiments aim to focus on identifying the role of protofibrillar $A\beta_{1\text{-}42}$ in VGCC-dependent calcium dyshomeostasis.

Chapter 4: Aβ mediated neurotoxicity

4.1. Introduction

Aβ cytotoxicity plays a key role in Alzheimer's disease pathology, with evidence suggesting that it is the aggregated form of the peptide that is responsible for the noted neurotoxicity (Hardy and Selkoe, 2002). Aβ can exist as a number of species and assemblies (Deshpande *et al.*, 2006; Nimmrich *et al.*, 2008; Pachahara *et al.*, 2012; Hermann *et al.*, 2013; Nichols *et al.*, 2015) (see Introduction). Although $A\beta_{1-40}$ consists the majority of Aβ species found in the brain, $A\beta_{1-42}$ is the species most prone to aggregation, therefore a number of studies have focused in studying cytotoxicity exerted by the 42 amino acid long sequence (Shao *et al.*, 1999; Barghorn *et al.*, 2005; Pachahara *et al.*, 2012; Cárdenas-Aguayo *et al.*, 2014). For this reason, this study focused on $A\beta_{1-42}$ with the reverse sequence $A\beta_{42-1}$ used as a control.

Aβ can exist in its monomeric form, where following changes to its secondary structure, it can undergo a conformational change from α-helices and random coils into β-sheets, which are more prone to aggregation (Shao *et al.*, 1999; DeTure and Dickson, 2019). The C-terminus of the Aβ peptide has a role in inducing the conformational change into β-sheets (Chen *et al.*, 2017). Following this, the peptide can then aggregate into dimers and small soluble oligomers, this is known as the nucleated polymerisation process. Oligomers can then further rearrange into elongated structures known as protofibrils and eventually mature fibrils, displaying crosslinking of β-sheets, which are primarily found within amyloid plaques (**Fig. 1.1.6.1**) (Podlisny *et al.*, 1998; Sandberg *et al.*, 2010; DeTure and Dickson, 2019). Evidence suggests that smaller Aβ aggregated assemblies such as small oligomers and protofibrils are more cytotoxic than mature fibrils, with neurotoxic mechanisms including synaptotoxicity, mitochondrial dysfunction, oxidative stress and ultimately neuronal loss (Hardy and Selkoe, 2002; Barghorn *et al.*, 2005; Deshpande *et al.*, 2006; Ryan *et al.*, 2010; Nicoll *et al.*, 2013; Hettiarachchi *et al.*, 2014; Morris, Clark and Vissel, 2014; Nichols *et al.*, 2015). Numerous studies are now using synthetic human $A\beta_{1-40/1-42}$ which can undergo aggregation in a similar manner to *in vivo* Aβ and can also exhibit similar degree of neurotoxicity (Ryan *et al.*, 2010). For the purpose of this study, Aβ neurotoxicity was investigated using synthetic human $A\beta_{1-42}$ in its protofibrillar form. Prior to investigating protofibrillar $A\beta_{1-}$

$_{42}$ neurotoxicity, various protocols designed to induce Aβ aggregation and protofibril formation were assessed.

Aggregated Aβ has shown to confer neurotoxicity in a number of manners, including calcium dysregulation (Anekonda *et al.*, 2011; Nimmrich and Eckert, 2013). One way by which it can cause calcium dysregulation is through modulation of VGCC expression and activity (Ueda *et al.*, 1997; Chiou, 2006; Nimmrich *et al.*, 2008; Kim and Rhim, 2011). The effect of protofibrillar $A\beta_{1-42}$ on neuronal VGCCs in undifferentiated and RTA-differentiated SH-SY5Y neuroblastoma cells was also investigated here. Lastly, the effects of CO, generated through CORM2 treatment, on protofibrillar $A\beta_{1-42}$-mediated changes in SH-SY5Y cell activity were also investigated.

4.1.1. Aim

The aim of the study was to develop a protocol that produces consistent $A\beta_{1-42}$ protofibrils and identify the effects of $A\beta_{1-42}$ protofibrils on VGCCs at molecular level, and overall cell function level using the neuronal cell line model SH-SY5Y neuroblastoma cells.

4.1.2. Objectives

- To compare time-dependent $A\beta_{1-42}$ protofibril formation using the NH_4OH protocol against the HFIP/DMSO protocol.
- To examine the effect of SDS on $A\beta_{1-42}$ protofibril formation.
- To identify $A\beta_{1-42}$/$A\beta_{42-1}$ -mediated changes in cell activity using SH-SY5Y cells in contrasting differentiation states.
- To investigate changes in VGCC gene expression by $A\beta_{1-42.}$
- To investigate $A\beta_{1-42}$ effect in modulating CCB-mediated changes in neuronal activity using undifferentiated and differentiated SH-SY5Y cells.
- To investigate CO effect in modulating $A\beta_{1-42}$ -mediated changes in neuronal activity using undifferentiated and differentiated SH-SY5Y cells.

4.1.3. Hypotheses

- SDS with its negatively charged surface, as it can mimic the cell microenvironment, it is expected to aid $A\beta_{1-42}$ aggregation.
- Protofibrillar $A\beta_{1-42}$ as one of the aggregated forms of $A\beta$ is expected to impair neuronal cell (metabolic) activity.
- Due to the important role of VGCCs in cell development, differentiation and survival, it is expected that protofibrillar $A\beta_{1-42}$ has an effect on VGCCs expression and survival.
- As CO is known to act neuroprotectively, it may interfere with protofibrillar $A\beta_{1-42}$-mediated changed in neuronal metabolic activity.

4.2. Results

4.2.1. Aβ Fibrillization

For the purpose of this study, experiments focused on investigating the effects of protofibrillar $A\beta_{1-42}$ on a neuronal cell line (SH-SY5Y cells). As a first step, prior to experimental use, advanced microscopy, specifically transmission electron microscopy (TEM) was used to study $A\beta_{1-42}$ aggregation, and to determine whether the widely used NH_4OH protocol (followed by 48hr incubation period) does indeed lead to $A\beta_{1-42}$ protofibril formation (see Materials & Methods for full protocol).

TEM images reveal that at 0hr the peptide was largely non-aggregated, which is observed as $A\beta_{1-42}$ clumps, with no fibril structures present (**Fig. 4.2.1.1A**). By 24hr the formation of small protofibrils can be seen (<100 nm length) (**Fig. 4.2.1.1B**) and by 48hr larger protofibrils were observed (**Fig. 4.2.1.1C**). Fibril length analysis revealed time-dependent formation of protofibrils, with a 41.4 $\pm$ 7.1% ($P<0.0001$) increase in protofibril length from 24 to 48hr incubation. At 24hr incubation 68.0% of the protofibrils were below 100 nm in length (average length 93.2 $\pm$ 3.9nm; n=25), whereas by 48hr 89.3% of the protofibrils were above 100 nm in length (average length 131.8 $\pm$ 5.8nm; n=28) (**Fig. 4.2.1.1E and F**).

$A\beta_{1-42}$ protofibril formation using the NH_4OH protocol was then compared to the widely used HFIP (hexafluoroisopropanol)/DMSO protocol (HFIP-peptide kindly provided by Dr Francesco Tamagnini, University of Reading). Preparing $A\beta_{1-42}$ using the HFIP/DMSO protocol also led to protofibril formation (2hr incubation), as determined via TEM (**Fig. 4.2.1.1D**). Of note, the length of the protofibrils were of similar size to the 24hr NH_4OH images rather than the 48hr protofibrils **(Fig. 4.2.1.1E and F)**. 63.4% of protofibrils generated using the HFIP/DMSO protocol were less than 100 nm in length (average length 85.7 $\pm$ 5.2nm; n=22). Protofibrils formed following the 48hr NH_4OH protocol were 53.7 $\pm$ 7.3% ($P<0.0001$) longer than the protofibrils formed following the HFIP/DMSO protocol. Due to this, all subsequent experiments were carried out with $A\beta$ prepared using the NH_4OH protocol.

Literature supports the notion that the reverse sequence of $A\beta_{1-42}$ does not confer cytotoxicity as it cannot aggregate (Paradis *et al.*, 1996; Wei, Wang and Kusiak, 2002;

Takuma *et al.*, 2004). Representative images taken via TEM revealed lack of fibrillization of $A\beta_{42\text{-}1}$ (48hr incubation) using the NH_4OH protocol (**Fig. 4.2.1.2A**), as compared to $A\beta_{1\text{-}42}$ (**Fig. 4.2.1.2B**). As a result, $A\beta_{42\text{-}1}$ was used as the inactive control for subsequent experiments.

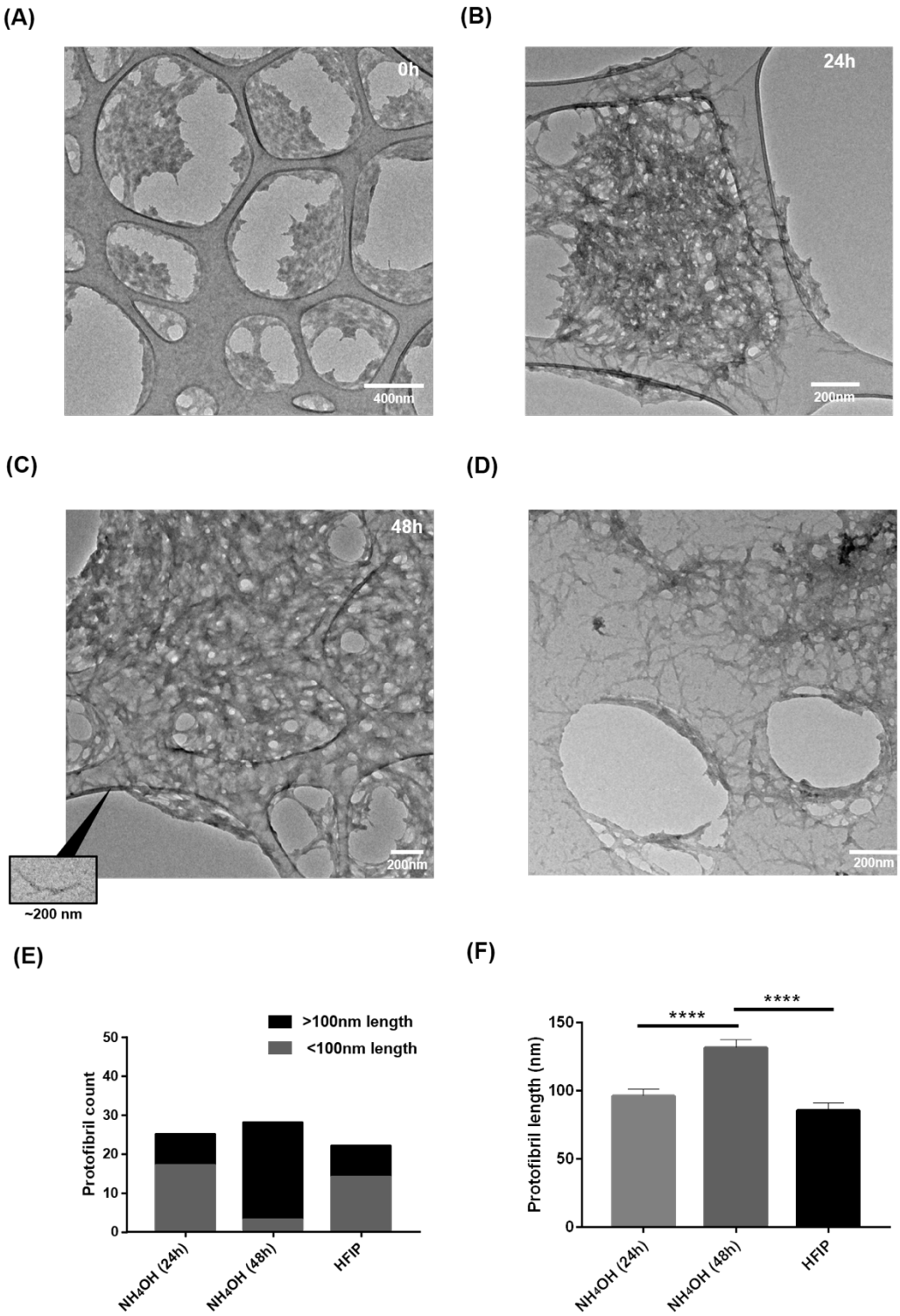

Figure 4.2.1.1: Aβ$_{1-42}$ fibrillization. *Transmission electron microscopy (TEM) was used to monitor Aβ$_{1-42}$ fibrillization. Representative images, using the NH$_4$OH protocol, show that at* ***(A)*** *0hr the peptide is largely not aggregated, at* ***(B)*** *24hr peptide fibrillization has started (protofibrils <100nm) and by* ***(C)*** *48hr the peptide aggregated into larger protofibrils (>100nm in length). Aβ$_{1-42}$ fibrillization using the NH$_4$OH protocol was also compared to* ***(D)*** *peptide aggregation via the HFIP/DMSO protocol (HFIP-peptide kindly provided by Dr Tamagnini) (n=22).* ***(E)*** *+* ***(F)*** *Image J analysis of protofibril length revealed that by 48hr (NH$_4$OH protocol) the majority of the protofibrils are over 100nm in length, with protofibrils obtained from the HFIP protocol demonstrating structural similarity to the protofibrils formed at 24hr with the NH$_4$OH protocol (n=22-28). Statistical analysis was carried out via One-way ANOVA, followed by post-hoc Tukey test. (****=P<0.0001)*

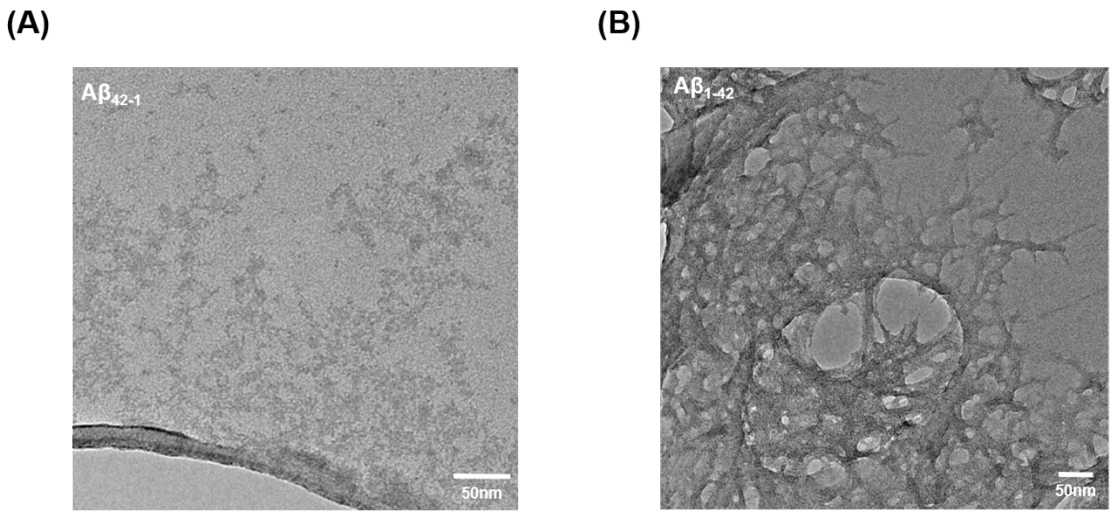

Figure 4.2.1.2: Aβ species dependent differences in aggregation. Aβ aggregation of $A\beta_{42-1}$ and $A\beta_{1-42}$ was monitored via TEM, using the NH_4OH protocol. Representative images show that **(A)** $A\beta_{42-1}$ did not aggregate into protofibrils and remained as unaggregated clamps compared to **(B)** $A\beta_{1-42}$ using the NH_4OH protocol followed by a 48hr incubation.

4.2.2. Use of SDS in Aβ aggregation

Evidence suggests that adding sodium-dodecyl sulfate (SDS) in Aβ preparations may promote Aβ aggregation (Barghorn *et al.*, 2005; Rangachari *et al.*, 2006; Wahlström *et al.*, 2008). In order to investigate the role of SDS in $A\beta_{1-42}$ aggregation, the peptide was prepared in the presence and absence of SDS. Representative TEM images reveal that lack of SDS leads to the formation of protofibrils 85.3 ± 6.9% ($P<0.0001$) smaller in length (average length 52.0 ± 2.1nm; n=21) compared to $A\beta_{1-42}$ prepared in the presence of SDS (average length 93.2 ± 3.9nm; n=25) at 24hr incubation. Although in the absence of SDS protofibril length was lower at 24hr incubation, $A\beta_{1-42}$ time-dependent protofibrillization was still observed, with a 49.1 ± 6.8% ($P<0.0001$) increase in length with an additional 24hr incubation (average length 103.0 ± 4.0nm; n=26). Protofibril length for $A\beta_{1-42}$ preparations in the presence or absence of SDS was also different at 48hr with 24.4 ± 6.3% ($P<0.01$) larger protofibrils seen in SDS containing $A\beta_{1-42}$ preparations (average length 131.7 ± 5.8nm; n=28) (**Fig. 4.2.2.1A and B)**. For this reason, for all subsequent experiments, SDS was added in the $A\beta_{1-42}$ preparations prior to aggregation.

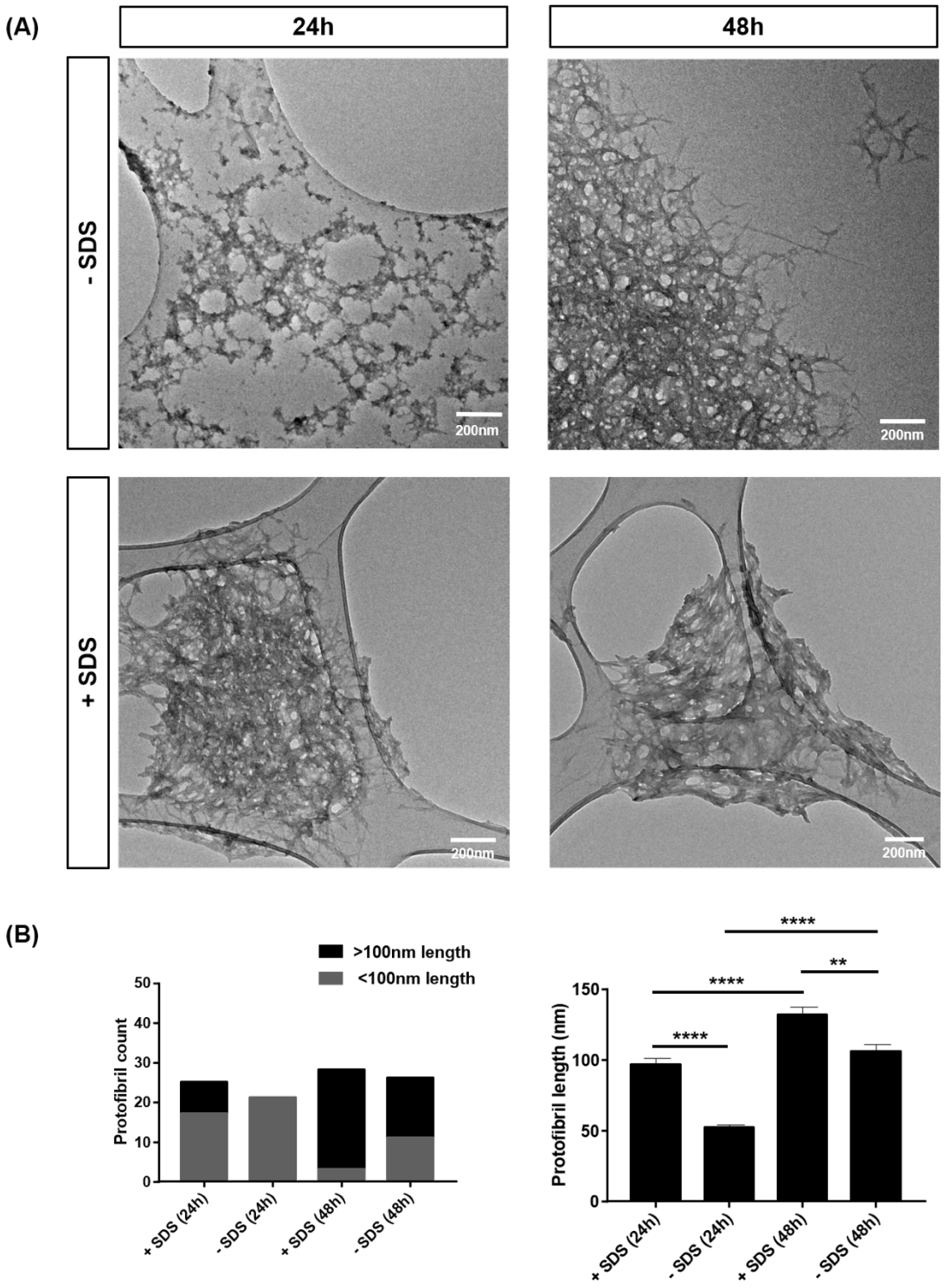

Figure 4.2.2.1: Aβ$_{1-42}$ fibrillization in the presence and absence of sodium dodecyl sulfate. *Aβ$_{1-42}$ fibrillization using the NH$_4$OH protocol was monitored via TEM.* ***(A)*** *Presence and absence of SDS at 24hr (left panel) and 48hr (right panel).* ***(B)*** *Image J analysis revealed that at 24hr, absence of SDS leads to formation of exclusively smaller than 100nm length protofibrils, whereas a combination of different sized protofibrils are observed in the presence of SDS. At 48hr incubation both in the absence and the presence of SDS average protofibril length is above 100nm, with larger protofibrils seen in the presence of SDS (n=21-28). Statistical analysis was carried out via unpaired T-test followed by Kolmogorov-Smirnov post-hoc test. (**=P< 0.01, ****=P<0.0001)*

4.2.3. Aβ-mediated neurotoxicity

Once protofibril formation was verified, the cytotoxic effects of both $A\beta_{1-42}$ and $A\beta_{42-1}$, via monitoring changes in cell (metabolic) activity, were investigated on both undifferentiated and RTA-differentiated SH-SY5Y cells via XTT assay. Studies suggest that Aβ can have neurotrophic or neurotoxic effects dependent on the concentration, with neurotrophic effects typically seen at lower (~pM) concentrations (Luo *et al.*, 1996; Plant *et al.*, 2003; Pearson and Peers, 2006; Garcia-Osta and Alberini, 2009). Therefore, for the purpose of this study, a range of concentrations (1nM - 10μM) were tested over a 24hr treatment to test for neurotoxicity.

In undifferentiated SH-SY5Y cells a concentration-dependent neurotoxic effect was seen with protofibrillar $A\beta_{1-42}$ from nM to μM range. A significant reduction by 21.2 ± 6.1% (n=11; P<0.05) and 23.9 ± 6.8% (n=8; P<0.01) in cell activity was seen with 3 and 10μM $A\beta_{1-42}$ respectively **(Fig. 4.2.3.1A)**. A significant change in cell activity with $A\beta_{1-42}$ treatment was also seen in differentiated cells, although only 10μM $A\beta_{1-42}$ treatment caused a significant reduction in activity (36.2 ± 11.6%; n=3; P<0.01) **(Fig. 4.2.3.2A)**. A more gradual reduction in cell activity was noted (HillSlope: 0.4 ± 0.2) in differentiated compared to undifferentiated cells (HillSlope: 0.7 ± 0.3) (P<0.05) **(Fig. 4.2.3.1D and 4.2.3.2D)**, suggesting that differentiated cells are less susceptible to protofibrillar $A\beta_{1-42}$ induced cytotoxicity.

Treatment of undifferentiated cells with non-aggregated $A\beta_{1-42}$ also demonstrated a degree of cytotoxicity, with 10μM $A\beta_{1-42}$ significantly reducing cell activity by 21.6 ± 6.6%; n=5; P<0.05) **(Fig. 4.2.3.1B)**. On the other hand, within differentiated cells, no significant changes in cell activity was observed with non-aggregated $A\beta_{1-42}$ (n=3) **(Fig. 4.2.3.2B)**. In contrast to protofibrillar $A\beta_{1-42}$, no significant difference in cell activity was observed in undifferentiated cells (HillSlope: 0.6 ± 0.3) compared to differentiated cells (HillSlope: 0.3 ± 0.2) treated with non-aggregated $A\beta_{1-42}$ (**Fig. 4.2.3.1D and 4.2.3.2D**).

Lastly, the effect of the reverse sequence ($A\beta_{42-1}$) as a negative control was also investigated in SH-SY5Y cells. No significant change in cell activity was observed in either undifferentiated (n=4) or differentiated (n=3) cells **(Fig. 4.2.3.1C and 4.2.3.2C)**.

In order to determine whether the effect of the reverse sequence on SH-SY5Y cells is cell-specific, the effect of $A\beta_{42-1}$ was also investigated on a murine microglia cell line

(BV2), which is widely used in both the wider neuroscience field and for Alzheimer's research (Stansley, Post and Hensley, 2012). In agreement with findings in SH-SY5Y cells, within BV2 cells, $A\beta_{42\text{-}1}$ at concentrations ranging from 0.1nM to 100nM had no significant effect on BV2 cell activity **(Fig. 4.2.3.3)**. By contrast, the positive control 10mM H_2O_2 led to a 86.5 ± 17.5% (n=4; $P<0.01$) reduction in BV2 activity.

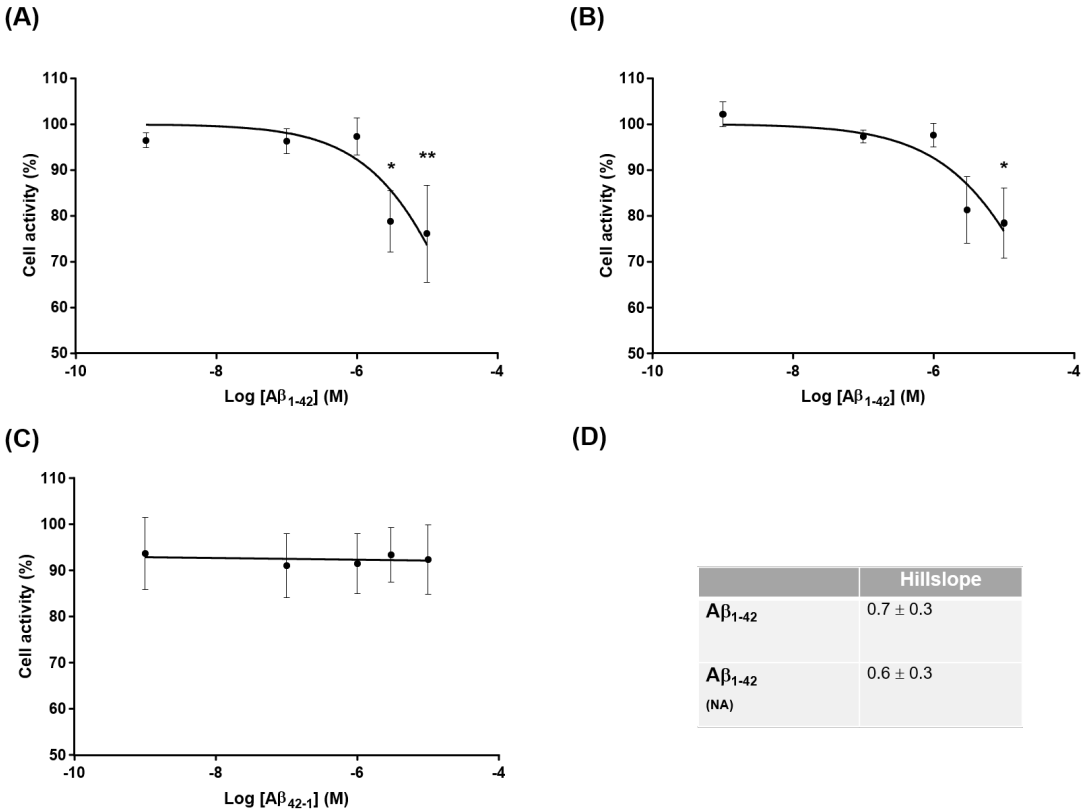

	Hillslope
$A\beta_{1-42}$	0.7 ± 0.3
$A\beta_{1-42}$ (NA)	0.6 ± 0.3

Figure 4.2.3.1: Aб mediated cytotoxicity in undifferentiated neuroblastoma cells. *The effect of Aб was investigated in undifferentiated SH-SY5Y cells via XTT assay.* ***(A)*** *Protofibrillar $Aб_{1-42}$ significantly reduced cell activity at 3 and 10µM (24hr; n=8-17).* ***(B)*** *Non-aggregated $Aб_{1-42}$ significantly reduced activity at 10µM only (24hr; n=5).* ***(C)*** *The reverse sequence, $Aб_{42-1}$ did not cause any changes in cell activity of undifferentiated SH-SY5Y cells (24hr; n=4).* ***(D)*** *HillSlope analysis for protofibrillar $Aб_{1-42}$ (graph A) and non-aggregated $Aб_{1-42}$ (graph B). Data (mean ±SEM) were normalised to the corresponding vehicle control (PBS). Statistical analysis was carried out via One-way ANOVA and post-hoc Tukey test. (*=P<0.05, **=P<0.01)*

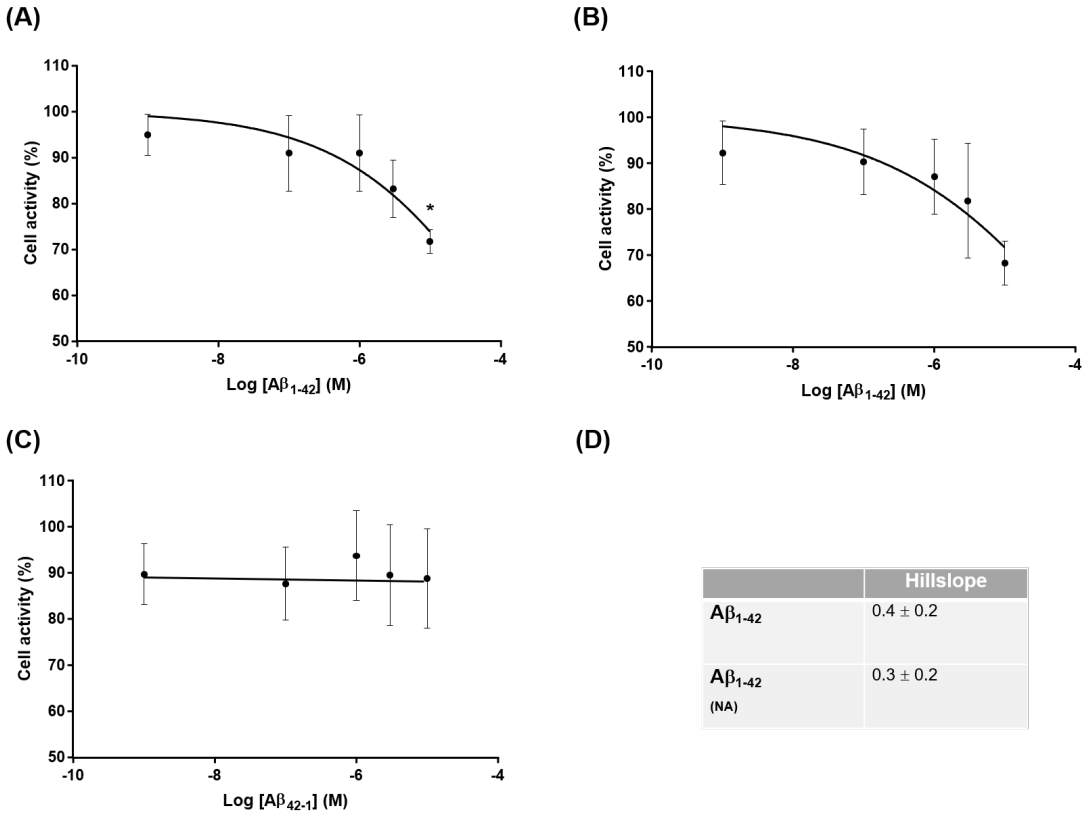

	Hillslope
$A\beta_{1-42}$	0.4 ± 0.2
$A\beta_{1-42}$ (NA)	0.3 ± 0.2

Figure 4.2.3.2: Aβ mediated cytotoxicity in differentiated neuroblastoma cells. *The effect of Aβ was investigated in differentiated SH-SY5Y cells via XTT assay.* ***(A)*** *Protofibrillar $A\beta_{1-42}$ significantly reduced cell activity at 10μM only (24hr; n=3).* ***(B)*** *Non-aggregated $A\beta_{1-42}$ did not cause any significant change in cell activity (24hr; n=3).* ***(C)*** *The reverse sequence $A\beta_{42-1}$ did not cause any changes in cell activity of differentiated SH-SY5Y cells (24hr; n=3).* ***(D)*** *HillSlope analysis for protofibrillar $A\beta_{1-42}$ (graph A) and non-aggregated $A\beta_{1-42}$ (graph B). Data (mean ±SEM) were normalised to the corresponding vehicle control (PBS). Statistical analysis was carried out via One-way ANOVA and post-hoc Tukey test. (*=P<0.05)*

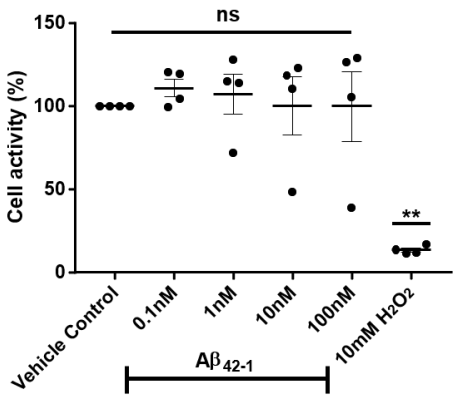

Figure 4.2.3.3: Aβ mediated cytotoxicity in microglia cells. *The effect of $A\beta_{42-1}$ was investigated in BV2 murine microglia cells via XTT assay. $A\beta_{42-1}$ (24hr; n=4) did not cause any changes in BV2 cell activity. Data (mean ±SEM) were normalised to the corresponding vehicle control (PBS). Statistical analysis was carried out via One-way ANOVA and post-hoc Tukey test. (**=P<0.01)*

4.2.4. Aβ$_{1-42}$ mediated changes in VGCC expression

Previously, mRNA for VGCCs in both undifferentiated and RTA-differentiated SH-SY5Y cells were detected (see Chapter 3), with differences in gene expression dependent on the differentiation state of the cells. Following a 24hr exposure to either 100nM (n=6) or 1μM (n=3) Aβ$_{1-42}$, undifferentiated SH-SY5Y cells showed no fold-changes in mRNA expression of Cav1.2, Cav1.3, Cav2.2 and Cav3.1 (**Fig. 4.2.4.1 and 4.2.4.2**), assessed via qPCR. By contrast, treatment of differentiated cells with 100nM Aβ$_{1-42}$ caused a significant reduction in Cav1.3 mRNA expression of 0.2 ± 0.04 fold-change (n=5; P<0.01) **(Fig. 4.2.4.3)**. Whereas treatment of differentiated cells with 1μM Aβ$_{1-42}$ led to a significant increase in Cav1.2 mRNA expression of 0.8 ± 0.2 fold-change (n=3; P<0.05) **(Fig. 4.2.4.4)**. No change in the mRNA expression of Cav2.2 and Cav3.1 was seen in differentiated cells treated with either Aβ$_{1-42}$ concentrations.

In order to identify whether the mechanism by which Aβ$_{1-42}$ causes reduction in cell (metabolic) activity involves VGCCs, Aβ$_{1-42}$ cytotoxicity was studied in the presence of various CCBs, assessed via changes in cell activity through MTT assay (**Fig. 4.2.4.5A-B**). Aβ$_{1-42}$ (3μM) alone caused a 44.5 ± 8.3% (n=5; P<0.001) and 42.8 ± 5.6% (n=5; P<0.0001) reduction in activity within undifferentiated and differentiated cells, respectively. Treating both undifferentiated and differentiated SH-SY5Y cells with 3μM Aβ$_{1-42}$ in the presence of selective-VGCC blockers, had no significant effect on Aβ-mediated cytotoxicity. Also, no significant change in toxicity was seen when differentiated cells were treated with Aβ$_{1-42}$ in the presence of the global-VGCC blocker $CdCl_2$ (10μM) (47.7 ± 5.6%; n=5) in comparison to 3μM Aβ$_{1-42}$ (42.8 ± 5.6%; n=5) alone **(Fig. 4.2.4.5B)**. In contrast to differentiated cells, within undifferentiated cells, the combination of 3μM Aβ$_{1-42}$ and 10μM $CdCl_2$ led to an additional 34.9 ± 8.3% (n=5; P<0.01) reduction in cell activity **(Fig. 4.2.4.5A)**. The positive control 10mM H_2O_2 caused a 97.9 ± 8.3% (n=5; P<0.0001) and 98.9 ± 5.6% (n=5; P<0.0001) reduction in undifferentiated and differentiated SH-SY5Y cell activity respectively.

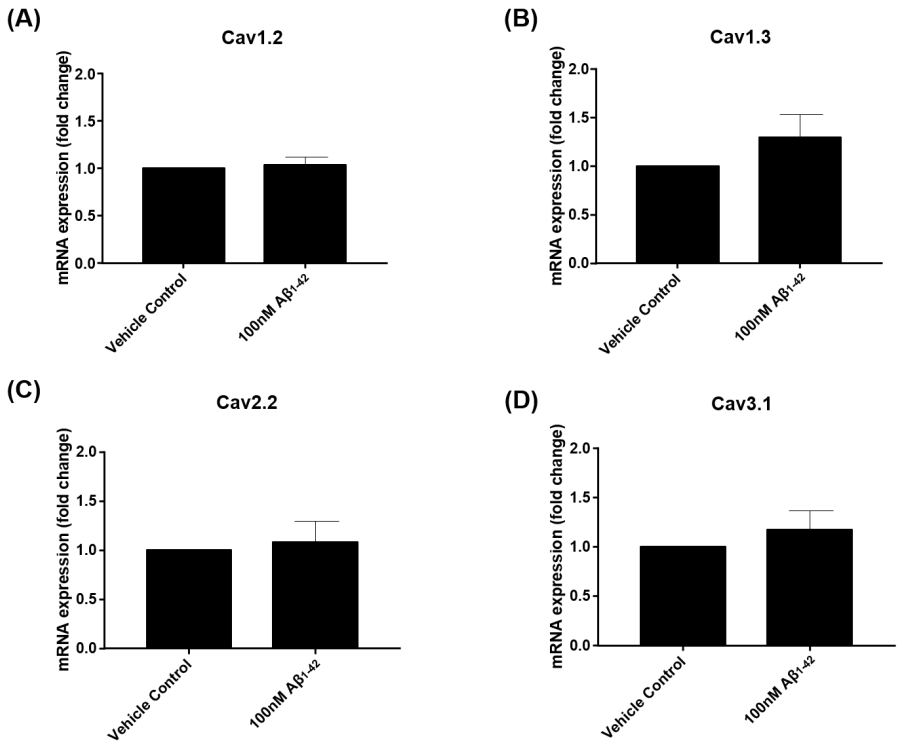

Figure 4.2.4.1: Modulation of neuronal VGCC mRNA expression in undifferentiated SH-SY5Y cells by 100nM protofibrillar Aβ$_{1-42}$. *Changes in VGCC mRNA expression by Aβ$_{1-42}$ were investigated via qPCR. Exposure to 100nM Aβ$_{1-42}$ (n=6) for 24hr did not cause any change in* ***(A)*** *Cav1.2,* ***(B)*** *Cav1.3,* ***(C)*** *Cav2.2 and* ***(D)*** *Cav3.1 mRNA expression in undifferentiated cells, as compared to vehicle control (PBS) treated cells. Data (mean ±SEM) were normalized to β-actin and subjected to one-tailed unpaired Welch T-test.*

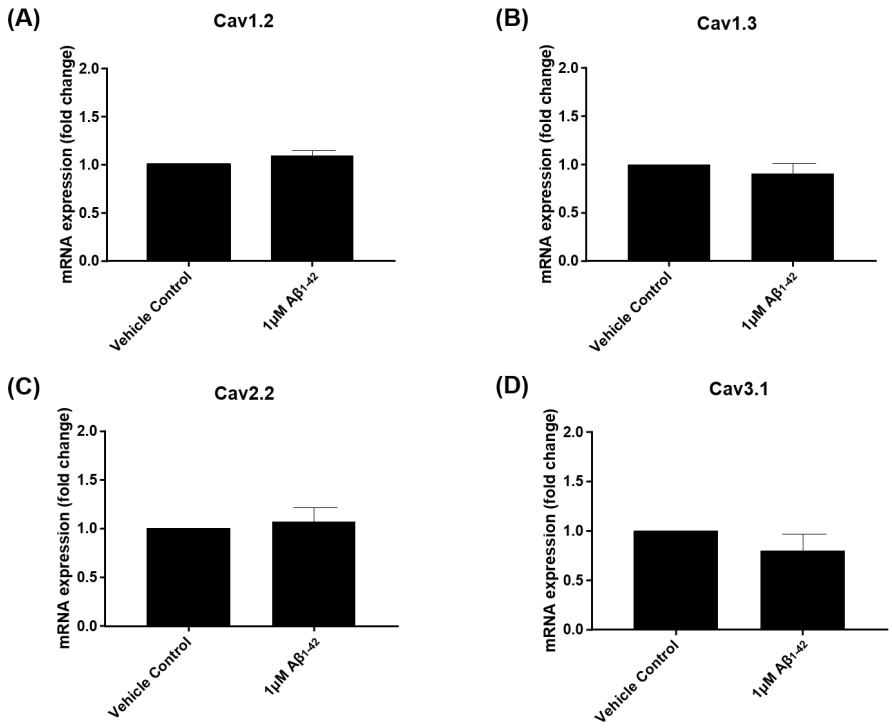

Figure 4.2.4.2: Modulation of neuronal VGCC mRNA expression in undifferentiated SH-SY5Y cells by 1μM protofibrillar Aβ$_{1-42}$. *Changes in VGCC mRNA expression by Aβ$_{1-42}$ were investigated via qPCR. Exposure to 1μM Aβ$_{1-42}$ (n=6) for 24hr did not cause any change in* ***(A)*** *Cav1.2,* ***(B)*** *Cav1.3,* ***(C)*** *Cav2.2 and* ***(D)*** *Cav3.1 mRNA expression in undifferentiated cells, as compared to vehicle control (PBS) treated cells. Data (mean ±SEM) were normalized to β-actin and subjected to one-tailed unpaired Welch T-test.*

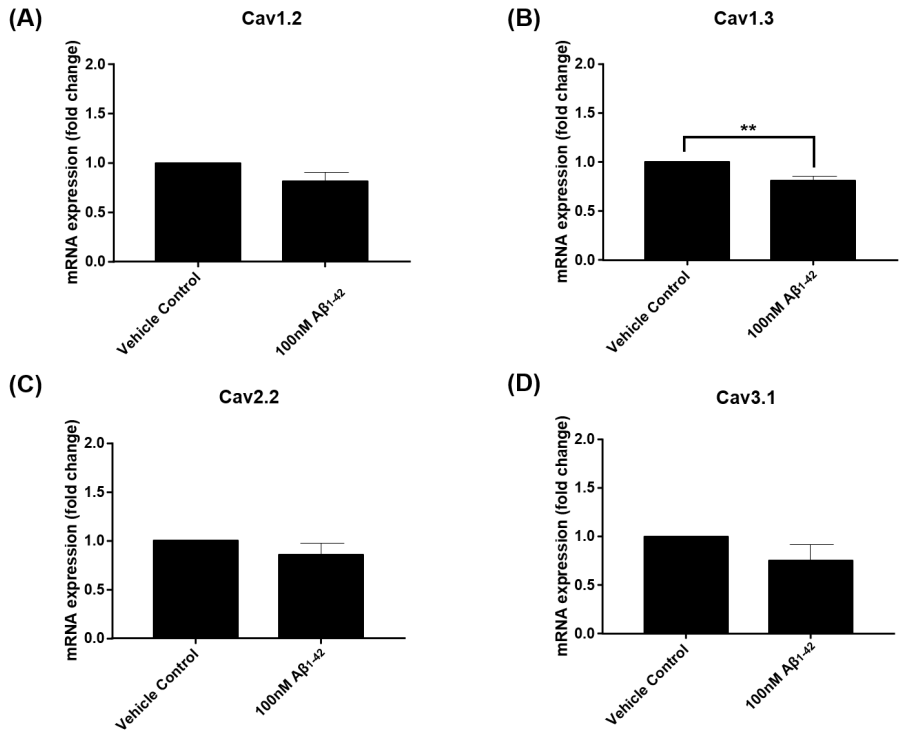

Figure 4.2.4.3: Modulation of neuronal VGCC mRNA expression in differentiated SH-SY5Y cells by 100nM protofibrillar Aβ1-42. *Changes in VGCC mRNA expression by $A\beta_{1-42}$ were investigated via qPCR. Exposure to 100nM $A\beta_{1-42}$ (n=5) did not cause any change in* ***(A)*** *Cav1.2,* ***(C)*** *Cav2.2 and* ***(D)*** *Cav3.1 mRNA expression within differentiated SH-SY5Y cells.* ***(B)*** *A significant reduction in Cav1.3 mRNA expression was seen. Data (mean ±SEM) were normalized to β-actin and subjected to one-tailed unpaired Welch T-test. (**=P<0.001)*

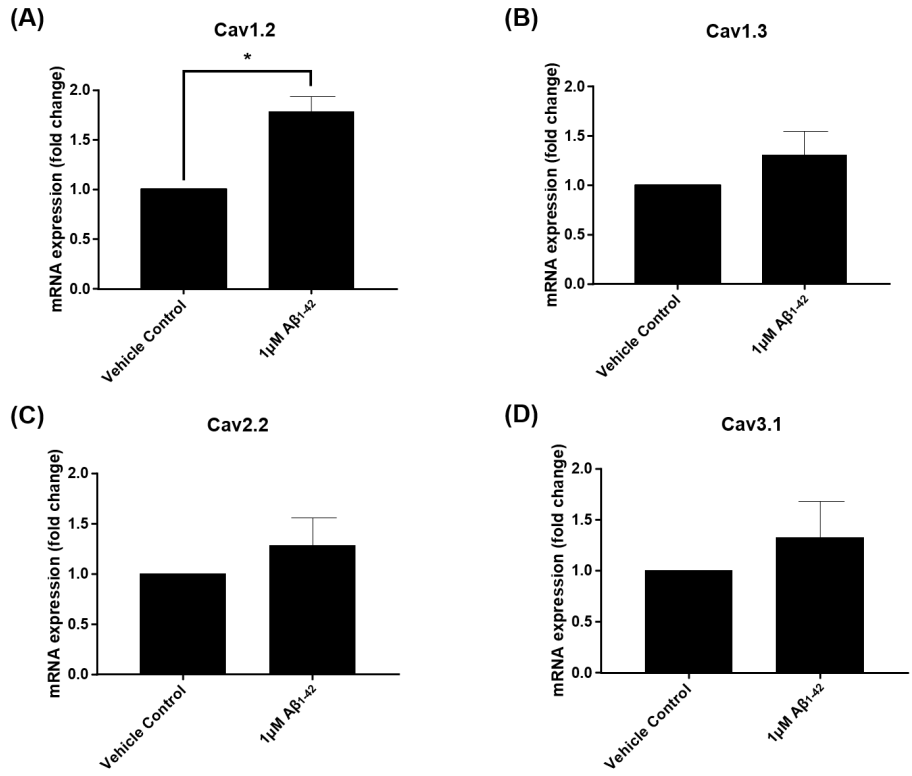

Figure 4.2.4.4: Modulation of neuronal VGCC mRNA expression in differentiated SH-SY5Y cells by 1μM protofibrillar Aβ$_{1-42}$. *Changes in VGCC mRNA expression by Aβ$_{1-42}$ were investigated via qPCR.* ***(A)*** *Exposure to 1μM Aβ$_{1-42}$ (n=3) caused a significant increase in Cav1.2 mRNA expression within differentiated SH-SY5Y cells. No changes in mRNA expression of* ***(B)*** *Cav1.3,* ***(C)*** *Cav2.2 and* ***(D)*** *Cav3.1 was seen. Data (mean ±SEM) were normalized to β-actin and subjected to one-tailed unpaired Welch T-test. (*=P<0.05)*

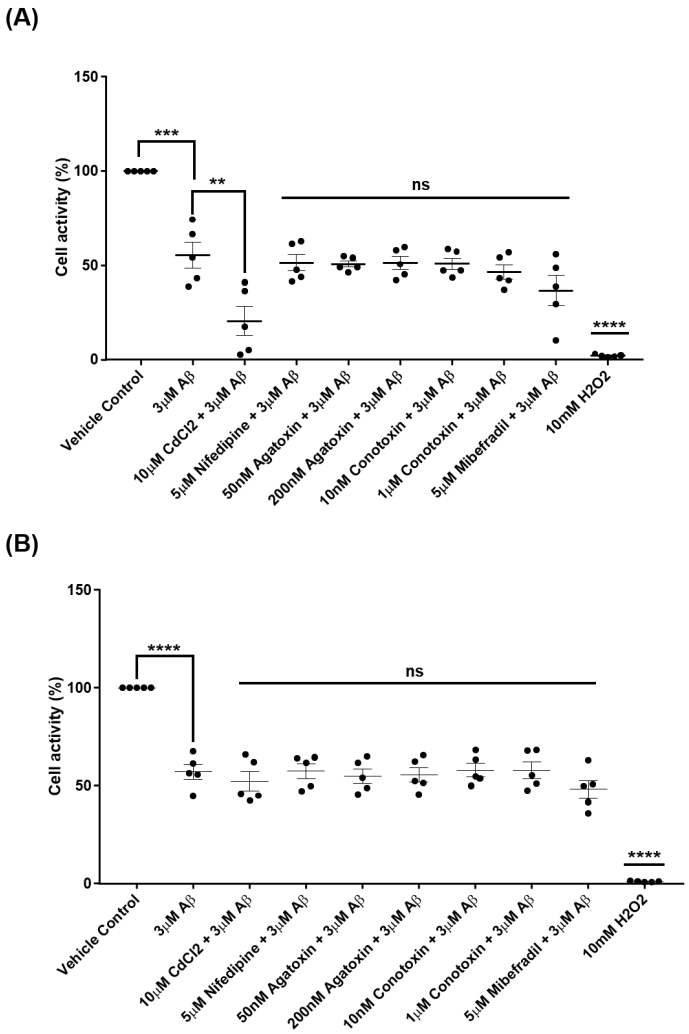

Figure 4.2.4.5: Calcium channel blocker effect on protofibrillar Aβ-mediated changes in cell activity. *Protofibrillar $Aβ_{1-42}$ neurotoxicity in undifferentiated and differentiated SH-SY5Y cells was evaluated in the presence of calcium channel blockers, via MTT assay.* ***(A)*** *Within undifferentiated SH-SY5Y cells, 3μM $Aβ_{1-42}$ in the presence of $CdCl_2$ demonstrated a significant reduction in cell activity, whereas $Aβ_{1-42}$ in the presence of more selective-CCBs did not show any additional reduction in activity (24h; n=5).* ***(B)*** *Within differentiated SH-SY5Y cells, no additional reduction in activity was seen when cells were treated with 3μM $Aβ_{1-42}$ in the presence of the global-CCB $CdCl_2$ and the more-selective CCBs (24h; n=5). Data (mean ±SEM) were normalised to their corresponding vehicle control. Statistical analysis was carried out via One-way ANOVA and post-hoc Tukey test. (**=P<0.01, ***=P<0.001, ****=P<0.0001)*

4.2.5. Aβ$_{1-42}$ -mediated mechanism of action

Once protofibrillar Aβ$_{1-42}$ neuronal cytotoxicity and its effect on VGCCs was identified, the role of CO in preventing Aβ$_{1-42}$-mediated reduction in cell (metabolic) activity was investigated in SH-SY5Y cells of both differentiation states via MTT assay.

To investigate whether CORM2 can reduce Aβ$_{1-42}$-mediated reduction in cell activity through a change in peptide aggregation, prior to cell treatment, Aβ$_{1-42}$ was left to aggregate (48hr) in the presence of CORM2 (using methodology described by De Simone *et al.* 2019). Protofibrillar 4μM Aβ$_{1-42}$ alone caused a 44.0 ± 2.9% (n=4; P<0.0001) reduction in undifferentiated SH-SY5Y cell activity. Although at the concentrations tested, direct interaction of CORM2 with the peptide could not be excluded, no change in Aβ$_{1-42}$-mediated cytotoxicity was observed when undifferentiated SH-SY5Y cells were treated with 4μM Aβ$_{1-42}$ left to aggregate in the presence of CORM2 at 0.5 (39.3 ± 2.9%; n=4) and 2.5 (37.4 ± 2.9%; n=4) concentration ratio. Also, no significant change in cytotoxicity was also seen when cells were treated with Aβ$_{1-42}$ left to aggregate in the presence of iCORM2 at a 2.5 concentration ratio (38.4 ± 3.2%; n=3) compared to Aβ$_{1-42}$ alone. The positive control 10mM H_2O_2 caused a 98.3 ± 2.9% (n=4; P<0.0001) reduction in cell activity **(Fig. 4.2.5.1)**.

When undifferentiated cells were treated with 3μM Aβ$_{1-42}$ in combination with 1 or 10μM CORM2 no significant change in Aβ$_{1-42}$ -mediated cytotoxicity (47.7 ± 4.1%; n=4 and 46.5 ± 4.1%; n=5 respectively) was observed compared to treatment with Aβ$_{1-42}$ alone (49.6 ± 4.1%; n=5; P<0.0001). No significant change in Aβ-mediated toxicity was also seen when undifferentiated cells were treated with Aβ$_{1-42}$ in combination with 1 or 10μM iCORM2 (48.9 ± 4.1%; n=5 and 50.0 ± 4.1%; n=5 respectively). Treatment of cells with the positive control 10mM H_2O_2 led to 97.8 ± 4.4% (n=5; P<0.0001) reduction in cell activity **(Fig. 4.2.5.2A)**.

When differentiated SH-SY5Y cells were treated with 3μM Aβ$_{1-42}$ in combination with 1 or 10μM CORM2 no significant change in toxicity (28.7 ± 1.1%; n=4 and 28.4 ± 1.9%; n=5 respectively) was observed compared to treatment with Aβ$_{1-42}$ alone (31.0 ± 6.7%;n=5; P<0.01). No significant change in Aβ-mediated toxicity was also seen when undifferentiated cells were treated with Aβ$_{1-42}$ in combination with 1 or 10μM iCORM2 (29.7 ± 2.2%; n=5 and 29.1 ± 2.2%; n=5 respectively). Treatment of cells with the positive

control 10mM H_2O_2 led to 97.5 ± 0.5% (n=5; P<0.0001) reduction in cell activity **(Fig. 4.2.5.2B)**.

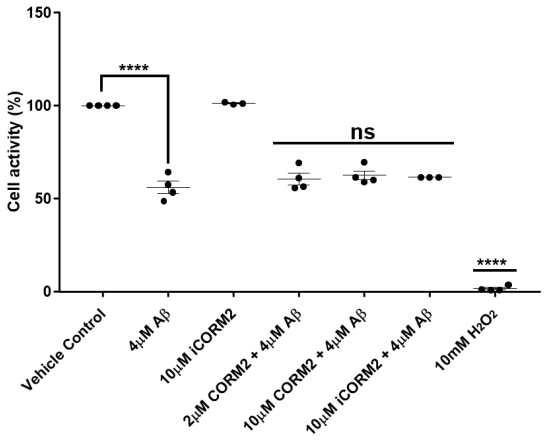

Figure 4.2.5.1: Effect of CO on protofibrillar Aβ$_{1-42}$ mediated neurotoxicity. *Protofibrillar Aβ$_{1-42}$ neurotoxicity in undifferentiated SH-SY5Y cells was evaluated in the presence of CORM2/iCORM2, via MTT assay. Prior to treating the cells, Aβ$_{1-42}$ was left to aggregate in the presence of CORM2 at 0.5 and 2.5 ratio.* In *undifferentiated SH-SY5Y cells CO was unable to prevent changes in cell activity induced by 4μM Aβ$_{1-42}$ (24h; n=4). Data (mean ±SEM) were normalised to their corresponding vehicle control. Statistical analysis was carried out via One-way ANOVA and post-hoc Tukey test. (****=P<0.0001)*

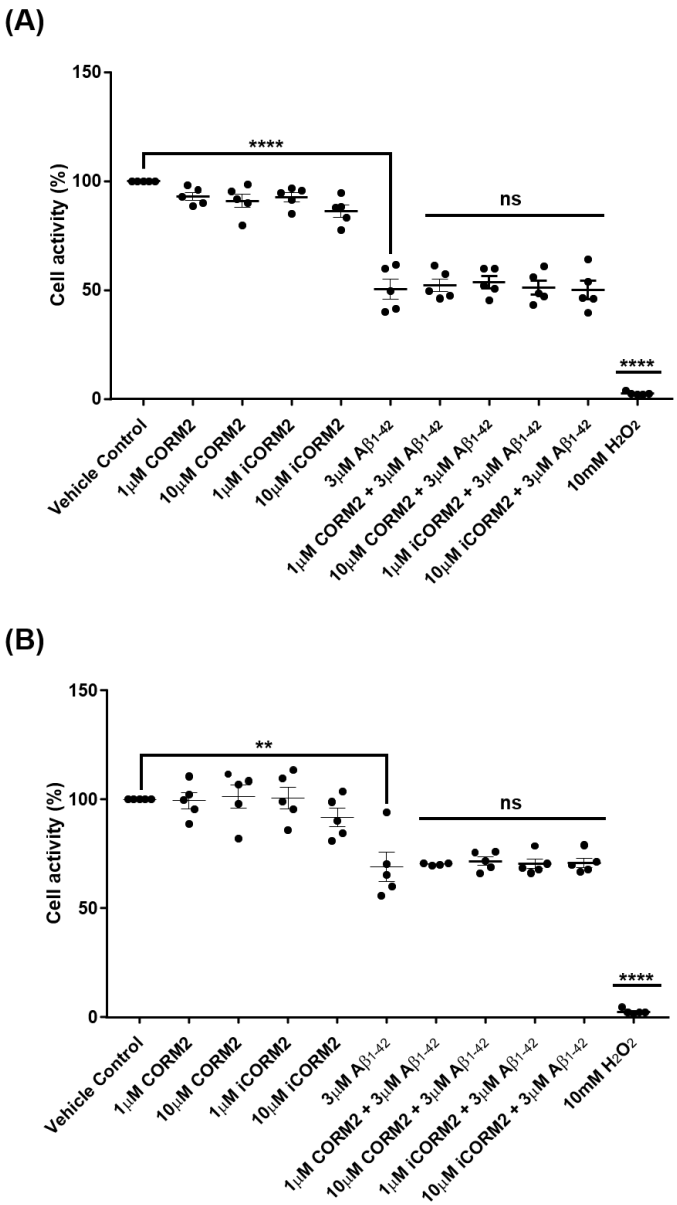

Figure 4.2.5.2: Effect of CO in combination with protofibrillar Aβ$_{1-42}$ on neuronal cell activity. *Protofibrillar Aβ$_{1-42}$ neurotoxicity in undifferentiated and differentiated SH-SY5Y cells was evaluated in the presence of CORM2/iCORM2, via MTT assay. In both* ***(A)*** *undifferentiated and* ***(B)*** *differentiated SH-SY5Y cells CO, via CORM2, was unable to prevent changes in cell activity induced by 3μM Aβ$_{1-42}$ (24h; n=5). Data (mean ±SEM) were normalised to their corresponding vehicle control. For undifferentiated SH-SY5Y cells, statistical analysis was carried out via One-way ANOVA and post-hoc Tukey test. For differentiated SH-SY5Y cells, statistical analysis was carried out via unpaired Kruskal-Wallis followed by Dunn's test. (**=P<0.01, ****=P<0.0001)*

4.3. Discussion

Aβ Fibrillization

- *Pre-treatment of $A\beta_{1-42}$ in NH_4OH led to complete dissolution of the peptide, and time-dependent protofibril formation.*
- *Allowing $A\beta_{1-42}$ to aggregate in the presence of SDS led to larger in length protofibrils formed.*
- *The reverse sequence ($A\beta_{42-1}$) was unable to undergo aggregation and consequently protofibril formation.*

In the present study, NH_4OH treatment of $A\beta_{1-42}$ peptide followed by exposure to NaOH led to the complete dissolution of the peptide, and a time-dependent formation of $A\beta_{1-42}$ protofibrils. Numerous protocols have been reported for preparing and inducing aggregation of Aβ into protofibrils (Nicoll *et al.*, 2013; Ryan *et al.*, 2013; Hettiarachchi *et al.*, 2014). Alkalines such as NH_4OH, have been widely used to pre-treat the peptide followed by dissolving the peptide film in NaOH for preparing Aβ for aggregation (Barghorn *et al.*, 2005; O'Nuallain *et al.*, 2010; Ryan *et al.*, 2013). The basic pH of NH_4OH and NaOH ensure Aβ is fully solubilized and kept in its monomeric state in preparation for subsequent aggregation, therefore ensuring no variability between Aβ preparations which could impact degree of aggregation and subsequent experimental findings when investigating Aβ cytotoxicity (Shirahama and Cohen, 1967; Fezoui *et al.*, 2000). In agreement to findings from this study, work done by Ryan *et al.* (2013) have proven that pre-treating human synthetic $A\beta_{1-42}$ in NH_4OH leads to the formation of stable aggregates with a low degree of variability and consistent *in vitro* cytotoxicity. The current study revealed that using the NH_4OH protocol, protofibril formation was evident as early as 24hr, with larger protofibrils in length seen by 48hr. Work done by other groups such as Nicoll *et al.* and Walsh *et al.* provide further support to findings in this study by demonstrating a time-dependent aggregation of $A\beta_{1-40/1-42}$ into protofibrils under similar timeframes. Whereas, longer than 72hr incubation has been reported to lead to the formation of larger assemblies such as mature fibrils, identified via ThT assay (Walsh *et al.*, 1999; Nicoll *et al.*, 2013). In addition to the use of monomeric $A\beta_{1-42}$ (at 0hr incubation period), we have also used the Aβ reverse sequence ($A\beta_{42-1}$). In our study, supported by previous research (Paradis *et al.*, 1996; Takuma *et al.*, 2004), $A\beta_{42-1}$ failed to aggregate using the NH_4OH protocol followed by a 48hr incubation. In contrast to use of NH_4OH or the HFIP/DMSO protocol, Hettiarachchi *et al.* (2014) demonstrated that

synthetic human $A\beta_{1-42}$ dissolved in fresh DMEM media and incubated over 24hr can also lead to the formation of protofibrillar $A\beta_{1-42}$ structures ranging from 25 - 90nm in length.

Although in the current study NH_4OH was used for generating stable and consistent protofibril $A\beta_{1-42}$ preparations, a number of other studies have used HFIP for preparing $A\beta$ for aggregation and investigating cytotoxicity (Rangachari *et al.*, 2006; Ryan *et al.*, 2010; Pachahara *et al.*, 2012; Tamagnini *et al.*, 2015). The present study revealed that although pre-treatment of the peptide using HFIP indeed led to protofibril formation after just a 2hr incubation, as described elsewhere (Tamagnini *et al.*, 2015), HFIP generated protofibrils were of similar structure and length as those observed with NH_4OH after 24hr. While it has been suggested that HFIP pre-treatment ensures $A\beta$ is entirely monomeric in preparation for aggregation, previous observations have reported that HFIP-prepared $A\beta$ can lead to premature $A\beta$ aggregation, evident by the formation of false 'enhanced' $A\beta$ aggregates, such as protofibrils and fibrils which would not normally form immediately post-preparation (Pachahara *et al.*, 2012). In support of this, in the current study, presence of protofibrils was evident as early as with 2hr incubation. This may be explained by taking into consideration the effect of the pH of the solvent on peptide aggregation. In contrast to using NH_4OH/NaOH, HFIP can alter pH levels to the acidic pH of $A\beta$ which can promote aggregation (Wood *et al.*, 1996; Ryan *et al.*, 2013). Previous observations also suggest that the NH_4OH protocol leads to the formation of stable aggregates with a lower degree of variability and higher *in vitro* cytotoxicity compared to the HFIP protocol (Ryan *et al.*, 2013). In agreement, our work has revealed that NH_4OH-prepared $A\beta$ followed by a 48hr incubation creates larger protofibrils, with low degree of variability in protofibil length between $A\beta$ preparations. Moreover, due to concerns with adding DMSO in the final $A\beta$ preparation, such as DMSO-dependent cytotoxicity, and DMSO reported interference with $A\beta$ aggregation and oxidative mechanisms (Shen and Murphy, 1995; Kahler, 2000; Hanslick *et al.*, 2009; Broersen *et al.*, 2011), the NH_4OH/NaOH protocol is considered more appropriate in studying $A\beta$ protofibril-dependent *in vitro* cytotoxicity. Due to all these observations, all subsequent experiments in this study focused on investigating the effects of protofibril $A\beta_{1-42}$ generated by the NH_4OH-48hr protocol.

Recently, there has been considerable interest in investigating how membrane mimetics, such as SDS, may influence peptide aggregation (Shao *et al.*, 1999; Wahlström *et al.*, 2008; Pedersen *et al.*, 2020). Research has shown that both synthetic human $A\beta_{1-40/1-42}$ and recombinant Aβ can aggregate from monomers into oligomers and larger aggregates when co-incubated with cells (Podlisny *et al.*, 1998; Shao *et al.*, 1999; Khondker, Alsop and Rheinstädter, 2017). These findings suggest that the interaction of Aβ with the cell lipid bilayer may enhance peptide aggregation. In line with this, recently, AD has been linked to altered lipid content, such as an increase in neuronal membrane lipid raft composition which is known to influence APP processing and Aβ aggregation (Rushworth and Hooper, 2011). This suggests that changes within the lipid membranes consists part of the AD pathology. Therefore, mimicking the microenvironment of biological membranes through the inclusion of negatively-charged SDS, capable of forming lipid micelles with an anionic surface, similarly to adding physiological fatty acids such as arachidonic and lauric acid, can influence peptide folding and aggregation. This may allow the study of Aβ aggregation and cytotoxicity in a manner which more closely represents the *in vivo* situation (Mattice, Riser and Clark, 1976; Shao *et al.*, 1999; Yamamoto *et al.*, 2004; Barghorn *et al.*, 2005; Wahlström *et al.*, 2008; Pedersen *et al.*, 2020). In the present study, SDS was shown to enhance $A\beta_{1-42}$ aggregation, evident by larger protofibrils formed. Currently there is contradictory evidence with respect to the use of SDS in Aβ studies (Shao *et al.*, 1999; Barghorn *et al.*, 2005; Wahlström *et al.*, 2008). Some studies suggest that SDS micelles which mimic the cell lipid bilayer, work by stabilizing the α-helix conformation of Aβ, a secondary structure favoured in monomeric Aβ, therefore preventing peptide aggregation (Shao *et al.*, 1999; Rangachari *et al.*, 2006). In contrast, other studies, similar to results from the current study, suggest that SDS induces aggregation, possibly through a conformational change from random coils into β-sheets, a secondary structure which is favoured for peptide aggregation (Barghorn *et al.*, 2005; Wahlström *et al.*, 2008). A possible explanation for contradictory results could be that the effect of SDS on the Aβ secondary structure and subsequent role in peptide folding and aggregation could be different dependent on SDS concentration used (Shao *et al.*, 1999; Barghorn *et al.*, 2005; Rangachari *et al.*, 2006; Wahlström *et al.*, 2008).

Taken together, evidence from the current study indicates that pre-treatment of human $A\beta_{1-42}$ with NH_4OH leads to a time-dependent protofibril formation, with low variability between $A\beta$ preparations. Moreover, low levels of SDS can act as an aggregation and nucleation inducer potentially through stabilising changes in the $A\beta$'s conformational structure. Therefore, NH_4OH pre-treatment of $A\beta_{1-42}$, and use of SDS, leads to the generation of $A\beta_{1-42}$ protofibrils structurally and functionally similar to those seen *in vivo.*

Aβ effect on neuronal viability

- *High μM concentrations of protofibrillar $A\beta_{1-42}$ caused a significant reduction in cell activity of SH-SY5Y cells of both differentiation states.*
- *Reduction in cell activity could not be replicated with the reverse sequence ($A\beta_{42-1}$) in either SH-SY5Y of both differentiation states, or BV2 microglia cells.*

In the present study, protofibrillar $A\beta_{1-42}$, at a concentration-dependent manner, caused a significant reduction in cell (metabolic) activity of both undifferentiated and RTA-differentiated SH-SY5Y cells, which could not be replicated with the use of the reverse sequence ($A\beta_{42-1}$). In support of this, several studies have proven that protofibrillar $A\beta_{1-42}$ can cause cell dysfunction through investigating early-apoptotic pathways (Walsh *et al.*, 1999; Sandberg *et al.*, 2010; Jan *et al.*, 2011; Hettiarachchi *et al.*, 2017). Previous research conducted *in vivo* (e.g. Aβ injections in rodent hippocampi) and *in vitro* models have proven that aggregated (oligomeric and protofibrillar) $A\beta_{1-40}/_{1-42}$ at μM concentrations, similar to the concentrations used in the current study, can induce cell death at a concentration-dependent manner via a manner involving the activation of caspase 3 and 7 (Takuma *et al.*, 2004; Sandberg *et al.*, 2010). Another manner by which aggregated Aβ, specifically fibrillar $A\beta_{1-40/1-42}$ has been suggested to induce apoptosis is through an increase in pro-apoptotic bax and decrease in anti-apoptotic bcl-2 expression and also through increasing neuronal susceptibility to oxidative-stress induced cell damage, which has also been linked to regulation of calcium homeostasis (Paradis *et al.*, 1996). A study conducted in SH-SY5Y neuroblastoma cells, although they failed to specify the size of the Aβ aggregates, revealed 50-60% neuroblastoma loss with $A\beta_{1-42}$ incubation (50μM) through a pathway involving JNK activation (Wei, Wang and Kusiak, 2002). Although cell activity experiments carried out in the current study are not a direct measure of cell survival and degree of apoptosis, but more of a measure of metabolic activity, findings from previous studies support the present study where μM concentrations of protofibrillar $A\beta_{1-42}$ caused cell dysfunction by reducing SH-SY5Y activity, and therefore protofibrillar $A\beta_{1-42}$ was shown to act in a neurotoxic manner. Although in the current study nM concentrations of protofibrillar $A\beta_{1-42}$ did not alter SH-SY5Y activity, changes in the expression of proteins which can induce cell death with longer incubation periods cannot be excluded. In contrast to findings from this study, Dahlgren *et al.* (2002) noted

a 50% reduction in neuronal viability with 40nM oligomeric peptide, whereas fibrillar $A\beta_{1-42}$ induced similar degree of neurotoxicity at 10 times higher concentration. Similarly, Huang and Liu demonstrated that incubating SH-SY5Y cells with 10μM fibrillar $A\beta_{1-42}$ for 24hr, and then measuring cell activity via MTT, did not cause cell apoptosis at 24hr but caused significant cell death following a 48hr incubation (Huang and Liu, 2015). Differences in degree of toxicity seen with protofibrillar Aβ treatment in this study compared to other studies could be due to differences in the Aβ aggregates used. Findings from the current study and the literature prove that smaller aggregates such as oligomers and protofibrils are more cytotoxic than fibrillar Aβ. In support of this, another study revealed a 60% reduction in viability of neuro-2A neuroblastoma cells with 20μM oligomeric $A\beta_{1-42}$ treatment, whereas fibrillar $A\beta_{1-42}$ caused significantly less toxicity, hence demonstrating that smaller Aβ aggregates are more toxic-potent (Tizon *et al.*, 2010). Similar effects by oligomeric and fibrillar $A\beta_{1-42}$ were observed in primary rat hippocampal neurons, although lower concentration of $A\beta_{1-42}$ were needed to induce toxicity (Tizon *et al.*, 2010). This suggesting that hippocampal neurons, as primary terminally differentiated neurons show higher susceptibility to Aβ-induced cytotoxicity. In contrast to Tizon *et al.*, our study suggests that although higher degree of toxicity was seen in differentiated cells with 10μM $A\beta_{1-42}$, a more gradual reduction in cell activity was seen in differentiated compared to undifferentiated cells. Differences in the $A\beta_{1-42}$ assembly used could be responsible for differences in the toxicity observed between studies. In contrast, another study demonstrated that co-incubation of rat primary cortical neurons with protofibrillar Aβ caused a significant reduction in viability with as low as 2hr treatment (Walsh *et al.*, 1999). Even though 20% reduction in viability was observed with less that 24hr treatment, concentrations higher than ~20μM were needed to achieve cell death (Walsh *et al.*, 1999). In our study, similar to other studies such as Jan *et al.* (2011) and Hettiarachchi *et al.* (2014) on SH-SY5Y cells, an approximate 30% reduction in cell activity was observed with protofibrillar $A\beta_{1-42}$ incubation with 3-7 times lower concentrations, although a longer treatment duration was needed. Interestingly, Jan *et al.* reported a reduction in degree of neurotoxicity when $A\beta_{1-42}$ monomers were removed from the protofibrillar preparation (Jan *et al.*, 2011). This

suggests that Aβ toxicity is not dependent on just one type of Aβ assembly, but a combination of Aβ assemblies are needed to induce maximum degree of toxicity.

In the current study, although non-aggregated (monomeric) $A\beta_{1-42}$ was expected to not change SH-SY5Y activity, 10μM $A\beta_{1-42}$ caused reduction of undifferentiated SH-SY5Y activity. Agreeing with results from this study, observations from other studies reveal that monomeric $A\beta_{1-42}$ either does not have any effect on neuronal function, or marginally induces an increase in caspase activity (Podlisny *et al.*, 1995; Shao *et al.*, 1999; Sandberg *et al.*, 2010). The reduction in cell activity noted by non-aggregated $A\beta_{1-42}$ in our study and the literature, may be justified by some degree of unavoidable aggregation when cells are co-incubated with the peptide, as it is known that exposure of Aβ to cell cultures can promote peptide aggregation. In contrast to our work, Dahlgren *et al.* (2002), showed that monomeric $A\beta_{1-42}$ at nM concentrations not only does not confer neurotoxicity, but it displayed neurotrophic properties, identified via MTT assay performed on mouse neuro-2A neuroblastoma cells.

Agreeing with the notion that the reverse sequence as it cannot undergo aggregation it therefore cannot induce cytotoxicity, previous observations from other studies (Paradis *et al.*, 1996; Wei, Wang and Kusiak, 2002; Takuma *et al.*, 2004) are in support to findings from the current study where $A\beta_{42-1}$ did not change BV2 microglia or SH-SY5Y cell activity. This proves that the reverse Aβ sequence can be used as an inactive control in AD research.

Taken together, although cell metabolic activity experiments carried out in the current study are not a direct measure of cell death, findings from this study prove that acute treatment with protofibrillar $A\beta_{1-42}$, although high μM concentrations are needed, can indeed cause neurotoxicity through changes in SH-SY5Y cell activity. The observation that no changes in either BV2 microglia or SH-SY5Y cell activity was seen when cells were treated with $A\beta_{42-1}$, which cannot undergo aggregation, proves that cytotoxicity noted by Aβ *in vivo* is indeed due to its aggregated form.

Aβ-mediated changes in neuronal VGCCs

- *Dependent on concentration, protofibrillar $A\beta_{1-42}$ altered Cav1 α1 mRNA expression in differentiated SH-SY5Y cells.*
- *Protofibrillar $A\beta_{1-42}$ at 1μM caused a significant increase in Cav1.2 mRNA expression, whereas a significant reduction in Cav1.3 mRNA expression was seen with 100nM $A\beta_{1-42}$.*
- *Use of a global and selective CCBs were unable to prevent $A\beta_{1-42}$-mediated changes in SH-SY5Y cell activity.*

The current study has shown that protofibrillar $A\beta_{1-42}$, dependent on concentration, impairs calcium homeostasis through selective changes in differentiated SH-SY5Y Cav1 mRNA expression. The use of selective CCBs demonstrated that they were unable to suppress $A\beta_{1-42}$-mediated neurotoxicity. Aβ is known to modulate VGCC-dependent intracellular Ca^{2+} levels in distinct ways; (i) changing the kinetics of calcium currents, (ii) changing the expression of specific VGCC subunits, and (iii) altering channel trafficking to the cell membrane (Chiou, 2006; Anekonda *et al.*, 2011; Gholamipour-Badie *et al.*, 2013).

Findings from this study indicate a significant increase in transcript expression for Cav1.2 with 1μM protofibrillar $A\beta_{1-42}$ treatment. Although in the current study we were unable to investigate whether this change in gene expression translates to a changes a protein level due to issues with the Cav-antibodies available (antibody specificity, no robust signal), work from previous studies indicate Aβ-mediated changes in VGCC expression at protein level as well. Coon *et al.* revealed an upregulation in hippocampal Cav1 channel expression in brains from individuals diagnosed with AD (Coon *et al.*, 1999). As this change in Cav1 expression was localised in areas of extensive neuronal loss, it was suggested that Cav1 channels are important in maintaining neuronal survival and that altered expression of VGCCs seen in AD could be responsible for activating pathways that induce neuronal apoptosis. In contrast to Cav1.2 upregulation at transcript level, the current study revealed that lower concentrations of protofibrillar $A\beta_{1-42}$ (100nM), which more closely represent Aβ physiological levels, caused a significant downregulation in Cav1.3 transcript expression. This is the first study to suggest differential effects of protofibrillar $A\beta_{1-42}$ on Cav1 expression dependent on the Aβ concentration. Although Coon *et al.* findings suggest an increase in global Cav1 expression in AD brains through CCB-autoradiography binding

experiments, it failed to address which Cav1 subfamily members Aβ causes an upregulation of.

Cav1 channels have been linked to neuronal survival and apoptosis. One manner by which changes in Cav1 activity can cause neuronal death is through activation of CAMKKII and phosphorylation of AMPK leading to caspase activation (Hettiarachchi *et al.*, 2014). Work done by Hettiarachchi *et al. (2014)* revealed that this apoptotic mechanism can be blocked by nifedipine, hence proving that protofibrillar $A\beta_{1-42}$ increases Cav1 activity and consequently Ca^{2+} influx, which may occur through changes in the expression of Cav1 channels. Release of ROS which then activates NF-κB, consequently causing an upregulation in Cav1 α1 subunit expression and subsequent increase in Cav1 conductance has been proposed as a pathway that aggregated Aβ can cause increase in Ca^{2+} influx (Green and Peers, 2002; Chiou, 2006). In contrast to the current study, work done by Chiou (2006) suggests that aggregated 20μM $A\beta_{25-35}$ not only causes an upregulation in both gene and protein expression of the α1 subunit of Cav1.2, but also of Cav2.1 and Cav2.2. Contradictory findings in regards to changes in Cav1.3 and Cav2 expression between the current study and Chiou (2006) could be due to a number of differences in the methodologies, for example the species, assembly and the concentration of Aβ used. Additionally, within the present study, changes in mRNA expression of Cav1 channels where only noted in RTA-differentiated SH-SY5Y cells, whereas Chiou investigated changes in VGCC expression in only undifferentiated SH-SY5Y cells which represent a pre-mature neuronal phenotype. It has been suggested that APP can form a direct protein-protein interaction with Cav1.2, consequently reducing Cav1.2 trafficking to the membrane (Yang *et al.*, 2009). This suggests that reduction in APP, due to increased APP processing into Aβ, may be responsible for the noted increase in Cav1.2 expression at the functional level, and not gene level, seen in some studies. In addition, Kim and Rhim (2011) revealed that 25nM $A\beta_{25-35}$ treatment led to an increase in the presence of functional Cav1.2 and Cav1.3 channels at hippocampal cell membranes. Moreover, the increase in Cav1.2 expression could also be linked to an increase at gene level. This suggests, that Aβ may not only alter the expression of the α1 pore-forming subunits, which were investigated in the current study, but may also act through changing the expression or direct interaction with the

VGCC accessory subunits which are responsible for the transport of the channels to the membrane, and hence changing the number of Cav functional channels present at the membrane. In support of this, evidence from co-immunoprecipitation experiments revealed that treatment of Cav1.3 (containing $\alpha 1_D$ and β_3 subunits) transfected HEK293 cells with $A\beta_{25\text{-}35}$ caused a marked increase in both Cav1.3 amplitude and conductance, achieved through direct interaction with the β_3 subunit (Kim and Rhim, 2011).

Although work done in this study clearly suggest Aβ-mediated calcium dyshomeostasis through changes in Cav1 expression at transcript level, the impact of such changes on neuronal function are yet to be resolved. Both Cav1.2 and Cav1.3 are known to have roles in neuronal excitability and neuronal firing (McKinney *et al.*, 2009; Liu *et al.*, 2014). Therefore, the noted increase in Cav1.2 expression at a gene level in this study, if translated to an upregulation at protein level, may suggest an increase in neuronal excitability and firing. Although a number of studies have linked AD to a reduction in neuronal and overall synaptic function, pre-clinical and early-stages AD reveal neuronal hyperexcitability (Busche *et al.*, 2008, 2012; Busche and Konnerth, 2015; Kazim *et al.*, 2017). Thus, this suggests a critical role for Cav1.2 at early stages of the disease. Additionally, Cav1.2-dependent Ca^{2+} influx has also been linked to CREB-dependent gene transcription of genes with roles in synaptic function, neuronal proliferation, differentiation, and neuronal survival (Moosmang *et al.*, 2005; Marschallinger *et al.*, 2015). Therefore, in further support of an upregulation of Cav1.2 at early-stages of the disease, increase in CREB-dependent activation of genes linked to synaptic activity and plasticity may cause the reported neuronal hyperactivity. Cav1.3 has also been shown to have a role in dentritic spine morphology and stability (Stanika, Flucher and Obermair, 2015; Stanika *et al.*, 2016). A reduction in Cav1.3 in this study may suggest structural changes in dendrites which could impair long-term potentiation and overall synaptic activity (McKinney *et al.*, 2009). In addition, adult neurogenesis, a process important in learning and memory, has also been shown to be regulated by Ca^{2+} influx through Cav1.3 (Marschallinger *et al.*, 2015). The reduction in Cav1.3 expression shown by treatment with protofibrillar $A\beta_{1\text{-}42}$ in this study may explain the cognitive deficits due to impaired neurogenesis seen at early stages of Alzheimer's disease (Scopa *et al.*, 2020).

It is widely accepted that not only pathological conditions, but also normal ageing can alter the expression of Cav1 channels, seen in studies on animal models and post-mortem tissue (Blalock *et al.*, 2003; Thibault *et al.*, 2012; Nunez-Santana *et al.*, 2014). Consequently, there is a considerable interest in investigating whether pathological conditions such as AD may induce changes in VGCC expression different than those seen during normal ageing. Work done by Nunez-Santana demonstrated an increase in the presence of both Cav1.2 and Cav1.3 on the cell surface of hippocampal neurons (Nunez-Santana *et al.*, 2014). Although an increase in functional Cav1 channels was observed, this was not due an upregulation at transcript level (Nunez-Santana *et al.*, 2014). Despite Nunez-Santana *et al.* not observing any changes in the mRNA expression of specific Cav1 members, their study focused on identifying changes in VGCC expression during normal ageing. Therefore, this suggests that during normal ageing, compared to pathological conditions such as AD, other factors may be responsible for changes in VGCC expression at the functional level such as post-translational modifications, or changes in neuronal excitability.

In further support of an important role for Cav1 channels at early-stages of AD pathology, Gholamipour-Badie and colleagues, through behavioural experiments revealed that the Cav1 CCBs nimodipine and isradipine were beneficial in reducing the decline of learning and memory in Wistar rats which were induced by $A\beta_{1-42}$ injections in the endorhinal cortex (Gholamipour-Badie *et al.*, 2013). Block of Cav1 channels by these CCBs led to a downregulation of calpain-2 at protein level, and subsequent reduction in caspase-12 and -3 protein expression, therefore reducing synaptic loss and neuronal apoptosis (Gholamipour-Badie *et al.*, 2013). In further support of Cav1 channels role in neuronal survival, Anekonda *et al.* (2011) revealed that isradipine, reduced oligomeric $A\beta_{1-42}$ -mediated neurotoxicity in APP-stably transfected MC65 neuroblastoma cells, although this occurred through a caspase-3 independent pathway. Similar to our study, oligomeric $A\beta_{1-42}$ was found to increase Cav1-dependent Ca^{2+} influx via a 2-fold upregulation of Cav1.2 mRNA expression, with a delayed increase in protein level seen by 72hr (Anekonda *et al.*, 2011). Ueda and colleagues revealed that incubation of both cortical and hippocampal neurons with protofibrillar 10μM $A\beta_{25-35}$ increased Ca^{2+} influx, possibly through an upregulation in VGCC expression, which in

turn induced cell apoptosis through a ROS manner (Ueda *et al.*, 1997). Agreeing with findings from the present study where no change in the Cav2.2 expression, and also use of Cav2 CCBs did not alter Aβ-mediated changes in cell activity, Ueda *et al.* shown that 3μM nimodipine significantly reduced both Ca^{2+} influx and cell death mediated by $A\beta_{25-35}$, whereas blockers of Cav2.1 and Cav2.2 channels, at the concentrations tested, were largely non-effective against Aβ-induced cell death (Ueda *et al.*, 1997). In contrast to Ueda's study, Brown *et al.* 2005, suggested that mitochondrial dysfunction and release of ROS precedes Aβ-mediated changes in VGCC activity. This in turn, induces aggregation of $A\beta_{1-40}$ which then causes an increasing in Cav1.2 α1 subunit trafficking, increasing the number of functional channels present at the membrane and increasing overall Ca^{2+} influx (Brown *et al.*, 2005). Differences in findings could be due to studying the effect of aggregated Aβ in transfected- HEK293 cell line, compared to primary neurons which natively express VGCCs. Contradictory to other studies, Thibault *et al.*, revealed that in hippocampal neurons of APP/PS1 mouse models of AD, a reduction in the activity of Cav1 currents is observed as compared to hippocampal neurons from control animals (Thibault *et al.*, 2012). Yagami *et al.* (2004), revealed that incubation of primary cortical neurons with 10μM aggregated $A\beta_{25-35}$ caused noted morphological changes and DNA damage, leading to 70% cell death by 48hr. Whereas adding $A\beta_{25-35}$ in combination with Cav1 CCBs S-312-d or nimodipine, significantly reduced the noted cell death (Yagami *et al.*, 2004). These results further prove that Cav1 channels have a critical role in Aβ-mediated neuronal death. On the other hand, similar to our study conducted on both undifferentiated and differentiated SH-SY5Y cells, treating primary cortical neurons with $A\beta_{25-35}$ and the Cav2 CCBs ω-conotoxin-MVIIC/ω-agatoxin-IVA (P/Q-type blockers) or ω-conotoxin-GVIA (N-type blocker) did not reduce $A\beta_{25-35}$ -mediated neurotoxicity (Yagami *et al.*, 2004). This suggests that neuronal cell apoptosis induced by aggregated Aβ occurs through a Cav1, but Cav2-independent pathway. In further support of Cav1 role in neuronal survival, use of the Cav1 CCB nimopridine can prevent Aβ-mediated neuronal loss further proving that part of Aβ's mechanism of action involves Cav1 channels, possibly through inducing their activation (Ho, Ortiz and Shea, 2001).

Overall, evidence from the present study and the literature, points to an important role for Cav1 channels in AD pathology through changes in neuronal survival. Although in this study, changes in the mRNA expression of Cav1 channels were noted with protofibrillar $A\beta_{1\text{-}42}$ treatment, the effect of the peptide on Cav1 channels at the functional level was not investigated. Likewise, although protofibrillar $A\beta_{1\text{-}42}$ did not alter transcript expression of Cav2 and Cav3 channels, the effect of the peptide on channel conductance, or through direct interaction and changes in the expression of accessory subunits cannot be excluded. Differences in results obtained in this study compared to the literature could be due to variations in methodology, such as the $A\beta$ peptide concentration and species used, degree of aggregation, cell type investigated and which VGCC members and subunit isoforms the studies focused on.

Effect of CO on Aβ-mediated neurotoxicity

- *Treating SH-SY5Y cells with either $A\beta_{1-42}$ left to aggregate in the presence of CORM2, or with a combination of protofibrillar $A\beta_{1-42}$ and CORM2 did not alter Aβ-mediated changes in cell activity.*

The current study demonstrates that allowing $A\beta_{1-42}$ to aggregate in the presence of CORM2, did not reduce Aβ-mediated changes in undifferentiated SH-SY5Y cell (metabolic) activity. In addition, treating both undifferentiated and differentiated SH-SY5Y cells with a combination of protofibrillar $A\beta_{1-42}$ and CORM2, also did not alter Aβ-mediated changes in cell activity.

CORM molecules can directly interact with Aβ through modification of specific amino acid residues. For example, Valensin *et al.* (2010) suggested a direct interaction of CORM3 with histidine (His) residues on the $A\beta_{1-28}$ peptide (His13 & His14), significantly reducing degree of cytotoxicity (Valensin *et al.*, 2010). In support of this, Santos-Silva and colleagues also demonstrated that CORM3 is able to form protein adducts by direct interaction of the ruthenium (Ru) structure with His residues on the Aβ peptide (Santos-Silva *et al.*, 2011). Arispe *et al.*, discovered that modulation of His residues of the Aβ peptide, such as through the use of His-related compounds, prevented Aβ pore formation on the membrane and subsequent calcium dyshomeostasis and cell death (Arispe, Diaz and Flora, 2008). Due to this, there has been considerable interest in identifying whether a potential Ru-Aβ complex could potentially reduce some of the toxic effects of the peptide *in vivo*. Building on these studies, De Simone *et al.* (2019) revealed that CORM3 can act as an anti-aggregator molecule through direct interaction of the CORM3 Ru structure with His residues of the peptide when $A\beta_{1-42}$ was left to aggregate in the presence of high non-physiological concentrations of CORM3 (250-500μM). Similarly, CORM2, which contains two Ru structures, was also shown to form CORM2/$A\beta_{1-42}$ stable adducts at a much lower CORM2/$A\beta_{1-42}$ molar ratio. ESI-mass spectrometry and ThT analysis revealed that in peptide preparations that contain CORM3 (1:1 ratio; 50μM), monomeric structures could still be detected by 48hr, whereas in the absence of CORM3 complete removal of monomeric structures is observed by 48hr (De Simone *et al.*, 2019). In our study, using the same methodology as the one used by De Simone *et al.* to let $A\beta_{1-42}$ aggregate in the presence of CORM2, did not protect SH-SY5Y cells from $A\beta_{1-42}$-mediated changes in

cell activity. Although no changes in cytotoxicity were noted, direct interaction of CORM2 with the peptide could not be excluded. Differences in observations within our study and other studies could be due to differences in methodology such as the type and concentration of CORM, and also Aβ concentration, species and assembly used. For example, De Simone *et al.*, used $A\beta_{1-42}$ at concentrations as high as 50μM which do not correspond to physiological concentrations seen *in vivo*. Additionally, pre-treatment of $A\beta_{1-42}$ was carried out in HFIP, in contrast to NH_4OH which was used in our study. Moreover, concentrations above 100μM of CORM2 tested by De Simone and colleagues do not correspond to physiological levels of CO.

In addition to CORM2 (via its ruthenium structure) interfering with the aggregation process of Aβ, Kim *et al.* (2019) was able to prove that CO is able to interfere with Aβ production. Injection of CORM3 to 3xTg-AD animal models, significantly reduced the expression of *BACE1* (β-secretase) at both mRNA and protein level through NF-κB binding *BACE1*, causing a reduction in Aβ production (Kim *et al.*, 2019).

In addition to CO demonstrating anti-aggregating properties, evidence suggests that CO may also exert anti-apoptotic effects. In the current study, CORM2 was unable to prevent $A\beta_{1-42}$ -mediated neurotoxicity. A number of pre-clinical studies conducted on animal models revealed that inhalation of physiological levels of CO, was able to protect further tissue damage by reducing neuronal loss in the hippocampus and the cortex, during times of restoration of oxygen flow following an ischemic stroke, possibly through an ion channel-dependent mechanism (Zeynalov and Doré, 2009; Mahan *et al.*, 2012). One pathway by which it may confer these anti-apoptotic effects, could be through increasing sGC activity, increasing NOS activity and NO production through an ion-channel manner (Vieira, Queiroga and Alves, 2008). As treatment with nM concentrations of oligomeric $A\beta_{1-42}$ have been linked to changes in the activity of sGC and subsequent expression of cGMP and phosphorylation of CREB, with can have detrimental effect in neuronal plasticity (Puzzo *et al.*, 2005), CO's effect on this pathway may prevent neuronal dysfunction and subsequent neuronal death seen in AD. Zuckerbraun *et al.* (2007) proposed a different pathway that CO may confer anti-apoptotic effects via a mechanism involving mitochondria targeting. CO cytoprotection included inhibition of cytochrome c oxidase, release of ROS from mitochondria, and

lastly activation of p38, similar to the mode of action seen by the gasotransmitter nitric oxide (Zuckerbraun *et al.*, 2007). Hettiarachchi *et al.* revealed that use of a selective and a pan-caspase blocker reduced protofibrillar $A\beta_{1-42}$ cytotoxicity, suggesting that activating pro-apoptotic pathways via caspases is part of the manner by which protofibrillar $A\beta_{1-42}$ causes cell dysfunction. Hettiarachchi *et al.* also revealed that part of the peptide's mode of action involves increasing Cav1 channel activity, which in turn can cause activation of CAMKKII and subsequent phosphorylation and activation of AMPK. Phosphorylation and subsequent activation of AMPK could be blocked with CORM2 treatment (Hettiarachchi *et al.*, 2014). In contrast to Hettiarachchi *et al.*, research done by Duckles proposed that CO can reduce Cav3 channel conductance, and therefore exhibit anti-proliferative properties (Duckles *et al.*, 2015). In contrast to Hettiarachchi *et al.* where CORM2 was shown to prevent Aβ-mediated cell death of both SH-SY5Y and hippocampal neurons through direct evaluation of cell apoptosis via measuring activation of caspase-3 and propidium iodine staining, our data suggest that CORM2 was unable to reduce $A\beta_{1-42}$-mediated change in cell activity in both undifferentiated and differentiated SH-SY5Y cells. Although our study suggests that CORM2 is unable to prevent $A\beta_{1-42}$ induced cytotoxicity, differences in findings could be due to differences in methodology. For example, in our study a higher concentration of $A\beta_{1-42}$ (3μM) was tested, whereas Hettiarachchi tested lower concentrations that better represent *in vivo* $A\beta_{1-42}$ levels (100 and 500nM). Additionally Hettiarachchi *et al.* reported CORM2 anti-apoptotic effects using a higher molar ratio (1:100) than the ones tested in the current study. Moreover, Hettiarachchi used techniques that directly measure degree of cell apoptosis (caspase-3 and propidium iodine staining), whereas in this study metabolic activity was evaluated which although can give indication of cell dysfunction, it does not directly investigate cell death. Lastly, although previous studies have suggested that CO can exhibit anti-apoptotic effects through increasing sGC and preventing the phosphorylation of CAMKII and AMPK, lack of anti-apoptotic effects seen in the current study by CORM2 may suggest that μM concentrations of $A\beta_{1-42}$ may induce apoptosis through independent pathways than those seen with more physiological concentrations of $A\beta_{1-42}$.

To recap, although CORMs via their ruthenium structure, and CO specifically have been shown by previous studies to act cytoprotectively, in the current study, CORM2 was unable to prevent Aβ-mediated changes in SH-SY5Y cell activity. Although direct interaction of CORM2 with $A\beta_{1-42}$ cannot be excluded, the findings suggest that $A\beta_{1-42}$ at the concentrations tested, and CORM2 may influence cell activity through independent pathways.

4.4. Summary

This study has demonstrated that NH_4OH pre-treatment of $A\beta_{1-42}$ leads to time-dependent protofibril formation that structurally and functionally resembles aggregated $A\beta_{1-42}$ cytotoxicity *in vivo*. In addition, this is the first study to compare $A\beta_{1-42}$ aggregation in the presence or absence of SDS. In support of the hypothesis that SDS can mimic the cell microenvironment, low levels of SDS were proven to aid protofibril formation.

Overall, findings from the current study, agreeing with the hypotheses, have proven that protofibrillar $A\beta_{1-42}$ does indeed impair neuronal function, through pathways including changes in voltage-gated calcium channel mRNA expression. Changes in Cav1.2 and Cav1.3 gene expression seen in this study may suggest a role for Cav1 channels at early stages of AD. Although CORM2 has been shown to act cytoprotectively, and although cell metabolic activity assays carried in this study cannot exclude a direct interaction of CORM2 with the peptide, in the current study CORM2 was unable to prevent $A\beta$-mediated cell dysfunction. Further experiments aim to investigate and identify the effect of protofibrillar $A\beta_{1-42}$ and CORM2 on Cav2.2 at the functional level, due to its high expression in the CNS and important role in synaptic function. This will further our understanding of protofibrillar $A\beta_{1-42}$ and CO role on neuronal function and specifically synaptic activity.

Chapter 5: Modulation of Cav2.2 channels by $A\beta_{1\text{-}42}$ and CO

5.1. Introduction

Oxidative stress forms part of the pathogenesis of many diseases, including AD (Subbarao *et al.*, 1990; Schipper *et al.*, 1995; Dallas *et al.*, 2011; Wojsiat *et al.*, 2018). Reduction in antioxidants, increase in lipid peroxidation products and redox active iron which induces ROS release, identified via post-mortem studies, have been reported in AD (Subbarao *et al.*, 1990; Schipper *et al.*, 1995). Oxidative stress has been linked to neuronal dysfunction and ultimately cell death seen in AD (Schipper *et al.*, 1995; Pappolla *et al.*, 1998; Schipper, 2004). In AD, oxidative stress and increase in heme levels have been linked to an upregulation in HO-1 expression, seen in neurons and astrocytes, which is believed to occur as a defence mechanism against free radicals (Schipper, Cissé and Stopa, 1995; Hettiarachchi *et al.*, 2014). As CO is one of the products of HO-dependent heme catabolism, recently there has been considerable interest in identifying whether CO can exert antioxidant properties and be effective against AD pathology.

It is widely accepted that post-translational modifications, such as redox modulation, can modulate the activity of ion channels including VGCCs (Li *et al.*, 1998; Lazniewska and Weiss, 2017; Qian *et al.*, 2017). Numerous studies have proposed that CO may modulate ion channels through a number of different mechanisms. In voltage-gated potassium channels, such as Kv2.1, which have been implicated with cell death, CO was shown to prevent oxidant-dependent neuronal death (Dallas *et al.*, 2011). In contrast, in Kv1.5 inhibition by CO was shown to occur through an oxidant-dependent manner via a pathway possibly involving release of ROS from mitochondria (Al-Owais *et al.*, 2017). In cardiac K_{ATP} channels findings revealed that CO can activate these channels through a heme binding domain (Kapetanaki *et al.*, 2018). CO requires heme to bind to K_{ATP}, forming a complex which CO can then interact with, and modulate these channels (Kapetanaki *et al.*, 2018). In VGCCs, specifically Cav1 and Cav3 channels, CO was also shown to change channel kinetics through an oxidation mechanism (Scragg *et al.*, 2008; Boycott *et al.*, 2013). Release of ROS from mitochondria and direct modulation of cysteine residues at specific sites on the α1 pore-forming subunit have been implicated as some of the mechanisms by which CO may modulate Cav channel kinetics, and consequently channel activity (Scragg *et al.*, 2008; Boycott *et al.*, 2013).

As AD has been linked to altered VGCC expression and activity (Nimmrich *et al.*, 2008; Mezler *et al.*, 2012; Hermann *et al.*, 2013), investigating the effect of protofibrillar $A\beta_{1-42}$ on calcium currents, and redox-dependent VGCC modulation may help us better understand AD pathology and the role of VGCCs in AD pathogenesis. Additionally, identifying novel mechanisms by which oxidative stress or its downstream effects can be targeted may have clinical significance in treating AD. Although a number of studies have proven that CO can modulate ion channels via a redox-dependent pathway, the effect of CO on Cav2.2 channels has not been investigated.

Cav2.2 channels merit further investigation given their prominent role in mediating presynaptic Ca^{2+} influx. The effect of CO on channel kinetics, through CORM2 treatment, was investigated in Cav2.2-stably transfected HEK293 cells. Moreover, the hypothesis that CO may modulate Cav2.2 channels through a redox manner was also tested.

5.1.1. Aim

The aim of the study was to identify the effects of protofibrillar $A\beta_{1-42}$ on Cav2.2 at the functional level. Additionally, the effect of CO on Cav2.2 was also investigated, while examining whether the mechanism of action of CO involves redox modulation of these channels.

5.1.2. Objectives

- To identify the effect of protofibrillar $A\beta_{1-42}$ on Cav2.2 channels at the functional level using Cav2.2 (α_{1B} ($Ca_v2.2$), β_{1b}, and $a_2\delta$ subunits) stably-transfected HEK293 cells.
- To investigate CO-dependent changes in Cav2.2 channel properties, using CORM2 treatment of Cav2.2 (α_{1B} ($Ca_v2.2$), β_{1b}, and $a_2\delta$ subunits) channels in stably-transfected HEK293 cells.
- To examine whether CO modulates Cav2.2 channels via a redox mechanism through the use of the oxidant DTDP and reducing agent DTT.

5.1.3. Hypotheses

- Due to the important role(s) of Cav2.2 in neuronal cells, it is expected that protofibrillar $A\beta_{1\text{-}42}$ may change channel kinetics.
- As CO has shown to modulate a number of ion channels, it is expected that CORM2 may change channel kinetics through post-translational modification.

5.2. Results

5.2.1. Effect of protofibrillar Aβ1-42 on Cav2.2. channels

Prior to investigating the effect of protofibrillar $A\beta_{1-42}$ on Cav2.2 kinetics, the presence of functional Cav2.2 (α_{1B} ($Ca_v2.2$), β_{1b}, and $a_2\delta$ subunits) in stably transfected HEK293 cells was verified via whole cell patch clamp. Treatment of cells with the Cav2.2 blocker ω-conotoxin-GVIA confirmed the presence of functional Cav2.2 channels (n=5) (**Fig. 5.2.1.1A and B**). Cells displayed maximum current at +10mV. Boltzmann fit analysis to current voltage (I/V) relationship was used to investigate changes in biophysical properties. Reversal potential (Rp), maximal conductance (G_{max}), V_{half}, and slope (k) remained unaltered following exposure to 10nM ω-conotoxin-GVIA (**Fig. 5.2.1.2A-D**). Cells were also subjected to a single-step protocol (+10mV) for investigating changes in current density over time (**Fig. 5.2.1.3A and B**). The CCB ω-conotoxin-GVIA (~10mins) caused a significant reduction in Cav2.2 current density by 21.0 ± 7.4 pA/pF ($P<0.05$) compared to untreated cells. Time-dependent reduction in Cav2.2 current amplitude can be seen in **Fig. 5.2.1.3C**.

Once the presence of functional Cav2.2 channels was verified, the effect of protofibrillar $A\beta_{1-42}$ on Cav2.2 currents was investigated via population experiments using whole cell patch clamp (n=15). A multi-step protocol was applied to Cav2.2 stably-transfected HEK293 cells treated with 100nM protofibrillar $A\beta_{1-42}$ for 24hr (**Fig. 5.2.1.4A**). Rp, G_{max}**,** V_{half} and current density remained unaffected (**Fig. 5.2.1.4A-C and F**). In contrast, 100nM protofibrillar $A\beta_{1-42}$ caused a significant change in Cav2.2 slope factor by 6.8 ± 3.0 mV ($P<0.05$) compared to vehicle control (PBS) treated cells (**Fig. 5.2.1.4D**).

In contrast, Cav2.2 currents treated with a higher concentrations of protofibrillar $A\beta_{1-42}$ (24hr; 1μM) revealed a significant reduction in both G_{max} (**Fig. 5.2.1.5A and C**) and current density (**Fig. 5.2.1.5F**) by 0.5 ± 0.2 ns/pF ($P<0.05$) and 20.1 ± 11.0 pA/pF ($P<0.05$) respectively. Other channel properties such as Rp (**Fig. 5.2.1.5B**), V_{half} (**Fig. 5.2.1.5D**) and k (**Fig. 5.2.1.5E**) remained unaffected.

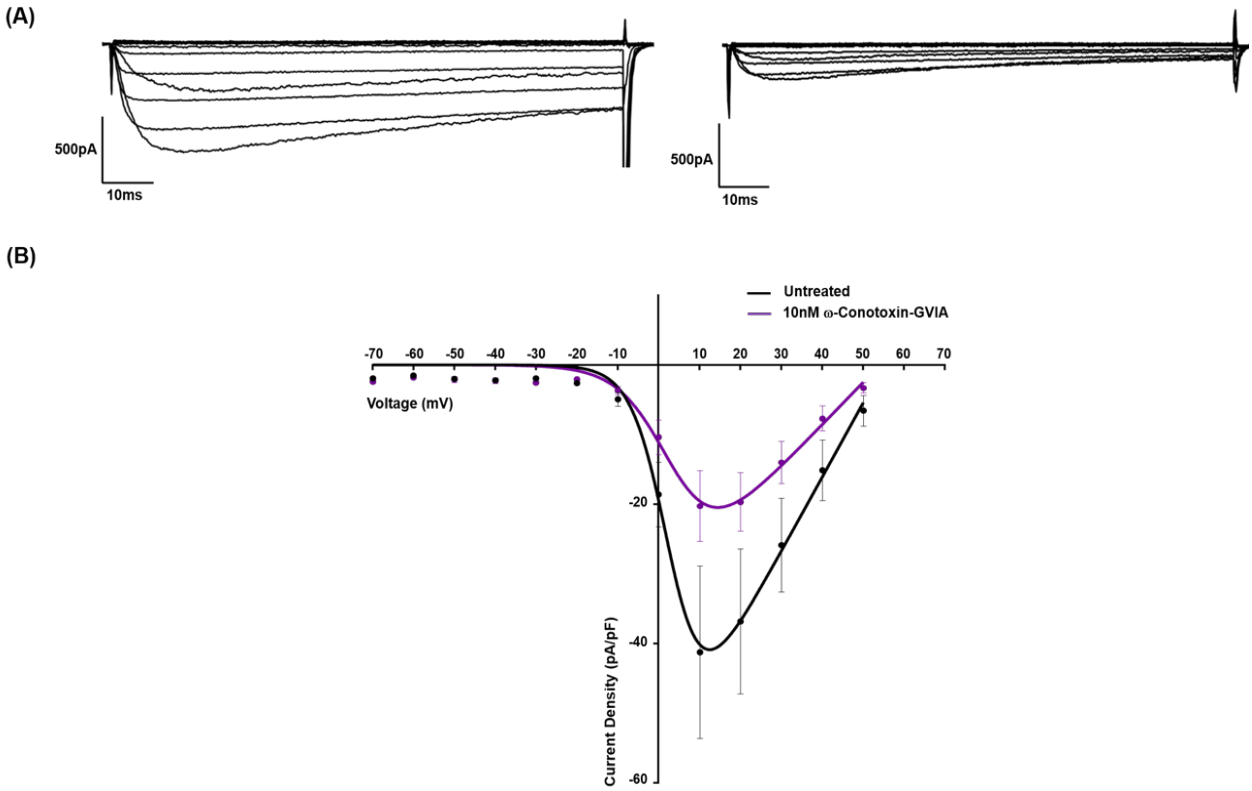

Figure 5.2.1.1: Effect of ω-Conotoxin-GVIA on Cav2.2 currents. *The effect of ω-conotoxin-GVIA on Cav2.2 channels of stably-transfected HEK293 cells was investigated via whole-cell patch clamp.* ***(A)*** *Example current-voltage traces (-70 to +50mV) prior (left) and after (right) 10nM ω-conotoxin-GVIA treatment.* ***(B)*** *Current-voltage (-70 to +50mV) relationship of Cav2.2 channels (mean ± SEM) of HEK293 cells prior and after 10nM ω-conotoxin-GVIA treatment, fitted with the Boltzmann fit equation (n=5). Clampfit 10.3 was used for trace analysis, and GraphPad for plotting current-voltage relationship and Boltzmann fit analysis.*

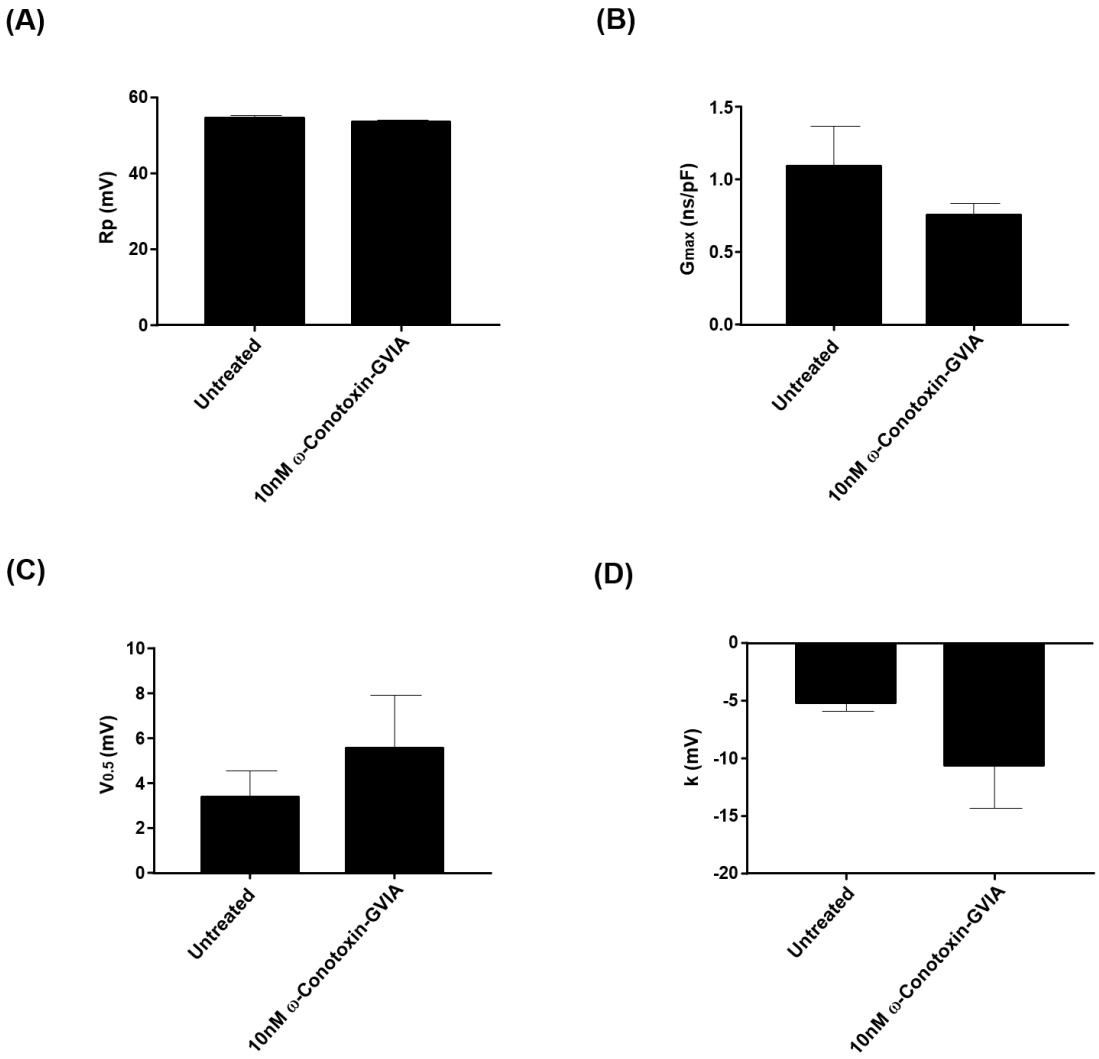

Figure 5.2.1.2: Effect of ω-conotoxin-GVIA on Cav2.2 kinetics. *The effect of ω-conotoxin-GVIA on Cav2.2 channel kinetics of stably transfected HEK293 cells was investigated via whole-cell patch clamp.* ***(A)*** *Reversal potential of Cav2.2 channels (mean ± SEM) prior (untreated) and after 10nM ω-conotoxin-GVIA treatment (n=5).* ***(B)*** *Maximal conductance of Cav2.2 channels (mean ± SEM) prior (untreated) and after 10nM ω-conotoxin-GVIA treatment (n=5).* ***(C)*** *Half-activation voltage of Cav2.2 channels (mean ± SEM) prior (untreated) and after 10nM ω-conotoxin-GVIA treatment (n=5).* ***(D)*** *Slope of Cav2.2 channels (mean ± SEM) prior (untreated) and after 10nM ω-conotoxin-GVIA treatment (n=5). Clampfit 10.3 was used for trace analysis, and GraphPad for analysing changes in channel kinetics obtained from Boltzmann fit analysis. Statistical analysis was carried out via one-tailed paired T-test.*

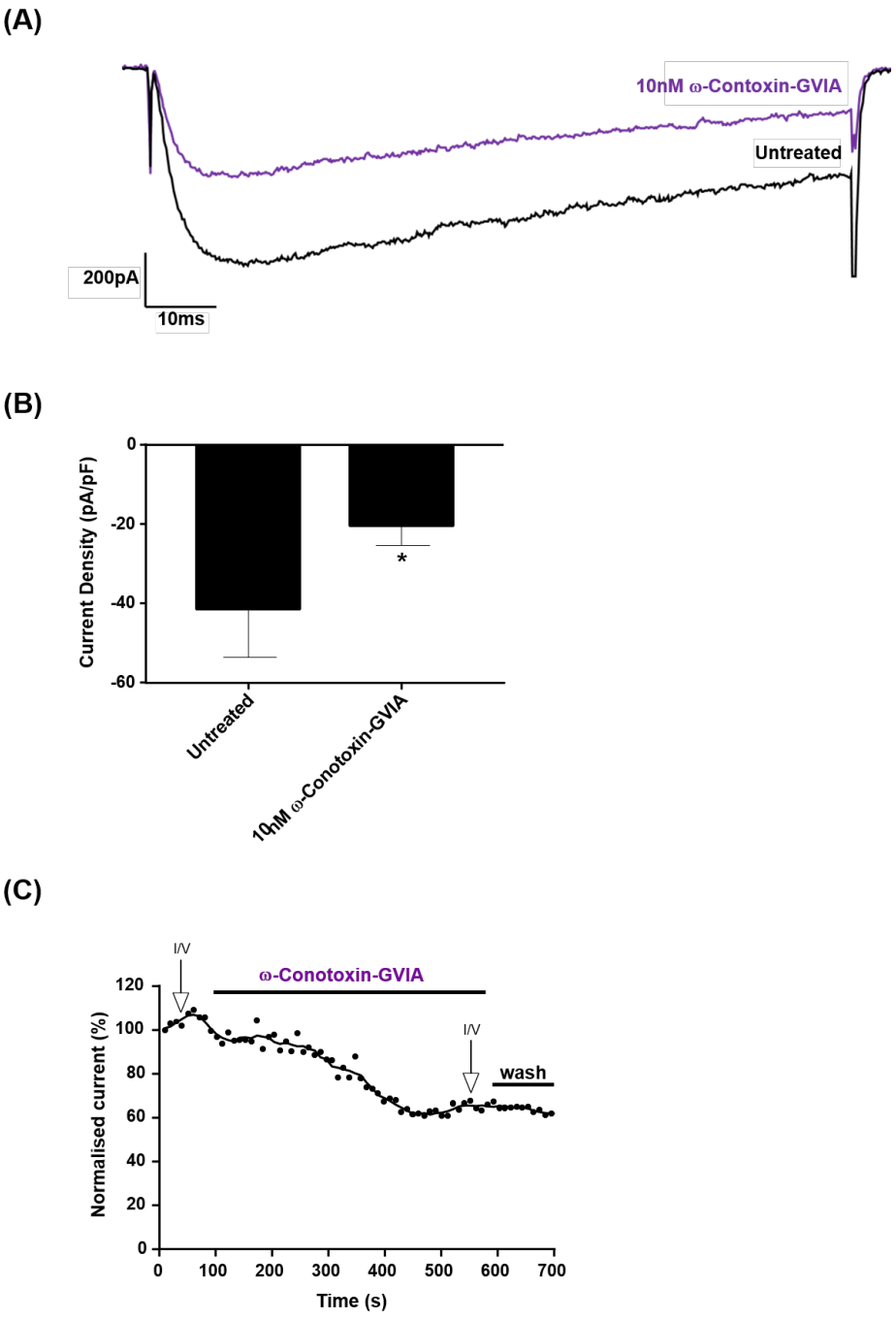

Figure 5.2.1.3: Effect of ω-conotoxin-GVIA on Cav2.2 current amplitude. *The effect of ω-conotoxin-GVIA on Cav2.2 current amplitude of Cav2.2-stably transfected HEK293 cells was investigated via whole-cell patch clamp.* ***(A)*** *Example trace of a single-step (+10mV) recording of Cav2.2 current prior (black) and after (purple) 10nM ω-conotoxin-GVIA treatment.* ***(B)*** *Reduction in Cav2.2 current amplitude (mean ± SEM) with ω-conotoxin-GVIA treatment (n=5).* ***(C)*** *Representative example of time-dependent changes in Cav2.2 current amplitude (+10mV) with ω-conotoxin-GVIA (purple) treatment. Clampfit 10.3 was used for trace analysis, and GraphPad for analysing changes in current amplitude. Statistical analysis was carried out via one-tailed paired T-test. (*=P<0.05)*

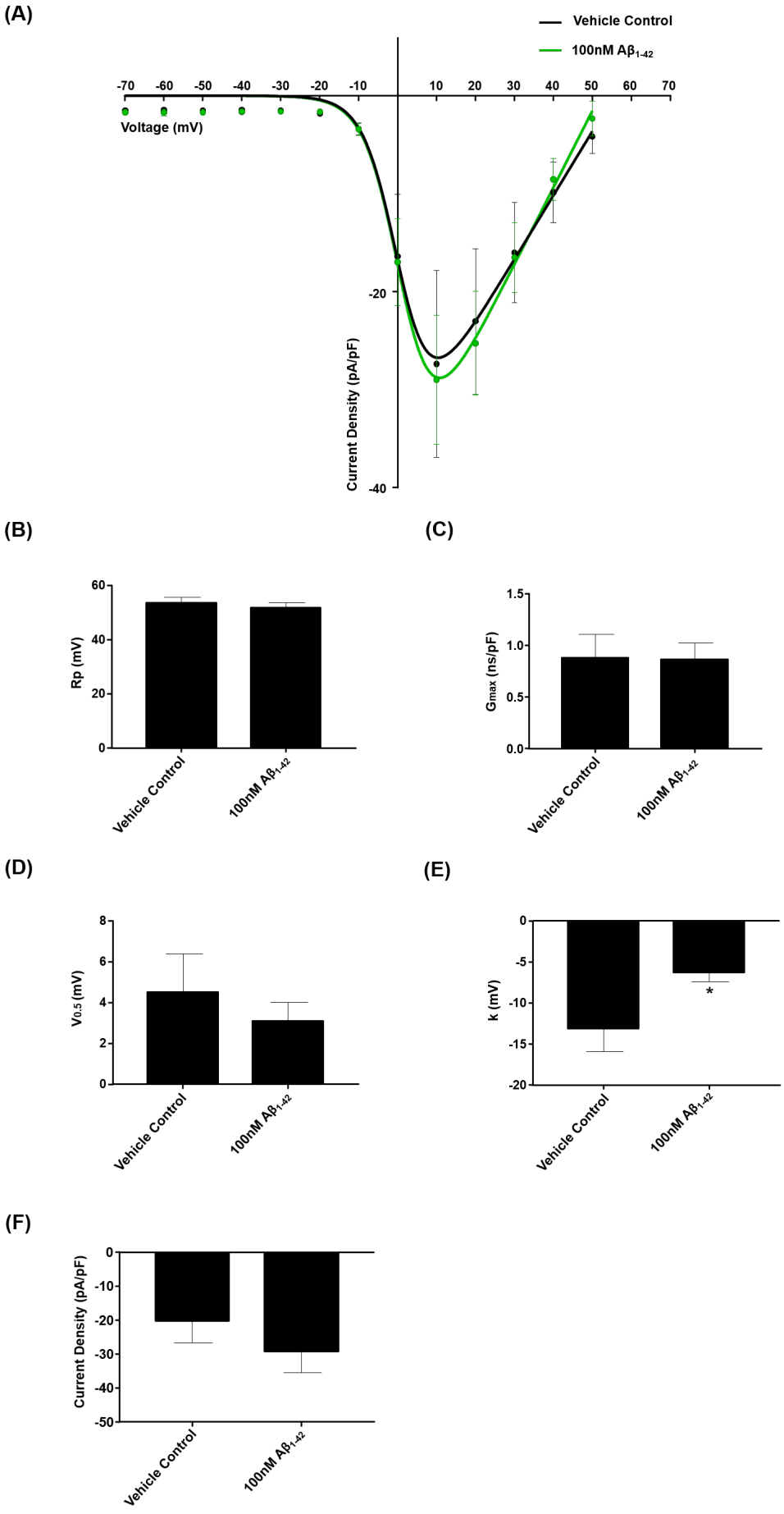
(A)
Vehicle Control
100nM Aβ1-42
-70 -60 -50 -40 -30 -20 -10 10 20 30 40 50 60 70
Voltage (mV)
-20
-40
Current Density (pA/pF)
(B)
Rp (mV)
60
40
20
0
Vehicle Control
100nM Aβ1-42
(C)
Gmax (ns/pF)
1.5
1.0
0.5
0.0
Vehicle Control
100nM Aβ1-42
(D)
V0.5 (mV)
8
6
4
2
0
Vehicle Control
100nM Aβ1-42
(E)
k (mV)
0
-5
-10
-15
-20
*
Vehicle Control
100nM Aβ1-42
(F)
Current Density (pA/pF)
0
-10
-20
-30
-40
-50
Vehicle Control
100nM Aβ1-42

Figure 5.2.1.4: Effect of protofibrillar 100nM Aβ_{1-42} on Cav2.2 kinetics. *Whole-cell patch clamp population experiments investigating the effect of protofibrillar 100nM Aβ_{1-42} on Cav2.2 channel kinetics of Cav2.2-stably transfected HEK293 cells.* ***(A)*** *Current-voltage (-70 to +50mV) relationship of Cav2.2 channels (mean ± SEM) treated with the vehicle control (PBS) compared to protofibrillar 100nM Aβ_{1-42} treatment (n=15).* ***(B)*** *Reversal potential of Cav2.2 channels (mean ± SEM) treated with the vehicle control(PBS) compared to protofibrillar 100nM Aβ_{1-42} (n=15).* ***(C)*** *Maximal conductance of Cav2.2 channels (mean ± SEM) treated with the vehicle control (PBS) compared to protofibrillar 100nM Aβ_{1-42} (n=15).* ***(D)*** *Half-activation voltage of Cav2.2 channels (mean ± SEM) treated with the vehicle control (PBS) compared to protofibrillar 100nM Aβ_{1-42} (n=15).* ***(E)*** *Changes in the slope of Cav2.2 channels (mean ± SEM) treated with protofibrillar 100nM Aβ_{1-42} (n=15).* ***(F)*** *Current density of Cav2.2 channels (mean ± SEM) of HEK293 cells treated with vehicle control (PBS) compared to protofibrillar 100nM Aβ_{1-42} treatment (n=15). Clampfit 10.3 was used for trace analysis. GraphPad was used for plotting current-voltage relationship and carrying out Boltzmann fit analysis. Statistical analysis was carried out via one-tailed unpaired Welch T-test. (*=P<0.05)*

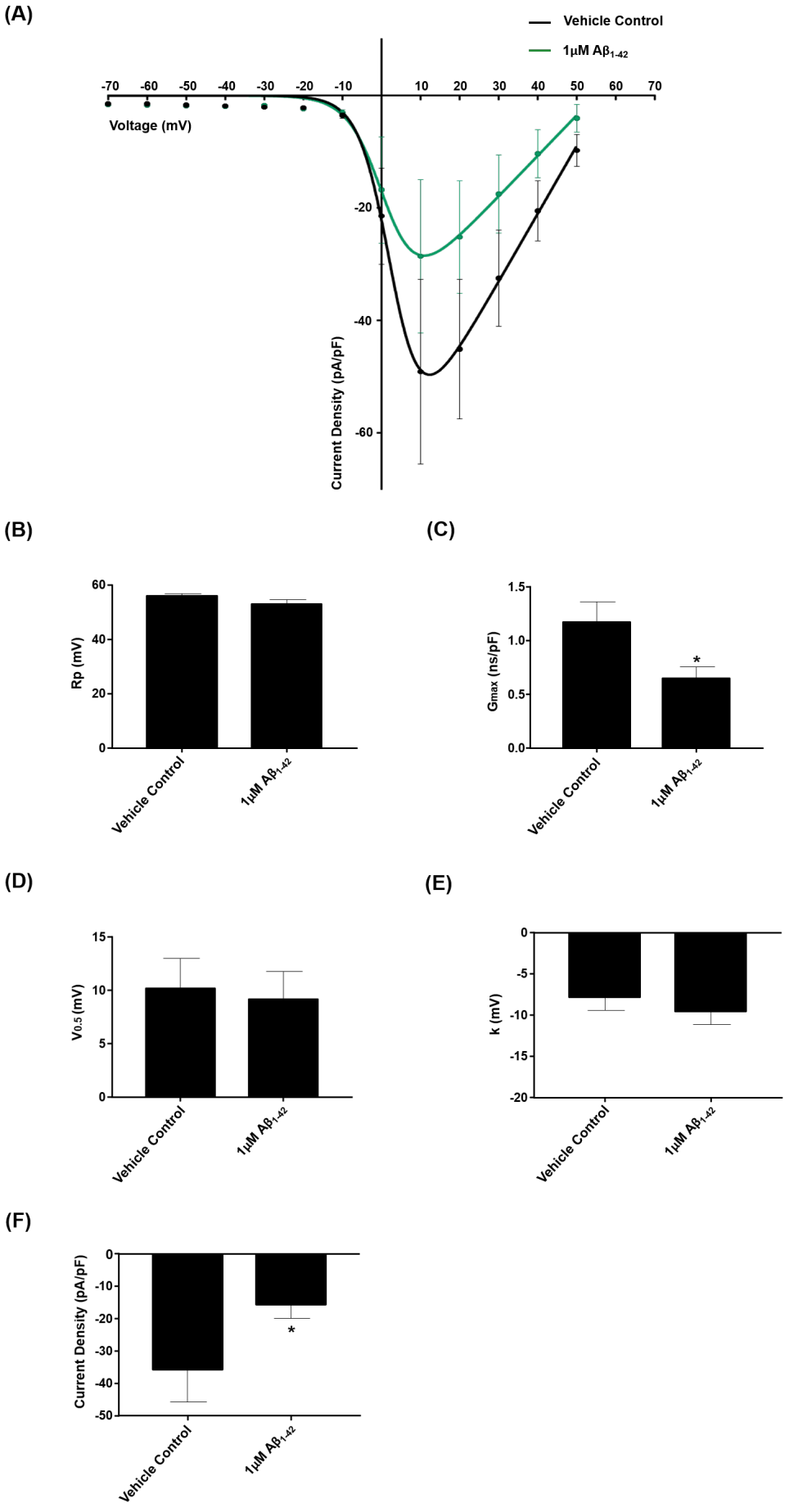
(A)
Vehicle Control
1μM Aβ1-42
-70 -60 -50 -40 -30 -20 -10 10 20 30 40 50 60 70
Voltage (mV)
-20
-40
-60
Current Density (pA/pF)
(B)
Rp (mV)
60
40
20
0
Vehicle Control
1μM Aβ1-42
(C)
Gmax (ns/pF)
1.5
1.0
0.5
0.0
*
Vehicle Control
1μM Aβ1-42
(D)
V0.5 (mV)
15
10
5
0
Vehicle Control
1μM Aβ1-42
(E)
k (mV)
0
-5
-10
-15
-20
Vehicle Control
1μM Aβ1-42
(F)
Current Density (pA/pF)
0
-10
-20
-30
-40
-50
*
Vehicle Control
1μM Aβ1-42

Figure 5.2.1.5: Effect of protofibrillar 1μM Aβ_{1-42} on Cav2.2 kinetics. *Whole-cell patch clamp population experiments investigating the effect of protofibrillar 1μM Aβ_{1-42} on Cav2.2 channel kinetics of Cav2.2-stably transfected HEK293 cells.* ***(A)*** *Current-voltage (-70 to +50mV) relationship of Cav2.2 channels (mean ± SEM) treated with vehicle control (PBS) compared to protofibrillar 1μM Aβ_{1-42} treatment (n=15).* ***(B)*** *Reversal potential of Cav2.2 channels (mean ± SEM) treated with the vehicle control (PBS) compared to protofibrillar 1μM Aβ_{1-42} (n=15).* ***(C)*** *Reduction in maximal conductance of Cav2.2 channels (mean ±SEM) treated with protofibrillar 1μM Aβ_{1-42} (n=15).* ***(D)*** *Half-activation voltage of Cav2.2 channels (mean ± SEM) treated with the vehicle control (PBS) compared to protofibrillar 1μM Aβ_{1-42} (n=15).* ***(E)*** *Slope of Cav2.2 channels (mean ± SEM) treated with the vehicle control (PBS) compared to protofibrillar 1μM Aβ_{1-42} (n=15).* ***(F)*** *Reduction in Cav2.2 current density (mean ± SEM) with protofibrillar 1μM Aβ_{1-42} treatment (n=15). Clampfit 10.3 was used for trace analysis. GraphPad was used for plotting current-voltage relationship and carrying out Boltzmann fit analysis. Statistical analysis was carried out via one-tailed unpaired Welch T-test. (*=P<0.05)*

5.2.2. Effect of CO on Cav2.2 channels

Prior to investigating the effect of CORM2 on Cav2.2 channels of HEK293 cells, the effect of DMSO (vehicle control) was investigated (**Fig. 5.2.2.1A-B**). DMSO (1/1000 dilution) alone had no significant effect on the Cav2.2 channel properties measured (Rp, G_{max}, V_{half} and k) (**Fig. 5.2.2.2A-D**). In addition, DMSO also had no effect on Cav2.2 current density over time (**Fig. 5.2.2.3A and B**).

Following DMSO control experiments, the effect of CORM2 on Cav2.2 channel kinetics, was then investigated via whole-cell patch clamp. Analysis of Cav2.2 channel properties, revealed that 100nM (n=6) and 500nM (n=8) CORM2 had no effect on all measured Cav2.2 channel properties (**Fig. 5.2.2.4A-F and Fig. 5.2.2.5A-F respectively**). In contrast, Cav2.2 currents (**Fig. 5.2.2.6A and B**) exposed to a higher concentration of CORM2 (10μM; n=6) revealed a significant reduction in G_{max} by 0.4 ± 0.1 ns/pF ($P<0.05$), an increase in the V_{half} by 7.1 ± 2.8 mV ($P<0.05$) and a significant change in the slope factor of Cav2.2 currents by 15.8 ± 6.7 mV ($P<0.05$) (**Fig. 5.2.2.7B,C and D**). Rp of Cav2.2 currents remained unchanged following 10μM application (**Fig. 5.2.2.7A**). 10μM CORM2 (~10mins) led to a time-dependent reduction in Cav2.2 current density by 15.9 ± 2.9 pA/pF ($P<0.01$) (**Fig. 5.2.2.8A-C**).

In order to verify that changes in channel properties seen by CORM2 treatment are indeed due to CO release, whole cell patch clamp experiments were also repeated in the presence of 10μM iCORM2 (n=9). Similarly to CORM2, plotting Cav2.2 current-voltage relationship (**Fig. 5.2.2.9A and B**) revealed that iCORM2 also caused a significant change in G_{max} by 0.5 ± 0.1 ns/pF ($P<0.01$), Vhalf by 1.5 ± 0.3 mV ($P<0.01$) and slope factor by 0.5 ± 0.2 mV ($P<0.05$) (**Fig. 5.2.2.10B-D**). Rp remained unaltered (**Fig. 5.2.2.10A**). Applying a single-step protocol to identify changes in Cav2.2 current density revealed a reduction in Cav2.2 amplitude by 10.7 ± 22.6 pA/pF ($P<0.001$) with 10μM iCORM2 treatment (**Fig. 5.2.2.11A and B**). Time-dependent changes in Cav2.2 current amplitude with 10μM iCORM2 treatment (~10mins) can be seen in **Fig. 5.2.2.11C**.

As both CORM2 and iCORM2 were shown to have an effect on Cav2.2 channel kinetics, stably-transfected HEK293 cells were also subjected to treatment with iCORM2 followed by CORM2 at 10μM concentration (n=6). Plotting Cav2.2 current-voltage

relationship (**Fig. 5.2.2.12A and B**) revealed that treating cells with 10μM iCORM2 followed by CORM2 caused a further significant reduction in G_{max} by 0.9 ± 0.2 ns/pF ($P<0.01$), whereas no change in the Rp, V_{half} or slope factor was noticed (**Fig. 5.2.2.13A-D**). Interestingly, when cells where subjected to a single-step protocol 10μM iCORM2 caused a 5.4 ± 1.6 pA/pF ($P<0.05$) reduction in current density, whereas iCORM2 followed by 10μM CORM2 treatment caused an additional 9.3 ± 2.4 pA/pF ($P<0.01$) reduction in current density (**Fig. 5.2.2.14A and B**). Time-dependent reduction in Cav2.2 current amplitude with iCORM2 followed by CORM2 can be seen in **Fig. 5.2.2.14C**.

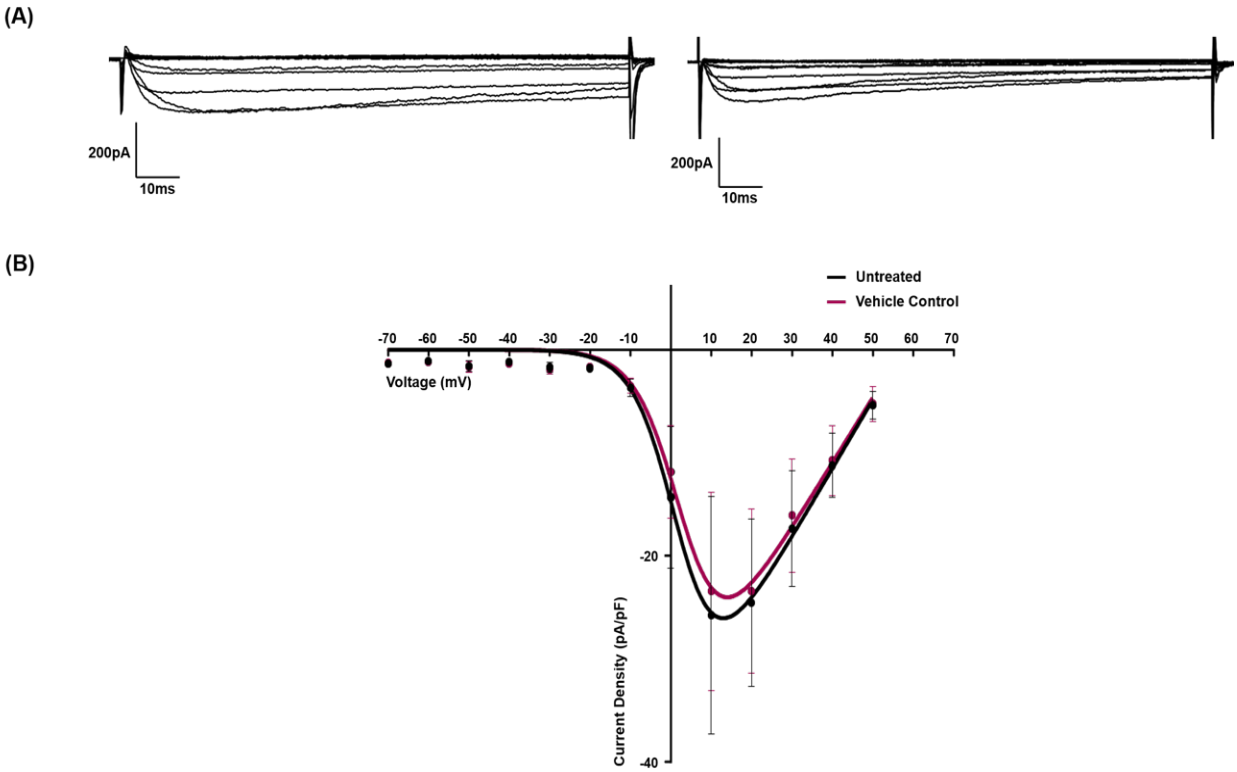

Figure 5.2.2.1: Effect of vehicle control (DMSO) on Cav2.2 currents. *The effect of the vehicle control (DMSO) on Cav2.2 channels of stably-transfected HEK293 cells was investigated via whole-cell patch clamp.* ***(A)*** *Example current-voltage traces (-70 to +50mV) prior (left) and after (right) vehicle control (DMSO) treatment.* ***(B)*** *Current-voltage (-70 to +50mV) relationship of Cav2.2 channels (mean ± SEM) of HEK293 cells prior (untreated) and after vehicle control (DMSO) treatment, fitted with the Boltzmann fit equation (n=6). Clampfit 10.3 was used for trace analysis, and GraphPad for plotting current-voltage relationship and Boltzmann fit analysis.*

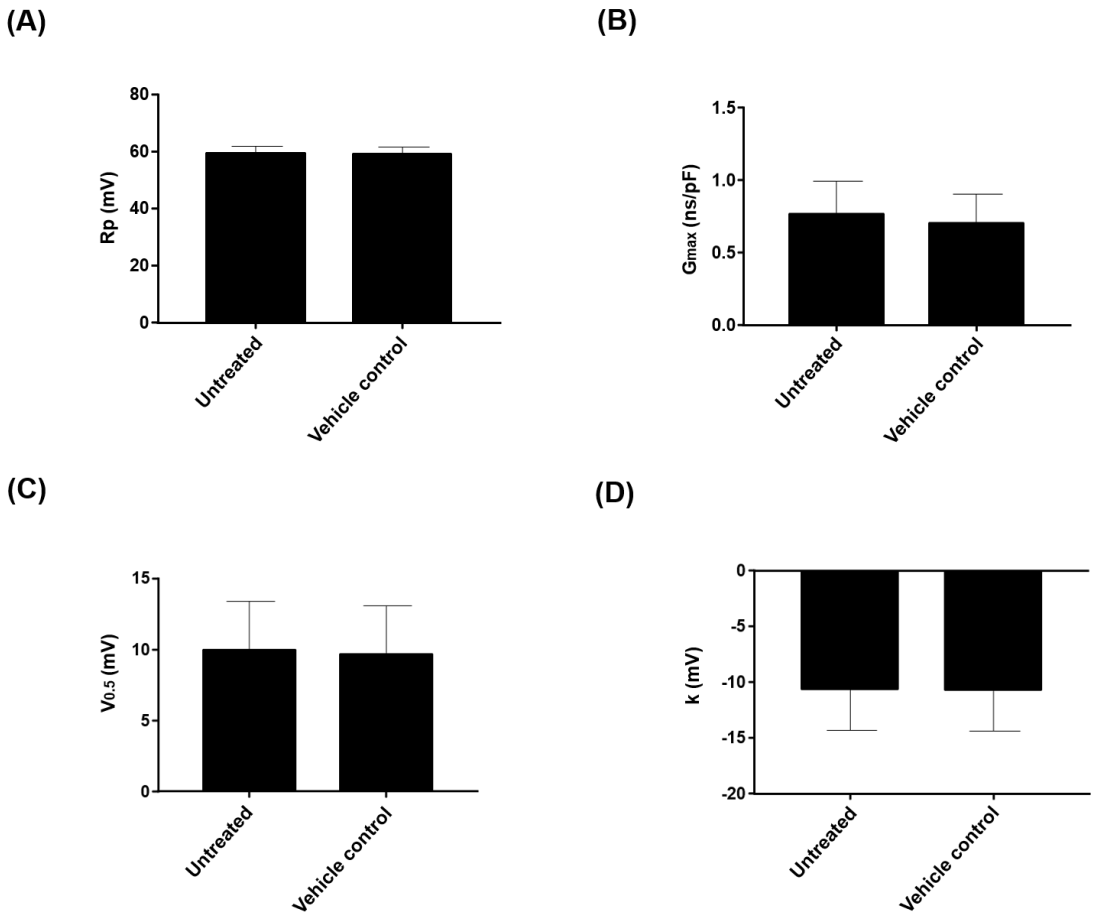

Figure 5.2.2.2: Effect of the vehicle control (DMSO) on Cav2.2 kinetics. *The effect of the vehicle control (DMSO) on Cav2.2 channel kinetics of stably transfected HEK293 cells was investigated via whole-cell patch clamp.* ***(A)*** *Reversal potential of Cav2.2 channels (mean ± SEM) prior (untreated) and after vehicle control (DMSO) treatment (n=6).* ***(B)*** *Maximal conductance of Cav2.2 channels (mean ± SEM) prior (untreated) and after vehicle control (DMSO) treatment (n=6).* ***(C)*** *Half-activation voltage of Cav2.2 channels (mean ± SEM) prior (untreated) and after vehicle control (DMSO) treatment (n=6).* ***(D)*** *Slope of Cav2.2 channels (mean ± SEM) prior (untreated) and after vehicle control (DMSO) treatment (n=6). Clampfit 10.3 was used for trace analysis, and GraphPad for analysing changes in channel kinetics obtained from Boltzmann fit analysis. Statistical analysis was carried out via one-tailed paired T-test.*

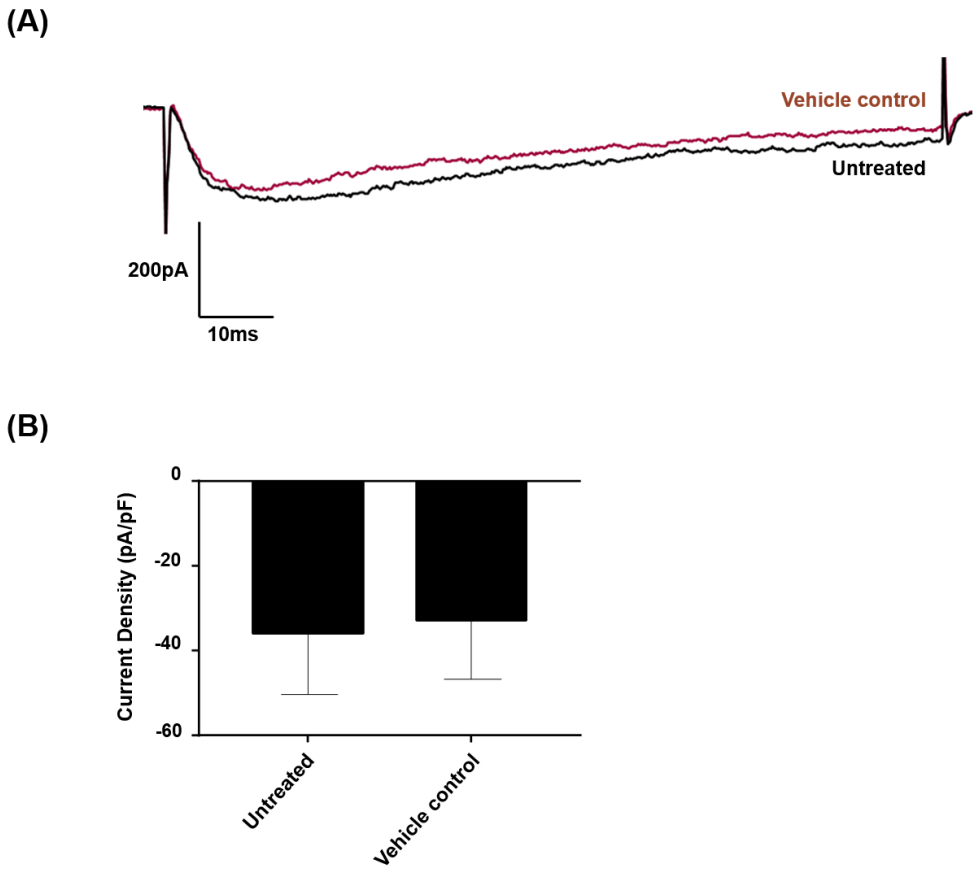

Figure 5.2.2.3: Effect of vehicle control (DMSO) on Cav2.2 current amplitude. *The effect of the vehicle control (DMSO) on Cav2.2 current amplitude of stably-transfected HEK293 cells was investigated via whole-cell patch clamp.* ***(A)*** *Example trace of single-step (+10mV) recording of Cav2.2 current prior (black) and after (maroon) vehicle control treatment (DMSO).* ***(B)*** *Current density of Cav2.2 channels (mean ± SEM) with vehicle control (DMSO) treatment (n=6). Clampfit 10.3 was used for trace analysis, and GraphPad for analysing changes in current amplitude. Statistical analysis was carried out via one-tailed paired T-test.*

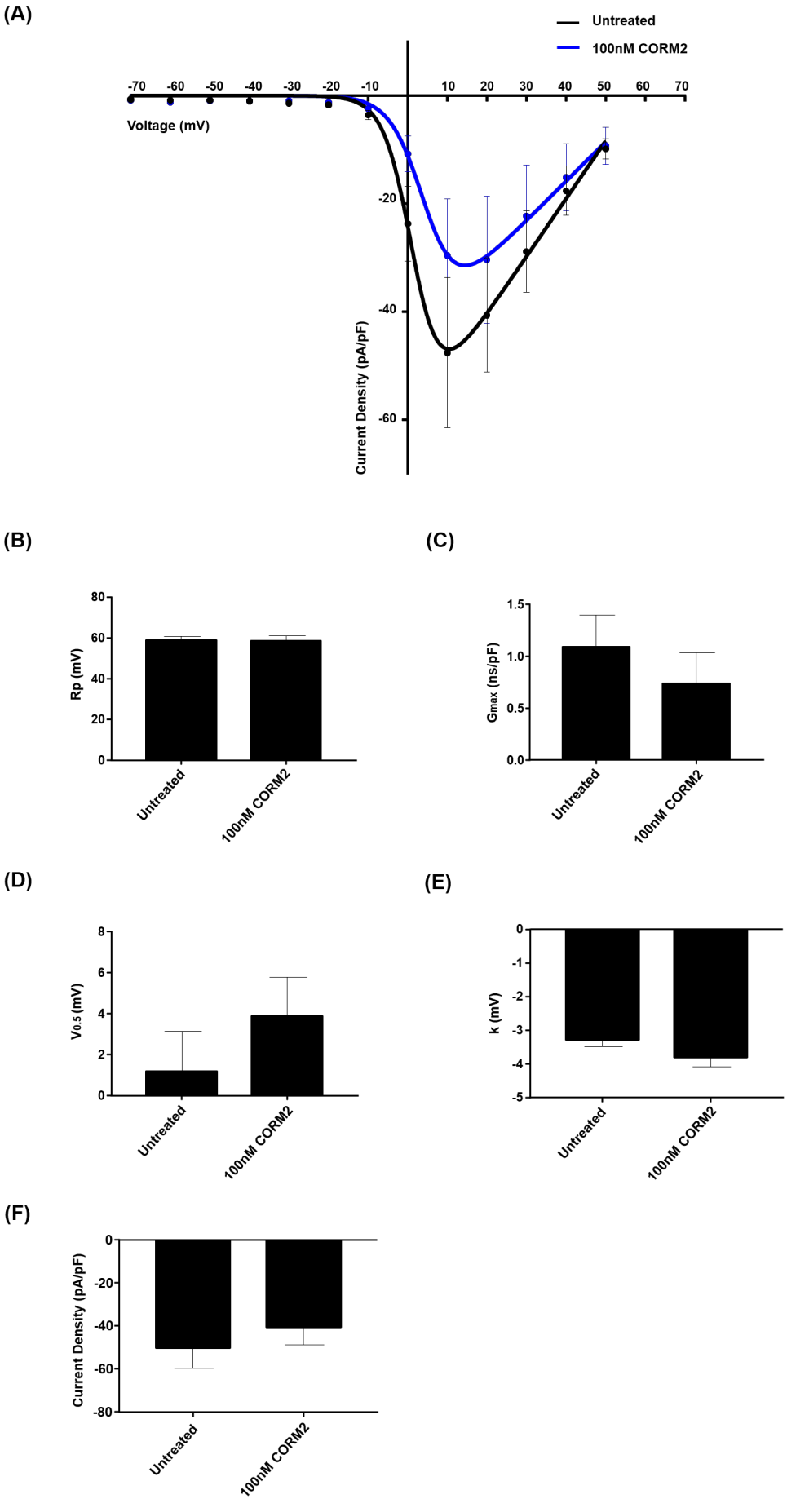
(A)
Untreated
100nM CORM2
-70 -60 -50 -40 -30 -20 -10 10 20 30 40 50 60 70
Voltage (mV)
-20
-40
-60
Current Density (pA/pF)
(B)
Rp (mV)
80
60
40
20
0
Untreated
100nM CORM2
(C)
Gmax (ns/pF)
1.5
1.0
0.5
0.0
Untreated
100nM CORM2
(D)
V0.5 (mV)
8
6
4
2
0
Untreated
100nM CORM2
(E)
k (mV)
0
-1
-2
-3
-4
-5
Untreated
100nM CORM2
(F)
Current Density (pA/pF)
0
-20
-40
-60
-80
Untreated
100nM CORM2

Figure 5.2.2.4: Effect of 100nM CORM2 on Cav2.2 kinetics. *The effect of 100nM CORM2 on Cav2.2 channel kinetics of stably-transfected HEK293 cells was investigated via whole-cell patch clamp.* ***(A)*** *Current-voltage (-70 to +50mV) relationship of Cav2.2 channels (mean ± SEM) of HEK293 cells prior (untreated) and after 100nM CORM2 treatment (n=6).* ***(B)*** *Reversal potential of Cav2.2 channels (mean ± SEM) prior (untreated) and after 100nM CORM2 treatment (n=6).* ***(C)*** *Maximal conductance of Cav2.2 channels (mean ± SEM) prior (untreated) and after 100nM CORM2 treatment (n=6).* ***(D)*** *Half-activation voltage of Cav2.2 channels (mean ± SEM) prior (untreated) and after 100nM CORM2 treatment (n=6).* ***(E)*** *Slope of Cav2.2 channels (mean ± SEM) prior (untreated) and after 100nM CORM2 treatment (n=6).* ***(F)*** *Cav2.2 current density (mean ± SEM) prior (untreated) and after 100nM CORM2 treatment (n=6). Clampfit 10.3 was used for trace analysis. GraphPad was used for plotting current-voltage relationship and carrying out Boltzmann fit analysis. Statistical analysis was carried out via one-tailed paired T-test.*

(A)

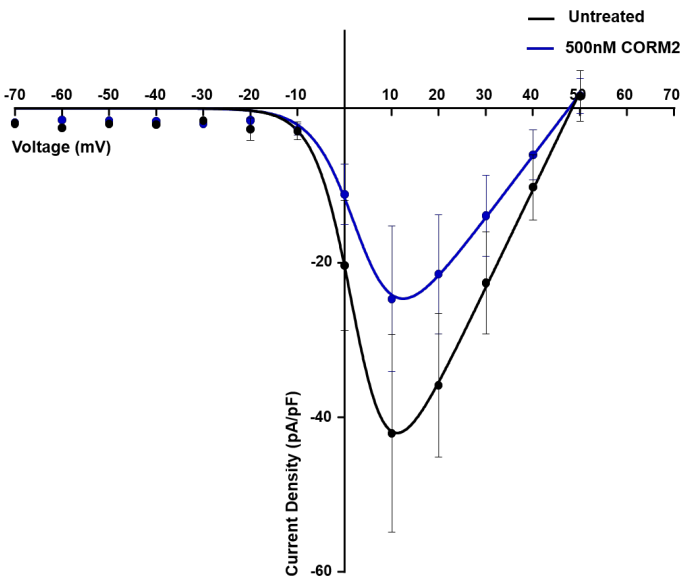
Untreated
500nM CORM2
-70 -60 -50 -40 -30 -20 -10 10 20 30 40 50 60 70
Voltage (mV)
-20
-40
-60
Current Density (pA/pF)

(B)

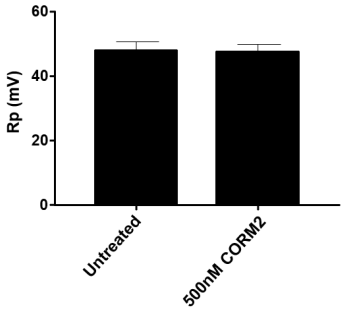
60
40
20
0
Rp (mV)
Untreated
500nM CORM2

(C)

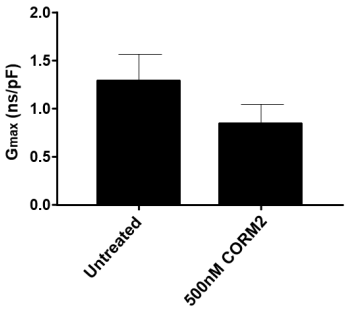
2.0
1.5
1.0
0.5
0.0
Gmax (ns/pF)
Untreated
500nM CORM2

(D)

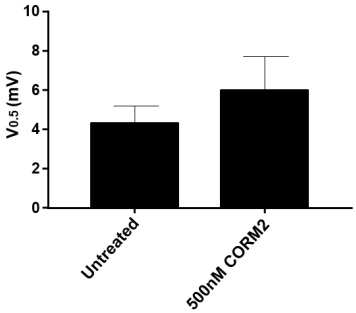
10
8
6
4
2
0
V0.5 (mV)
Untreated
500nM CORM2

(E)

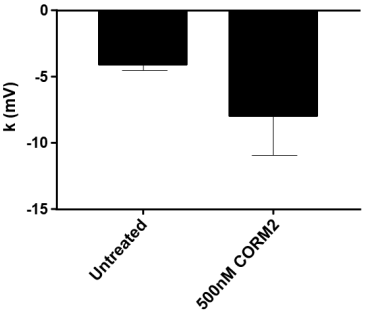
0
-5
-10
-15
k (mV)
Untreated
500nM CORM2

(F)

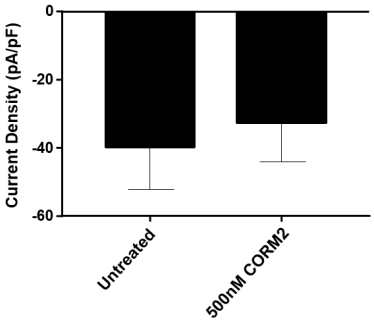
0
-20
-40
-60
Current Density (pA/pF)
Untreated
500nM CORM2

Figure 5.2.2.5: Effect of 500nM CORM2 on Cav2.2 kinetics. *The effect of 500nM CORM2 on Cav2.2 channel kinetics of stably-transfected HEK293 cells was investigated via whole-cell patch clamp.* ***(A)*** *Current-voltage (-70 to +50mV) relationship of Cav2.2 channels (mean ± SEM) prior (untreated) and after 500nM CORM2 treatment, fitted with the Boltzmann fit equation (n=8).* ***(B)*** *Reversal potential of Cav2.2 channels (mean ± SEM) prior (untreated) and after 500nM CORM2 treatment (n=8).* ***(C)*** *Maximal conductance of Cav2.2 channels (mean ± SEM) prior (untreated) and after 500nM CORM2 treatment (n=8).* ***(D)*** *Half-activation voltage of Cav2.2 channels (mean ± SEM) prior (untreated) and after 500nM CORM2 treatment (n=8).* ***(E)*** *Slope of Cav2.2 channels (mean ± SEM) prior (untreated) and after 500nM CORM2 treatment (n=8).* ***(F)*** *Cav2.2 current density (mean ± SEM) prior (untreated) and after 500nM CORM2 treatment (n=8). Clampfit 10.3 was used for trace analysis. GraphPad was used for plotting current-voltage relationship and carrying out Boltzmann fit analysis. Statistical analysis was carried out via one-tailed paired T-test.*

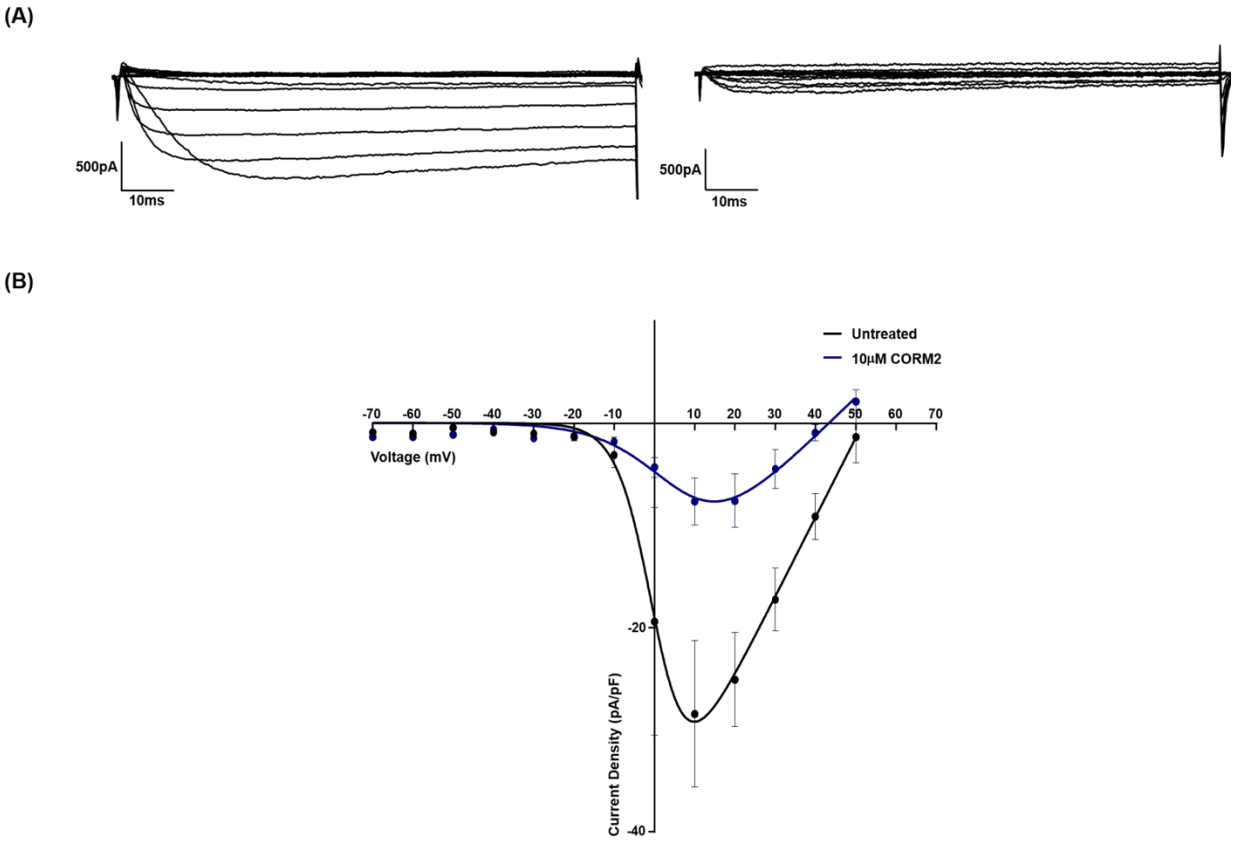

Figure 5.2.2.6: Effect of 10μM CORM2 on Cav2.2 currents. *The effect of 10μM CORM2 on Cav2.2 channels of stably-transfected HEK293 cells was investigated via whole-cell patch clamp.* ***(A)*** *Example current-voltage traces (-70 to +50mV) prior (left) and after (right) 10μM CORM2 treatment.* ***(B)*** *Current-voltage (-70 to +50mV) relationship of Cav2.2 channels (mean ± SEM) of HEK293 cells prior (untreated) and after 10μM CORM2 treatment, fitted with the Boltzmann fit equation (n=6). Clampfit 10.3 was used for trace analysis, and GraphPad for plotting current-voltage relationship and Boltzmann fit analysis.*

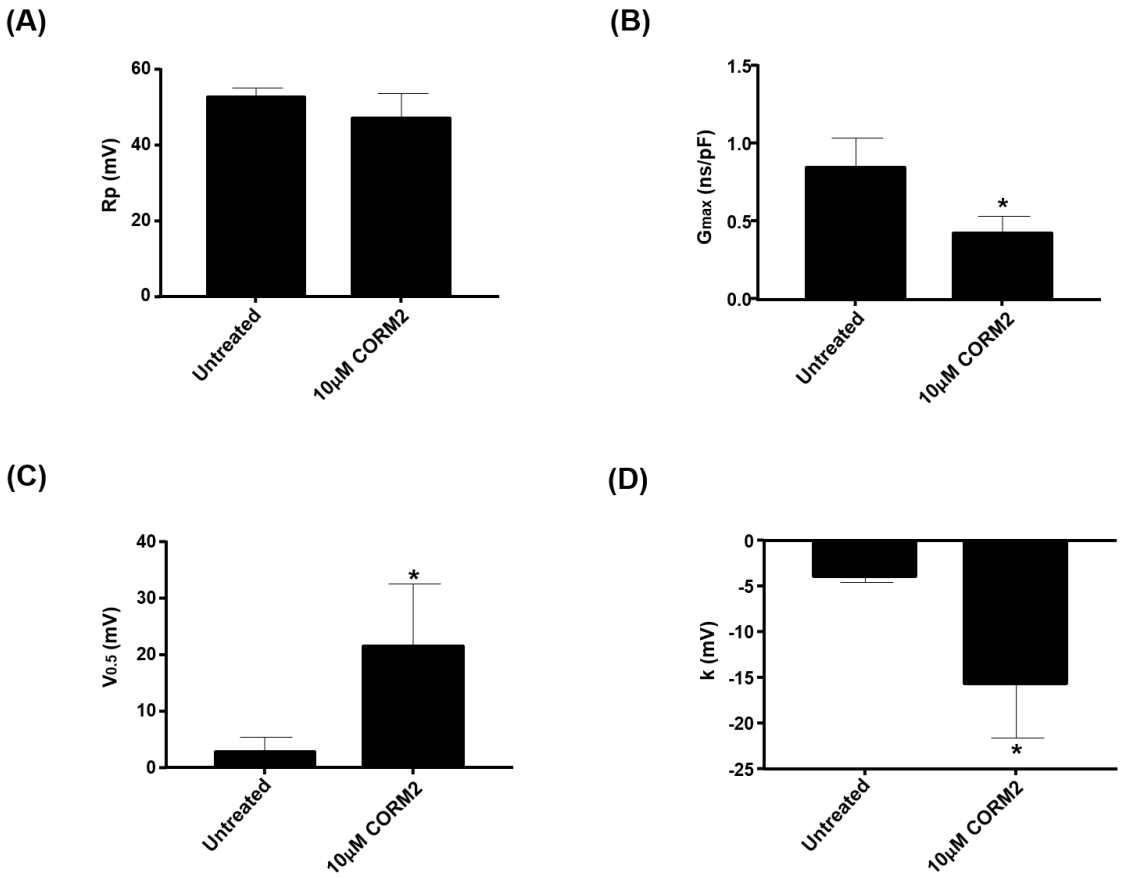

Figure 5.2.2.7: Effect of the 10μM CORM2 on Cav2.2 kinetics. *The effect of 10μM CORM2 on Cav2.2 channel kinetics of stably transfected HEK293 cells was investigated via whole-cell patch clamp.* ***(A)*** *Reversal potential of Cav2.2 channels (mean ± SEM) prior (untreated) and after 10μM CORM2 treatment (n=6).* ***(B)*** *Reduction in maximal conductance of Cav2.2 channels (mean ± SEM) with 10μM CORM2 treatment (n=6).* ***(C)*** *Increase in half-activation voltage of Cav2.2 channels (mean ± SEM) with 10μM CORM2 treatment (n=6).* ***(D)*** *Change in the slope of Cav2.2 channels (mean ± SEM) with 10μM CORM2 treatment (n=6). Clampfit 10.3 was used for trace analysis, and GraphPad for analysing changes in channel kinetics obtained from Boltzmann fit analysis. Statistical analysis was carried out via one-tailed paired T-test. (*=P<0.05)*

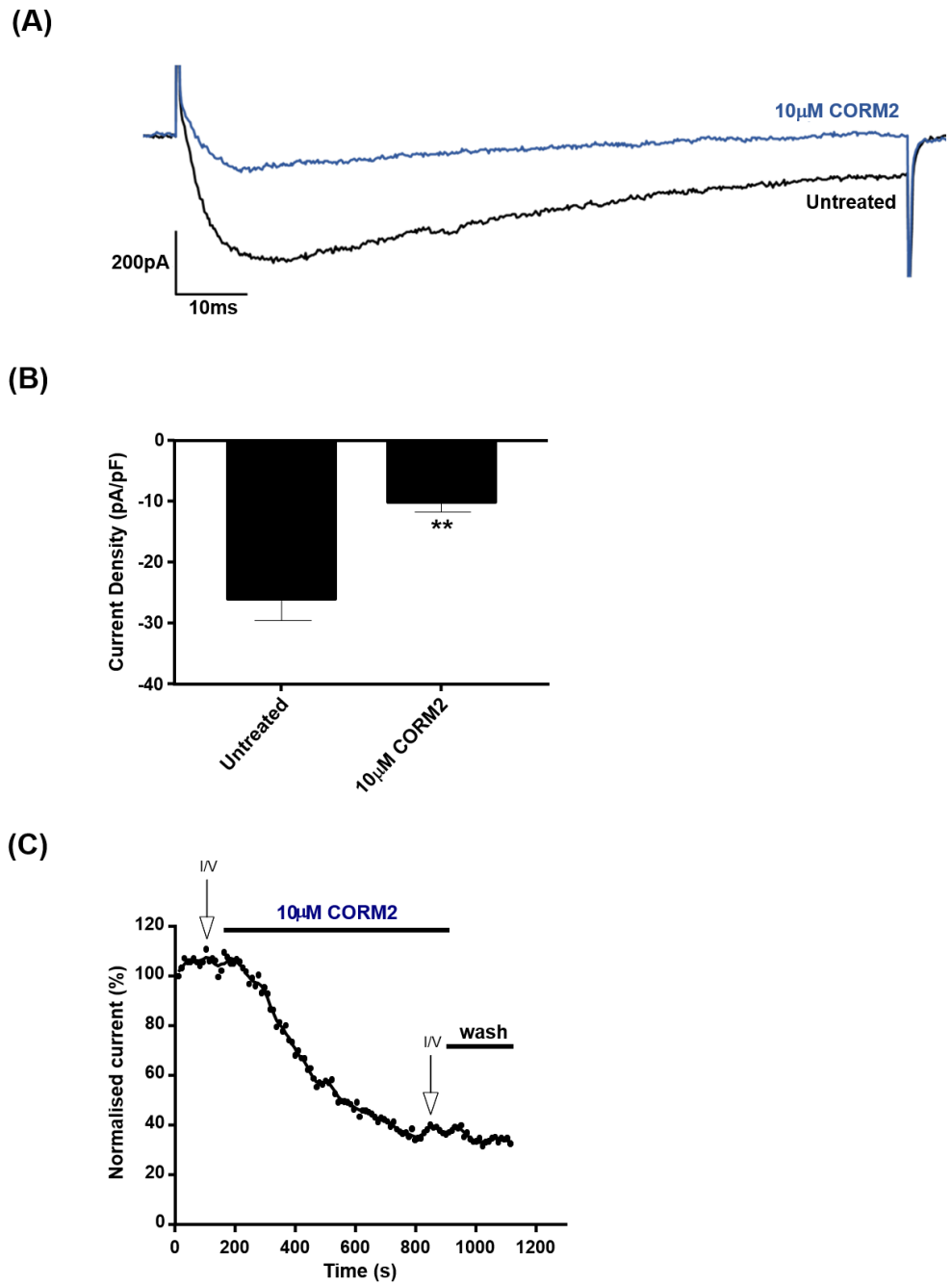

Figure 5.2.2.8: Effect of 10μM CORM2 on Cav2.2 current amplitude. *The effect of 10μM CORM2 on Cav2.2 current amplitude of stably-transfected HEK293 cells was investigated via whole-cell patch clamp.* ***(A)*** *Example trace of single-step (+10mV) recording of Cav2.2 current prior (black) and after (blue) 10μM CORM2 treatment.* ***(B)*** *Reduction in Cav2.2 current density (mean ± SEM) with 10μM CORM2 treatment (n=6).* ***(C)*** *Representative example of time-dependent changes in Cav2.2 current (+10mV) with 10μM CORM2 (blue) treatment. Clampfit 10.3 was used for trace analysis, and GraphPad for analysing changes in current amplitude. Statistical analysis was carried out via one-tailed paired T-test. (**=P<0.01)*

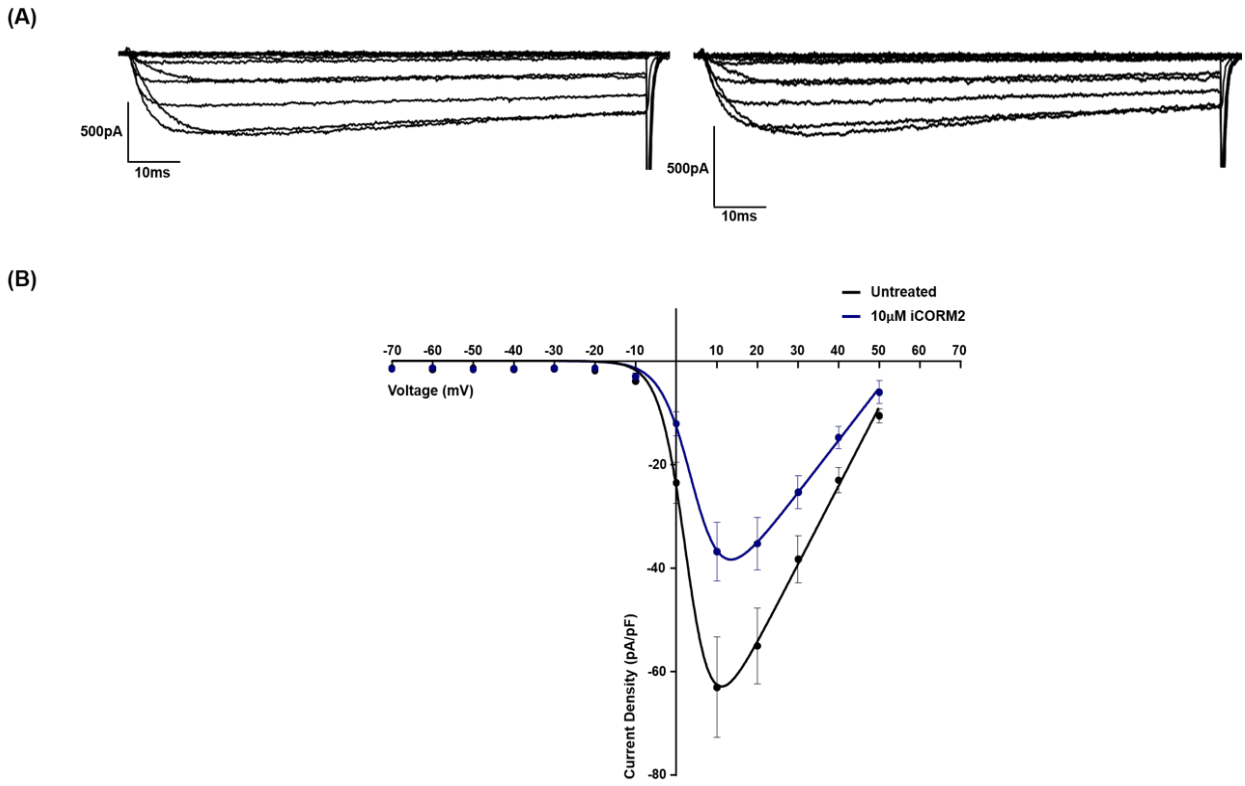

Figure 5.2.2.9: Effect of 10μM iCORM2 on Cav2.2 currents. *The effect of 10μM iCORM2 on Cav2.2 channels of stably-transfected HEK293 cells was investigated via whole-cell patch clamp.* ***(A)*** *Example current-voltage traces (-70 to +50mV) prior (left) and after (right) 10μM iCORM2 treatment.* ***(B)*** *Current-voltage (-70 to +50mV) relationship of Cav2.2 channels (mean ± SEM) of HEK293 cells prior (untreated) and after 10μM iCORM2 treatment, fitted with the Boltzmann fit equation (n=9). Clampfit 10.3 was used for trace analysis, and GraphPad for plotting current-voltage relationship and Boltzmann fit analysis.*

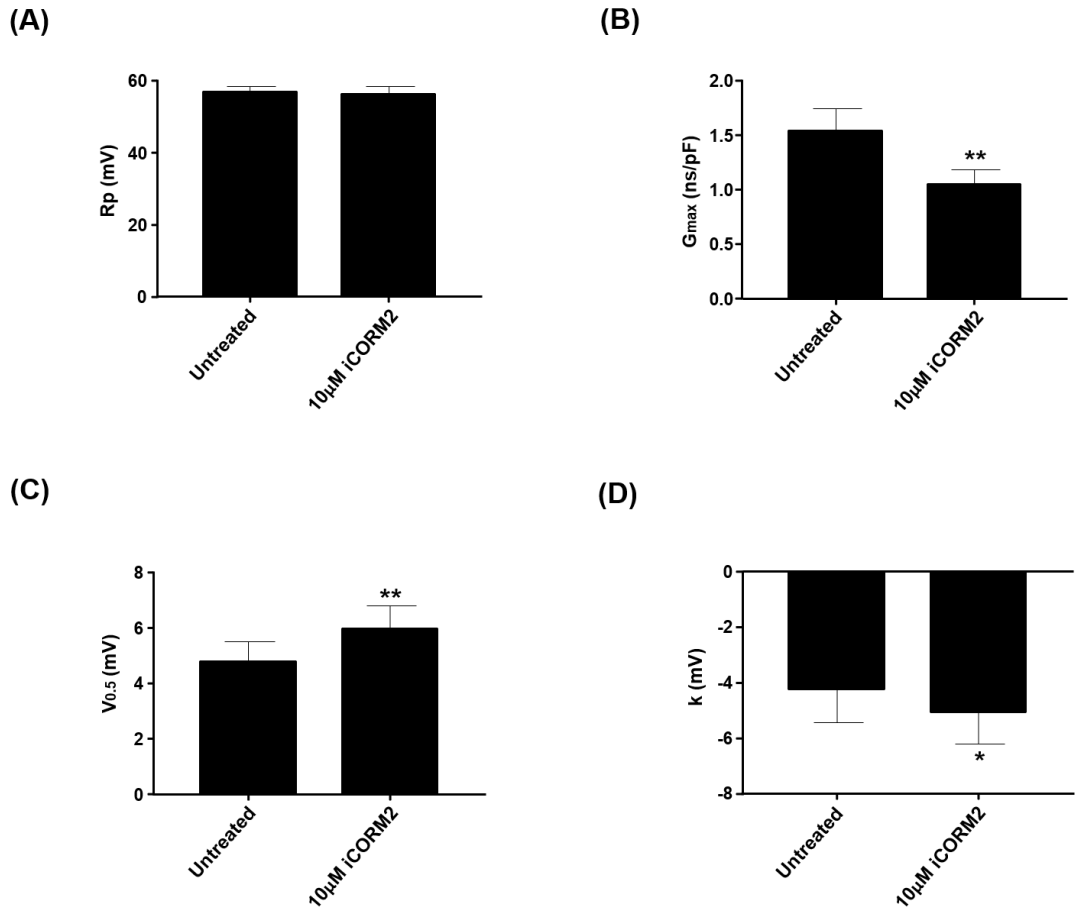

Figure 5.2.2.10: Effect of 10μM iCORM2 on Cav2.2 kinetics. *The effect of 10μM iCORM2 on Cav2.2 channel kinetics of stably transfected HEK293 cells was investigated via whole-cell patch clamp.* ***(A)*** *Reversal potential of Cav2.2 channels (mean ± SEM) prior (untreated) and after 10μM iCORM2 treatment (n=9).* ***(B)*** *Reduction in maximal conductance of Cav2.2 channels (mean ± SEM) with 10μM iCORM2 treatment (n=9).* ***(C)*** *Increase in half-activation voltage of Cav2.2 channels (mean ± SEM) with 10μM iCORM2 treatment (n=9).* ***(D)*** *Change in slope of Cav2.2 channels (mean ± SEM) with 10μM iCORM2 treatment (n=9). Clampfit 10.3 was used for trace analysis, and GraphPad for analysing changes in channel kinetics obtained from Boltzmann fit analysis. Statistical analysis was carried out via one-tailed paired T-test. (*=P<0.05; **=P<0.01)*

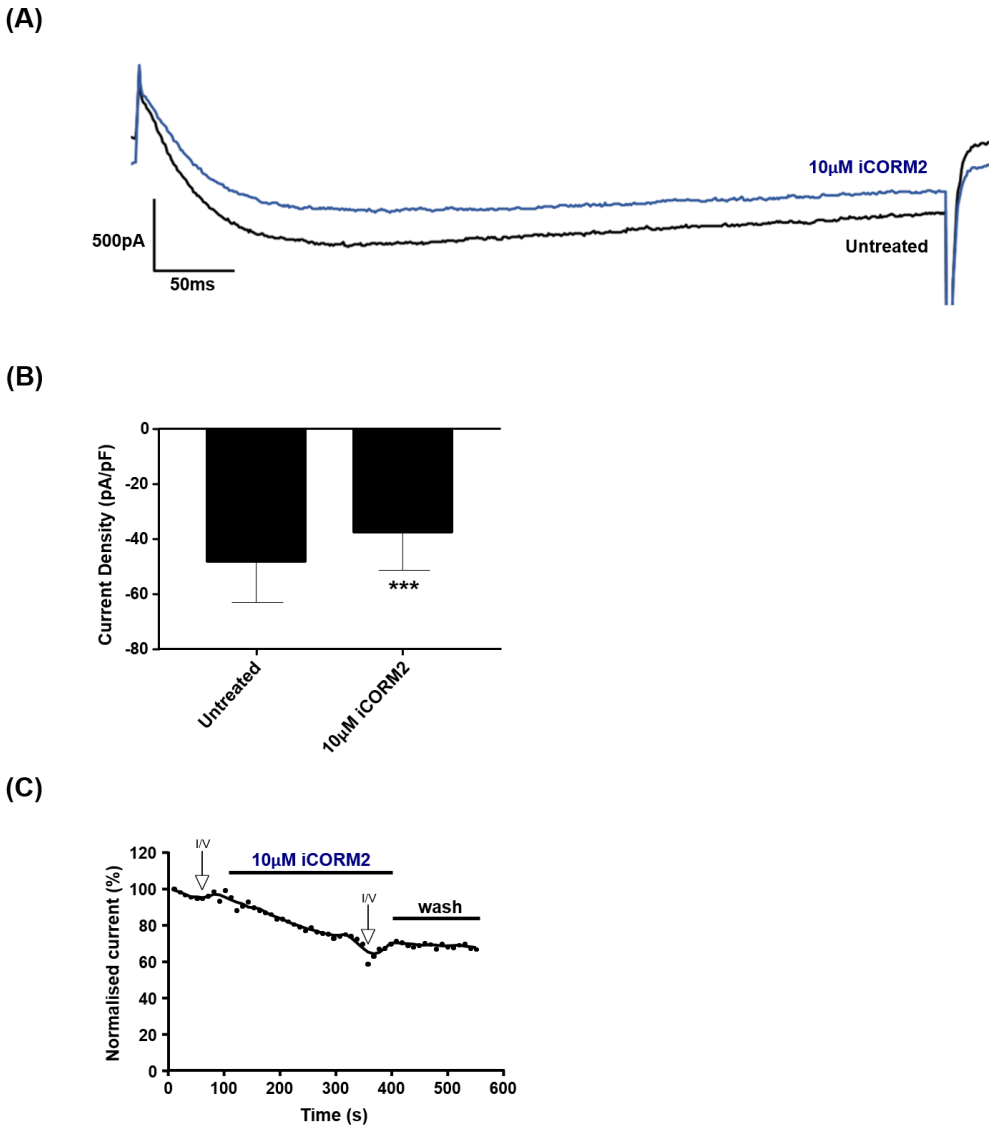

Figure 5.2.2.11: Effect of 10μM iCORM2 on Cav2.2 current amplitude. *The effect of 10μM iCORM2 on Cav2.2 current amplitude of stably-transfected HEK293 cells was investigated via whole-cell patch clamp.* ***(A)*** *Example trace of single-step (+10mV) recording of Cav2.2 current prior (black) and after (blue) 10μM iCORM2 treatment.* ***(B)*** *Reduction in Cav2.2 current density (mean ± SEM) with 10μM iCORM2 treatment (n=9).* ***(C)*** *Representative example of time-dependent changes in Cav2.2 current (+10mV) with 10μM iCORM2 (blue) treatment. Clampfit 10.3 was used for trace analysis, and GraphPad for analysing changes in current amplitude. Statistical analysis was carried out via one-tailed paired T-test. (***=P<0.001)*

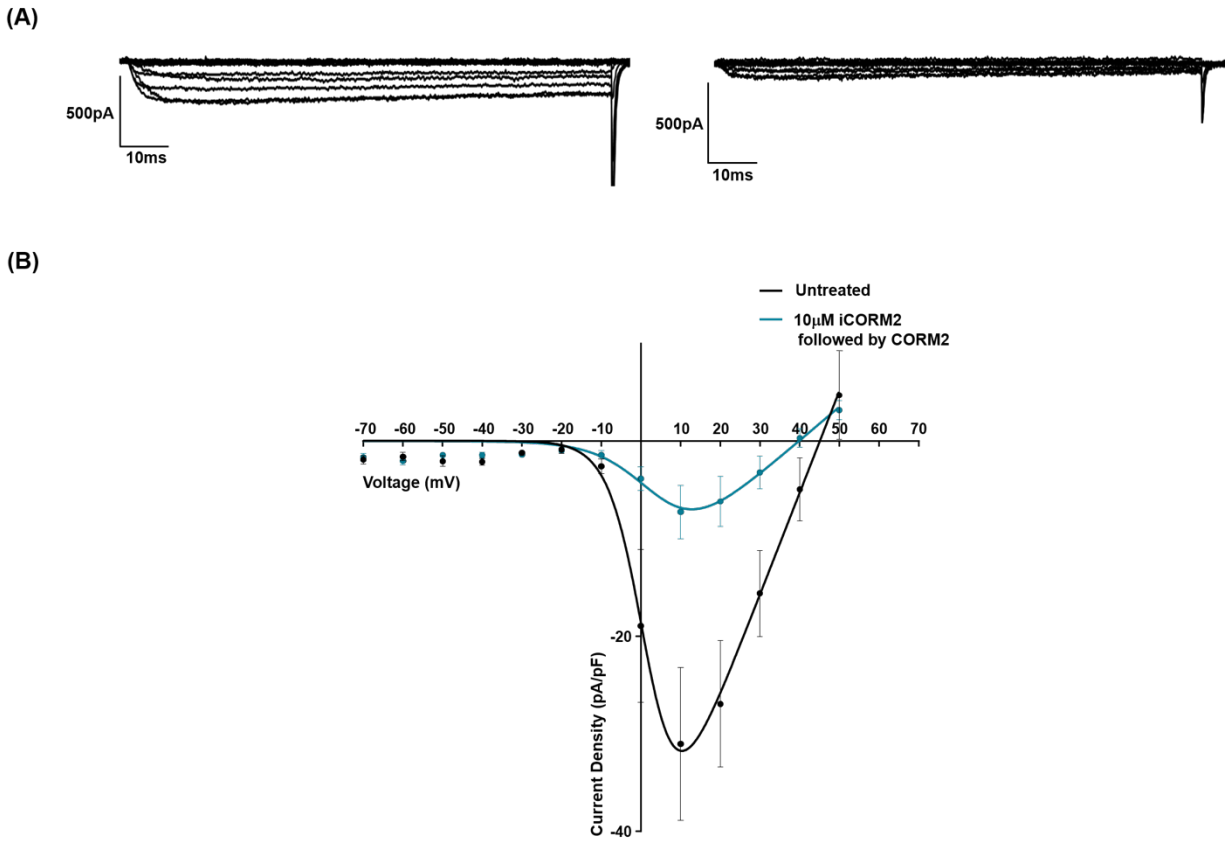

Figure 5.2.2.12: Effect of CORM2 on Cav2.2 currents. *The effect of CO, through iCORM2 followed by CORM2 treatment, on Cav2.2 channels of stably-transfected HEK293 cells was investigated via whole-cell patch clamp through treatment.* ***(A)*** *Example current-voltage traces (-70 to +50mV) prior (left) and after (right) 10μM iCORM2 followed by CORM2 treatment.* ***(B)*** *Current-voltage (-70 to +50mV) relationship of Cav2.2 channels (mean ±SEM) prior (untreated) and after 10μM iCORM2 followed by CORM2 treatment, fitted with the Boltzmann fit equation (n=6). Clampfit 10.3 was used for trace analysis, and GraphPad for plotting current-voltage relationship and Boltzmann fit analysis.*

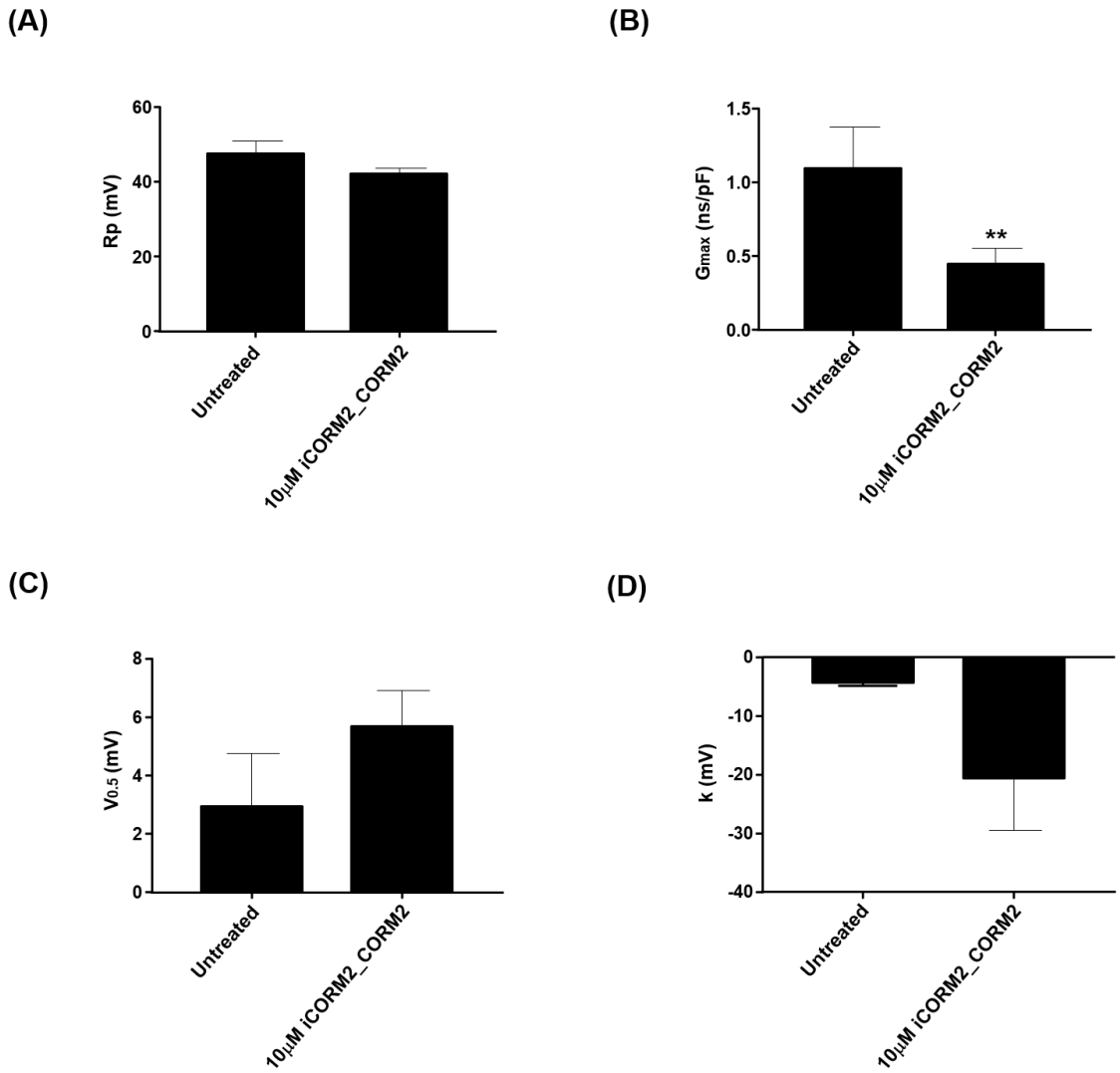

Figure 5.2.2.13: Effect of CO on Cav2.2 kinetics. *The effect of CO, through iCORM2 followed by CORM2 treatment on Cav2.2 channel kinetics of stably-transfected HEK293 cells investigated via whole-cell patch clamp.* ***(A)*** *Reversal potential of Cav2.2 channels (mean ±SEM) prior (untreated) and after 10μM iCORM2 followed by CORM2 treatment (n=6).* ***(B)*** *Reduction in maximal conductance of Cav2.2 channels (mean ±SEM) with 10μM iCORM2 followed by CORM2 treatment (n=6).* ***(C)*** *Half-activation voltage of Cav2.2 channels (mean ±SEM) prior (untreated) and after 10μM iCORM2 followed by CORM2 treatment (n=6).* ***(D)*** *Slope of Cav2.2 channels (mean ±SEM) prior (untreated) and after 10μM iCORM2 followed by CORM2 treatment (n=6). Clampfit 10.3 was used for trace analysis, and GraphPad for analysing changes in channel kinetics obtained from Boltzmann fit analysis. Statistical analysis was carried out via one-tailed paired T-test. (**=P<0.01)*

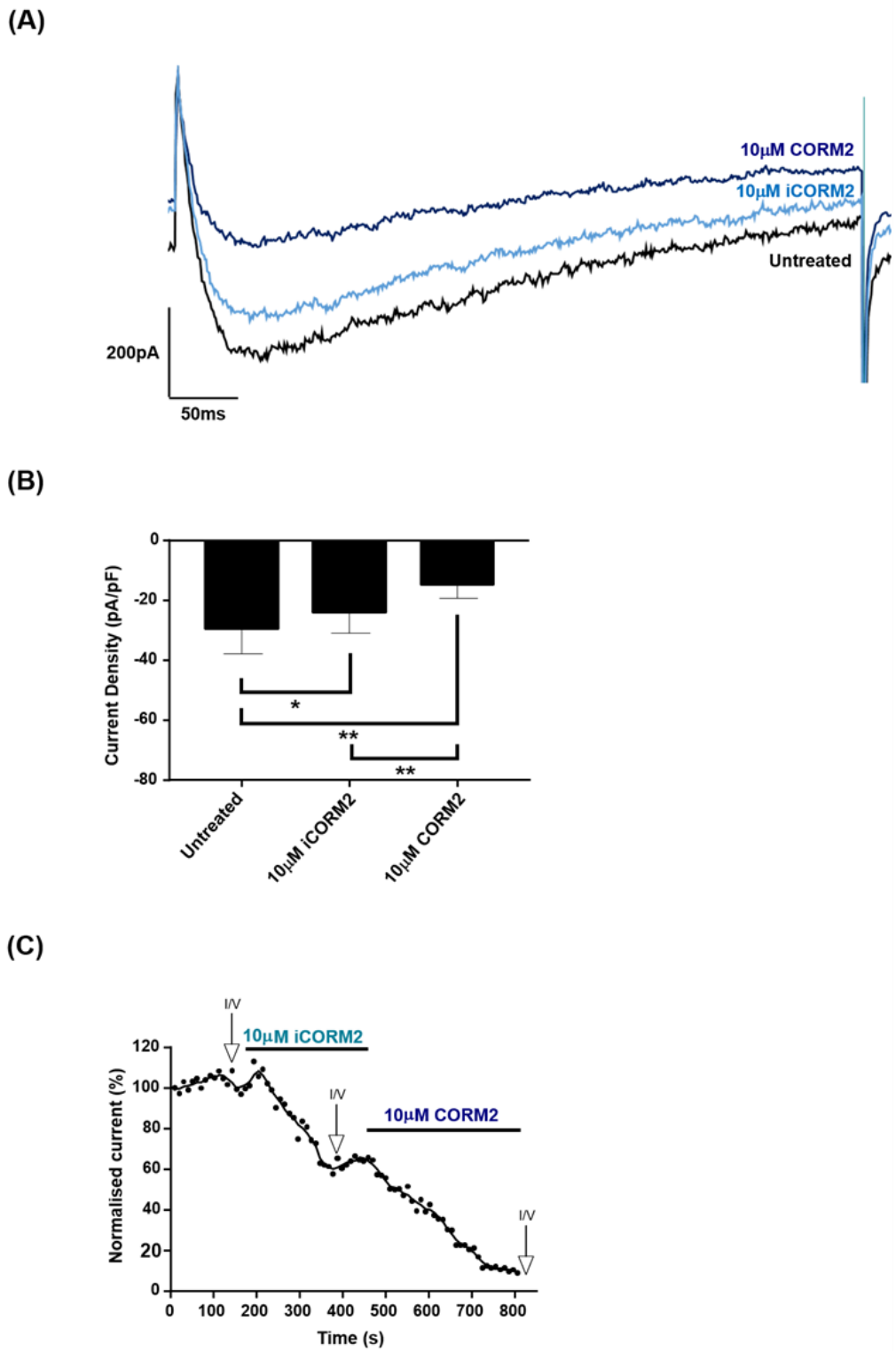

Figure 5.2.2.14: Effect of CO on Cav2.2 current amplitude. *The effect of CO, through iCORM2 followed by CORM2 treatment, on Cav2.2 current amplitude of stably-transfected HEK293 cells was investigated via whole-cell patch clamp.* ***(A)*** *Example trace of single-step (+10mV) recording of Cav2.2 current prior (black), followed by 10μM iCORM2 (light blue) and 10μM CORM2 (dark blue) treatment.* ***(B)*** *Reduction in Cav2.2 current amplitude (mean ±SEM) with 10μM iCORM2 followed by CORM2 treatment (n=6).* ***(C)*** *Representative example of time-dependent changes in Cav2.2 current (+10mV) with 10μM iCORM2 (light blue) followed by CORM2 (dark blue) treatment. Clampfit 10.3 was used for trace analysis, and GraphPad for analysing changes in current amplitude. Statistical analysis was carried out via one-tailed paired T-test. (*=P<0.05; **=P<0.01)*

5.2.3. Redox modulation of Cav2.2 channels by CO

Once CORM2 was verified to have an effect on Cav2.2 channel kinetics, the hypothesis that CORM2 may modulate Cav2.2 channels through a redox manner was then investigated via whole-cell patch clamp.

Plotting Cav2.2 current-voltage relationship (**Fig. 5.2.3.1A**) of HEK293 cells treated with the oxidising agent DTDP (2,2-dithiodipyridine) revealed that 1μM DTDP (n=6) has no significant effect on any of the Cav2.2 channel kinetics (**Fig. 5.2.3.1B-F**). In contrast, plotting the Cav2.2 current-voltage relationship (**Fig. 5.2.3.2A and B**) of cells treated with 10μM DTDP (n=5) although did not have any effect on Rp, G_{max}, V_{half} and slope factor (**Fig 5.2.3.3A-D**), 10μM DTDP caused a significant reduction in current density by 7.7 ± 1.7 pA/pF (P<0.001) (**Fig. 5.2.3.4A and B**). Time-dependent changes in Cav2.2 current amplitude with 10μM DTDP treatment (~10mins) can be seen in **Fig. 5.2.3.4C**.

As the oxidising agent DTDP caused a significant reduction in current density similar to treatment with CORM2, CORM2 modulation of Cav2.2 channels through an oxidising manner was also investigated via whole-cell patch clamp. Plotting Cav2.2 current-voltage relationship (**Fig. 5.2.3.5A-B**) of HEK293 cells treated with 10μM DTDP followed by 10μM CORM2 (n=7) revealed a significant reduction in G_{max} by 0.4 ± 0.2 ns/pF (P<0.05) and 9.3 ± 4.4 mV (P<0.05) in slope factor (**Fig. 5.2.3.6B and D**). Whereas no change in the Rp and V_{half} of Cav2.2 channels was noted (**Fig. 5.2.3.6A and C**). When cells where subjected to a single-step protocol 10μM DTDP caused a 7.4 ± 2.2 pA/pF (P<0.01) reduction in current density, whereas 10μM DTDP followed by 10μM CORM2 treatment caused an additional 4.7 ± 0.7 pA/pF (P<0.01) reduction in current density, suggesting CORM2 may act similarly to an oxidising agent (**Fig. 5.2.3.7A**). Time-dependent reduction in Cav2.2 current amplitude with DTDP followed by CORM2 can be seen in **Fig. 5.2.3.7B**.

In order to verify that CORM2 acts as a redox modulator of Cav2.2 channel by acting as an oxidizing agent, the effect of the reducing agent DTT (dithiothreitol) on CORM2-dependent changes in Cav2.2 channel kinetics was also investigated (n=6). Plotting Cav2.2 current-voltage relationship (**Fig. 5.2.3.8A and B**) revealed that 1mM

DTT had no effect on the Rp, G_{max} and slope factor of Cav2.2 currents (**Fig. 5.2.3.9A, B and D**). Whereas, 1mM treatment caused a significant change in V_{half} of Cav2.2 currents by 3.0 ± 1.4 mV (P<0.05) (**Fig. 5.2.3.9C**). Applying a single-step protocol to study changes in current density revealed that 1mM DTT (~10mins) had no effect on Cav2.2 current density (**Fig. 5.2.3.10A and B**).

As a last-step, in order to verify that CORM2 modulates Cav2.2 through an oxidising mechanism, Cav2.2 stably-transfected HEK293 cells were also treated with 10μM CORM2 followed by 1mM DTT (n=5). Plotting Cav2.2 current-voltage relationship (**Fig. 5.2.3.11A and B**) revealed that although CORM2 alone treatment did not cause any change in Rp or V_{half}, treating cells with 10μM CORM2 followed by 1mM DTT caused a 10.39 ± 2.9 mV (P<0.01) and 6.2 ± 1.0 mV (P<0.01) change respectively (**Fig. 5.2.3.12A and C**). Treating cells with 10μM CORM2 alone caused a 0.9 ± 0.3 ns/pF (P<0.05) reduction in G_{max}. Whereas, treating cells with 10μM CORM2 followed by 1mM DTT caused complete restoration in G_{max} (0.3 ± 0.3 ns/pF) (**Fig. 5.2.3.12B**). In contrast, treating cells with 10μM CORM2 followed by 1mM DTT had no effect on Cav2.2 slope factor (**Fig. 5.2.3.12D**). Applying a single-step protocol to study changes in current density revealed that 10μM CORM2 reduces Cav2.2 current density by 25.2 ± 7.7 pA/pF (P<0.05). Whereas treating cells with 10μM CORM2 followed by 1mM DTT caused complete restoration in Cav2.2 current density (12.8 ± 10.1 pA/pF) (**Fig. 5.2.3.13A**). Time-dependent changes in current amplitude of Cav2.2 channels of HEK293 cells treated with 10μM CORM2 followed by 1mM DTT can be seen in **Fig. 5.2.3.13B**.

(A)

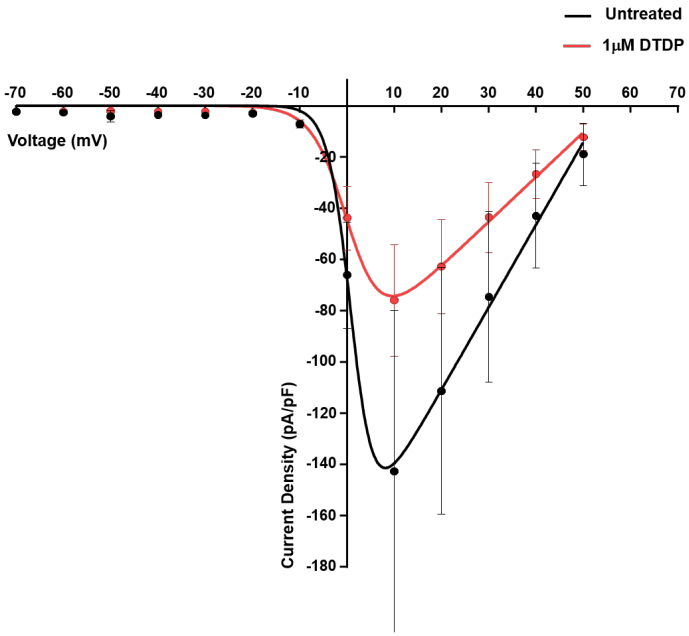
Untreated
1μM DTDP
-70 -60 -50 -40 -30 -20 -10 10 20 30 40 50 60 70
Voltage (mV)
-20 -40 -60 -80 -100 -120 -140 -160 -180
Current Density (pA/pF)

(B)

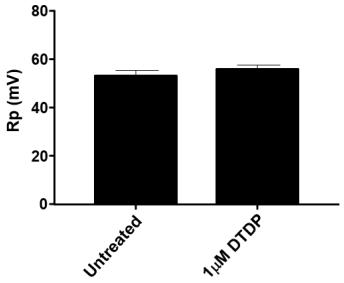
80 60 40 20 0
Rp (mV)
Untreated
1μM DTDP

(C)

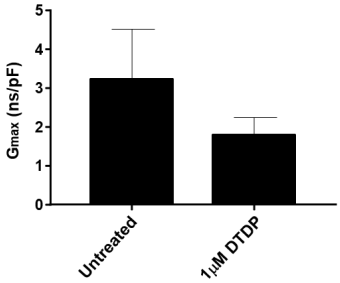
5 4 3 2 1 0
Gmax (ns/pF)
Untreated
1μM DTDP

(D)

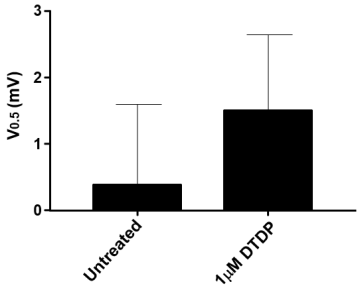
3 2 1 0
V0.5 (mV)
Untreated
1μM DTDP

(E)

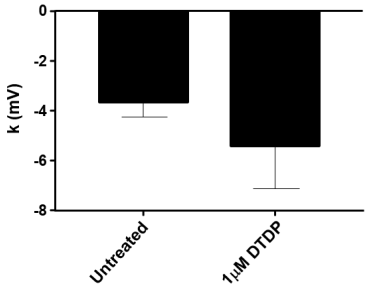
0 -2 -4 -6 -8
k (mV)
Untreated
1μM DTDP

(F)

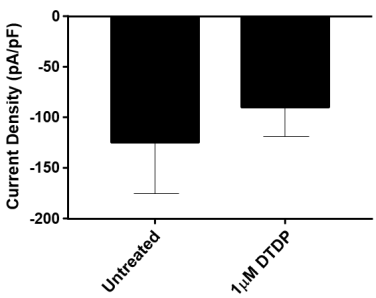
0 -50 -100 -150 -200
Current Density (pA/pF)
Untreated
1μM DTDP

Figure 5.2.3.1: Effect of 1μM DTDP on Cav2.2 kinetics. *The effect of 1μM DTDP on Cav2.2 channel kinetics of stably-transfected HEK293 cells was investigated via whole-cell patch clamp.* ***(A)*** *Current-voltage (-70 to +50mV) relationship of Cav2.2 channels (mean ± SEM) of HEK293 cells prior (untreated) and after 1μM DTDP treatment (n=6).* ***(B)*** *Reversal potential of Cav2.2 channels (mean ± SEM) prior (untreated) and after 1μM DTDP treatment (n=6).* ***(C)*** *Maximal conductance of Cav2.2 channels (mean ± SEM) prior (untreated) and after 1μM DTDP treatment (n=6).* ***(D)*** *Half-activation voltage of Cav2.2 channels (mean ± SEM) prior (untreated) and after 1μM DTDP treatment (n=6).* ***(E)*** *Slope of Cav2.2 channels (mean ± SEM) prior (untreated) and after 1μM DTDP treatment (n=6).* ***(F)*** *Amplitude of Cav2.2 channels (mean ± SEM) prior (untreated) and after 1μM DTDP treatment (n=6). Clampfit 10.3 was used for trace analysis. GraphPad was used for plotting current-voltage relationship and carrying out Boltzmann fit analysis. Statistical analysis was carried out via one-tailed paired T-test.*

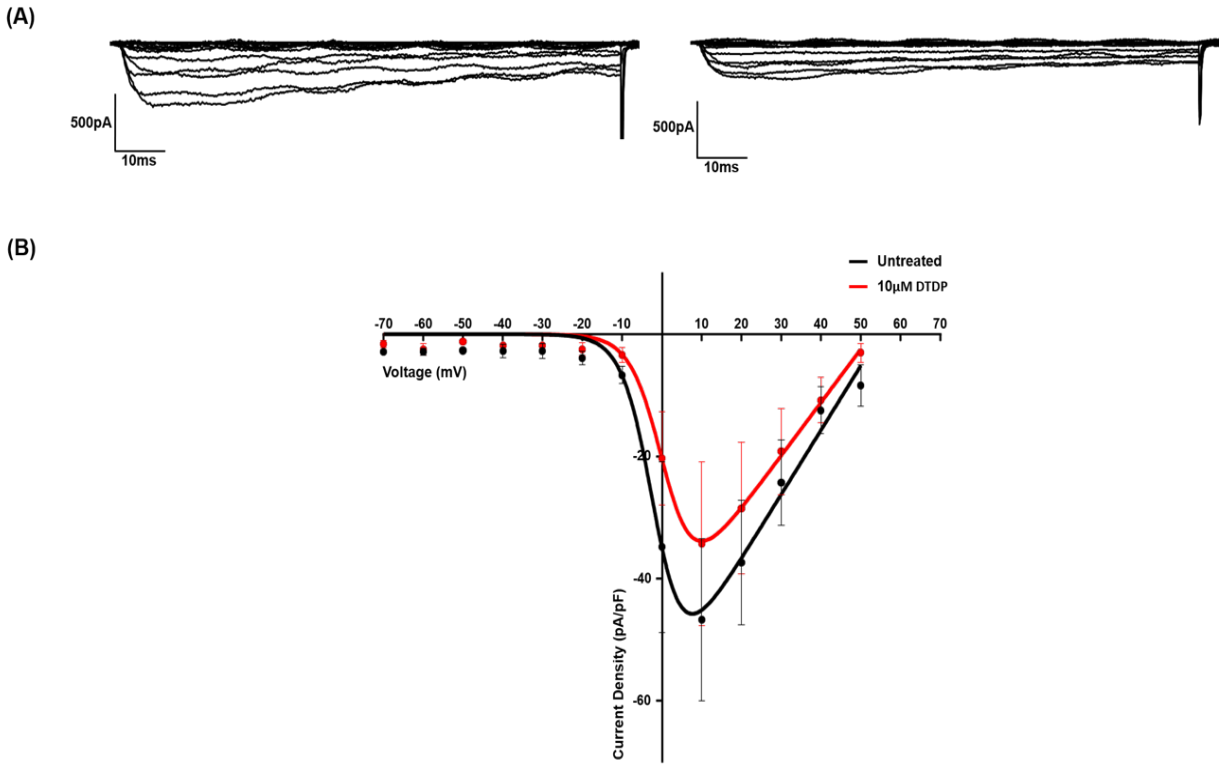

Figure 5.2.3.2: Effect of 10μM DTDP on Cav2.2 currents. *The effect of 10μM DTDP on Cav2.2 channels of stably-transfected HEK293 cells was investigated via whole-cell patch clamp.* ***(A)*** *Example current-voltage traces (-70 to +50mV) prior (left) and after (right) 10μM DTDP treatment.* ***(B)*** *Current-voltage (-70 to +50mV) relationship of Cav2.2 channels (mean ± SEM) of HEK293 cells prior and after 10μM DTDP treatment, fitted with the Boltzmann fit equation (n=5). Clampfit 10.3 was used for trace analysis, and GraphPad for plotting current-voltage relationship and Boltzmann fit analysis.*

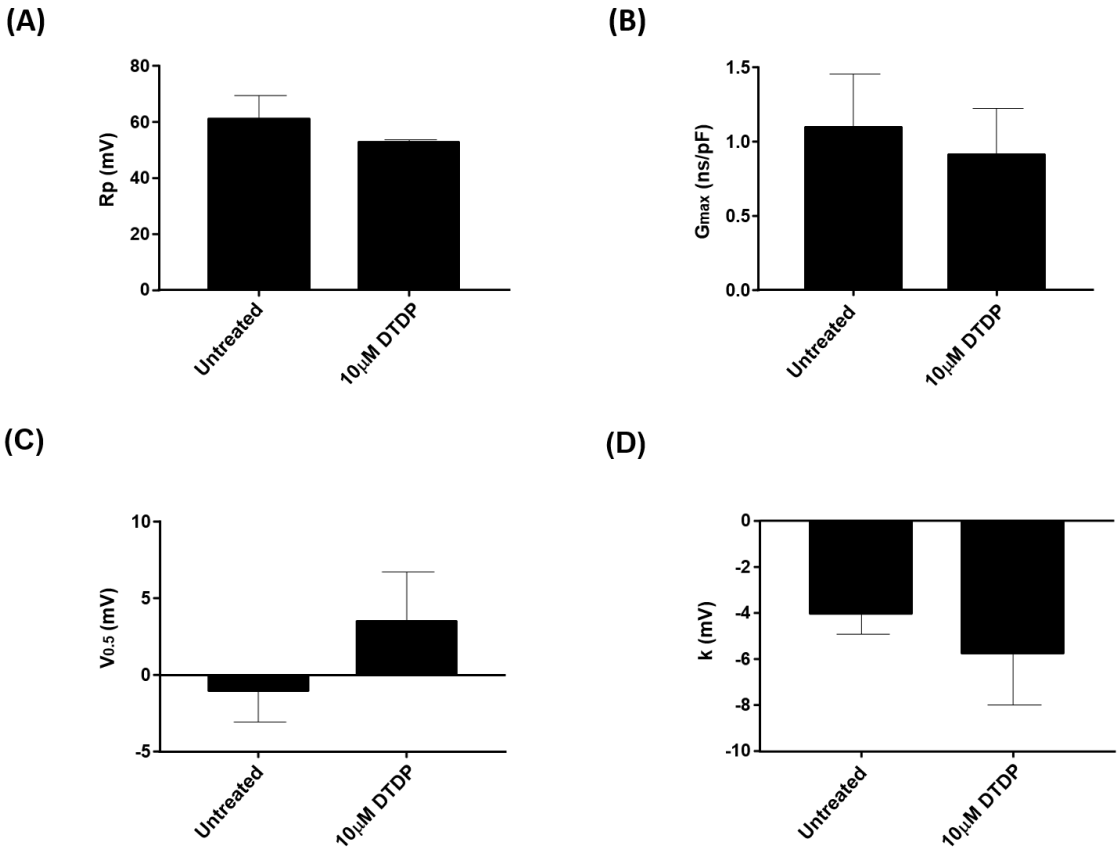

Figure 5.2.3.3: Effect of 10μM DTDP on Cav2.2 kinetics. *The effect of 10μM DTDP on Cav2.2 channel kinetics of stably transfected HEK293 cells was investigated via whole-cell patch clamp.* ***(A)*** *Reversal potential of Cav2.2 channels (mean ± SEM) prior (untreated) and after 10μM DTDP treatment (n=5).* ***(B)*** *Maximal conductance of Cav2.2 channels (mean ± SEM) prior (untreated) and after 10μM DTDP treatment (n=5).* ***(C)*** *Half-activation voltage of Cav2.2 channels (mean ± SEM) prior (untreated) and after 10μM DTDP treatment (n=5).* ***(D)*** *Slope of Cav2.2 channels (mean ± SEM) prior (untreated) and after 10μM DTDP treatment (n=5). Clampfit 10.3 was used for trace analysis, and GraphPad for analysing changes in channel kinetics obtained from Boltzmann fit analysis. Statistical analysis was carried out via one-tailed paired T-test.*

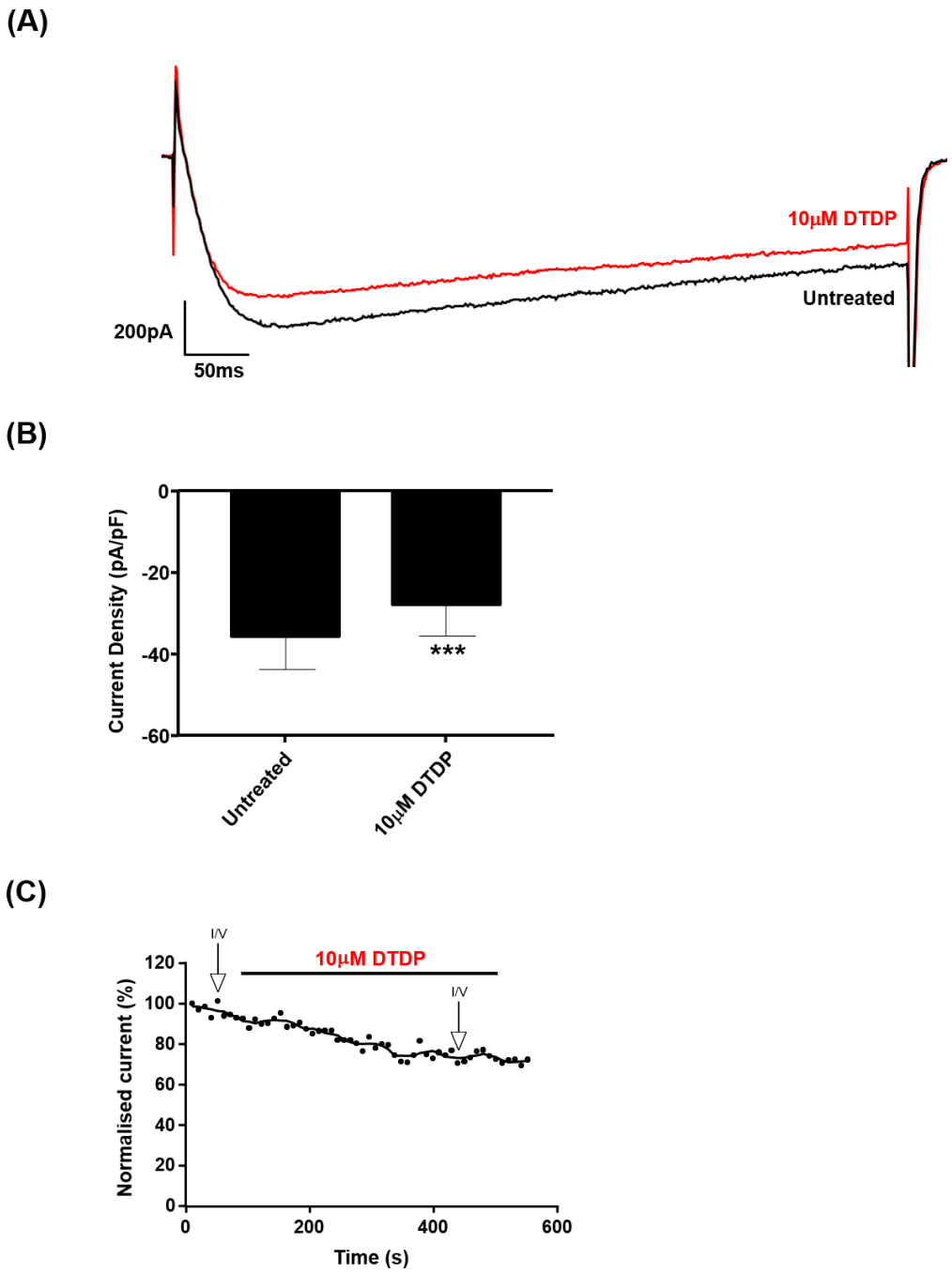

Figure 5.2.3.4: Effect of 10μM DTDP on Cav2.2 current amplitude. *The effect of 10μM DTDP on Cav2.2 current amplitude of stably-transfected HEK293 cells was investigated via whole-cell patch clamp.* ***(A)*** *Example trace of single-step (+10mV) recording of Cav2.2 current prior (black) and after (red) 10μM DTDP treatment.* ***(B)*** *Reduction in Cav2.2 current amplitude (mean ± SEM) with 10μM DTDP treatment (n=5).* ***(C)*** *Representative example of time-dependent changes in Cav2.2 current (+10mV) with 10μM DTT (red) treatment. Clampfit 10.3 was used for trace analysis, and GraphPad for analysing changes in current amplitude. Statistical analysis was carried out via one-tailed paired T-test. (***=P<0.001)*

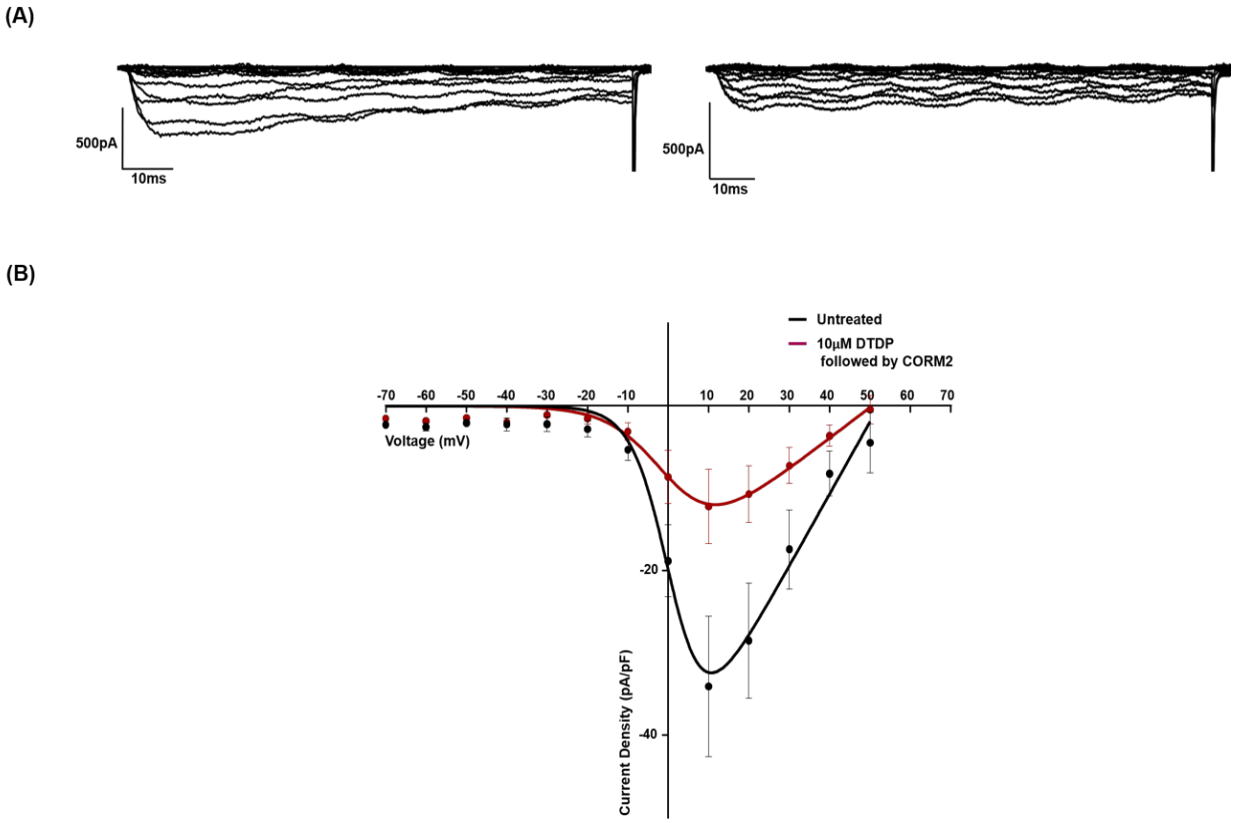

Figure 5.2.3.5: Redox modulation of CO on Cav2.2 currents. *The effect of CO, through 10μM DTDP followed by CORM2 treatment, on Cav2.2 channels of stably-transfected HEK293 cells was investigated via whole-cell patch clamp.* ***(A)*** *Example current-voltage traces (-70 to +50mV) prior (left) and after (right) 10μM DTDP followed by CORM2 treatment.* ***(B)*** *Current-voltage (-70 to +50mV) relationship of Cav2.2 channels (mean ±SEM) prior (untreated) and after 10μM DTDP followed by CORM2 treatment, fitted with the Boltzmann fit equation (n=7). Clampfit 10.3 was used for trace analysis, and GraphPad for plotting current-voltage relationship and Boltzmann fit analysis.*

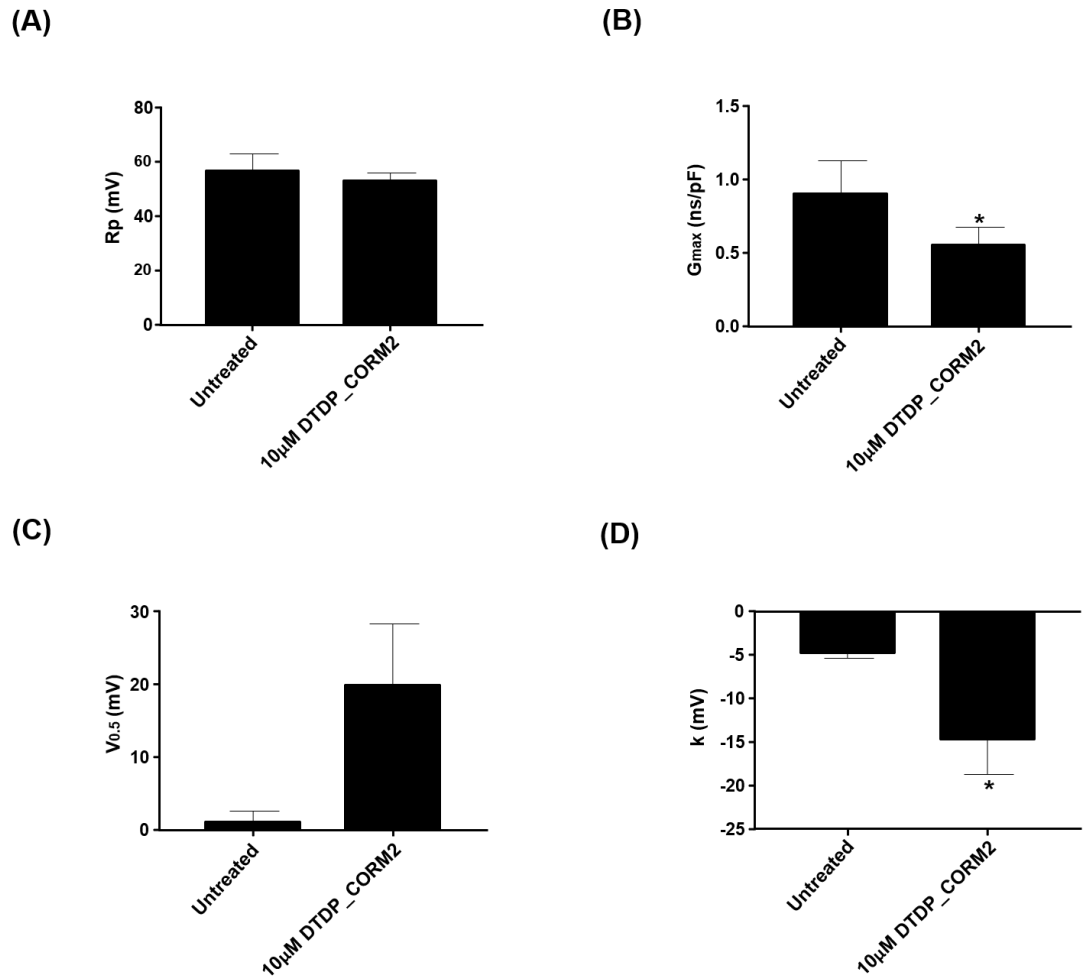

Figure 5.2.3.6: Redox-dependent effect of CO on Cav2.2 kinetics. *The effect of CO, through 10μM DTDP followed by CORM2 treatment on Cav2.2 channel kinetics of stably-transfected HEK293 cells investigated via whole-cell patch clamp.* ***(A)*** *Reversal potential of Cav2.2 channels (mean ±SEM) prior (untreated) and after 10μM DTDP followed by CORM2 treatment (n=7).* ***(B)*** *Reduction in maximal conductance of Cav2.2 channels (mean ±SEM) treated with 10μM DTDP followed by CORM2 (n=7).* ***(C)*** *Half-activation voltage of Cav2.2 channels (mean ±SEM) prior (untreated) and after 10μM DTDP followed by CORM2 treatment (n=7).* ***(D)*** *Change in slope of Cav2.2 channels (mean ±SEM) treated with 10μM DTDP followed by CORM2 (n=7). Clampfit 10.3 was used for trace analysis, and GraphPad for analysing changes in channel kinetics obtained from Boltzmann fit analysis. Statistical analysis was carried out via one-tailed paired T-test. (*=P<0.05)*

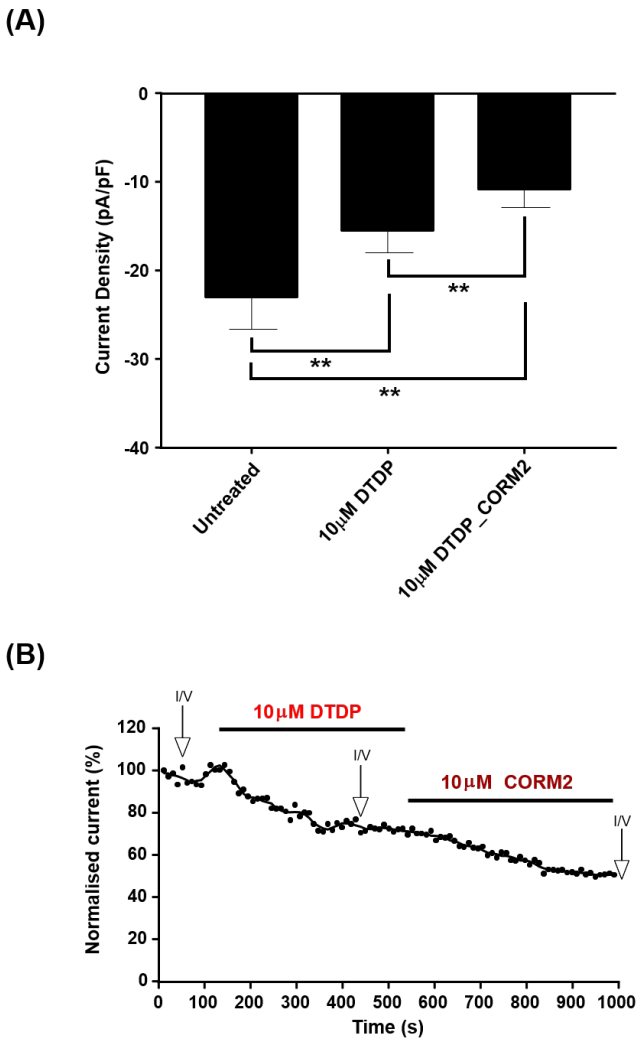

Figure 5.2.3.7: Redox-dependent effect of CO on Cav2.2 current amplitude. *The effect of CO, through 10μM DTDP followed by CORM2 treatment on Cav2.2 current amplitude of stably-transfected HEK293 cells was investigated via whole-cell patch clamp.* ***(A)*** *Reduction in Cav2.2 current amplitude (mean ± SEM) with 10μM DTDP followed by CORM2 treatment (n=7).* ***(B)*** *Representative example of time-dependent changes in Cav2.2 current (+10mV) with 10μM CORM2 (light red) followed by CORM2 (dark red) treatment. Clampfit 10.3 was used for trace analysis, and GraphPad for analysing changes in current amplitude. Statistical analysis was carried out via one-tailed paired T-test. (**=P<0.01)*

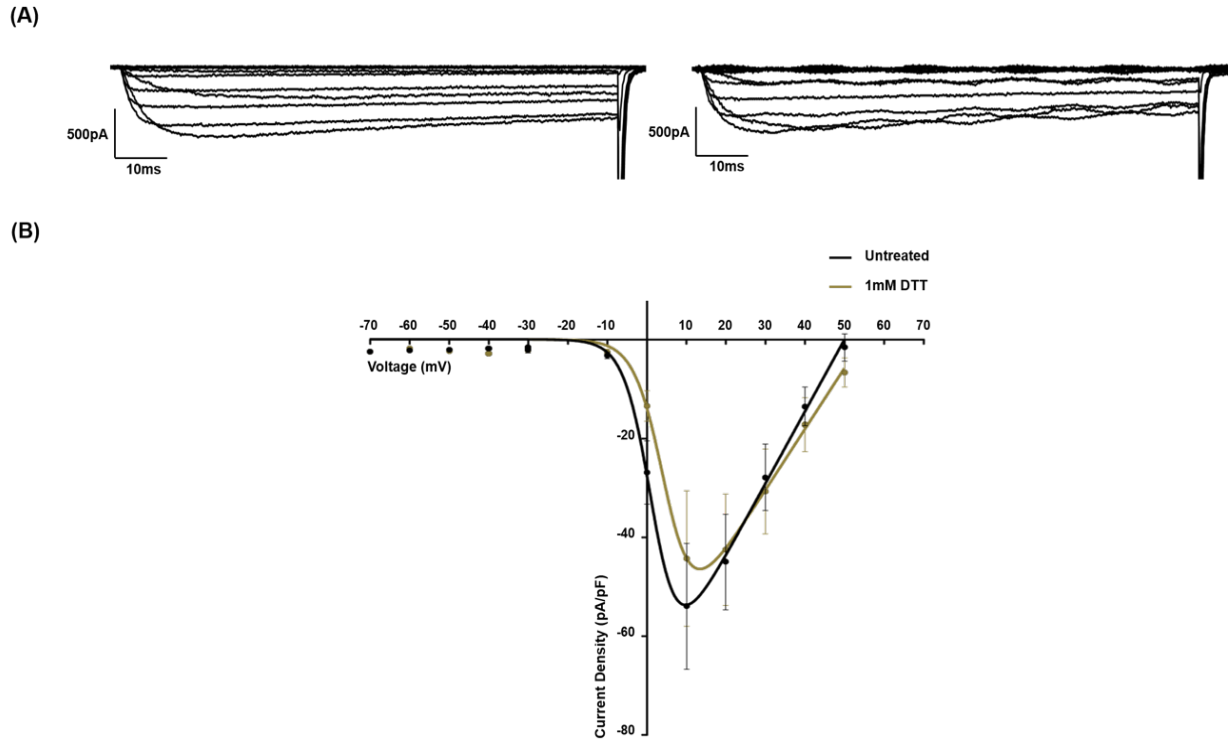

Figure 5.2.3.8: Effect of 1mM DTT on Cav2.2 currents. *The effect of 10μM DTDP on Cav2.2 channels of stably-transfected HEK293 cells was investigated via whole-cell patch clamp.* ***(A)*** *Example current-voltage traces (-70 to +50mV) prior (left) and after (right) 1mM DTT treatment.* ***(B)*** *Current-voltage (-70 to +50mV) relationship of Cav2.2 channels (mean ± SEM) of HEK293 cells prior and after 1mM DTT treatment, fitted with the Boltzmann fit equation (n=6). Clampfit 10.3 was used for trace analysis, and GraphPad for plotting current-voltage relationship and Boltzmann fit analysis.*

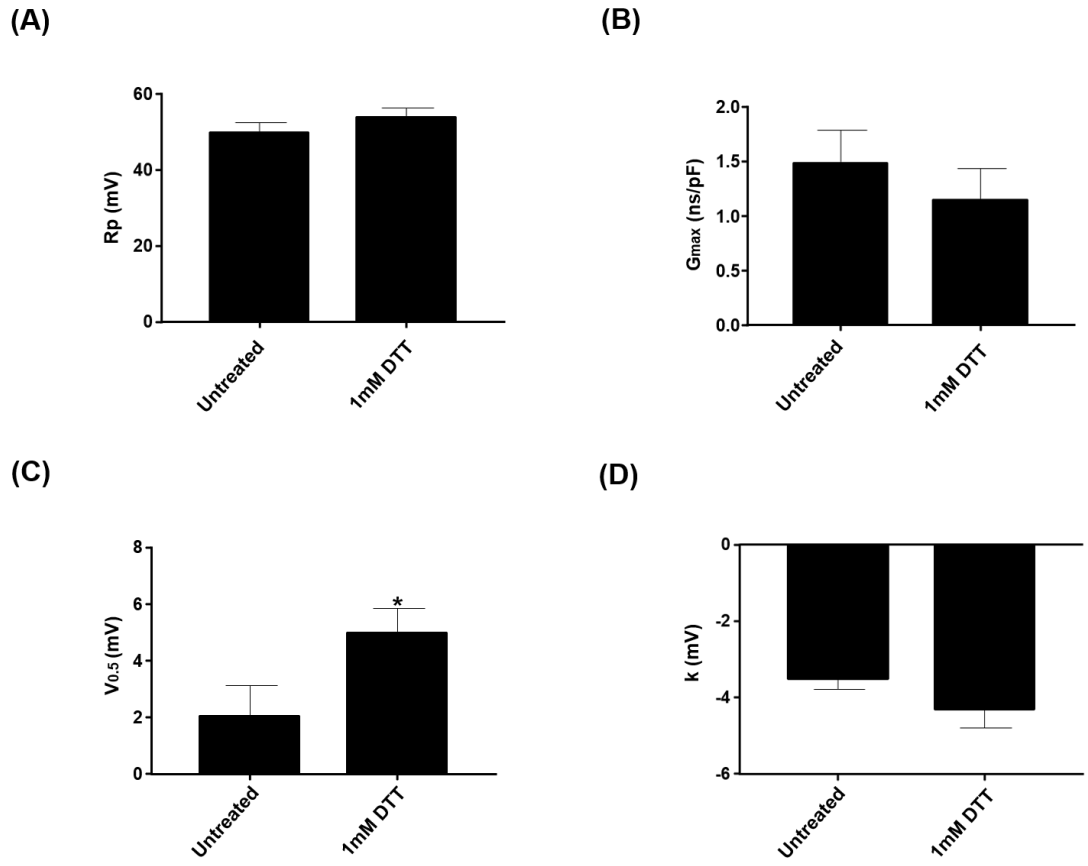

Figure 5.2.3.9: Effect of 1mM DTT on Cav2.2 kinetics. *The effect of 1mM DTT on Cav2.2 channel kinetics of stably transfected HEK293 cells was investigated via whole-cell patch clamp.* ***(A)*** *Reversal potential of Cav2.2 channels (mean ± SEM) prior (untreated) and after 1mM DTT treatment (n=6).* ***(B)*** *Maximal conductance of Cav2.2 channels (mean ± SEM) prior (untreated) and after 1mM DTT treatment (n=6).* ***(C)*** *Increase in half-activation voltage of Cav2.2 channels (mean ± SEM) treated with 1mM DTT treatment (n=6).* ***(D)*** *Slope of Cav2.2 channels (mean ± SEM) prior (untreated) and after 1mM DTT treatment (n=6). Clampfit 10.3 was used for trace analysis, and GraphPad for analysing changes in channel kinetics obtained from Boltzmann fit analysis. Statistical analysis was carried out via one-tailed paired T-test. (*=P<0.05)*

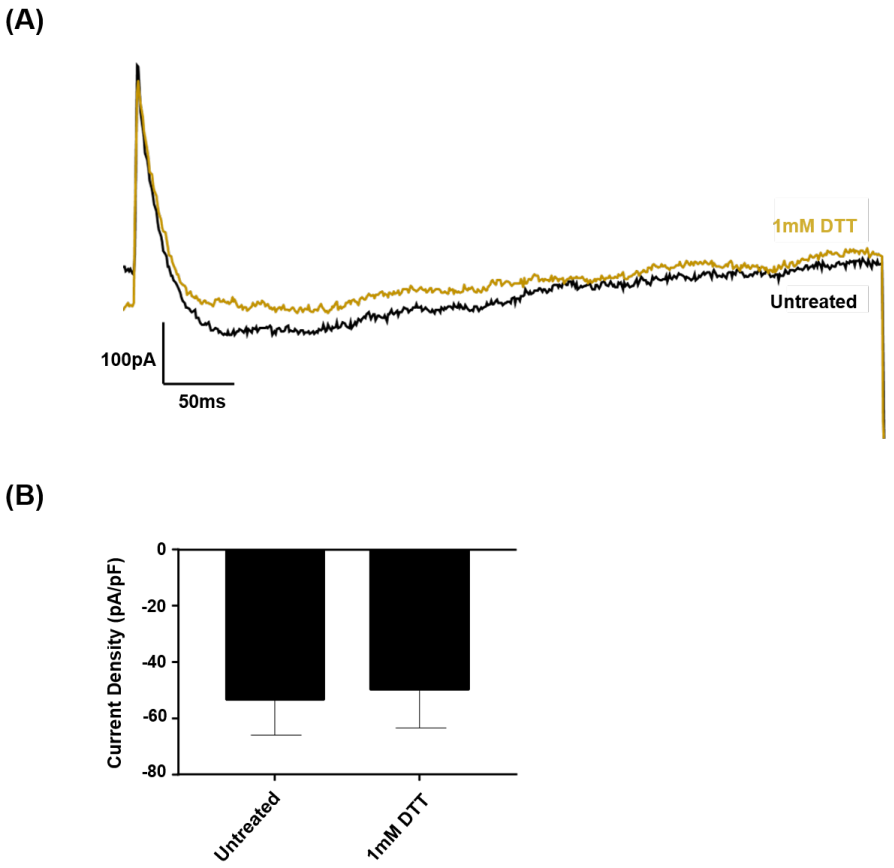

Figure 5.2.3.10: Effect of 1mM DTT on Cav2.2 current amplitude. *The effect of 10μM DTDP on Cav2.2 current amplitude of stably-transfected HEK293 cells was investigated via whole-cell patch clamp.* ***(A)*** *Example trace of single-step (+10mV) recording of Cav2.2 current prior (black) and after (brown) 1mM DTT treatment.* ***(B)*** *Amplitude of Cav2.2 channels (mean ± SEM) with 1mM DTT treatment (n=6). Clampfit 10.3 was used for trace analysis, and GraphPad for analysing changes in current amplitude. Statistical analysis was carried out via one-tailed paired T-test.*

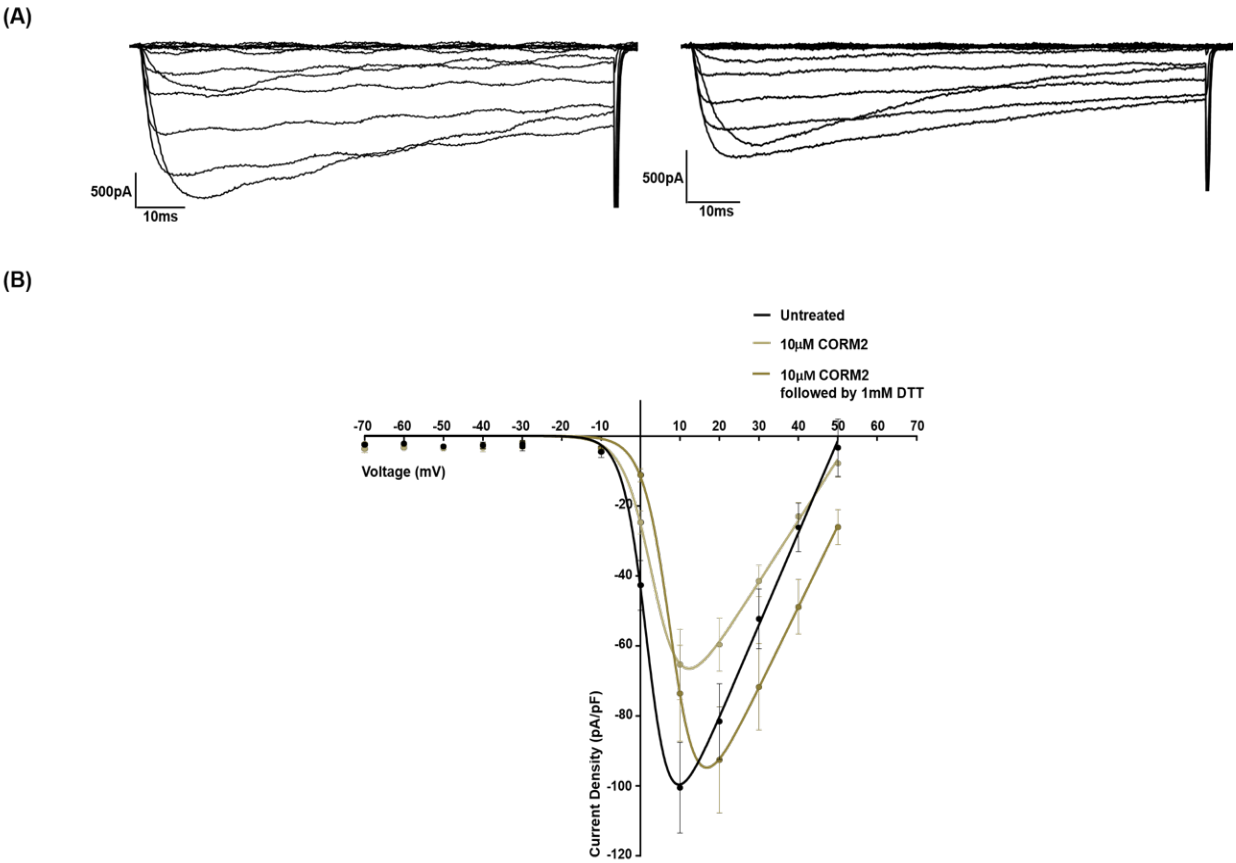

Figure 5.2.3.11: Modulation of Cav2.2 channels by CO through a redox manner. *The effect of CO, through 10μM CORM2 followed by 1mM DTT treatment, on Cav2.2 channels of stably-transfected HEK293 cells was investigated via whole-cell patch clamp through treatment.* ***(A)*** *Example current-voltage traces (-70 to +50mV) prior (left) and after (right) 10μM CORM2 followed by 1mM DTT treatment.* ***(B)*** *Current-voltage (-70 to +50mV) relationship of Cav2.2 channels (mean ±SEM) prior (untreated) and after 10μM CORM2 followed by 1mM DTT treatment, fitted with the Boltzmann fit equation (n=5). Clampfit 10.3 was used for trace analysis, and GraphPad for plotting current-voltage relationship and Boltzmann fit analysis.*

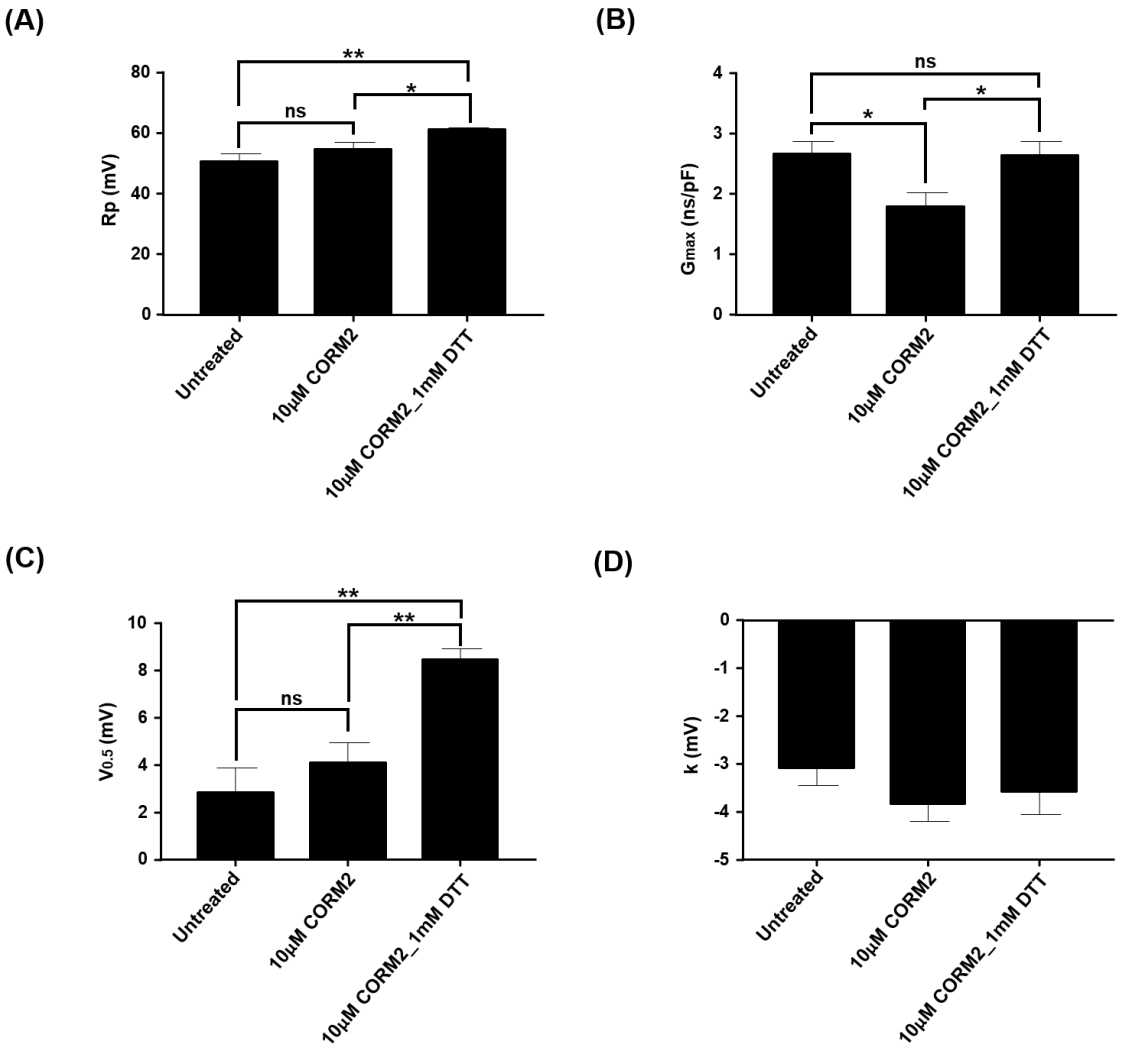

Figure 5.2.3.12: Redox-dependent effect of CO on Cav2.2 kinetics. *The effect of CO, through 10μM CORM2 followed by 1mM DTT treatment on Cav2.2 channel kinetics of stably-transfected HEK293 cells investigated via whole-cell patch clamp.* ***(A)*** *Increase in reversal potential of Cav2.2 channels (mean ±SEM) treated with 10μM CORM2 followed by 1mM DTT (n=5).* ***(B)*** *Reduction in maximal conductance of Cav2.2 channels (mean ±SEM) treated with 10μM CORM2. Complete reversal in conductance was noted with 10μM CORM2 followed by 1mM DTT treatment (n=5).* ***(C)*** *Increase in half-activation voltage of Cav2.2 channels (mean ±SEM) treated with 10μM CORM2 followed by 1mM DTT (n=5).* ***(D)*** *Slope of Cav2.2 channels (mean ±SEM) prior (untreated) and after 10μM CORM2 followed by 1mM DTT treatment (n=5). Clampfit 10.3 was used for trace analysis, and GraphPad for analysing changes in channel kinetics obtained from Boltzmann fit analysis. Statistical analysis was carried out via one-tailed paired T-test. (*=P<0.05; **=P<0.01)*

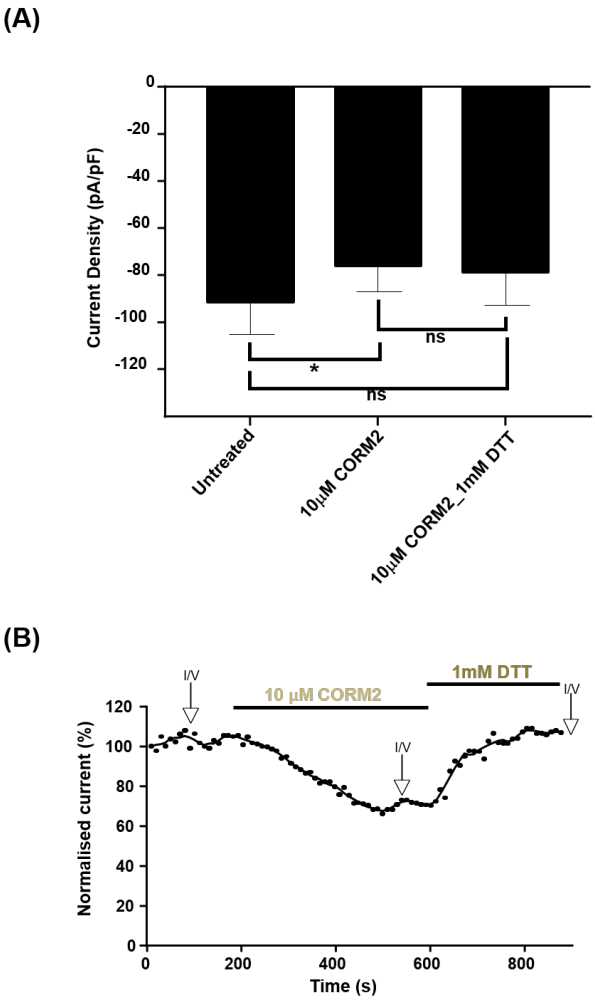

Figure 5.2.3.13: Redox-dependent effect of CO on Cav2.2 current amplitude. *The effect of CO, through 10μM CORM2 followed by DTT treatment on Cav2.2 current amplitude of stably-transfected HEK293 cells was investigated via whole-cell patch clamp.* ***(A)*** *Reduction in Cav2.2 current amplitude (mean ± SEM) with 10μM CORM2. Complete reversal in current amplitude with 10μM CORM2 followed by DTT treatment (n=5).* ***(B)*** *Representative example of time-dependent changes in Cav2.2 current (+10mV) with 10μM CORM2 (light brown) followed by 1mM DTT (dark brown) treatment. Clampfit 10.3 was used for trace analysis, and GraphPad for analysing changes in current amplitude. Statistical analysis was carried out via one-tailed paired T-test. (*=P<0.05)*

5.3. Discussion

Effect of protofibrillar Aβ_{1-42} on Cav2.2 channels

- *Protofibrillar Aβ_{1-42} at 100nM significantly changed the slope factor of Cav2.2 currents in stably-transfected HEK293 cells.*
- *Protofibrillar Aβ_{1-42} at 1μM reduces Cav2.2 currents in stably-transfected HEK293 cells.*

As a first step in investigating the effects of protofibrillar Aβ_{1-42} on VGCCs, functional Cav2.2 (α_{1B} ($Ca_v2.2$), β_{1b}, and $a_2\delta$ subunits) channels expression in stably-transfected HEK293 cells was verified via the use of ω-conotoxin-GVIA. Treatment with 100nM protofibrillar Aβ_{1-42} although it significantly changed the slope factor, it did not change Cav2.2 conductance or other channel properties. In contrast, higher concentration (1μM) of protofibrillar Aβ_{1-42} caused a significant reduction in both Cav2.2 conductance and amplitude. While it has been proven by a number of studies that aggregated Aβ_{1-42} can alter the activity of VGCCs, contradictory evidence exist in relation to the effect of Aβ_{1-42} on these channels (Nimmrich *et al.*, 2008; Mezler *et al.*, 2012; Hermann *et al.*, 2013). Previous studies have shown that exposure to high (200-830) nM concentrations of human synthetic oligomeric Aβ_{1-42} caused a significant increase in both Cav2.1 and Cav2.2 amplitude, and additionally a leftward shift of V_{half} towards more hyperpolarised values (Mezler *et al.*, 2012; Hermann *et al.*, 2013). The changes in Cav2.1 kinetics was found to occur due to a physical interaction of globulomer Aβ_{1-42} with the α1 subunit of the channel (Mezler *et al.*, 2012). Although Mezler *et al.* revealed a direct interaction for globulomer Aβ_{1-42} with the α1 subunit of Cav2.1, the mechanism by which Aβ_{1-42} interacts with the peptide, such as modulation of specific residues, was not investigated. In contrast, a study conducted in 2002 by Ramsden and colleagues, agreeing with the results in the current study revealed that aggregated Aβ_{1-40} (1μM) reduces Cav2.2 currents, whereas unaggregated Aβ_{1-40} increases Ca^{2+} currents (Ramsden, Henderson and Pearson, 2002). Differences in findings within the literature and the current study could be explained due to differential effects of Aβ on Cav2 channels dependent on Cav2 subtype, and also differential effects dependent on the Aβ species, aggregation status and concentration used. Moreover, the current study investigated the effect of Aβ_{1-42} on cells exposed to the amyloid peptide over 24hr, whereas Hermann *et al.* (2013) and Mezler *et al.* (2012) investigated the effect of acute

treatment (10mins) with $A\beta_{1-42}$. This suggests that short term exposure to Aβ may cause an initial increase in channel conductance and therefore synaptic activity, whereas prolonged exposure and exposure to higher levels of Aβ, can ultimately lead to changes in the synapses and synaptic decline, possibly through a pathway involving a reduction in VGCC conductance (Sheng *et al.*, 1996; Koppensteiner *et al.*, 2016; Arbel-Ornath *et al.*, 2017). In line with this, studies have revealed that pre-clinical and early-stages of AD are characterised by neuronal hyperactivity, possibly as a compensatory mechanism, that can eventually lead to synaptic loss which is especially noted at later stages of AD (Miller *et al.*, 2008; Yassa *et al.*, 2010; Putcha *et al.*, 2011; Busche *et al.*, 2012; Busche and Konnerth, 2015). Thus, reduction in Cav2.2 currents noted in the current study may be representative of synaptic dysfunction seen at later stages of AD rather than pre-clinical or early-stages. Although Nimmrich *et al.* used primary neurons in contrast to SH-SY5Y neuronal line used in the current study, Nimmrich *et al.* (2008) demonstrated that one manner by which treatment with low nM $A\beta_{1-42}$ globulomers caused a marked downregulation in synaptic activity of hippocampal neurons was through a reduction in Cav2.1 channel conductance. A reduction in Ca^{2+} influx due to Aβ-mediated changes in VGCC currents can have detrimental effects in neuronal function, for example through interfering with neurotransmission. For example, oligomeric Aβ has been implicated with neuronal morphological changes, such as reduction in spine density and in overall dendritic spine number which can subsequently influence synaptic activity (Arbel-Ornath *et al.*, 2017). Another manner by which VGCC dysfunction may lead to reduction in neurotransmission is through less Ca^{2+} binding to the Ca^{2+} sensor synaptotagmin which is known to interact with the SNARE complex, facilitating vesicular fusion and subsequent neurotransmitter release (Bennett *et al.*, 1992; Pang *et al.*, 2006; Xu *et al.*, 2009; Südhof, 2013).

Taken together, the current study, supported by previous research, proves that protofibrillar $A\beta_{1-42}$ can impair Ca^{2+} influx through changes in Cav2.2 channel properties.

Effect of CO on Cav2.2 channels

- *CO, through CORM2 reduces Cav2.2 currents of stably-transfected HEK293 cells in a concentration-dependent manner.*
- *The mechanism by which CO reduces Cav2.2 currents involves redox modulation.*

A growing number of ion channels have been reported to be modulated by CO (Scragg *et al.*, 2008; Dallas *et al.*, 2011; Mezler *et al.*, 2012; Boycott *et al.*, 2013; Al-Owais *et al.*, 2017; Kapetanaki *et al.*, 2018). The current study is the first study to prove that CO, through CORM2 treatment, can modulate Cav2.2 channels through a reduction in the conductance and also changes in other channel properties.

Similarly to the current study, previous evidence, although conducted on Cav1 rather than Cav2 channels, has revealed that in both rodent native and human and rodent recombinant Cav1.2 channels 30μM CORM2 inhibits Cav1 currents, whereas iCORM2 has no effect on Ca^{2+} currents (Scragg *et al.*, 2008). Similarly, Boycott *et al.* (2013) proposed that CORM2 also inhibits LVA Cav3 channels. Although in the current study, iCORM2 was shown to also reduce Cav2.2 conductance, a larger reduction in conductance and amplitude was seen with CORM2 suggesting that the effect of CORM2 on these channels is at least partly due to the release of CO.

In addition to revealing that CO through CORM2 treatment modulates Cav2.2 channels and reduces Ca^{2+} influx through these channels, use of the oxidant DTDP and the reducing agent DTT revealed that the mode of action of CO involves redox modulation of these channels. The current study is the first study to suggest redox modulation of Cav2 channels by CO. In the current study both CORM2 and the oxidant DTDP caused a significant reduction in Cav2.2 currents. Treating cells with DTDP alone caused a small reduction in Cav2.2 currents, whereas treating cells with DTDP followed by CORM2 caused a larger degree of reduction. This suggests that CORM2 may act in a similar manner to DTDP. As iCORM2 did not cause the same degree of changes in Cav2.2 kinetics as with treatment with CORM2, it is believed that at least partly, the inhibitory effects seen by CORM2 are due to release of CO. In further support of a redox role for CO, treating cells with CORM2 followed by DTT, an antioxidant, partly prevented CO-mediated Cav2.2 inhibition.

Numerous studies have proven that redox modulation of VGCCs, through either indirect modulation such as lipid peroxidation, or direct redox modulation of specific

residues on these channels can have an impact on their overall function, with clinical significance in diseases such as AD (Li *et al.*, 1998). For example, treatment of neuronal Cav2.1 channels with H_2O_2 has been shown to increase Cav2.1 current amplitude by causing the channels to open at more hyperpolarised values (Li *et al.*, 1998). Although the manner by which oxidation with H_2O_2 modulates these channels was not investigated, direct interaction with the $\alpha 2\delta$ subunit was excluded (Li *et al.*, 1998). In contrast, work done on cardiac Cav1.2 revealed that oxidation with DTDP causes a decrease in Cav1.2 currents through directly modulating specific cysteine residues found on the $\alpha 1$ pore-forming subunit (Chiamvimonvat *et al.*, 1995; Scragg *et al.*, 2008).

A number of studies have proven that CO may also modulate ion channels through a redox manner (Scragg *et al.*, 2008; Dallas *et al.*, 2011; Al-Owais *et al.*, 2017). Even though redox modulation has been proposed as one manner by which CO may modulate VGCCs, some studies suggest that it works similar to an oxidising, where other studies suggest it may act similar to a reducing agent. In agreement to findings from the current study, where CORM2 was shown to reduce Cav2.2 currents, Scragg *et al.* (2008) and Boycott *et al.* (2013) have proven that the use of the reducing agent DTT (low mM concentrations) can partly or completely reverse the inhibitory effects of CORM2 on VGCCs. This suggests that CO, through CORM2 treatment, may act as an oxidant and therefore may change channel properties in a redox-dependent manner. Although these studies agree with the current study, these studies focused on Cav1 and Cav3 channels. The current study is the first study to suggest redox modulation of Cav2 channels by CO. In contrast, Dallas *et al.* (2011) although agreeing that CO may act as a redox modulator, in neuronal Kv2.1 channels was shown to act as a reducing agent rather than an oxidant.

A number of mechanisms have been proposed as to how CO modulate ion channels such as VGCCs through a redox manner, with a number of studies implicating specific cysteine residues as the ion-channel site required for CO-channel sensitivity. For example, in K_{ATP} channels findings revealed that CO can activate these channels through a change in conformational structure via a mechanism that requires heme binding onto the channel forming a heme-SUR2A complex. Following the formation of the complex, CO can then displace a cysteine residue in order to interact and bind to the heme-SUR2A complex. This change in conformational structure can then induce K_{ATP} activation

(Kapetanaki *et al.*, 2018). In VGCCs, specifically Cav1 channels, it was revealed that specific cysteine residues within the α1 subunit cytoplasmic C-terminus of the channels were required for CO binding, identified through site-mutagenesis (Scragg *et al.*, 2008). CO-dependent redox modulation of Cav1 channels involved release of ROS from ETC mitochondrial complex III, where similar to the current study, use of the reducing agent DTT prevented the effect of CO on the Cav1 channels (Scragg *et al.*, 2008). Whereas in LVA VGCCs, specifically Cav3.2 channels, CORM2 (μM concentrations) significantly reduces VGCC current amplitude through targeting cysteines present at an extracellular site of the α1 subunit (cysteines linking region S5 and S6 in domain I) (Boycott *et al.*, 2013). Some of these cysteine residues are conserved between all Cav families (Karmazinova *et al.*, 2010). Substitution of these cysteine residues with alanine residues can either change channel kinetics, reduce channel conductance or result in a non-functional channel, proving that these residues have an important role in the gating properties of the channel (Karmazinova *et al.*, 2010). Use of DTT has shown to cause an increase in reduced channel conductance seen with substitution of these cysteine residues (Karmazinova *et al.*, 2010). It has been suggested that compounds containing metals such as CORM2 which contains ruthenium, may work by interacting with these cysteine residues, therefore disrupting the stability of the VGCC structure, and consequently blocking Cav currents. Whereas DTT is believed to work by either disrupting disulphide bonds or as a scavenger by removing the metal interacting with the channel (Chiamvimonvat *et al.*, 1995; Karmazinova *et al.*, 2010). Boycott *et al.* (2013) revealed that AuF, an agent that blocks the reduction of Trx (thioredoxin), with known ion-channel redox modulator roles, reduced Cav3.2 currents similarly to CORM2 treatment, whereas DTT restored currents. Similarly to our findings, Boycott *et al.* (2013) revealed that treatment of Cav3 channels with DTT alone only caused a marginal change in the size of the current, whereas treatment with CORM2, followed by DTT caused a significant increase in current, and therefore partially reversed the inhibitory effect of CORM2. Therefore, it is believed that CO may modulate Cav3.2 channels through a Trx-manner (Boycott *et al.*, 2013). Although CO-dependent modulation of Cav3.2 channels was shown to involve Trx, CORM2 was not shown to influence Cav3.1 and Cav3.3 channels using the same mechanism (Boycott *et al.*, 2013).

Taken together, CORM2 was shown to reduce Cav2.2 currents through a redox-dependent manner. Although iCORM2 was also shown to reduce Cav2.2 currents, a higher degree of reduction was seen with CORM2. This suggests that although some of these inhibitory effects seen by CORM2 could be due to the presence of the metal ruthenium structure, part of the changes in channel kinetics seen by CORM2 are due to CO. The effect of CORM2 on Cav2.2 is reversed with treatment with the reducing agent DTT, suggesting that CORM2 acts as an oxidant. Although previous work done by other groups reveal differential redox effects of CO on ion channels, CO may act differently dependent on the ion channel type and the ion channel subunit composition. Similar mechanisms to Cav1 and Cav3 channels noted from previous studies, such as indirect modulation via release of ROS from mitochondria, or direct interaction with cysteine residues at specific sites on the $\alpha 1$ pore-forming subunit may also underlie the mechanism by which CORM2 reduces Cav2.2 currents in the current study.

5.4. Summary

In support of the hypothesis protofibrillar $A\beta_{1-42}$ induced concentration-dependent changes in Cav2.2 channel properties. The reduction in channel conductance seen with 1μM $A\beta_{1-42}$ may reflect late-stages of AD where a high degree of synaptic dysfunction is reported.

Parallel studies, in support of the hypothesis that CO modulates ion channels, revealed that CORM2 inhibits Cav2.2 channels. Although a role for the ruthenium dimer present in CORM2 cannot be excluded, this redox-dependent inhibitory effect is believed to occur at least partly due to CORM2 dependent CO release.

Chapter 6: Overall discussion

6.1. Overall discussion

Calcium dysregulation comprises a main feature of numerous neurodegenerative diseases. In AD, Aβ misfolding, accumulation and aggregation has been linked to changes in VGCCs and neuronal dysfunction (e.g. synaptic loss) and eventually even neuronal death (Ueda *et al.*, 1997; Arbel-Ornath *et al.*, 2017). Similarly, in ALS (amyotrophic lateral sclerosis), a motor neuron disease, through both molecular and electrophysiology approaches an increase in HVA VGCC, particularly Cav1 activity has been proposed as part of the mechanism accounting for the noted protein misfolding and accumulation, which drives the noted neurodegeneration (Mosier *et al.*, 1995; Pullen *et al.*, 2004; Pambo-Pambo, Durand and Gueritaud, 2009; Leal *et al.*, 2013; Chang and Martin, 2016). Epilepsy, Parkinson's disease (PD) and psychiatric disorders are some other conditions where Ca^{2+} dysregulation has also been reported (Nedergaard, Flatman and Engberg, 1993; Talley *et al.*, 2000; Zhang *et al.*, 2002; Chan *et al.*, 2007; Miki *et al.*, 2008; Hurley *et al.*, 2013; Ripke *et al.*, 2013; Ostacher *et al.*, 2014).

The current study focuses on the effect of protofibrillar $A\beta_{1\text{-}42}$ on VGCCs and modulation of these channels by CO. It provides evidence that different VGCCs, specifically Cav1.2, Cav1.3 and Cav2.2 may be modulated by Aβ during AD. Moreover CORM2, either through CO release or/and due to the presence of the metal ruthenium, was shown to have a redox-dependent inhibitory effect on Cav2.2.

AD has been linked to changes in both the expression and activity of Cav1 channels (Coon *et al.*, 1999; Chiou, 2006; Kim and Rhim, 2011; Hettiarachchi *et al.*, 2014). The current study has shown that protofibrillar $A\beta_{1\text{-}42}$, dependent on concentration, impairs calcium homeostasis through selective changes in differentiated SH-SY5Y Cav1 mRNA expression. Findings from this study indicate a significant increase in transcript expression for Cav1.2 with 1μM protofibrillar $A\beta_{1\text{-}42}$ treatment, whereas a significant reduction in Cav1.3 expression with 100nM protofibrillar $A\beta_{1\text{-}42}$ was seen. Similar to AD, where changes in Cav1 expression are seen, in PD where extensive dopaminergic neuronal loss is seen, changes in Cav1.2 and Cav1.3 expression and activity have been linked to neuronal hyperexcitability (Nedergaard, Flatman and Engberg, 1993; Chan *et al.*, 2007; Hurley *et al.*, 2013). Changes in VGCC activity are also seen in ALS at early stages of the disease, during stages of hyperexcitability and

excitotoxicity (Bories *et al.*, 2007; Pambo-Pambo, Durand and Gueritaud, 2009). As changes in Cav1 expression and activity has been shown to be part of the pathological mechanisms of numerous neurodegenerative diseases, including AD, a number of cohort studies have suggested that the use of dihydropyridines may provide neuroprotection. In hypertensive patients use of dihydropyridines revealed that it may confer some neuroprotection against risk in developing PD, shown through a reduction in the incidence of PD (Ritz *et al.*, 2010; Lee *et al.*, 2014). Although this may suggest that use of dihydropyridines would also be effective against AD, clinical trials have revealed mixed findings. Potential reasons for clinical trials failing to exhibit significant effects in interrupting or delaying AD pathology could be due to low brain bioavailability of the CCB tested, the disease stage at which the drug was tested and also selectivity issues could also affect findings, such as nimodipine which targets all Cav1 isoforms (Birks and López-Arrieta, 2002; Anekonda *et al.*, 2011; Gholamipour-Badie *et al.*, 2013; Zamponi, 2016). Neuronal hyperexcitability is a feature of both pre-clinical AD and early-stage AD (Busche *et al.*, 2008; Busche and Konnerth, 2015; Kazim *et al.*, 2017). As in the CNS Cav1 channels have shown to be vital for neuronal excitability and firing, changes in the expression of Cav1 channels highlighted in the current study may be indicative of early stages of AD (McKinney *et al.*, 2009; Liu *et al.*, 2014). In addition to neuronal excitability and firing, Cav1.2 has also been implicated in regulating CREB-dependent gene expression of genes linked to synaptic function, cell proliferation, development and apoptosis, whereas Cav1.3 has a role in dendritic spine morphology, stability and adult neurogenesis which is a vital process for learning and memory (Moosmang *et al.*, 2005; McKinney *et al.*, 2009; Liu *et al.*, 2014; Marschallinger *et al.*, 2015; Stanika, Flucher and Obermair, 2015; Stanika *et al.*, 2016). Neuronal hyperactivity which can occur due to impairments in neuronal morphology, synaptic activity and overall synaptic plasticity, as well as deficits in adult neurogenesis, are both known as features of early-stage AD (Busche *et al.*, 2008; Busche and Konnerth, 2015; Kazim *et al.*, 2017; Scopa *et al.*, 2020). As Cav1 channels have been shown to have important roles in all these processes, changes in their expression and activity may be part of the pathogenic mechanism(s) seen at early stages of AD progression. Therefore, using dihydropyridines at a later stage in the disease, where progressive levels of neurodegeneration is observed may render them ineffective. In support, a cohort study conducted on individuals with hypertension

and PD revealed that although Cav1 blockers may have promising effects against PD risk at early stages of the disease, taken at later disease stages, CCBs were unable to prevent disease progression and to limit neurodegeneration (Marras *et al.*, 2012). A similar trend in effectiveness of CCBs, dependent on disease stage, may also be true for AD. This suggests that use of compounds that modulate VGCCs would be most effective when given to patients at risk of developing AD or patients displaying MCI rather than at progressed (moderate or severe) AD stages where significant neuronal loss and brain atrophy is already evident (**Fig. 6.1.1**).

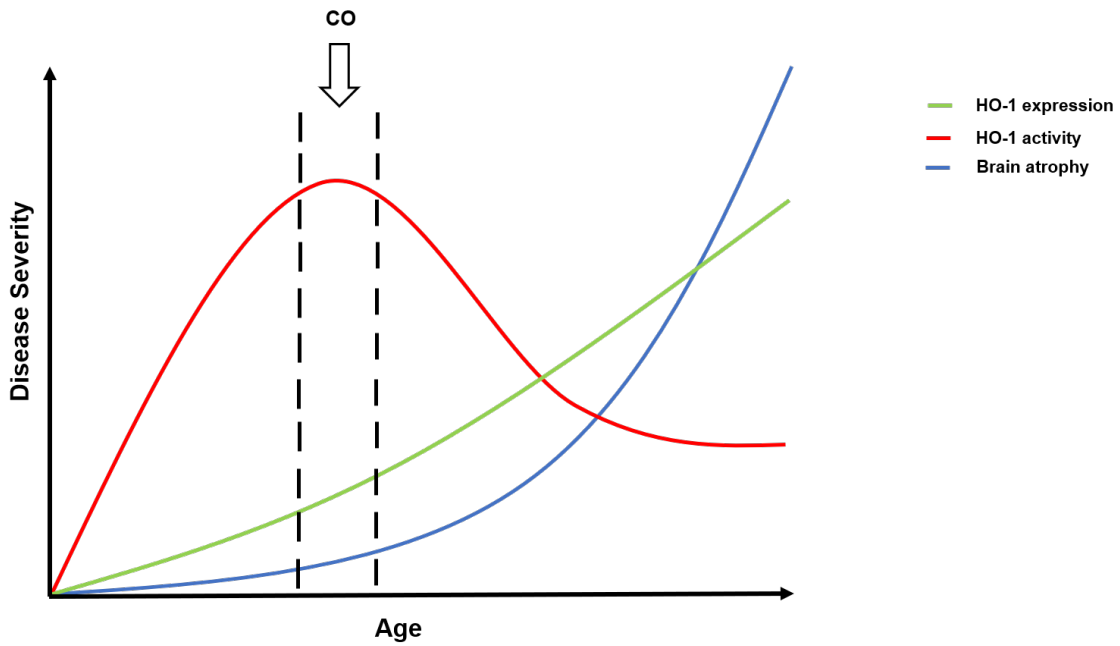

Figure 6.1.1: Progression of Alzheimer's disease and CO as a therapeutic. *Trend for Alzheimer's disease progression can be seen in the graph. Age is known as a major risk factor for Alzheimer's development and progression. As AD progresses, more brain atrophy is seen. Although HO-1 has been shown to be neuroprotective, and its expression is upregulated in Alzheimer's disease, its activity is impaired, consequently rendering it ineffective. Use of CO, or activating CO- dependent mechanisms during early stages of the disease, where neuronal dysfunction is evident, but limited degree of brain atrophy is seen, might be an effective treatment against Alzheimer's disease.*

The current study has also revealed a reduction in Cav2.2 Ca^{2+} influx with protofibrillar $A\beta_{1-42}$ treatment. In contrast to Cav1 channels, Cav2 channels are found predominately at presynaptic sites with specialised functions such as in neurotransmission. As late stages of AD are characterised by pathological processes such as neurotransmitter depletion, reduction in spine density and overall number which aid synaptic decline (Miller *et al.*, 2008; Yassa *et al.*, 2010; Putcha *et al.*, 2011; Busche *et al.*, 2012; Busche and Konnerth, 2015; Arbel-Ornath *et al.*, 2017), it is suggested that the inhibitory effect noted by protofibrillar $A\beta_{1-42}$ on Cav2.2 currents in the current study may represent a pathological mechanism seen at a later stage in disease progression where significant degree of synaptic dysfunction and neuronal loss is already evident.

In AD, particularly in regions where amyloid plaques and neurofibrillary tangles are present, HO-1 expression has been shown to be upregulated as a defence mechanism against oxidative stress and free radicals (Pappolla *et al.*, 1998; Schipper, 2000, 2004). In transgenic animals that suffered an ischemic stroke, neuronal overexpression of HO-1 has been shown to minimize neuronal cell damage and maintain cell viability by reducing release of ROS as well as upregulating expression of anti-apoptotic proteins (Panahian, Yoshiura and Maines, 1999; Schipper, 2004). While upregulation of HO-1 expression can be neuroprotective and could be beneficial in fighting Aβ-dependent pathology, impaired HO-1 activity can drive AD pathology (Schipper, 2000; Takahashi *et al.*, 2000). Therefore, there has been considerable interest in investigating whether CO, a HO-1 by-product can also act as a neuroprotectant. In the current study CORM2, similarly to protofibrillar $A\beta_{1-42}$, was shown to reduce Cav2.2 currents. Although the manner by which protofibrillar $A\beta_{1-42}$ modulates Cav2 channels was not further investigated here, findings from the literature suggest changes at transcript level and direct interaction with specific subunits such as the accessory β subunit, consequently changing the number of functional VGCCs found at the cell membrane (Coon *et al.*, 1999; Green and Peers, 2002; Chiou, 2006; Kim and Rhim, 2011). In contrast to protofibrillar $A\beta_{1-42}$, the current study was able to prove that CORM2, at least partly to CO release, can inhibit Cav2.2 channels through post-translation modifications, specifically via redox modulation. This may potentially occur

through modulation of specific cysteine residues (Scragg *et al.*, 2008; Boycott *et al.*, 2013; Kapetanaki *et al.*, 2018). The current study suggests that activating CO-dependent mechanisms at an early-stage in disease progression, prior to significant brain atrophy is seen (**Fig. 6.1.1**), where initially Ca^{2+} influx is elevated, may prevent some of the cytotoxic pathways associated with VGCC-dependent calcium dysregulation seen in AD, through redox modulation of these channels. In contrast, activating CO-dependent mechanisms at a later stage of the disease, where significant reduction in VGCC activity is observed, may have deleterious effects, further impairing processes such as neurotransmission, dendritic spine morphology and stability, and subsequently adding to the synaptic decline and overall neuronal loss observed. In support, experiments in the current study revealed that co-incubation of neuroblastoma cells with $A\beta_{1-42}$ and CORM2, CO was unable to prevent reduction in neuronal viability. This suggests that CO may have been unable to suppress neurotoxicity, because cell apoptosis pathways have already been activated.

Findings from the current study have significant clinical implications as they demonstrate that activating CO-dependent processes that can modulate VGCCs via a redox manner, at an early stage in disease progression, may be neuroprotective and may significantly reduce the progression of dementia. Such interventions may not only provide symptomatic relief, but also target some of the cytotoxic mechanisms mediated by $A\beta$. Such a therapeutic would not only delay the progression of the disease, but may also have an economic impact by reducing healthcare costs.

6.2. Future work

Although the work conducted in this study proves that CORM2 can modulate VGCCs, specifically Cav2.2 channels, through redox modulation, all work was conducted in cell lines. HEK293 cells, which can easily be manipulated through transfections can provide an ideal *in vitro* model for studying ion channels 'in isolation' using techniques such as whole cell patch clamp. SH-SY5Y cells as an immature neuronal cell line model that can easily be differentiated into neuronal-like cells more closely resembling primary neurons are also widely used within the neuroscience field (Biedler and Schachner, 1978; Morton *et al.*, 1992; Kovalevich and Langford, 2013; Sousa *et al.*, 2013; de Medeiros *et al.*, 2019). Although SH-SY5Y cells are capable of undergo differentiation into neuronal-like cells, the effects identified here by protofibrillar $A\beta_{1-42}$ and CORM2 on VGCCs, would also need to be validated in primary neurons. Use of transgenic animal models such as the mice overexpressing human APP751 (mutation London (V717I) and Swedish (K670M/N671L)) which are capable of displaying both Aβ accumulation and aggregation into small oligomers and eventually plaques (Sturchler-Pierrat *et al.*, 1997), may not only allow the validation of the effects of Aβ and CO on VGCCs in primary neurons, but it would also provide an opportunity to investigate how CO not only modulates neuronal VGCCs, but how it can influence the whole brain network by looking at neuronal and glial interactions.

Although a role for the CORM2 ruthenium structure cannot be excluded, the current study is the first study to prove that CORM2, at least partly due to CO release, can influence Cav2.2 channel kinetics through redox modulation. Future studies can validate the inhibitory effect of CO through the use of other CORM compounds that do not contain a ruthenium structure, or even through the use of CO gas. Although it was proven that CORM2 works similarly to an oxidant, the mechanism by which it can confer this inhibitory effect will require further investigation. A number of studies have suggested that CO may modulate ion channels through interaction with specific cysteine subunits within the α1 pore-forming subunit (Scragg *et al.*, 2008; Boycott *et al.*, 2013). Future studies using site-directed mutagenesis, where specific cysteine residues within the α1 pore-forming subunit can be substituted by other residues such as alanine, could

help in identifying whether CO can modulate VGCCs through changing the gating properties of these channels via cysteine interaction.

Chapter 7: References

Aguado, C. *et al.* (2016) 'Ontogenic changes and differential localization of T-type Ca^{2+} channel subunits Cav3.1 and Cav3.2 in mouse hippocampus and cerebellum', *Frontiers in Neuroanatomy*, 10(83), pp. 1–16. doi: 10.3389/fnana.2016.00083.

Al-Owais, M. M. *et al.* (2017) 'Multiple mechanisms mediating carbon monoxide inhibition of the voltage-gated K+ channel Kv1.5', *Cell Death and Disease*, 8(11), pp. e3163. doi: 10.1038/cddis.2017.568.

Al-Owais, M. M. A. *et al.* (2012) 'Carbon monoxide mediates the anti-apoptotic effects of heme oxygenase-1 in medulloblastoma DAOY cells via K+ channel inhibition', *Journal of Biological Chemistry*, 287(29), pp. 24754–24764. doi: 10.1074/jbc.M112.357012.

Ali, T. B. *et al.* (2015) 'Adverse effects of cholinesterase inhibitors in dementia, according to the pharmacovigilance databases of the United-States and Canada', *PLoS ONE*, 10(12), pp. e0144337. doi: 10.1371/journal.pone.0144337.

Almeida, A. S. *et al.* (2012) 'Carbon monoxide modulates apoptosis by reinforcing oxidative metabolism in astrocytes: Role of Bcl-2', *Journal of Biological Chemistry*, 287(14), pp. 10761–10770. doi: 10.1074/jbc.M111.306738.

Anekonda, T. S. *et al.* (2011) 'L-type voltage-gated calcium channel blockade with isradipine as a therapeutic strategy for Alzheimer's disease', *Neurobiology of Disease*, 41(1), pp. 62–70. doi: 10.1016/j.nbd.2010.08.020.

Applegate, L. A., Luscher, P. and Tyrrell, R. M. (1991) 'Induction of heme oxygenase: A general response to oxidant stress in cultured mammalian cells', *Cancer Research*, 51(3), pp. 974–978.

Arbel-Ornath, M. *et al.* (2017) 'Soluble oligomeric amyloid-β induces calcium dyshomeostasis that precedes synapse loss in the living mouse brain', *Molecular Neurodegeneration*. Molecular Neurodegeneration, 12(27), pp. 1–14. doi: 10.1186/s13024-017-0169-9.

Arber, C., Lovejoy, C. and Wray, S. (2017) 'Stem cell models of Alzheimer's disease: Progress and challenges', *Alzheimer's Research and Therapy*. Alzheimer's Research & Therapy, 9(42), pp. 1–17. doi: 10.1186/s13195-017-0268-4.

Arispe, N., Diaz, J. C. and Flora, M. (2008) 'Efficiency of histidine-associating compounds for blocking the Alzheimer's Aβ channel activity and cytotoxicity', *Biophysical Journal*, 95(10), pp. 4879–4889. doi: 10.1529/biophysj.108.135517.

Arriagada, P. V. *et al.* (1992) 'Neurofibrillary tangles but not senile plaques parallel duration and severity of Alzheimer's disease', *Neurology*, 42(3), pp. 631–639. doi: 10.1212/wnl.42.3.631.

Bales, K. R. *et al.* (1999) 'Apolipoprotein E is essential for amyloid deposition in the APP(V717F) transgenic mouse model of Alzheimer's disease', *Proceedings of the National Academy of Sciences of the United States of America*, 96(26), pp. 15233–15238. doi: 10.1073/pnas.96.26.15233.

Barghorn, S. *et al.* (2005) 'Globular amyloid β-peptide 1-42 oligomer- A homogenous and stable neuropathological protein in Alzheimer's disease', *Journal of*

Neurochemistry, 95(3), pp. 834–847. doi: 10.1111/j.1471-4159.2005.03407.x.

Barnes, C. J. *et al.* (1998) 'Age alters expression and inducibility of heme oxygenase isozymes in mice', *Journal of the American Aging Association*, 21(3), pp. 123–128. doi: 10.1007/s11357-998-0019-3.

Barnes, S. and Haynes, L. W. (1992) 'Low-voltage-activated calcium channels in human retinoblastoma cells', *Brain Research*, 598, pp. 19–22. doi: 10.1016/0006-8993(92)90162-3.

Bell, K. F. S. *et al.* (2006) 'The amyloid pathology progresses in a neurotransmitter-specific manner', *Neurobiology of Aging*, 27(11), pp. 1644–1657. doi: 10.1016/j.neurobiolaging.2005.09.034.

Belleville, S. *et al.* (2017) 'Neuropsychological measures that predict progression from mild cognitive impairment to Alzheimer's type dementia in older adults: a systematic review and meta-analysis', *Neuropsychology Review*. Neuropsychology Review, 27(4), pp. 328–353. doi: 10.1007/s11065-017-9361-5.

Bennett, M. K., Calakos, N. and Scheller, R. H. (1992) 'Syntaxin : A synaptic protein implicated in docking of synaptic vesicles at presynaptic active zones', *Science*, 257(5067), pp. 255–259. doi: 10.1126/science.1321498.

Bernabeu-Zornoza, A. *et al.* (2019) 'Aβ42 peptide promotes proliferation and gliogenesis in human neural stem cells', *Molecular Neurobiology*. Molecular Neurobiology, 56(6), pp. 4023–4036. doi: 10.1007/s12035-018-1355-7.

Bertolesi, G. E. *et al.* (2002) 'The Ca^{2+} channel antagonists mibefradil and pimozide inhibit cell growth via different cytotoxic mechanisms', *Molecular Pharmacology*, 62(2), pp. 210–219. doi: 10.1124/mol.62.2.210.

Bertolesi, G. E. *et al.* (2003) 'Regulation of alpha1G T-type calcium channel gene (CACNA1G) expression during neuronal differentiation', *European Journal of Neuroscience*, 17(9), pp. 1802–1810. doi: 10.1046/j.1460-9568.2003.02618.x.

Bertrand, E. *et al.* (2001) 'A short cytoplasmic domain of the amyloid precursor protein induces apoptosis in vitro and in vivo', *Molecular and Cellular Neuroscience*, 18(5), pp. 503–511. doi: 10.1006/mcne.2001.1030.

Biedler, J. L. and Schachner, M. (1978) 'Multiple neurotransmitter synthesis by human neuroblastoma cell lines and clones', *Cancer Research*, 38(November), pp. 3751–3757.

Birks, J. and López-Arrieta, J. (2002) 'Nimodipine for primary degenerative, mixed and vascular dementia', *Cochrane Database of Systematic Reviews*, (3), pp. CD000147. doi: 10.1002/14651858.CD000147.

Birks, J. S. and Harvey, R. J. (2018) 'Donepezil for dementia due to Alzheimer's disease', *Cochrane Database of Systematic Reviews*, 6(6), p. CD001190. doi: 10.1002/14651858.CD001190.pub3.

Blalock, E. M. *et al.* (2003) 'Gene microarrays in hippocampal aging : statistical profiling identifies novel processes correlated with cognitive impairment', *Journal of*

Neuroscience, 23(9), pp. 3807–3819. doi: 10.1523/JNEUROSCI.23-09-03807.2003.

Bock, G. *et al.* (2011) 'Functional properties of a newly identified C-terminal splice variant of Cav1.3 L-type Ca^{2+} channels', *Journal of Biological Chemistry*, 286(49), pp. 42736–42748. doi: 10.1074/jbc.M111.269951.

Bolmont, T. *et al.* (2007) 'Induction of tau pathology by intracerebral infusion of amyloid-β-containing brain extract and by amyloid-β deposition in APP x tau transgenic mice', *American Journal of Pathology*, 171(6), pp. 2012–2020. doi: 10.2353/ajpath.2007.070403.

Boncristiano, S. *et al.* (2005) 'Neocortical synaptic bouton number is maintained despite robust amyloid deposition in APP23 transgenic mice', *Neurobiology of Aging*, 26(5), pp. 607–613. doi: 10.1016/j.neurobiolaging.2004.06.010.

Bories, C. *et al.* (2007) 'Early electrophysiological abnormalities in lumbar motoneurons in a transgenic mouse model of amyotrophic lateral sclerosis', *European Journal of Neuroscience*, 25(2), pp. 451–459. doi: 10.1111/j.1460-9568.2007.05306.x.

Bourinet, E. *et al.* (1999) 'Splicing of a1A subunit gene generates phenotypic variants of P- and Q-type calcium channels', *Nature Neuroscience*, 2(5), pp. 407–415. doi: 10.1038/8070.

Boxer, A. L. *et al.* (2019) 'Safety of the tau-directed monoclonal antibody BIIB092 in progressive supranuclear palsy: a randomised, placebo-controlled, multiple ascending dose phase 1b trial', *The Lancet Neurology*, 18(6), pp. 549–558. doi: 10.1016/S1474-4422(19)30139-5.

Boycott, H. E. *et al.* (2013) 'Carbon monoxide inhibition of Cav3.2 T-type Ca^{2+} channels reveals tonic modulation by thioredoxin', *FASEB Journal*, 27, pp. 3395–3407. doi: 10.1096/fj.13-227249.

Bozzali, M. *et al.* (2002) 'White matter damage in Alzheimer's disease assessed in vivo using diffusion tensor magnetic resonance imaging', *Journal of Neurology Neurosurgery and Psychiatry*, 72(6), pp. 742–746. doi: 10.1136/jnnp.72.6.742.

Braak, H. and Braak, E. (1997) 'Frequency of stages of Alzheimer-related lesions in different age categories', *Neurobiology of Aging*, 18(4), pp. 351–357. doi: 10.1016/S0197-4580(97)00056-0.

Brini, M. *et al.* (2014) 'Neuronal calcium signaling: function and dysfunction', *Cellular and Molecular Life Sciences*, 71(15), pp. 2787–2814. doi: 10.1007/s00018-013-1550-7.

Broersen, K. *et al.* (2011) 'A standardized and biocompatible preparation of aggregate-free amyloid beta peptide for biophysical and biological studies of Alzheimers disease', *Protein Engineering, Design and Selection*, 24(9), pp. 743–750. doi: 10.1093/protein/gzr020.

Brown, S. T. *et al.* (2005) 'Hypoxic augmentation of Ca2+ channel currents requires a functional electron transport chain', *Journal of Biological Chemistry*, 280(23), pp. 21706–21712. doi: 10.1074/jbc.M503144200.

Busche, M. A. *et al.* (2008) 'Clusters of hyperactive neurons near amyloid plaques in a mouse model of Alzheimer's disease', *Science*, 321, pp. 1686–1689. doi: 10.1126/science.1162844.

Busche, M. A. *et al.* (2012) 'Critical role of soluble amyloid-β for early hippocampal hyperactivity in a mouse model of Alzheimer's disease', *Proceedings of the National Academy of Sciences of the United States of America*, 109(22), pp. 8740–8745. doi: 10.1073/pnas.1206171109.

Busche, M. A. and Konnerth, A. (2015) 'Neuronal hyperactivity - A key defect in Alzheimer's disease?', *BioEssays*, 37(6), pp. 624–632. doi: 10.1002/bies.201500004.

Buttini, M. *et al.* (2010) 'Cellular source of apolipoprotein E4 determines neuronal susceptibility to excitotoxic injury in transgenic mice', *American Journal of Pathology*, 177(2), pp. 563–569. doi: 10.2353/ajpath.2010.090973.

Cacabelos, R. (2007) 'Donepezil in Alzheimer's disease: From conventional trials to pharmacogenetics', *Neuropsychiatric Disease and Treatment*, 3(3), pp. 303–333.

Cai, Y., An, S. S. A. and Kim, S. (2015) 'Mutations in presenilin 2 and its implications in Alzheimer's disease and other dementia-associated disorders', *Clinical Interventions in Aging*, 10, pp. 1163–1172. doi: 10.2147/CIA.S85808.

Cárdenas-Aguayo, M. del C. *et al.* (2014) 'Physiological role of amyloid beta in neural cells: The cellular trophic activity', *Intech*, pp. 257–281. doi: 10.5772/57398.

Carrillo-Mora, P., Luna, R. and Colín-Barenque, L. (2014) 'Amyloid beta: Multiple mechanisms of toxicity and only some protective effects?', *Oxidative Medicine and Cellular Longevity*, 2014, pp. 795375. doi: 10.1155/2014/795375.

Carter, D. A., Desmarais, E. and Bellis, M. (1992) 'More missense in amyloid gene', *Nature Genetics*, 2, pp. 255–256.

Cerejeira, J., Lagarto, L. and Mukaetova-Ladinska, E. B. (2012) 'Behavioral and psychological symptoms of dementia', *Frontiers in Neurology*, 3(73), pp. 1–21. doi: 10.3389/fneur.2012.00073.

Chan, C. S. *et al.* (2007) '"Rejuvenation" protects neurons in mouse models of Parkinson's disease', *Nature*, 447(7148), pp. 1081–1086. doi: 10.1038/nature05865.

Chang, Q. and Martin, L. J. (2016) 'Voltage-gated calcium channels are abnormal in cultured spinal motoneurons in the G93A-SOD1 transgenic mouse model of ALS', *Neurobiology of Disease*, 93, pp. 78–95. doi: 10.1016/j.nbd.2016.04.009.

Chen, G. F. *et al.* (2017) 'Amyloid beta: structure, biology and structure-based therapeutic development', *Acta Pharmacologica Sinica*, 38(9), pp. 1205–1235. doi: 10.1038/aps.2017.28.

Chen, Y. and Dong, C. (2009) 'Aβ40 promotes neuronal cell fate in neural progenitor cells', *Cell Death and Differentiation*, 16(3), pp. 386–394. doi: 10.1038/cdd.2008.94.

Chiamvimonvat, N. *et al.* (1995) 'Functional consequences of sulfhydryl modification in

the pore-forming subunits of cardiovascular Ca^{2+} and Na^{+} channels', *Circulation research*, 76(3), pp. 325–334. doi: 10.1161/01.

Chin, H. (1998) 'Molecular biology of neuronal voltage-gated calcium channels', *Experimental and Molecular Medicine*, 30(3), pp. 123–130. doi: 10.1038/emm.1998.18.

Chiou, W.-F. (2006) 'Effect of Aβ exposure on the mRNA expression patterns of voltage-sensitive calcium channel α1 subunits (α1A–α1D) in human SK-N-SH neuroblastoma', *Neurochemistry International*, 49(3), pp. 256–261. doi: 10.1016/j.neuint.2006.01.022.

Chow, R. H. (1991) 'Cadmium block of squid calcium currents: Macroscopic data and a kinetic model', *Journal of General Physiology*, 98(4), pp. 751–770. doi: 10.1085/jgp.98.4.751.

Chow, V. W. *et al.* (2010) 'An overview of APP processing enzymes and products', *Neuromolecular Medicine*, 12(1), pp. 1–12. doi: 10.1007/s12017-009-8104-z.

Chui, H. C. and Ramirez-Gomez, L. (2015) 'Clinical and imaging features of mixed Alzheimer and vascular pathologies', *Alzheimer's Research and Therapy*, 7(1), pp. 1–13. doi: 10.1186/s13195-015-0104-7.

Citron, M. *et al.* (1997) 'Mutant presenilins of Alzheimer's disease increase production of 42-residue amyloid b-protein in both transfected cells and transgenic mice', *Nature Medicine*, 3(1), pp. 67–72. doi: 10.1038/nm0197-67.

Clark, C. M. *et al.* (2012) 'Cerebral PET with florbetapir compared with neuropathology at autopsy for detection of neuritic amyloid-β plaques: A prospective cohort study', *The Lancet Neurology*, 11(8), pp. 669–678. doi: 10.1016/S1474-4422(12)70142-4.

Clark, J. E. *et al.* (2003) 'Cardioprotective actions by a water-soluble carbon monoxide-releasing molecule.', *Circulation research*, 93(2), pp. e2–e8. doi: 10.1161/01.res.0000084381.86567.08.

Congdon, E. E. and Sigurdsson, E. M. (2018) 'Tau-targeting therapies for Alzheimer disease', *Nature Reviews Neuroscience*, 14(7), pp. 399–415. doi: 10.1038/s41582-018-0013-z.

Coon, A. L. *et al.* (1999) 'L-type calcium channels in the hippocampus and cerebellum of Alzheimer's disease brain tissue', *Neurobiology of Aging*, 20(6), pp. 597–603. doi: 10.1016/s0197-4580(99)00068-8.

Counts, S. E. *et al.* (2014) 'Synaptic gene dysregulation within hippocampal CA1 pyramidal neurons in mild cognitive impairment', *Neuropharmacology*, 79, pp. 172–179. doi: 10.1016/j.neuropharm.2013.10.018.

Creavin, S. T. *et al.* (2016) 'Mini-mental state examination (MMSE) for the detection of dementia in clinically unevaluated people aged 65 and over in community and primary care populations', *Cochrane Database of Systematic Reviews*, (1), pp. CD011145. doi: 10.1002/14651858.CD011145.pub2.

Cribbs, L. L. *et al.* (1998) 'Cloning and characterization of a1H from human heart, a member of the T-Type Ca^{2+} channel gene family', *Circulation Research*, 83, pp. 103–109.

doi: 10.1161/01.res.83.1.103.

Curtis, B. M. and Catterall, W. A. (1984) 'Purification of the calcium antagonist receptor of the voltage-sensitive calcium channel from skeletal muscle transverse tubules', *Biochemistry*, 23(10), pp. 2113–2118. doi: 10.1021/bi00305a001.

Dahlgren, K. N. *et al.* (2002) 'Oligomeric and fibrillar species of amyloid-β peptides differentially affect neuronal viability', *Journal of Biological Chemistry*, 277(35), pp. 32046–32053. doi: 10.1074/jbc.M201750200.

Dallas, M. L. *et al.* (2011) 'Carbon monoxide protects against oxidant-induced apoptosis via inhibition of Kv2.1', *FASEB Journal*, 25(5), pp. 1519–1530. doi: 10.1096/fj.10-173450.

Dallas, M. L. *et al.* (2012) 'Carbon monoxide induces cardiac arrhythmia via induction of the late Na+ current', *American Journal of Respiratory and Critical Care Medicine*, 186(7), pp. 648–656. doi: 10.1164/rccm.201204-0688OC.

DaRocha-Souto, B. *et al.* (2011) 'Brain oligomeric β-amyloid but not total amyloid plaque burden correlates with neuronal loss and astrocyte inflammatory response in amyloid precursor protein/tau transgenic mice', *Journal of Neuropathology Experimental Neurology*, 70(5), pp. 360–376. doi: 10.1097/NEN.0b013e318217a118.

Daschil, N. *et al.* (2013) 'Cav1.2 calcium channel expression in reactive astrocytes is associated with the formation of amyloid-β plaques in an Alzheimer's disease mouse model', *Journal of Alzheimer's Disease*, 37(2), pp. 439–451. doi: 10.3233/JAD-130560.

Deane, R. *et al.* (2008) 'ApoE isoform–specific disruption of amyloid β peptide clearance from mouse brain', *The Journal of Clinical Investigation*, 118(12), pp. 4002–4013. doi: 10.1172/JCI36663.

Deardorff, W. J. and Grossberg, G. T. (2017) 'Targeting neuroinflammation in Alzheimer's disease: evidence for NSAIDs and novel therapeutics', *Expert Review of Neurotherapeutics*, 17(1), pp. 17–32. doi: 10.1080/14737175.2016.1200972.

Deshpande, A. *et al.* (2006) 'Different conformations of amyloid β induce neurotoxicity by distinct mechanisms in human cortical neurons', *Journal of Neuroscience*, 26(22), pp. 6011–6018. doi: 10.1523/JNEUROSCI.1189-06.2006.

DeTure, M. A. and Dickson, D. W. (2019) 'The neuropathological diagnosis of Alzheimer's disease', *Molecular Neurodegeneration*. Molecular Neurodegeneration, 14(32), pp. 1–18. doi: 10.1186/s13024-019-0333-5.

Dolphin, A. C. (2013) 'The α2δ subunits of voltage-gated calcium channels', *Biochimica et Biophysica Acta - Biomembranes*, 1828(7), pp. 1541–1549. doi: 10.1016/j.bbamem.2012.11.019.

Doody, R. S. *et al.* (2013) 'A phase 3 trial of semagacestat for treatment of Alzheimer's disease', *New England Journal of Medicine*, 369(4), pp. 341–350. doi: 10.1056/NEJMoa1210951.

Dubnovitsky, A. *et al.* (2013) 'Amyloid-β protofibrils: size, morphology and synaptotoxicity of an engineered mimic', *PLoS ONE*, 8(7), pp. 1–8. doi:

10.1371/journal.pone.0066101.

Duckles, H. *et al.* (2015) 'Heme oxygenase-1 regulates cell proliferation via carbon monoxide-mediated inhibition of T-type Ca^{2+} channels', *Pflugers Archiv European Journal of Physiology*, 467(2), pp. 415–427. doi: 10.1007/s00424-014-1503-5.

Dumenieu, M. *et al.* (2018) 'The low-threshold calcium channel Cav3.2 mediates burst firing of mature dentate granule cells', *Cerebral Cortex*, 28(7), pp. 2594–2609. doi: 10.1093/cercor/bhy084.

Egan, M. F. *et al.* (2018) 'Randomized trial of verubecestat for mild-to-moderate Alzheimer's disease', *New England Journal of Medicine*, 378(18), pp. 1691–1703. doi: 10.1056/NEJMoa1706441.

El-Amouri, S. S. *et al.* (2008) 'Neprilysin: An enzyme candidate to slow the progression of Alzheimer's disease', *American Journal of Pathology*, 172(5), pp. 1342–1354. doi: 10.2353/ajpath.2008.070620.

Ertel, E. A. *et al.* (2000) 'Nomenclature of voltage-gated calcium channels', *Neuron*, 25(3), pp. 533–535. doi: 10.1016/s0896-6273(00)81057-0.

Etnier, J. L. *et al.* (2018) 'The physical activity and Alzheimer's disease (PAAD) study: Cognitive outcomes', *Annals of Behavioral Medicine*, 52(2), pp. 175–185. doi: 10.1093/abm/kax035.

Fahnestock, M. (2011) 'Brain-derived neurotrophic factor: The link between amyloid-β and memory loss', *Future Neurology*, 6(5), pp. 627–639. doi: 10.2217/fnl.11.44.

Farrer, L. A. *et al.* (1997) 'Effects of age, sex, and ethnicity on the association between apolipoprotein E genotype and Alzheimer disease: A meta-analysis', *Journal of the American Medical Association*, 278(16), pp. 1349–1356. doi: 10.1001/jama.1997.03550160069041.

Farris, W. *et al.* (2003) 'Insulin-degrading enzyme regulates the levels of insulin, amyloid β-protein, and the β-amyloid precursor protein intracellular domain in vivo', *Proceedings of the National Academy of Sciences of the United States of America*, 100(7), pp. 4162–4167. doi: 10.1073/pnas.0230450100.

Fein, J. A. *et al.* (2008) 'Co-localization of amyloid beta and tau pathology in Alzheimer's disease synaptosomes', *American Journal of Pathology*, 172(6), pp. 1683–1692. doi: 10.2353/ajpath.2008.070829.

Fernández-Mendívil, C. *et al.* (2020) 'Protective role of microglial HO-1 blockade in aging: implication of iron metabolism', *Redox Biology*, doi: 10.1016/j.redox.2020.101789.

Fezoui, Y. *et al.* (2000) 'An improved method of preparing the amyloid β-protein for fibrillogenesis and neurotoxicity experiments', *Amyloid*, 7(3), pp. 166–178. doi: 10.3109/13506120009146831.

Finder, V. H. and Glockshuber, R. (2007) 'Amyloid-β aggregation', *Neurodegenerative*

Diseases, 4(1), pp. 13–27. doi: 10.1159/000100355.

Flockerzi, V. *et al.* (1986) 'Purified dihydropyridine-binding site from skeletal muscle t-tubules is a functional calcium channel', *Nature*, 323(6083), pp. 66–68. doi: 10.1038/323066a0.

Fonseca, M. B. *et al.* (2013) 'Amyloid β peptides promote autophagy-dependent differentiation of mouse neural stem cells: Aβ-mediated neural differentiation', *Molecular Neurobiology*, 48(3), pp. 829–840. doi: 10.1007/s12035-013-8471-1.

Gakhar-Koppole, N. *et al.* (2008) 'Activity requires soluble amyloid precursor protein α to promote neurite outgrowth in neural stem cell-derived neurons via activation of the MAPK pathway', *European Journal of Neuroscience*, 28(5), pp. 871–882. doi: 10.1111/j.1460-9568.2008.06398.x.

Garcia-Osta, A. and Alberini, C. M. (2009) 'Amyloid beta mediates memory formation', *Cold Spring Harbor Laboratory Press*, 16, pp. 267–272. doi: 10.1101/lm.1310209.

Garzon, D. J. and Fahnestock, M. (2007) 'Oligomeric amyloid decreases basal levels of brain-derived neurotrophic factor (BDNF) mRNA via specific downregulation of BDNF transcripts IV and V in differentiated human neuroblastoma cells', *Journal of Neuroscience*, 27(10), pp. 2628–2635. doi: 10.1523/JNEUROSCI.5053-06.2007.

Gholamipour-Badie, H. *et al.* (2013) 'L-type calcium channel blockade alleviates molecular and reversal spatial learning and memory alterations induced by entorhinal amyloid pathology in rats', *Behavioural Brain Research*, 237, pp. 190–199. doi: 10.1016/j.bbr.2012.09.045.

Giedraitis, V. *et al.* (2007) 'The normal equilibrium between CSF and plasma amyloid beta levels is disrupted in Alzheimer's disease', *Neuroscience Letters*, 427(3), pp. 127–131. doi: 10.1016/j.neulet.2007.09.023.

Gilman, S. *et al.* (2005) 'Clinical effects of Aβ immunization (AN1792) in patients with AD in an interrupted trial', *Neurology*, 64(9), pp. 1553–1562. doi: 10.1212/01.WNL.0000159740.16984.3C.

Gómez-Isla, T. *et al.* (1996) 'Profound loss of layer II entorhinal cortex neurons occurs in very mild Alzheimer's disease', *Journal of Neuroscience*, 16(14), pp. 4491–4500. doi: 10.1523/JNEUROSCI.16-14-04491.1996.

Gorman, D. *et al.* (2003) 'The clinical toxicology of carbon monoxide', *Toxicology*, 187(1), pp. 25–38. doi: 10.1016/S0300-483X(03)00005-2.

Green, K. N. and Peers, C. (2002) 'Divergent pathways account for two distinct effects of amyloid b peptides on exocytosis and Ca^{2+} currents : involvement of ROS and NF-kB', *Journal of Neurochemistry*, 81(5), pp. 1043–1051. doi: 10.1046/j.1471-4159.2002.00907.x.

Guo, T., Noble, W. and Hanger, D. P. (2017) 'Roles of tau protein in health and disease', *Acta Neuropathologica*, 133(5), pp. 665–704. doi: 10.1007/s00401-017-1707-9.

Haam, J. and Yakel, J. L. (2017) 'Cholinergic modulation of the hippocampal region and

memory function', *Journal of Neurochemistry*, 142(Suppl 2), pp. 111–121. doi: 10.1111/jnc.14052.

Hajjar, I. *et al.* (2002) 'The impact of the use of statins on the prevalence of dementia and the progression of cognitive impairment', *Journals of Gerontology: Medical Sciences*, 57(7), pp. M414-418. doi: 10.1093/gerona/57.7.M414.

Hanslick, J. L. *et al.* (2009) 'Dimethyl sulfoxide (DMSO) produces widespread apoptosis in the developing central nervous system', *Neurobiology of Disease*, 34(1), pp. 1–10. doi: 10.1016/j.nbd.2008.11.006.

Hardy, J. and Selkoe, D. J. (2002) 'The amyloid hypothesis of Alzheimer's disease: Progress and problems on the road to therapeutics', *Science*, 297(5580), pp. 353–356. doi: 10.1126/science.1072994.

Hayashi, S. *et al.* (2004) 'Characterization of rat heme oxygenase-3 gene. Implication of processed pseudogenes derived from heme oxygenase-2 gene', *Gene*, 336(2), pp. 241–250. doi: 10.1016/j.gene.2004.04.002.

Heilig, E. A. *et al.* (2010) 'A presenilin-1 mutation identified in familial Alzheimer disease with cotton wool plaques causes a nearly complete loss of γ-secretase activity', *Journal of Biological Chemistry*, 285(29), pp. 22350–22359. doi: 10.1074/jbc.M110.116962.

Heilig, E. A. *et al.* (2013) 'Trans-dominant negative effects of pathogenic PSEN1 mutations on γ-secretase activity and Aβ production', *Journal of Neuroscience*, 33(28), pp. 11606–11617. doi: 10.1523/JNEUROSCI.0954-13.2013.

Hell, J. W. *et al.* (1993) 'Identification and differential subcellular localization of the neuronal class C and class D L-type calcium channel α1 subunits', *Journal of Cell Biology*, 123(4), pp. 949–962. doi: 10.1083/jcb.123.4.949.

Henley, D. B. *et al.* (2014) 'Safety profile of semagacestat, a gamma-secretase inhibitor: IDENTITY trial findings', *Current Medical Research and Opinion*, 30(10), pp. 2021–2032. doi: 10.1185/03007995.2014.939167.

Hermann, D. *et al.* (2013) 'Synthetic Aβ oligomers (Aβ1–42 globulomer) modulate presynaptic calcium currents: Prevention of Aβ-induced synaptic deficits by calcium channel blockers', *European Journal of Pharmacology*, 702(1–3), pp. 44–55. doi: 10.1016/j.ejphar.2013.01.030.

Hettiarachchi, N. T. *et al.* (2014) 'Heme oxygenase-1 protects against Alzheimer ''s amyloid-β1-42-induced toxicity via carbon monoxide production', *Cell Death and Disease*, 5(12), pp. e1569-11. doi: 10.1038/cddis.2014.529.

Hettiarachchi, N. T. *et al.* (2017) 'Heme oxygenase-1 derived carbon monoxide suppresses Aβ1-42 toxicity in astrocytes', *Cell Death and Disease*, 8(6), pp. e2884-11. doi: 10.1038/cddis.2017.276.

Hippius, H. and Neundörfer, G. (2003) 'The discovery of Alzheimer's disease', *Dialogues in Clinical Neuroscience*, 5(1), pp. 101–108.

Ho, R., Ortiz, D. and Shea, T. B. (2001) 'Amyloid-β promotes calcium influx and

neurodegeneration via stimulation of L voltage-sensitive calcium channels rather than NMDA channels in cultured neurons', *Journal of Alzheimer's Disease*, 3(5), pp. 479–483. doi: 10.3233/jad-2001-3507.

Hopperton, K. E. *et al.* (2018) 'Markers of microglia in post-mortem brain samples from patients with Alzheimer's disease: A systematic review', *Molecular Psychiatry*, 23(2), pp. 177–198. doi: 10.1038/mp.2017.246.

Huang, L. K., Chao, S. P. and Hu, C. J. (2020) 'Clinical trials of new drugs for Alzheimer disease', *Journal of Biomedical Science*. Journal of Biomedical Science, 27(18), pp. 1–13. doi: 10.1186/s12929-019-0609-7.

Huang, Y. and Liu, T. (2015) 'Amyloid beta peptide 1-42 induces SH-SY5Y cell apoptosis via the promotion of Meg3 long noncoding RNA expression', *Integrative Medicine International*, 2(1–2), pp. 73–79. doi: 10.1159/000438702.

Hurley, M. J. *et al.* (2013) 'Parkinson's disease is associated with altered expression of Cav1 channels and calcium-binding proteins', *Brain*, 136(7), pp. 2077–2097. doi: 10.1093/brain/awt134.

Iacono, L. Lo *et al.* (2011) 'A carbon monoxide-releasing molecule (CORM-3) uncouples mitochondrial respiration and modulates the production of reactive oxygen species', *Free Radical Biology and Medicine*, 50(11), pp. 1556–1564. doi: 10.1016/j.freeradbiomed.2011.02.033.

Ikonomovic, M. D. *et al.* (2008) 'Post-mortem correlates of in vivo PiB-PET amyloid imaging in a typical case of Alzheimer's disease', *Brain*, 131(6), pp. 1630–1645. doi: 10.1093/brain/awn016.

Infante, J. *et al.* (2010) 'Gene-gene interaction between heme oxygenase-1 and liver X receptor-β and Alzheimer's disease risk', *Neurobiology of Aging*, 31(4), pp. 710–714. doi: 10.1016/j.neurobiolaging.2008.05.025.

Jack, C. R. J. *et al.* (1999) 'Prediction of AD with MRI-based hippocampal volume in mild cognitive impairment', *Neurology*, 52(7), pp. 1397–1403. doi: 10.1212/wnl.52.7.1397.

Jahn, K. *et al.* (2017) 'A cell culture model for investigation of synapse influenceability: epigenetics, expression and function of gene targets important for synapse formation and preservation in SH-SY5Y neuroblastoma cells differentiated by retinoic acid', *Journal of Neural Transmission*, 124(11), pp. 1341–1367. doi: 10.1007/s00702-017-1769-9.

James, B. D. *et al.* (2012) 'Dementia from Alzheimer disease and mixed pathologies in the oldest old', *Journal of the American Medical Association*, 307(17), pp. 1798–1800. doi: 10.1001/jama.2012.3556.

Jan, A. *et al.* (2011) 'Aβ42 neurotoxicity is mediated by ongoing nucleated polymerization process rather than by discrete Aβ42 species', *Journal of Biological Chemistry*, 286(10), pp. 8585–8596. doi: 10.1074/jbc.M110.172411.

Janson, J. *et al.* (2004) 'Increased risk of Type 2 diabetes in Alzheimer disease', *Diabetes*, 53(2), pp. 474–481. doi: 10.2337/diabetes.53.2.474.

Jayanti, S. *et al.* (2020) 'The Role of bilirubin and the other "Yellow Players" in neurodegenerative diseases', *Antioxidants*, 9(900), pp. 1–26. doi: 10.3390/antiox9090900.

Kaczara, P. *et al.* (2020) 'Antiplatelet effect of carbon monoxide is mediated by NAD^+ and ATP depletion', *Arteriosclerosis, Thrombosis, and Vascular Biology*, 40, pp. 2376–2390. doi: 10.1161/ATVBAHA.120.314284.

Kahler, C. P. (2000) 'Evaluation of the use of the solvent dimethyl sulfoxide in chemiluminescent studies', *Blood Cells, Molecules, and Diseases*, 26(6), pp. 626–633. doi: 10.1006/bcmd.2000.0340.

Kamp, M. A. *et al.* (2005) 'Presynaptic "Cav2.3-containing" E-type Ca^{2+} channels share dual roles during neurotransmitter release', *European Journal of Neuroscience*, 21(6), pp. 1617–1625. doi: 10.1111/j.1460-9568.2005.03984.x.

Kantarci, K. *et al.* (2012) 'Multimodality imaging characteristics of dementia with Lewy bodies', *Neurobiology of Aging*, 33(9), pp. 2091–2105. doi: 10.1016/j.neurobiolaging.2011.09.024.

Kapetanaki, S. M. *et al.* (2018) 'A mechanism for CO regulation of ion channels', *Nature Communications*, 9(907), pp. 1–10. doi: 10.1038/s41467-018-03291-z.

Karmazinova, M. *et al.* (2010) 'Cysteines in the loop between IS5 and the pore helix of Cav3.1 are essential for channel gating', *European Journal of Physiology*, 460(6), pp. 1015–1028. doi: 10.1007/s00424-010-0874-5.

Katsouri, L. *et al.* (2020) 'Ablation of reactive astrocytes exacerbates disease pathology in a model of Alzheimer's disease', *Glia*, 68(5), pp. 1017–1030. doi: 10.1002/glia.23759.

Katz, B. and Miledi, R. (1970) 'Further study of the role of calcium in synaptic transmission', *The Journal of Physiology*, 207(3), pp. 789–801. doi: 10.1113/jphysiol.1970.sp009095.

Kazim, S. F. *et al.* (2017) 'Early-onset network hyperexcitability in presymptomatic Alzheimer's disease transgenic mice in suppressed by passive immunization with anti-human APP/Aβ antibody and by mGluR5 blockade', *Frontiers in Aging Neuroscience*, 9(71), pp. 1–17. doi: 10.3389/fnagi.2017.00071.

Kellett, K. A. B. and Hooper, N. M. (2009) 'Prion protein and Alzheimer disease', *Prion*, 3(4), pp. 190–194. doi: 10.4161/pri.3.4.9980.

Khondker, A., Alsop, R. J. and Rheinstädter, M. C. (2017) 'Membrane-accelerated Amyloid-β aggregation and formation of cross-β sheets', *Membranes*, 7(49), pp. 1–19. doi: 10.3390/membranes7030049.

Kim, H. J. *et al.* (2019) 'Carbon monoxide attenuates amyloidogenesis via down-regulation of NF-κB-mediated BACE1 gene expression', *Aging Cell*, 18(1), pp. e12864. doi: 10.1111/acel.12864.

Kim, J.-W. *et al.* (2018) 'T-type calcium channels are required to maintain viability of neural progenitor cells', *Biomolecules & Therapeutics*, 26(5), pp. 439–445. doi:

10.4062/biomolther.2017.223.

Kim, S. and Rhim, H. (2011) 'Effects of amyloid-β peptides on voltage-gated L-Type Cav1.2 and Cav1.3 Ca^{2+} channels', *Molecules and Cells*, 32(3), pp. 289–294. doi: 10.1007/s10059-011-0075-x.

Koppensteiner, P. *et al.* (2016) 'Time-dependent reversal of synaptic plasticity induced by physiological concentrations of oligomeric Aβ42: An early index of Alzheimer's disease', *Scientific Reports*, 6(32553). doi: 10.1038/srep32553.

Kovalevich, J. and Langford, D. (2013) 'Considerations for the use of SH-SY5Y neuroblastoma cells in neurobiology', *Methods in Molecular Biology*, 1078, pp. 9–21. doi: 10.1007/978-1-62703-640-5_2.

Lazniewska, J. and Weiss, N. (2017) 'Glycosylation of voltage-gated calcium channels in health and disease', *Biochimica et Biophysica Acta - Biomembranes*, 1859(5), pp. 662–668. doi: 10.1016/j.bbamem.2017.01.018.

Leal, S. S. *et al.* (2013) 'Calcium ions promote superoxide dismutase 1 (SOD1) aggregation into non-fibrillar amyloid: A link to toxic effects of calcium overload in amyotrophic lateral sclerosis (ALS)?', *Journal of Biological Chemistry*, 288(35), pp. 25219–25228. doi: 10.1074/jbc.M113.470740.

Lecht, S. *et al.* (2012) 'Neuroprotective effects of nimodipine and nifedipine in the NGF-differentiated PC12 cells exposed to oxygen-glucose deprivation or trophic withdrawal', *International Journal of Developmental Neuroscience*, 30(6), pp. 465–469. doi: 10.1016/j.ijdevneu.2012.05.007.

Lee, Y. C. *et al.* (2014) 'Antihypertensive agents and risk of Parkinson's disease: A nationwide cohort study', *PLoS ONE*, 9(6), pp. e98961. doi: 10.1371/journal.pone.0098961.

Levy-Lahad, E. *et al.* (1995) 'A Familial Alzheimer's disease locus on chromosome I', *Science*, 269(5226), pp. 970–973. doi: 10.1126/science.7638621.

Lewis, R. J. *et al.* (2000) 'Novel ω-conotoxins from Conus catus discriminate among neuronal calcium channel subtypes', *Biological Chemistry*, 275(45), pp. 35335–35344. doi: 10.1074/jbc.M002252200.

Li, A. *et al.* (1998) 'Oxidation regulates cloned neuronal voltage-dependent Ca^{2+} channels expressed in Xenopus oocytes', *Journal of Neuroscience*, 18(17), pp. 6740–6747. doi: 10.1523/jneurosci.18-17-06740.1998.

Li, G. *et al.* (2010) 'Age-varying association between statin use and incident Alzheimer disease', *Journal of the Americal geriatrics society*, 58(7), pp. 1311–1317. doi: 10.1111/j.1532-5415.2010.02906.x.

Li, Y. *et al.* (2001) 'Differential functions of members of the low density lipoprotein receptor family suggested by their distinct endocytosis rates', *Journal of Biological Chemistry*, 276(21), pp. 18000–18006. doi: 10.1074/jbc.M101589200.

Lim, I. *et al.* (2005) 'Carbon monoxide activates human intestinal smooth muscle L-type Ca^{2+} channels through a nitric oxide-dependent mechanism', *Am J Physiol Gastrointest Liver Physio*, 288, pp. 7–14. doi: 10.1152/ajpgi.00205.2004.

Liu, C.-C. *et al.* (2013) 'Apoliprotein E and Alzheimer's disease: risk, mechanisms, and therapy', *Nature Reviews Neuroscience*, 9(2), pp. 106–118. doi: 10.1038/nrneurol.2012.263.

Liu, C.-C. *et al.* (2017) 'ApoE4 accelerates early seeding of amyloid pathology', *Neuron*, 96(5), pp. 1024–1032. doi: 10.1016/j.neuron.2017.11.013.

Liu, Y. *et al.* (2014) 'Cav1.2 and Cav1.3 L-type calcium channels regulate dopaminergic firing activity in the mouse ventral tegmental area', *Journal of Neurophysiology*, 112(5), pp. 1119–1130. doi: 10.1152/jn.00757.2013.

Livingston, G. *et al.* (2020) 'Dementia prevention, intervention, and care: 2020 report of the Lancet Commission', *The Lancet*, 396(10248), pp. 413–446. doi: 10.1016/S0140-6736(20)30367-6.

Lobo, A. *et al.* (2000) 'Prevalence of dementia and major subtypes in Europe: A collaborative study of population-based cohorts', *Neurology*, 54(11 Suppl 5), pp. S4-9.

Lopes, F. M. *et al.* (2010) 'Comparison between proliferative and neuron-like SH-SY5Y cells as an in vitro model for Parkinson disease studies', *Brain Research*, 1337, pp. 85–94. doi: 10.1016/j.brainres.2010.03.102.

Lopez, J. R. *et al.* (2008) 'Increased intraneuronal resting [Ca^{2+}] in adult Alzheimer's disease mice', *Journal of Neurochemistry*, 105(1), pp. 262–271. doi: 10.1111/j.1471-4159.2007.05135.x.

Lovell, M. A. *et al.* (2015) 'Calcium channel blockers, progression to dementia, and effects on amyloid beta peptide production', *Oxidative Medicine and Cellular Longevity*, 2015, pp. 787805. doi: 10.1155/2015/787805.

Lu, D. C. *et al.* (2003) 'Caspase cleavage of the amyloid precursor protein modulates amyloid β-protein toxicity', *Journal of Neurochemistry*, 87(3), pp. 733–741. doi: 10.1046/j.1471-4159.2003.02059.x.

Luo, Y. *et al.* (1996) 'Physiological levels of β-amyloid peptide promote PC12 cell proliferation', *Neuroscience Letters*, 217(2–3), pp. 125–128.

Mahan, V. L. *et al.* (2012) 'Inhaled carbon monoxide provides cerebral cytoprotection in pigs', *PLoS ONE*, 7(8), pp. e41982. doi: 10.1371/journal.pone.0041982.

Maines, M. D. (1997) 'The heme oxygenase system: A regulator of second messenger gases', *Annual Review of Pharmacology and Toxicology*, 37, pp. 517–554. doi: 10.1146/annurev.pharmtox.37.1.517.

Marchetti, C. (2013) 'Role of calcium channels in heavy metal toxicity', *ISRN Toxicology*, pp. 184360. doi: 10.1155/2013/184360.

Marjaux, E., Hartmann, D. and De Strooper, B. (2004) 'Presenilins in memory,

Alzheimer's disease, and therapy', *Neuron*, 42(2), pp. 189–192. doi: 10.1016/S0896-6273(04)00218-1.

Marras, C. *et al.* (2012) 'Dihydropyridine calcium channel blockers and the progression of Parkinsonism', *Annals of Neurology*, 71(3), pp. 362–369. doi: 10.1002/ana.22616.

Marschallinger, J. *et al.* (2015) 'The L-type calcium channel Cav1.3 is required for proper hippocampal neurogenesis and cognitive functions', *Cell Calcium*, 58(6), pp. 606–616. doi: 10.1016/j.ceca.2015.09.007.

Masliah, E. *et al.* (2005) 'Aβ vaccination effects on plaque pathology in the absence of encephalitis in Alzheimer disease', *Neurology*, 64(1), pp. 129–131. doi: 10.1212/01.WNL.0000148590.39911.DF.

Mattice, W. L., Riser, J. M. and Clark, D. S. (1976) 'Conformational properties of the complexes formed by proteins and sodium dodecyl sulfate', *Biochemistry*, 15(19), pp. 4264–4272. doi: 10.1021/bi00664a020.

Mattson, M. P. *et al.* (1993) 'Evidence for excitoprotective and intraneuronal calcium-regulating roles for secreted forms of the β-amyloid precursor protein', *Neuron*, 10(2), pp. 243–254. doi: 10.1016/0896-6273(93)90315-I.

Mattson, M. P. (1997) 'Cellular actions of β-amyloid precursor protein and its soluble and fibrillogenic derivatives', *Physiological Reviews*, 77(4), pp. 1081–1132. doi: 10.1152/physrev.1997.77.4.1081.

May, P. C. *et al.* (2011) 'Robust central reduction of amyloid-β in humans with an orally available, non-peptidic β-secretase inhibitor', *Journal of Neuroscience*, 31(46), pp. 16507–16516. doi: 10.1523/JNEUROSCI.3647-11.2011.

May, P. C. *et al.* (2015) 'The potent BACE1 inhibitor LY2886721 elicits robust central Aβ pharmacodynamic responses in mice, dogs, and humans', *Journal of Neuroscience*, 35(3), pp. 1199–1210. doi: 10.1523/JNEUROSCI.4129-14.2015.

McCoubrey, W. K. and Maines, M. D. (1994) 'The structure, organization and differential expression of the gene encoding rat heme oxygenase-2', *Gene*, 139(2), pp. 155–161. doi: 10.1016/0378-1119(94)90749-8.

McDavid, S. and Currie, K. P. M. (2006) 'G-proteins modulate cumulative inactivation of N-type (Cav2.2) calcium channels', *Journal of Neuroscience*, 26(51), pp. 13373–13383. doi: 10.1523/JNEUROSCI.3332-06.2006.

McKinney, B. C. *et al.* (2009) 'Impaired long-term potentiation and enhanced neuronal excitability in the amygdala of Cav1.3 knockout mice', *Neurobiology of Learning and Memory*, 92(4), pp. 519–528. doi: 10.1016/j.nlm.2009.06.012.

de Medeiros, L. M. *et al.* (2019) 'Cholinergic Differentiation of Human Neuroblastoma SH-SY5Y Cell Line and Its Potential Use as an In vitro Model for Alzheimer's Disease Studies', *Molecular Neurobiology*. Molecular Neurobiology, 56(11), pp. 7355–7367. doi: 10.1007/s12035-019-1605-3.

Mezler, M. *et al.* (2012) 'Aβ-amyloid oligomer directly modulates P/Q-type calcium

currents in Xenopus oocytes', *British Journal of Pharmacology*, 165(5), pp. 1572–1583. doi: 10.1111/j.1476-5381.2011.01646.x.

Miki, T. *et al.* (2008) 'Two novel alleles of tottering with distinct Cav2.1 calcium channel neuropathologies', *Neuroscience*, 155(1), pp. 31–44. doi: 10.1016/j.neuroscience.2008.05.028.

Mileusnic, R. *et al.* (2000) 'APP is required during an early phase of memory formation', *European Journal of Neuroscience*, 12(12), pp. 4487–4495.

Miller, S. L. *et al.* (2008) 'Hippocampal activation in adults with mild cognitive impairment predicts subsequent cognitive decline', *Journal of Neurology, Neurosurgery and Psychiatry*, 79(6), pp. 630–635. doi: 10.1136/jnnp.2007.124149.

Moosmang, S. *et al.* (2005) 'Role of hippocampal Cav1.2 Ca^{2+} channels in NMDA receptor-independent synaptic plasticity and spatial memory', *Journal of Neuroscience*, 25(43), pp. 9883–9892. doi: 10.1523/JNEUROSCI.1531-05.2005.

Morris, G. P., Clark, I. A. and Vissel, B. (2014) 'Inconsistencies and controversies surrounding the amyloid hypothesis of Alzheimer's disease', *Acta Neuropathologica Communications*, 2, p. 135. doi: 10.1186/s40478-014-0135-5.

Morton, A. J. *et al.* (1992) 'Characterisation of the L- and N-type calcium channels in differentiated SH-SY5Y neuroblastoma cells: calcium imaging and single channel recording', *Molecular Brain Research*, 13(1–2), pp. 53–61. doi: 10.1016/0169-328X(92)90044-C.

Mosier, D. R. *et al.* (1995) 'Amyotrophic lateral sclerosis immunoglobulins increase Ca2+ currents in a motoneuron cell line', *Annals of Neurology*, 37, pp. 102–109. doi: 10.1002/ana.410370119.

Motterlini, R. *et al.* (2002) 'Carbon monoxide–releasing molecules characterization of biochemical and vascular activities', *Circulation research*, 90, pp. e17–e24. doi: 10.1161/hh0202.104530.

Motterlini, R., Mann, B., *et al.* (2005) 'Bioactivity and pharmacological actions of carbon monoxide-releasing molecules', *Current Pharmaceutical Design*, 9(30), pp. 2525–2539. doi: 10.2174/1381612033453785.

Motterlini, R., Sawle, P., *et al.* (2005) 'CORM-A1: a new pharmacologically active carbon monoxide-releasing molecule', *The FASEB Journal*, 19(2), pp. 284–6. doi: 10.1096/fj.04-2169fje.

Motterlini, R. (2007) 'Carbon monoxide-releasing molecules (CO-RMs): vasodilatory, anti-ischaemic and anti-inflammatory activities', *Biochemical Society Transactions*, 35(pt 5), pp. 1142–1146. doi: 10.1042/BST0351142.

Mouchard, A. *et al.* (2019) 'ApoE-fragment/Aβ heteromers in the brain of patients with Alzheimer's disease', *Scientific Reports*, 9(3989). doi: 10.1038/s41598-019-40438-4.

Moya, K. L. *et al.* (1994) 'The amyloid precursor protein is developmentally regulated and correlated with synaptogenesis', *Developmental Biology*, 161(2), pp. 597–603. doi:

10.1006/dbio.1994.1055.

Müller-Schiffmann, A. *et al.* (2016) 'Amyloid-β dimers in the absence of plaque pathology impair learning and synaptic plasticity', *Brain*, 139(2), pp. 509–525. doi: 10.1093/brain/awv355.

Nedergaard, B. Y. S., Flatman, J. A. and Engberg, I. (1993) 'Nifedipine- and ω-conotoxin-sensitive Ca^{2+} conductances in guinea-pig sustantia nigra pars compacta neurones', *Journal of Physiology*, 466, pp. 727–747.

Nelson, P. T. *et al.* (2012) 'Correlation of Alzheimer disease neuropathologic changes with cognitive status: A review of the literature', *Journal of Neuropathology and Experimental Neurology*, 71(5), pp. 362–381. doi: 10.1097/NEN.0b013e31825018f7.

Newcombe, E. A. *et al.* (2018) 'Inflammation: the link between comorbidities, genetics, and Alzheimer's disease', *Journal of Neuroinflammation*, 15(276), pp. 1–26. doi: 10.1186/s12974-018-1313-3.

Ng, J. B., Turek, M. and Hakim, A. M. (2013) 'Hear disease as a risk factor for dementia', *Clinical Epidemiology*, 5, pp. 135–145. doi: 10.2147/CLEP.S30621.

Nichols, M. R. *et al.* (2015) 'Biophysical comparison of soluble amyloid-β(1-42) protofibrils, oligomers, and protofilaments', *Biochemistry*, 54(13), pp. 2193–2204. doi: 10.1021/bi500957g.

Nicoll, A. J. *et al.* (2013) 'Amyloid-β nanotubes are associated with prion protein-dependent synaptotoxicity', *Nature Communications*, 4, pp. 2416. doi: 10.1038/ncomms3416.

Nikolaev, A. *et al.* (2009) 'N-APP binds DR6 to cause axon pruning and neuron death via distinct caspases', *Nature*, 457(7232), pp. 981–989. doi: 10.1038/nature07767.

Nimmrich, V. *et al.* (2008) 'Amyloidβ oligomers (Aβ1-42 globulomer) S suppress spontaneous synaptic activity by inhibition of P/Q-type calcium currents', *Journal of Neuroscience*, 28(4), pp. 788–797. doi: 10.1523/JNEUROSCI.4771-07.2008.

Nimmrich, V. and Eckert, A. (2013) 'Calcium channel blockers and dementia', *British Journal of Pharmacology*, 169(6), pp. 1203–1210. doi: 10.1111/bph.12240.

Nowycky, M. C., Fox, A. P. and Tsien, R. W. (1985) 'Three types of neuronal calcium channel with different calcium agonist sensitivity', *Nature*, 316(6027), pp. 440–443. doi: 10.1038/316440a0.

Nunez-Santana, F. L. *et al.* (2014) 'Surface L-type Ca2+ channel expression levels are increased in aged hippocampus', *Aging Cell*, 13, pp. 111–120. doi: 10.1111/acel.12157.

O'Nuallain, B. *et al.* (2010) 'Amyloid β-protein dimers rapidly form stable synaptotoxic protofibrils', *Journal of Neuroscience*, 30(43), pp. 14411–14419. doi: 10.1523/JNEUROSCI.3537-10.2010.

Omaye, S. T. (2002) 'Metabolic modulation of carbon monoxide toxicity', *Toxicology*, 180(2), pp. 139–150. doi: 10.1016/S0300-483X(02)00387-6.

Ortner, N. J. and Striessnig, J. (2016) 'L-type calcium channels as drug targets in CNS disorders L-type calcium channels as drug targets in CNS disorders', *Channels*, 10(1), pp. 7–13. doi: 10.1080/19336950.2015.1048936.

Ostacher, M. J. *et al.* (2014) 'Pilot investigation of isradipine in the treatment of bipolar depression motivated by genome-wide association', *Bipolar Disorders*, 16(2), pp. 199–203. doi: 10.1111/bdi.12143.

Pachahara, S. K. *et al.* (2012) 'Hexafluoroisopropanol induces self-assembly of β-amyloid peptides into highly ordered nanostructures', *Journal of Peptide Science*, 18(4), pp. 233–241. doi: 10.1002/psc.2391.

Palmqvist, S. *et al.* (2015) 'Detailed comparison of amyloid PET and CSF biomarkers for identifying early Alzheimer disease', *Neurology*, 85(14), pp. 1240–1249. doi: 10.1212/WNL.0000000000001991.

Pambo-Pambo, A., Durand, J. and Gueritaud, J. P. (2009) 'Early excitability changes in lumbar motoneurons of transgenic SOD1 G85R and SOD1G93A-Low mice', *Journal of Neurophysiology*, 102(6), pp. 3627–3642. doi: 10.1152/jn.00482.2009.

Panahian, N., Yoshiura, M. and Maines, M. D. (1999) 'Overexpression of heme oxygenase-1 is neuroprotective in a model of permanent middle cerebral artery occlusion in transgenic mice', *Journal of Neurochemistry*, 72(3), pp. 1187–1203. doi: 10.1111/j.1471-4159.1999.721187.x.

Pang, Z. P. *et al.* (2006) 'A gain-of-function mutation in synaptotagmin-1 reveals a critical role of Ca^{2+}-dependent soluble N-ethylmaleimide-sensitive factor attachment protein receptor complex binding in synaptic exocytosis', *Journal of Neuroscience*, 26(48), pp. 12556–12565. doi: 10.1523/JNEUROSCI.3804-06.2006.

Pappolla, M. A. *et al.* (1998) 'Evidence of Oxidative Stress and in Vivo Neurotoxicity of β-Amyloid in a Transgenic Mouse Model of Alzheimer 's Disease', *American Journal of Patology*, 152(4), pp. 871–877.

Paradis, E. *et al.* (1996) 'Amyloid β peptide of Alzheimer's disease downregulates bcl-2 and upregulates bax expression in human neurons', *Journal of Neuroscience*, 16(23), pp. 7533–7539. doi: 10.1523/jneurosci.16-23-07533.1996.

Parsons, C. G., Stöffler, A. and Danysz, W. (2007) 'Memantine: a NMDA receptor antagonist that improves memory by restoration of homeostasis in the glutamatergic system - too little activation is bad, too much is even worse', *Neuropharmacology*, 53(6), pp. 699–723. doi: 10.1016/j.neuropharm.2007.07.013.

Pasqualetti, P. *et al.* (2009) 'A randomized controlled study on effects of ibuprofen on cognitive progression of Alzheimer's disease', *Aging Clinical and Experimental Research*, 21(2), pp. 102–110. doi: 10.1007/BF03325217.

Pearson, H. A. and Peers, C. (2006) 'Physiological roles for amyloid β peptides', *Journal of Physiology*, 575(1), pp. 5–10. doi: 10.1113/jphysiol.2006.111203.

Pedersen, J. N. *et al.* (2020) 'A complete picture of protein unfolding and refolding in surfactants', *Chemical Science*. Royal Society of Chemistry, 11(3), pp. 699–712. doi:

10.1039/c9sc04831f.

Peers, C. (2011) 'Ion channels as target effectors for carbon monoxide', *Experimental Physiology*, 96(9), pp. 836–839. doi: 10.1113/expphysiol.2011.059063.

Peers, C., Dallas, M. L. and Scragg, J. L. (2009) 'Ion channels as effectors in carbon monoxide signaling.', *Communicative & integrative biology*. Taylor & Francis, 2(3), pp. 241–2. doi: 10.1074/jbc.M803037200.

Perez-Reyes, E. *et al.* (1998) 'Molecular characterization of a neuronal low-voltage-activated T-type calcium channel', *Nature*, 391(6670), pp. 896–900. doi: 10.1038/36110.

Perez-Reyes, E., Lee, J.-H. and Cribbs, L. L. (1999) 'Molecular characterization of two members of the T-type calcium channel family', *Annals New York Academy of Sciences*, 868, pp. 131–143. doi: 10.1111/j.1749-6632.1999.tb11283.x.

Perri, R. *et al.* (2007) 'Preclinical dementia: An Italian multicentre study on amnestic mild cognitive impairment', *Dementia and Geriatric Cognitive Disorders*, 23(5), pp. 289–300. doi: 10.1159/000100871.

Petersen, R. C. *et al.* (2001) 'Current concepts in mild cognitive impairment', *Archives of Neurology*, 58(12), pp. 1985–1992. doi: 10.1001/archneur.58.12.1985.

Petersen, R. C. *et al.* (2006) 'Neuropathologic features of amnestic mild cognitive impairment', *Archives of Neurology*, 63(5), pp. 665–672. doi: 10.1001/archneur.63.5.665.

Peterson, J. E. and Stewart, R. D. (1975) 'Predicting the carboxyhemoglobin levels resulting from carbon monoxide exposures', *Journal of Applied Physiology*, 39(4), pp. 633–638. doi: 10.1152/jappl.1975.39.4.633.

Pham, E. *et al.* (2010) 'Alterations in Synaptic Scaffold Proteins', *FEBS Journal*, 277(14), pp. 3051–3067. doi: 10.1111/j.1742-4658.2010.07719.x.

Pike, C. J., Cummings, B. J. and Cotman, C. W. (1995) 'Early association of reactive astrocytes with senile plaques in Alzheimer's disease', *Experimental Neurology*, 132(2), pp. 172–179. doi: 10.1016/0014-4886(95)90022-5.

Plant, L. D. *et al.* (2003) 'The production of amyloid β peptide is a critical requirement for the viability of central neurons', *Journal of Neuroscience*, 23(13), pp. 5531–5535. doi: 10.1523/jneurosci.23-13-05531.2003.

Podlisny, M. B. *et al.* (1995) 'Aggregation of secreted amyloid β-protein into sodium dodecyl sulfate- stable oligomers in cell culture', *Journal of Biological Chemistry*, pp. 9564–9570. doi: 10.1074/jbc.270.16.9564.

Podlisny, M. B. *et al.* (1998) 'Oligomerization of endogenous and synthetic amyloid β-protein at nanomolar levels in cell culture and stabilization of monomer by Congo red', *Biochemistry*, 37(11), pp. 3602–3611. doi: 10.1021/bi972029u.

Pravettoni, E. *et al.* (2000) 'Different localizations and functions of L-type and N-type calcium channels during development of hippocampal neurons', *Developmental Biology*, 227(2), pp. 581–594. doi: 10.1006/dbio.2000.9872.

Prince M, Wimo A, Guerchet M, A. D. I. (2015) 'World Alzheimer Report 2015: The Global Impact of Dementia | Alzheimer's Disease International', *Alzheimer's disease international*, pp. 1–87.

Prince, M., Guerchet, M. and Prina, M. (2015) 'The epidemiology and impact of dementia. Current state and future trends', *World Health Organization*.

Prince, M. and Jackson, J. (2009) 'World Alzheimer Report', *Alzheimer's disease international*.

Pringle, A. K. *et al.* (1996) 'Selective N-Type Calcium Channel Antagonist Omega Conotoxin MVIIA Is Neuroprotective Against Hypoxic Neurodegeneration in Organotypic Hippocampal-Slice Cultures', *Stroke*, 27(11), pp. 2124–2130. doi: 10.1161/01.str.27.11.2124.

Pullen, A. H. *et al.* (2004) 'Passive transfer of purified IgG from patients with amyotrophic lateral sclerosis to mice results in degeneration of motor neurons accompanied by Ca2+ enhancement', *Acta Neuropathologica*, 107(1), pp. 35–46. doi: 10.1007/s00401-003-0777-z.

Putcha, D. *et al.* (2011) 'Hippocampal hyperactivation associated with cortical thinning in Alzheimer's disease signature regions in non-demented elderly adults', *Journal of Neuroscience*, 31(48), pp. 17680–17688. doi: 10.1523/JNEUROSCI.4740-11.2011.

Puzzo, D. *et al.* (2005) 'Amyloid-β peptide inhibits activation of the nitric oxide/cGMP/cAMP-responsive element-binding protein pathway during hippocampal synaptic plasticity', *Journal of Neuroscience*, 25(29), pp. 6887–6897. doi: 10.1523/JNEUROSCI.5291-04.2005.

Qian, H. *et al.* (2017) 'Phosphorylation of Ser1928 mediates the enhanced activity of the L-type Ca2+ channel Cav 1.2 by the β2-adrenergic receptor in neurons', *Science signaling*, 10(463), pp. eaaf9659. doi: 10.1126/scisignal.aaf9659.

Qiu, C., Kivipelto, M. and Strauss, E. von (2009) 'Epidemiology of Alzheimer's disease: occurrence, determinants, and strategies toward intervention', *Dialogues in Clinical Neuroscience*, 11(2), pp. 111–128.

Queiroga, C. S. F. *et al.* (2010) 'Glutathionylation of adenine nucleotide translocase induced by carbon monoxide prevents mitochondrial membrane permeabilization and apoptosis', *Journal of Biological Chemistry*, 285(22), pp. 17077–17088. doi: 10.1074/jbc.M109.065052.

Queiroga, C. S. F. *et al.* (2012) 'Preconditioning triggered by carbon monoxide (CO) provides neuronal protection following perinatal hypoxia-ischemia', *PLoS ONE*, 7(8), pp. e42632. doi: 10.1371/journal.pone.0042632.

Ramsden, M., Henderson, Z. and Pearson, H. A. (2002) 'Modulation of Ca^{2+} channel currents in primary cultures of rat cortical neurones by amyloid β protein (1-40) is dependent on solubility status', *Brain Research*, 956(2), pp. 254–261. doi:

10.1016/S0006-8993(02)03547-3.

Randall, A. and Tsien, R. W. (1995) 'Pharmacological dissection of multiple types of Ca^{2+} channel currents in rat cerebellar granule neurons', *Journal of Neuroscience*, 15(4), pp. 2995–3012. doi: 10.1523/jneurosci.15-04-02995.1995.

Rangachari, V. *et al.* (2006) 'Secondary structure and interfacial aggregation of amyloid-β(1-40) on sodium dodecyl sulfate micelles', *Biochemistry*, 45(28), pp. 8639–8648. doi: 10.1021/bi060323t.

Reeve, H. L., Vaughan, P. F. T. and Peers, C. (1994) 'Calcium channel currents in undifferentiated human neuroblastoma (SH-SY5Y) cells: actions and possible interactions of dihydropyridines and ω-conotoxin', *European Journal of Neuroscience*, 6, pp. 943–952.

Resende, R. R. *et al.* (2010) 'Intracellular Ca^{2+} regulation during neuronal differentiation of murine embryonal Carcinoma and Mesenchymal stem cells', *Stem Cells and Development*, 19(3), pp. 379–393. doi: 10.1089/scd.2008.0289.

Reuveny, E. and Narahashi, T. (1993) 'Two types of high voltage-activated calcium channels in SH-SY5Y human neuroblastoma cells', *Brain Research*, 603(1), pp. 64–73. doi: 10.1016/0006-8993(93)91300-h.

Ripke, S. *et al.* (2013) 'Genome-wide association analysis identifies 14 new risk loci for Schizophrenia', *Nature Genetics*, 45(10), pp. 1150–1159. doi: 10.1038/ng.2742.

Risacher, S. L. *et al.* (2020) 'Visual contrast sensitivity is associated with the presence of cerebral amyloid and tau deposition', *Brain Communications*, 2(1), pp. 1–14. doi: 10.1093/braincomms/fcaa019.

Ritz, B. *et al.* (2010) 'L-type calcium channel blockers and Parkinson's disease in Denmark', *Annals of Neurology*, 67(5), pp. 600–606. doi: 10.1002/ana.21937.

Rogaev, E. I. *et al.* (1995) 'Familial Alzheimer's disease in kindreds with missense mutations in a gene on chromosome 1 related to the Alzheimer's disease type 3 gene', *Nature*, 376(6543), pp. 775–778. doi: 10.1038/376775a0.

Rönnemaa, E. *et al.* (2008) 'Impaired insulin secretion increases the risk of Alzheimer disease', *Neurology*, 71(14), pp. 1065–1071. doi: 10.1212/01.wnl.0000310646.32212.3a.

Rovelet-Lecrux, A. *et al.* (2006) 'APP locus duplication causes autosomal dominant early-onset Alzheimer disease with cerebral amyloid angiopathy', *Nature Genetics*, 38(1), pp. 24–26. doi: 10.1038/ng1718.

Rushworth, J. V. and Hooper, N. M. (2011) 'Lipid rafts: Linking Alzheimer's amyloid-β production, aggregation, and toxicity at neuronal membranes', *International Journal of Alzheimer's Disease*, pp. 1–14. doi: 10.4061/2011/603052.

Ryan, D. A. *et al.* (2010) 'An improved method for generating consistent soluble amyloid-beta oligomer preparations for in vitro neurotoxicity studies', *Journal Neuroscience Methods*, 190(2), pp. 171–179. doi: 10.1016/j.jneumeth.2010.05.001.

Ryan, T. M. *et al.* (2013) 'Ammonium hydroxide treatment of Aβ produces an aggregate free solution suitable for biophysical and cell culture characterization', *PeerJ*, (1), pp. e73. doi: 10.7717/peerj.73.

Saddala, M. S. *et al.* (2017) 'Novel 1,4-dihydropyridines for L-type calcium channel as antagonists for cadmium toxicity', *Scientific Reports*, 7, pp. 1–13. doi: 10.1038/srep45211.

Sadigh-Eteghad, S. *et al.* (2015) 'Amyloid-Beta: A crucial factor in Alzheimer's disease', *Medical Principles and Practice*, 24(1), pp. 1–10. doi: 10.1159/000369101.

Salloway, S. *et al.* (2014) 'Two phase 3 trials of Bapineuzumab in mild-to-moderate Alzheimer's disease', *New England Journal of Medicine*, 370(4), pp. 322–333. doi: 10.1056/NEJMoa1304839.

Sandberg, A. *et al.* (2010) 'Stabilization of neurotoxic Alzheimer amyloid-β oligomers by protein engineering', *Proceedings of the National Academy of Sciences of the United States of America*, 107(35), pp. 15595–15600. doi: 10.1073/pnas.1001740107.

Sano, M. *et al.* (2011) 'A randomized, double-blind, placebo-controlled trial of simvastatin to treat Alzheimer disease', *Neurology*, 77(6), pp. 556–563. doi: 10.1212/WNL.0b013e318228bf11.

Santos-Silva, T. *et al.* (2011) 'CORM-3 reactivity toward proteins: The crystal structure of a Ru(II) dicarbonyl-lysozyme complex', *Journal of the American Chemical Society*, 133(5), pp. 1192–1195. doi: 10.1021/ja108820s.

Satizabal, C. L. *et al.* (2016) 'Incidence of dementia over three decades in the Framingham heart study', *The New England Journal of Medicine*, 374(6), pp. 523–532. doi: 10.1056/NEJMoa1504327.

Scarmeas, N. *et al.* (2006) 'Mediterranean diet and risk for Alzheimer's disease', *Annals of Neurology*, 59(6), pp. 912–921. doi: 10.1002/ana.20854.

Schenk, D. *et al.* (1999) 'Immunization with amyloid-β attenuates Alzheimer disease-like pathology in the PDAPP mouse', *Nature*, 400(6740), pp. 173–177. doi: 10.1038/22124.

Schipper, H. M. (2000) 'Heme oxygenase-1: Role in brain aging and neurodegeneration', *Experimental Gerontology*, 35(6–7), pp. 821–830. doi: 10.1016/S0531-5565(00)00148-0.

Schipper, H. M. (2004) 'Heme oxygenase expression in human central nervous system disorders', *Free Radical Biology and Medicine*, 37(12), pp. 1995–2011. doi: 10.1016/j.freeradbiomed.2004.09.015.

Schipper, H. M., Cissé, S. and Stopa, E. G. (1995) 'Expression of heme oxygenase-1 in the senescent and alzheimer-diseased brain', *Annals of Neurology*, 37(6), pp. 758–768. doi: 10.1002/ana.410370609.

Schneider, L. (2019) 'A resurrection of aducanumab for Alzheimer's disease', *The Lancet Neurology*, 19(2), pp. 111–112. doi: 10.1016/S1474-4422(19)30480-6.

Schneider, T. *et al.* (2005) 'Presynaptic "Cav2.3-containing" E-type Ca^{2+} channels share dual roles during neurotransmitter release', *European Journal of Neuroscience*, 21, pp. 1617–1625. doi: 10.1111/j.1460-9568.2005.03984.x.

Scopa, C. *et al.* (2020) 'Impaired adult neurogenesis is an early event in Alzheimer's disease neurodegeneration, mediated by intracellular Aβ oligomers', *Cell Death and Differentiation*, 27(3), pp. 934–948. doi: 10.1038/s41418-019-0409-3.

Scragg, J. L. *et al.* (2008) 'Carbon monoxide inhibits L-type Ca^{2+} channels via redox modulation of key cysteine residues by mitochondrial reactive oxygen species', *Journal of Biological Chemistry*, 283(36), pp. 24412–24419. doi: 10.1074/jbc.M803037200.

Senatore, A. *et al.* (2012) 'Mutant PrP suppresses glutamatergic neurotransmission in cerebellar granule neurons by impairing membrane delivery of VGCC α2δ-1 subunit', *Neuron*, 74(2), pp. 300–313. doi: 10.1016/j.neuron.2012.02.027.

Serra, L. *et al.* (2010) 'Grey and white matter changes at different stages of Alzheimer's disease', *Journal of Alzheimer's Disease*, 19(1), pp. 147–159. doi: 10.3233/JAD-2010-1223.

Shao, H. *et al.* (1999) 'Solution structures of micelle-bound amyloid β-(1-40) and β-(1-42) peptides of Alzheimer's disease', *Journal of Molecular Biology*, 285(2), pp. 755–773. doi: 10.1006/JMBI.1998.2348.

Sheehan, J. P. *et al.* (2013) 'Inhibition of glioblastoma and enhancement of survival via the use of mibefradil in conjunction with radiosurgery', *Journal of Neurosurgery*, 118(4), pp. 830–837. doi: 10.3171/2012.11.JNS121087.

Shen, C. L. and Murphy, R. M. (1995) 'Solvent effects on self-assembly of beta-amyloid peptide', *Biophysical Journal*, 69(2), pp. 640–651. doi: 10.1016/S0006-3495(95)79940-4.

Sheng, Z. H. *et al.* (1996) 'Calcium-dependent interaction of N-type calcium channels with the synaptic core complex', *Nature*, pp. 451–454. doi: 10.1038/379451a0.

Shin, J.-Y. *et al.* (2010) 'Swedish mutation within amyloid precursor protein modulates global gene expression towards the pathogenesis of Alzheimer's disease', *BMB Reports*, 43(10), pp. 704–709. doi: 10.5483/bmbrep.2010.43.10.704.

Shirahama, T. and Cohen, A. S. (1967) 'Reconstitution of amyloid fibrils from alkaline extracts.', *Journal of Cell Biology*, 35(2), pp. 459–464. doi: 10.1083/jcb.35.2.459.

de Simone, A. *et al.* (2019) 'Investigating in vitro amyloid peptide 1–42 aggregation: impact of higher molecular weight stable adducts', *ACS Omega*, 4(7), pp. 12308–12318. doi: 10.1021/acsomega.9b01531.

Sinnegger-Brauns, M. J. *et al.* (2009) 'Expression and 1,4-dihydropyridine-binding properties of brain L-type calcium channel isoforms', *Molecular Pharmacology*, 75(2), pp. 407–414. doi: 10.1124/mol.108.049981.

Song, R. *et al.* (2003) 'Carbon monoxide induces cytoprotection in rat orthotopic lung transplantation via anti-inflammatory and anti-apoptotic effects', *American Journal of Pathology*, 163(1), pp. 231–242. doi: 10.1016/S0002-9440(10)63646-2.

Song, R. *et al.* (2004) 'Carbon monoxide inhibits T lymphocyte proliferation via caspase-dependent pathway', *The Journal of Immunology*, 172(2), pp. 1220–1226. doi: 10.4049/jimmunol.172.2.1220.

Soong, T. W. *et al.* (1993) 'Structure and functional expression of a member of the low voltage-activated calcium channel family', *Science*, 260(5111), pp. 1133–1136. doi: 10.1126/science.8388125.

Sousa, S. R. *et al.* (2013) 'Expression and pharmacology of endogenous Cav channels in SH-SY5Y human neuroblastoma cells', *PLoS ONE*, 8(3), pp. e59293. doi: 10.1371/journal.pone.0059293.

Spoerri, P. E., Dozier, A. K. and Roisen, F. J. (1990) 'Calcium regulation of neuronal differentiation : the role of calcium in GMl-mediated neuritogenesis', *Developmental Brain Research*, 56, pp. 177–188. doi: 10.1016/0165-3806(90)90080-I.

Stalder, M. *et al.* (1999) 'Association of microglia with amyloid plaques in brains of APP23 transgenic mice', *American Journal of Pathology*, 154(6), pp. 1673–1684. doi: 10.1016/S0002-9440(10)65423-5.

Stanika, R. *et al.* (2016) 'Splice variants of the Cav1.3 L-type calcium channel regulate dendritic spine morphology', *Scientific Reports*, 6, p. 34528. doi: 10.1038/srep34528.

Stanika, R., Flucher, B. and Obermair, G. (2015) 'Regulation of postsynaptic stability by the L-type calcium channel CaV1.3 and its interaction with PDZ proteins', *Current Molecular Pharmacology*, 8(1), pp. 95–101. doi: 10.2174/1874467208666150507103716.

Stansley, B., Post, J. and Hensley, K. (2012) 'A comparative review of cell culture systems for the study of microglial biology in Alzheimer's disease', *Journal of Neuroinflammation*, 9(115), pp. 1–8. doi: 10.1086/302477.

Stephen, J. M. *et al.* (2010) 'Somatosensory responses in normal aging, mild cognitive impairment, and Alzheimer's disease', *Journal of Neural Transmission*, 117(2), pp. 217–225. doi: 10.1007/s00702-009-0343-5.

Strada, O. *et al.* (1992) 'Decreased choline acetyltransferase mRNA expression in the nucleus basalis of Meynert in Alzheimer disease: An in situ hybridization study', *Proceedings of the National Academy of Sciences of the United States of America*, 89(20), pp. 9549–9553. doi: 10.1073/pnas.89.20.9549.

Striessnig, J. *et al.* (2014) 'L-type Ca^{2+} channels in heart and brain', *Wiley Interdisciplinary Reviews: Membrane Transport and Signaling*, 3(2), pp. 15–38. doi: 10.1002/wmts.102.

de Strooper, B. (2007) 'Loss-of-function presenilin mutations in Alzheimer disease. Talking Point on the role of presenilin mutations in Alzheimer disease', *European Molecular Biology Organization*, 8(2), pp. 141–146. doi: 10.1038/sj.embor.7400897.

Sturchler-Pierrat, C. *et al.* (1997) 'Two amyloid precursor protein transgenic mouse models with Alzheimer disease-like pathology', *Proceedings of the National Academy of Sciences of the United States of America*, 94(24), pp. 13287–13292. doi:

10.1073/pnas.94.24.13287.

Subbarao, K. V, Richardson, T. J. S. and Ang, L. C. (1990) 'Autopsy samples of Alzheimer's cortex show increased peroxidation in vitro', *Journal of Neurochemistry*, 55(1), pp. 342–345. doi: 10.1111/j.1471-4159.1990.tb08858.x.

Südhof, T. C. (2013) 'Neurotransmitter release: The last millisecond in the life of a synaptic vesicle', *Neuron*, 80(3), pp. 675–690. doi: 10.1016/j.neuron.2013.10.022.

Sun, L. *et al.* (2016) 'Analysis of 138 pathogenic mutations in presenilin-1 on the in vitro production of Aβ42 and Aβ40 peptides by γ-secretase', *Proceedings of the National Academy of Sciences of the United States of America*, 114(4), pp. e476-E485. doi: 10.1073/pnas.1618657114.

Suppiah, S., Didier, M.-A. and Vinjamuri, S. (2019) 'The who, when, why, and how of PET amyloid imaging in management of Alzheimer's disease-review of literature and interesting images', *Diagnostics*, 9(65), pp. 1–18.

Suva, D. *et al.* (1999) 'Primary Motor Cortex involvement in Alzheimer disease', *Neuropathology and Experimental Neurology*, 58(11), pp. 1125–1134. doi: 10.1097/00005072-199911000-00002.

Swandulla, D. and Armstrong, C. M. (1989) 'Calcium channel block by cadmium in chicken sensory neurons', *Proceedings of the National Academy of Sciences of the United States of America*, 86(5), pp. 1736–1740. doi: 10.1073/pnas.86.5.1736.

Swerdlow, R. H. (2007) 'Pathogenesis of Alzheimer ' s disease', *Clinical Interventions in Aging*, 2(3), pp. 347–359.

Szabò, I., Zoratti, M. and Gulbins, E. (2010) 'Contribution of voltage-gated potassium channels to the regulation of apoptosis', *FEBS Letters*, 584, pp. 2049–2056. doi: 10.1016/j.febslet.2010.01.038.

Takahashi, M. *et al.* (1987) 'Subunit structure of dihydropyridine-sensitive calcium channels from skeletal muscle', *Proceedings of the National Academy of Sciences of the United States of America*, 84(15), pp. 5478–5482. doi: 10.1073/pnas.84.15.5478.

Takahashi, M. *et al.* (2000) 'Amyloid precursor proteins inhibit heme oxygenase activity and augment neurotoxicity in Alzheimer's disease', *Neuron*, 28(2), pp. 461–473. doi: 10.1016/S0896-6273(00)00125-2.

Takuma, H. *et al.* (2004) 'Amyloid beta peptide-induced cerebral neuronal loss is mediated by caspase-3 in vivo', *Journal of Neuropathology and Experimental Neurology*, 63(3), pp. 255–261. doi: 10.1093/jnen/63.3.255.

Talley, E. M. *et al.* (2000) 'Low-voltage-activated calcium channel subunit expression in a genetic model of absence epilepsy in the rat', *Molecular Brain Research*, 75(1), pp. 159–165. doi: 10.1016/S0169-328X(99)00307-1.

Tamagnini, F. *et al.* (2015) 'Intrinsic excitability changes induced by acute treatment of hippocampal CA1 pyramidal neurons with exogenous amyloid β peptide', *Hippocampus*,

25(7), pp. 786–797. doi: 10.1002/hipo.22403.

Taylor, S. C., Batten, T. F. C. and Peers, C. (1999) 'Hypoxic enhancement of quantal catecholamine secretion. Evidence for the involvement of amyloid β-peptides', *Journal of Biological Chemistry*, 274(44), pp. 31217–31222. doi: 10.1074/jbc.274.44.31217.

Tenhunen, R., Marvel, H. S. and Schmid, R. (1969) 'Microsomal heme oxygenase. Characterization of the enzyme', *Journal of Biological Chemistry*, 244(23), pp. 6388–6394.

Teppola, H. *et al.* (2016) 'Morphological differentiation towards neuronal phenotype of SH-SY5Y neuroblastoma cells by estradiol, retinoic acid and cholesterol', *Neurochemical Research*, 41(4), pp. 731–747. doi: 10.1007/s11064-015-1743-6.

Thévenod, F. and Jones, S. W. (1992) 'Cadmium block of calcium current in frog sympathetic neurons', *Biophysical Journal*, 63(1), pp. 162–168. doi: 10.1016/S0006-3495(92)81575-8.

Thibault, O. *et al.* (2012) 'Reduction in neuronal L-type calcium channel activity in a double knock-in mouse model of Alzheimer's disease', *Biochimica et Biophysica Acta*, 1822(4), pp. 546–549. doi: 10.1016/j.bbadis.2012.01.004.

Tierney, M. C. *et al.* (2005) 'Neuropsychological tests accurately predict incident Alzheimer disease after 5 and 10 years', *Neurology*, 64(11), pp. 1853–1859. doi: 10.1212/01.WNL.0000163773.21794.0B.

Tizon, B. *et al.* (2010) 'Cystatin C Protects Neuronal Cells from Amyloid-β-induced Toxicity', *Journal of Alzheimer's Disease*, 19(3), pp. 885–894. doi: 10.3233/JAD-2010-1291.

de la Torre, J. C. (2012) 'Cardiovascular risk factors promote brain hypoperfusion leading to cognitive decline and dementia', *Cardiovascular Psychiatry and Neurology*, 2012(367516), pp. 1–15. doi: 10.1155/2012/367516.

Ueda, K. *et al.* (1997) 'Amyloid β protein potentiates Ca^{2+} influx through L-Type voltage-sensitive Ca^{2+} channels: A possible involvement of free radicals', *Journal of Neurochemistry*, 68(1), pp. 265–271. doi: 10.1046/j.1471-4159.1997.68010265.x.

Urbanc, B. *et al.* (2002) 'Neurotoxic effects of thioflavin S-positive amyloid deposits in transgenic mice and Alzheimer's disease', *Proceedings of the National Academy of Sciences of the United States of America*, 99(22), pp. 13990–13995. doi: 10.1073/pnas.222433299.

Valensin, D. *et al.* (2010) 'Fac-{Ru(CO)3}2+ selectively targets the histidine residues of the β-amyloid peptide 1-28. Implications for new Alzheimer's disease treatments based on ruthenium complexes', *Inorganic Chemistry*, 49(11), pp. 4720–4722. doi: 10.1021/ic902593e.

Valerie, N. C. K. *et al.* (2013) 'Inhibition of T-type calcium channels disrupts Akt signaling and promotes apoptosis in glioblastoma cells', *Biochemical Pharmacology*, 85(7), pp. 888–897. doi: 10.1016/j.bcp.2012.12.017.

Vehmas, A. K. *et al.* (2003) 'Immune reactive cells in senile plaques and cognitive decline in Alzheimer's disease', *Neurobiology of Aging*, 24(2), pp. 321–331. doi: 10.1016/S0197-4580(02)00090-8.

Verma, M., Vats, A. and Taneja, V. (2015) 'Toxic species in amyloid disorders: Oligomers or mature fibrils.', *Annals of Indian Academy of Neurology*, 18(2), pp. 138–45. doi: 10.4103/0972-2327.144284.

Vieira, H. L. A., Queiroga, C. S. F. and Alves, P. M. (2008) 'Pre-conditioning induced by carbon monoxide provides neuronal protection against apoptosis', *Journal of Neurochemistry*, 107(2), pp. 375–384. doi: 10.1111/j.1471-4159.2008.05610.x.

Vogl, C. *et al.* (2015) 'Synaptic vesicle glycoprotein 2A modulates vesicular release and calcium channel function at peripheral sympathetic synapses', *European Journal of Neuroscience*, 41(4), pp. 398–409. doi: 10.1111/ejn.12799.

Volloch, V. and Rits, S. (2018) 'Results of Beta secretase-inhibitor clinical trials support amyloid precursor protein-independent generation of beta amyloid in sporadic Alzheimer's disease', *Medical Sciences*, 6(2), p. 45. doi: 10.3390/medsci6020045.

Wahlström, A. *et al.* (2008) 'Secondary structure conversions of Alzheimer's Aβ(1-40) peptide induced by membrane-mimicking detergents', *FEBS Journal*, 275(20), pp. 5117–5128. doi: 10.1111/j.1742-4658.2008.06643.x.

Walsh, D. M. *et al.* (1999) 'Amyloid b-protein fibrillogenesis. Structure and biological activity of protofibrillar intermediates', *Journal of Biological Chemistry*, 274(36), pp. 25945–25952. doi: 10.1074/jbc.274.36.25945.

Wang, B. *et al.* (2011) 'Carbon monoxide-activated Nrf2 pathway leads to protection against permanent focal cerebral ischemia Bing', *Stroke*, 42(9), pp. 2605–2610. doi: 10.1161/STROKEAHA.110.607101.

Wang, C. Y. *et al.* (2015) 'Meta-analysis of public microarray datasets reveals voltage-gated calcium gene signatures in clinical cancer patients', *PLoS ONE*, 10(7), p. e0125766. doi: 10.1371/journal.pone.0125766.

Wang, Y. *et al.* (2004) 'Involvement of Notch signaling in hippocampal synaptic plasticity', *Proceedings of the National Academy of Sciences of the United States of America*, 101(25), pp. 9458–9462. doi: 10.1073/pnas.0308126101.

Ward, R. V *et al.* (2000) 'Fractionation and characterization of oligomeric, protofibrillar and fibrillar forms of β-amyloid peptide', *Biochemistry*, 348(Pt 1), pp. 137–144.

Wei, W., Wang, X. and Kusiak, J. W. (2002) 'Signaling events in amyloid β-peptide-induced neuronal death and insulin-like growth factor I protection', *Journal of Biological Chemistry*, 277(20), pp. 17649–17656. doi: 10.1074/jbc.M111704200.

Weller, J. and Budson, A. (2018) 'Current understanding of Alzheimer's disease diagnosis and treatment', *F1000 Research*, 7, p. 1161. doi: 10.12688/f1000research.14506.1.

Westergard, L., Christensen, H. M. and Harris, D. A. (2007) 'The Cellular Prion Protein (PrPC): Its Physiological Function and Role in Disease', *Biochimica et Biophysica Acta*,

1772(6), pp. 629–644. doi: 10.1016/j.bbadis.2007.02.011.

Whitehouse, P. J. *et al.* (1982) 'Alzheimer's disease and senile dementia: loss of neurons in the basal forebrain', *American Association for the Advancement of Science*, 215(4537), pp. 1237–1239. doi: 10.1126/science.7058341.

Wilcock, G. K. *et al.* (1982) 'ALZHEIMER'S DISEASE Correlation of cortical choline acetyltransferase activity with the severity of dementia and histological abnormalities', *Journal of the Neurological Sciences*, 57(2–3), pp. 407–417. doi: 10.1016/0022-510X(82)90045.

Wildburger, N. C. *et al.* (2009) 'Neuroprotective effects of blockers for T-type calcium channels', *Molecular Neurodegeneration*, 4(44). doi: 10.1186/1750-1326-4-44.

Wilkinson, W. J. and Kemp, P. J. (2011) 'Carbon monoxide: An emerging regulator of ion channels', *Journal of Physiology*, 589(13), pp. 3055–3062. doi: 10.1113/jphysiol.2011.206706.

Wisniewski, T. *et al.* (1994) 'Acceleration of Alzheimer's fibril formation by Apolipoprotein E in vitro', *American Journal of Pathology*, 145(5), pp. 1030–1035.

Witcher, D. R. *et al.* (1993) 'Subunit identification and reconstitution of the N-Type Ca^{2+} channel complex purified from brain', *Science*, 261(5120), pp. 486–489. doi: 10.1126/science.8392754.

Wojsiat, J. *et al.* (2018) 'Oxidant/antioxidant imbalance in Alzheimer's disease: Therapeutic and diagnostic prospects', *Oxidative Medicine and Cellular Longevity*, p. 6435861. doi: 10.1155/2018/6435861.

Wolters, F. J. *et al.* (2020) 'Twenty-seven-year time trends in dementia incidence in Europe and the United States: The Alzheimer Cohorts Consortium', *Neurology*, 95(5), pp. e519–e531. doi: 10.1212/WNL.0000000000010022.

Wong, T. P. *et al.* (1999) 'Reorganization of cholinergic terminals in the cerebral cortex and hippocampus in transgenic mice carrying mutated presenilin-1 and amyloid precursor protein transgenes', *Journal of Neuroscience*, 19(7), pp. 2706–2716. doi: 10.1523/jneurosci.19-07-02706.1999.

Wood, S. J. *et al.* (1996) 'Physical, morphological and functional differences between pH 5.8 and 7.4 aggregates of the Alzheimer's amyloid peptide Aβ', *Journal of Molecular Biology*, 256(5), pp. 870–877. doi: 10.1006/jmbi.1996.0133.

Wu, H. Y. *et al.* (2018) 'B-Amyloid Induces Pathology-Related Patterns of Tau Hyperphosphorylation At Synaptic Terminals', *Journal of Neuropathology and Experimental Neurology*, 77(9), pp. 814–826. doi: 10.1093/jnen/nly059.

Wu, L. and Wang, R. (2005) 'Carbon monoxide: Endogenous production, physiological functions, and pharmacological applications', *Pharmacological Reviews*, 57(4), pp. 585–630. doi: 10.1124/pr.57.4.3.

Xu, B. *et al.* (2011) 'Calcium signaling is involved in cadmium-induced neuronal apoptosis via induction of reactive oxygen species and activation of MAPK/mTOR

network', *PLoS ONE*, 6(4), p. e19052. doi: 10.1371/journal.pone.0019052.

Xu, J. *et al.* (2009) 'Synaptotagmin-1 functions as a Ca^{2+} sensor for spontaneous release', *Nature Neuroscience*, 12(6), pp. 759–766. doi: 10.1038/nn.2320.

Xu, J. *et al.* (2019) 'Regional protein expression in human Alzheimer's brain correlates with disease severity', *Communications Biology*, 2(1). doi: 10.1038/s42003-018-0254-9.

Xue, C. *et al.* (2017) 'Thioflavin T as an amyloid dye: Fibril quantification, optimal concentration and effect on aggregation', *Royal Society Open Science*, 4(1), p. 160696. doi: 10.1098/rsos.160696.

Yagami, T. *et al.* (2004) 'Protective effects of a selective L-type voltage-sensitive calcium channel blocker , S -312- d , on neuronal cell death', *Biochemical Pharmacology*, 67, pp. 1153–1165. doi: 10.1016/j.bcp.2003.11.005.

Yamamoto, N. *et al.* (2004) 'Environment- and mutation-dependent aggregation behavior of Alzheimer amyloid β-protein', *Journal of Neurochemistry*, 90(1), pp. 62–69. doi: 10.1111/j.1471-4159.2004.02459.x.

Yang, L. *et al.* (2009) 'Amyloid precursor protein regulates Cav1.2 L-type calcium channel levels and function to influence GABAergic short-term plasticity', *Neurobiology of Disease*, 29(50), pp. 15660–15668. doi: 10.1523/JNEUROSCI.4104-09.2009.

Yassa, M. A. *et al.* (2010) 'High-resolution structural and functional MRI of hippocampal CA3 and dentate gyrus in patients with amnestic Mild cognitive impairment', *NeuroImage*, 51(3), pp. 1242–1252. doi: 10.1016/j.neuroimage.2010.03.040.

Yeo, J. M. *et al.* (2015) 'A systematic review and meta-analysis of 18F-labeled amyloid imaging in Alzheimer's disease', *Alzheimer's and Dementia: Diagnosis, Assessment and Disease Monitoring*, 1(1), pp. 5–13. doi: 10.1016/j.dadm.2014.11.004.

Younan, N. D. and Viles, J. H. (2015) 'A Comparison of Three Fluorophores for the Detection of Amyloid Fibers and Prefibrillar Oligomeric Assemblies. ThT (Thioflavin T); ANS (1-Anilinonaphthalene-8-sulfonic Acid); and bisANS (4,4′-Dianilino-1,1′-binaphthyl-5,5′-disulfonic Acid)', *Biochemistry*, 54(28), pp. 4297–4306. doi: 10.1021/acs.biochem.5b00309.

Zamponi, G. W. (2015) 'Targeting voltage-gated calcium channels in neurological and psychiatric diseases', *Nature Reviews Drug Discovery*, 15(1), pp. 19–34. doi: 10.1038/nrd.2015.5.

Zamponi, G. W. (2016) 'Targeting voltage-gated calcium channels in neurological and psychiatric diseases', *Nature Reviews Drug Discovery*, 15, pp. 19–34. doi: 10.1038/nrd.2015.5.

Zandi, P. P. *et al.* (2004) 'Reduced risk of Alzheimer disease in users of antioxidant vitamin supplements: The Cache County study', *Archives of Neurology*, 61(1), pp. 82–88. doi: 10.1001/archneur.61.1.82.

Zawadzki, A. *et al.* (2008) 'Verapamil inhibits L-type calcium channel mediated apoptosis in human colon cancer cells', *Diseases of the Colon and Rectum*, 51(11), pp. 1696–1702.

doi: 10.1007/s10350-008-9372-7.

Zeynalov, E. and Doré, S. (2009) 'Low doses of carbon monoxide protect against experimental focal brain ischemia', *Neurotoxicity Research*, 15(2), pp. 133–137. doi: 10.1007/s12640-009-9014-4.

Zhang, H. *et al.* (2006) 'Cav1.2 and Cav1.3 neuronal L-type calcium channels: differential targeting and signaling to pCREB', *European Journal of Neuroscience*, 23(9), pp. 2297–2310. doi: 10.1111/j.1460-9568.2006.04734.x.

Zhang, J. F. *et al.* (1993) 'Distinctive pharmacology and kinetics of cloned neuronal Ca^{2+} channels and their possible counterparts in mammalian CNS neurons', *Neuropharmacology*, 32(11), pp. 1075–1088. doi: 10.1016/0028-3908(93)90003-L.

Zhang, Y. *et al.* (2002) 'Mutations in high-voltage-activated calcium channel genes stimulate low-voltage-activated currents in mouse thalamic relay neurons', *Journal of Neuroscience*, 22(15), pp. 6362–6371. doi: 10.1523/jneurosci.22-15-06362.2002.

Zou, K. *et al.* (2002) 'A Novel function of monomeric amyloid β-protein serving as an antioxidant molecule against metal-induced oxidative damage', *Journal of Neuroscience*, 22(12), pp. 4833–4841. doi: 10.1523/jneurosci.22-12-04833.2002.

Zuckerbraun, B. S. *et al.* (2007) 'Carbon monoxide signals via inhibition of cytochrome c oxidase and generation of mitochondrial reactive oxygen species', *FASEB Journal*, 21(4), pp. 1099–1106. doi: 10.1096/fj.06-6644com.